

UNCLASSIFIED

AD NUMBER

ADB006136

LIMITATION CHANGES

TO:

Approved for public release; distribution is unlimited.

FROM:

Distribution authorized to U.S. Gov't. agencies only; Test and Evaluation; JAN 1974. Other requests shall be referred to Air Force Flight Dynamics Laboratory, FBS, Structures Division, Wright-Patterson AFB, OH 45433.

AUTHORITY

afal ltr, 22 may 1978

THIS PAGE IS UNCLASSIFIED

AFFDL-TR-74-140

ADB006136

F-4 BERYLLIUM RUDDERS

**A Précis of the Design, Fabrication,
Ground and Flight Test Demonstrations**

*STRUCTURES DIVISION
AIR FORCE FLIGHT DYNAMICS DIVISION*

TECHNICAL REPORT AFFDL-TR-74-140

MAY 1975

FINAL REPORT FOR PERIOD JUNE 1965 - AUGUST 1971

Distribution limited to U.S. Government agencies only; test and evaluation; statement applied January 1974. Other requests for this document must be referred to AF Flight Dynamics Laboratory (FBS), Wright-Patterson Air Force Base, Ohio 45433.

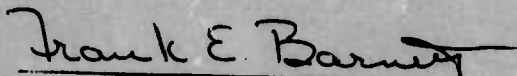


**AIR FORCE FLIGHT DYNAMICS LABORATORY
AIR FORCE SYSTEMS COMMAND
WRIGHT-PATTERSON AIR FORCE BASE, OHIO 45433**

NOTICE

When Government drawings, specifications, or other data are used for any purpose other than in connection with a definitely related Government procurement operation, the United States Government thereby incurs no responsibility nor any obligation whatsoever; and the fact that the government may have formulated, furnished, or in any way supplied the said drawings, specifications, or other data, is not to be regarded by implication or otherwise as in any manner licensing the holder or any other person or corporation, or conveying any rights or permission to manufacture, use, or sell any patented invention that may in any way be related thereto.

This technical report has been reviewed and is approved for publication.



FRANK E. BARNETT
Project Engineer

FOR THE COMMANDER:



FRANCIS J. JANIK
Chief, Advanced Structures Branch
Structures Division
Air Force Flight Dynamics Laboratory

Copies of this report should not be returned unless return is required by security considerations, contractual obligations, or notice on a specific document.

UNCLASSIFIED

SECURITY CLASSIFICATION OF THIS PAGE (When Data Entered)

REPORT DOCUMENTATION PAGE		READ INSTRUCTIONS BEFORE COMPLETING FORM
1. REPORT NUMBER AFFDL-TR-74-140	2. GOVT ACCESSION NO.	3. RECIPIENT'S CATALOG NUMBER
4. TITLE (and Subtitle) F-4 BERYLLIUM RUDDERS; A Précis of the Design, Fabrication, Ground and Flight Test Demonstrations		5. TYPE OF REPORT & PERIOD COVERED Final Summary Report June 1965 - August 1971
7. AUTHOR(s) Frank E. Barnett		6. PERFORMING ORG. REPORT NUMBER
9. PERFORMING ORGANIZATION NAME AND ADDRESS Air Force Flight Dynamics Laboratory/FBS Wright-Patterson AFB, OH 45433		8. CONTRACT OR GRANT NUMBER(s)
11. CONTROLLING OFFICE NAME AND ADDRESS Air Force Flight Dynamics Laboratory/FBS Structures Division, Advanced Structures Branch Wright-Patterson AFB, OH 45433		10. PROGRAM ELEMENT, PROJECT, TASK AREA & WORK UNIT NUMBERS PE: 62201F Proj - Task - WU 1368 01 03
14. MONITORING AGENCY NAME & ADDRESS (if different from Controlling Office)		12. REPORT DATE May 1975
		13. NUMBER OF PAGES 291
		15. SECURITY CLASS. (of this report) Unclassified
		15a. DECLASSIFICATION/DOWNGRADING SCHEDULE
16. DISTRIBUTION STATEMENT (of this Report) Distribution limited to U.S. Government agencies only; test and evaluation; statement applied January 1974. Other requests for this document must be referred to AF Flight Dynamics Laboratory, (FBS), Wright-Patterson AFB, OH 45433.		
17. DISTRIBUTION STATEMENT (of the abstract entered in Block 20, if different from Report) Approved for public release; distribution unlimited.		
18. SUPPLEMENTARY NOTES		
19. KEY WORDS (Continue on reverse side if necessary and identify by block number) Acoustics, acoustic measurements, aircraft, aerial rudders, airframes, air- craft rudders, aircraft structures, beryllium, beryllium fabrication, beryllium structures, industrial processes, structural analysis, structural design, radio- graphic inspection, fatigue test, flight test, static test.		
20. ABSTRACT (Continue on reverse side if necessary and identify by block number) This report contains a summary of the total effort expended to design, fabri- cate, qualify and demonstrate by actual flight tests an aircraft structural component constructed of beryllium. The low density and high modulus of this metal is unmatched by any alloy making it particularly attractive for applica- tions where weight and stiffness are critical. Limited ductility does put a premium on proper design and fabrication techniques. One F-4 beryllium rudder produced to the same configuration and load envelopes as the production aluminum rudder at a weight savings of 41.5%, was extensively ground tested		

DD FORM 1 JAN 73 1473

EDITION OF 1 NOV 65 IS OBSOLETE

UNCLASSIFIED

SECURITY CLASSIFICATION OF THIS PAGE (When Data Entered)

UNCLASSIFIED

SECURITY CLASSIFICATION OF THIS PAGE(When Data Entered)

(20. cont.)

first to qualify the configuration for flight testing and then to determine additional data on the acoustic fatigue life and residual strength of the damaged rudder. These sequential ground tests include:

- Test 1 - A 50,000 cycle fatigue test of upper balance weight support structure.
- Test 2 - A static test to design ultimate load (DUL) representing the yaw flight condition.
- Test 3 - A static test to DUL representing the rolling pull-out maneuver. Flight test qualified.
- Test 4 - A repeat of Test 2 to 167% DUL. Minor damage.
- Test 5 - Acoustic fatigue endurance test to about seven normal lives of the rudder. Major damage.
- Test 6 - A residual strength static test with loading conditions similar to Test 3. Failure occurred at 133% DUL.

An instrumented flight test rudder, with a weight savings of 34.6% over the production aluminum rudder, made 158 flights over a 39 month time span with a total flight time of 184 hours and 24 minutes under a variety of operating conditions. A maximum recorded load of 205% design limit load (137% DUL) was applied to the rudder due to an inadvertent maneuver on the 10th flight; however, no serious damage occurred and the rudder was still considered flight worthy when circumstances dictated removal of the beryllium rudder from the aircraft.

UNCLASSIFIED

SECURITY CLASSIFICATION OF THIS PAGE(When Data Entered)

FOREWORD

The development and demonstration of structural integrity of the F-4 beryllium rudders was accomplished under Project 1368, "Advanced Structures for Military Aerospace Vehicles", under a series of contractual and in-house work units sponsored by the Air Force Flight Dynamics Laboratory under the direction of Mr. F.E. Barnett(FBS) Project Engineer. The residual strength static test of the ground test rudder and the preparation of this report was accomplished under Work Unit 13680103, "Residual Life Testing of an F-4 Beryllium Rudder".

The total technical effort reported herein covers a time span from start of the initial contract in June 1965 through removal of the flight test rudder from the aircraft in August 1971 and NDI assessment of its structural condition. The initial effort to design fabricate and demonstrate flight worthiness through ground test of a beryllium rudder was accomplished under Air Force Contract AF33(615)-2974 by the McDonnell Aircraft Company (MCAIR), McDonnell Douglas Corporation under the technical guidance of J.M. Finn. The flight test rudder fabrication and flight demonstration was accomplished by MCAIR with Mr. Finn's leadership under Contract F33615-67-C-1618. The acoustic fatigue test was conducted in the AFFDL Wide Band Test Facility under technical cognizance of Messrs. N.D. Wolf and R. van der Heyde of the Vehicle Dynamics Division, Aero-Acoustics Branch (AFFDL/FYA). Mr. J.A. Holloway of the Air Force Materials Laboratory NDT & Mechanics Branch (AFML/LLP), conducted the radiographic inspection and evaluation of the ground test rudder during the acoustic

fatigue test series and independently assessed the flight test rudder radiographs provided by MCAIR for comparison with radiographic inspection results of the ground test rudder. The residual strength static test was conducted in the AFFDL Structural Test Facility with Mr. M.D. Richardson, Structures Division, Experimental Branch (AFFDL/EBT) as Test Engineer. Reports of these individual efforts are noted in the References of this report and served as the basis for this presentation. The credit for the successful development and demonstration of the F-4 Beryllium Rudders rightfully belong to these engineers and scientists along with their co-workers.

This manuscript was submitted by the author in January 1974 for publication.

TABLE OF CONTENTS

<u>SECTION</u>		<u>PAGE</u>
I	INTRODUCTION	1
II	RUDDER DESIGN	7
	1. Introduction	7
	2. Design Data	8
	3. Design Considerations	25
	4. Design Conditions	30
	5. Design Details	33
	6. Design Analysis	42
	7. Rudder Mass Balance	49
	8. Rudder Moment of Inertia	52
	9. Rudder Weight	52
III	RUDDER FABRICATION AND ASSEMBLY	54
	1. Introduction	54
	2. General Shop Practices	54
	3. Sawing Beryllium	55
	4. Machining Beryllium	56
	5. Drilling Beryllium	56
	6. Countersinking Beryllium	60
	7. Forming Beryllium	60
	8. Chemical Milling Beryllium	61
	9. Joining Beryllium	61
	a. Adhesive Bonding	62
	b. Mechanical Fasteners	62
	10. Corrosion Protection	64
	11. Inspection	66
	12. Rudder Assembly	66
IV	FLIGHT QUALIFICATION TESTS	77
	1. Introduction	77
	2. Instrumentation	79
	3. Test 1 - Fatigue Test of Upper Balance Weight Support Structure	83
	4. Test 2 - Rudder Ultimate Static Test with Maximum Airload at 30% Chord	85
	5. Test 3 - Rudder Ultimate Static Test with Maximum Loading on Vertical Tail	98
	6. Test 4 - Repeat of Test 2 with Loading Carried Beyond Design Ultimate	114

TABLE OF CONTENTS (cont'd)

<u>SECTION</u>		<u>PAGE</u>
	7. Epilogue	121
V	TEST 5 - ACOUSTIC FATIGUE ENDURANCE TEST	127
	1. Introduction	127
	2. Description of Test Facility and Instrumentation	127
	3. Measured Noise Levels on the Rudder of the F-4 Aircraft	129
	4. Test Set-Up, Procedure and Results	140
	5. Analysis of Rudder Frequency, Strain and Life Characteristics	145
	6. Conclusions	170
VI	RADIOGRAPHIC INSPECTION OF THE BERYLLIUM RUDDERS	174
	1. Introduction	174
	2. Equipment and Procedure - Ground Test Rudder X-Rays	175
	3. Results and Discussion - Ground Test Rudder X-Rays	176
	4. Equipment and Procedure - Flight Test Rudder X-Rays	180
	5. Results and Discussion - Flight Test Rudder X-Rays	183
	6. Commentary	187
VII	TEST 6 - RESIDUAL STRENGTH STATIC TEST	189
	1. Introduction	189
	2. Instrumentation	191
	3. Residual Strength Test Set-Up and Procedure	193
	4. Test Results and Discussion	203
VIII	BERYLLIUM RUDDER FLIGHT TEST PROGRAM	220
	1. Introduction	220
	2. Differences Between the Ground Test and Flight Test Rudders	223
	3. Flight Test Rudder Instrumentation	226
	4. Rudder Mass Balancing	228
	5. Proof Testing the Flight Test Beryllium Rudder	231
	6. Beryllium Rudder Flight Test	234
	7. Flight Test Inspections	251
	8. Summary	257

TABLE OF CONTENTS (cont'd)

SECTION	PAGE
IX	258
REFERENCES	259
BIBLIOGRAPHY	261
APPENDIX A	269
APPENDIX B	

LIST OF ILLUSTRATIONS

<u>Figure Nr</u>		<u>Page</u>
1	Effect of Temperature on Tensile Strength of Beryllium Sheet	9
2	Effect of Temperature on Bearing and Shear Strength of Beryllium Sheet	9
3	Effect of Temperature and Stress Concentration on Ultimate Tensile Strength of Beryllium Sheet	11
4	Fatigue Strength of Hot Rolled, Stress Relieved Ground and Etched Beryllium Sheet	12
5	Design Curves for Initial and Post-Buckling Shear of Flat Beryllium Panels	14
6	Design Curves for Initial Compression Buckling Strength of Flat, Unstiffened Beryllium Panels	15
7	Nondimensional Crippling Design Curves for Beryllium	17
8	Effective Width of Stiffened Sheet	18
9	Stiffened Panel Configurations	20
10	Beryllium Lug Design Chart	22
11	Fatigue Strength of Notched Sheet: Beryllium, Aluminum and Titanium	27
12	Fatigue Strength-to-Weight Efficiency of Notched Material: Beryllium, Aluminum and Titanium	28
13	Beryllium Rudder Structure Schematic	29
14	F-4 Rudder Structural Configurations	31
15	Ultimate Running Load	34
16	Condition I Ultimate Shear and Moment	35
17	Condition II Ultimate Shear and Moment	36

<u>Figure Nr</u>	<u>LIST OF ILLUSTRATIONS (cont'd)</u>	<u>Page</u>
18	Condition III Ultimate Shear and Moment	37
19	Ultimate Torque	38
20	Panel Flutter Criteria	39
21	Beryllium Rudder Rib and Spar Cross-Sections	41
22	Beryllium Rudder Leading Edge Skin Splice Configurations	43
23	Cover Skin Thickness Requirements	44
24	Ultimate Shear Flows	46
25	Rudder Bending and Torsional Stiffness	48
26	Stability of Rudder with Upper Damper Removed	50
27	Beryllium Rudder Power Cylinder Stability	51
28	Tools Used to Machine, Drill and Countersink Beryllium	57
29	Rudder Trailing Edge Assembly Structural Details	63
30	Rudder Front Torque Box Beryllium Detail Parts	65
31	Pre-Fit Assembly of Beryllium Rudder in Assembly Fixture	68
32	Beryllium Rudder Bonded Trailing Edge Assembly	69
33	Repair of Lower Closure Rib	71
34	Final Assembly of Beryllium Rudder	73
35	Beryllium Rib with Broken Flange and Repair Splice	75
36	Completed Beryllium Rudder Assembly	76
37	Beryllium Rudder Strain Gage Locations	80
38	Beryllium Rudder Deflection Point Locations	81

<u>Figure Nr</u>	<u>LIST OF ILLUSTRATIONS (cont'd)</u>	<u>Page</u>
39	Beryllium Rudder Deflection Instrumentation	82
40	Set-Up for Balance Weight Support Structure Fatigue Test	84
41	Set-Up for Static Tests of Beryllium Rudder	86
42	Aft Fuselage Support Fixture for Beryllium Rudder Static Test	87
43	Rudder Tension Pad Layout and Ultimate Loads for Test 2	89
44	Comparison of Test and Design Loads: Design Condition I	90
45	Beryllium Rudder Front Spar Strains: Test 2	91
46	Rear Spar and Trailing Edge Strains: Test 2	92
47	Forward Cover Skin Strains: Test 2	93
48	Front Spar Deflections: Test 2	94
49	Rear Spar Deflections: Test 2	95
50	Trailing Edge Deflections: Test 2	96
51	Hinge Deflections: Test 2	97
52	Rudder Deflections: Design Condition I	99
53	Vertical Fin Tension Pad Layout and Ultimate Loads for Test 3	100
54	Rudder Tension Pad Layout and Ultimate Loads for Test 3	101
55	Comparison of Fin Test and Design Loads: Design Condition III	103
56	Comparison of Rudder Test and Design Loads: Design Condition III	104

LIST OF ILLUSTRATIONS (cont'd)

<u>Figure Nr</u>		<u>Page</u>
57	F-4 Fin and Beryllium Rudder Prior to Loading	105
58	F-4 Fin and Beryllium Rudder with Condition III Ultimate Loads Applied	105
59	Front Spar Strains: Test 3	106
60	Rear Spar and Trailing Edge Strains: Test 3	107
61	Forward Cover Skin Strains: Test 3	108
62	Front Spar Deflections: Test 3	109
63	Rear Spar Deflections: Test 3	110
64	Trailing Edge Deflections: Test 3	111
65	Hinge Deflections: Test 3	112
66	Rudder Deflections: Design Condition III	113
67	Deflected Hinge Line: Design Condition III	115
68	Crack in Trailing Edge Lower Closure Rib of Beryllium Rudder	117
69	Front Spar Strains: Test 4	118
70	Rear Spar and Trailing Edge Strains: Test 4	119
71	Forward Cover Skin Strains: Test 4	120
72	Front Spar Deflections: Test 4	122
73	Rear Spar Deflections: Test 4	123
74	Trailing Edge Deflections: Test 4	124
75	Hinge Deflections: Test 4	125
76	Rudder Deflections: Design Condition I	126
77	Wide Band Test Facility	128

<u>Figure Nr</u>	<u>LIST OF ILLUSTRATIONS (cont'd)</u>	<u>Page</u>
78	Beryllium Rudder Strain Gage and Microphone Locations	130
79	Close-Up of the Strain Gage and Microphone Instrumentation Used on the Bottom Panel of the Rudder During the Acoustic Tests	131
80	SPL's Measured on Rudder of F-4 AFFDL Data Location 1	133
81	SPL's Measured on Rudder of F-4 AFFDL Data Location 2	134
82	SPL Data on the Rudder of the F-4 Aircraft McDonnell Douglas Corp. Location 1	135
83	SPL Data on the Rudder of the F-4 Aircraft McDonnell Douglas Corp. Location 2	136
84	Summary of SPL Data on the Rudder of the F-4 Aircraft for the Take-Off	138
85	SPL Data on the Rudder of the F-4 Aircraft for Two Operational Conditions: McDonnell Douglas Corp. Data	139
86	Rudder Mounted in Test Stand Ready for Testing	142
87	Test Spectra - Microphone Position 2	144
88	Left Side of Rudder After Acoustic Fatigue Tests Showing Failure	146
89	Left Side of Rudder After Acoustic Fatigue Tests (Close-Up)	147
90	Left Side of Rudder After Acoustic Fatigue Tests Showing Extent of Crack	148
91	Right Side of Rudder After Acoustic Fatigue Tests Showing Damage	148
92	Parts Broken Out of Rib R2	149
93	Rib R2 After Acoustic Fatigue Tests	149

<u>Figure Nr</u>	<u>LIST OF ILLUSTRATIONS (cont'd)</u>	<u>Page</u>
94	Output of Gage Nr 1	151
95	Output of Gage Nr 2	152
96	Output of Gage Nr 5	153
97	Output of Gage Nr 6	154
98	Output of Gage Nr 7	155
99	Output of Gage Nr 8	156
100	Output of Gage Nr 9	157
101	Output of Gage Nr 10	158
102	Output of Gage Nr 11	159
103	Ourput of Gage Nr 12	160
104	Output of Gage Nr 13	161
105	Output of Strain Gage Nr 8 as a Function of O/A SPL Frequency 470 Hz	165
106	Output of Strain Gage Nr 9 as a Function of O/A SPL Frequency 470 Hz	166
107	Output of Strain Gage Nr 10 as a Function of O/A SPL Frequency 470 Hz	167
108	Output of Gage Nr 1, O/A RMS Strain as a Function of O/A SPL	171
109	Output of Gage Nr 8, O/A RMS Strain as a Function of O/A SPL	172
110	Photograph of the Radiograph Showing Crack in in Rib R2 Before Start of Acoustic Fatigue Test	177
111	Photograph of the Radiograph Showing Crack in Rib R2 After 4 Hours of Testing at 150 dB	178
112	Photograph of the Radiograph Showing Crack in Rib R2 After 8 Hours of Testing at 150 dB	179

<u>Figure Nr</u>	<u>LIST OF ILLUSTRATIONS (cont'd)</u>	<u>Page</u>
113	Picker X-Ray Unit	181
114	Radiographic Inspection Set-Up	182
115	Layout for Radiographic Inspection of Beryllium Flight Test Rudder	183
116	Areas of Beryllium Rudder Where Indications of Possible Damage Were Discovered During Radiographic Inspection	184
117	Indication Located in Area 1	185
118	Indications Located in Area 2	185
119	Indications Located in Area 3	186
120	Post Acoustic Fatigue Test Damage to Lower Closure Rib	190
121	F-4 Beryllium Rudder Deflection Transducer Locations	192
122	F-4 Beryllium Rudder Strain Gage Locations	194
123	F-4 Beryllium Rudder with Tension Pads and Strain Gages Installed on Left Side	195
124	F-4 Beryllium Rudder with Deflection Transducer Pads and Strain Gages Installed on Right Side	196
125	Acoustic Damage to Lower Hinge Back-Up Rib of F-4 Beryllium Rudder	197
126	F-4 Beryllium Rudder Residual Static Strength Test Set-Up	199
127	F-4 Beryllium Rudder at Zero Load	200
128	Applied Load vs Time, Load Cell 1	201
129	Applied Load vs Time, Load Cell 2	202
130	F-4 Beryllium Rudder at 200% Design Limit Load	204

<u>Figure Nr</u>	<u>LIST OF ILLUSTRATIONS (cont'd)</u>	<u>Page</u>
131	Residual Static Strength Failure of F-4 Beryllium Rudder	205
132	F-4 Beryllium Rudder - Failure Area on Left Side	206
133	F-4 Beryllium Rudder - Failure Area on Right Side	207
134	Stresses vs Time, Strain Gage Locations 1, 3 & 20	208
135	Stresses vs Time, Strain Gage Locations 2, 4 & 21	209
136	Stresses vs Time, Strain Gage Locations 7 & 8	210
137	Stresses vs Time, Strain Gage Locations 11, 13, 22	211
138	Stresses vs Time, Strain Gage Locations 12, 14, 23, 25 & 27	212
139	Deflections vs Time, Potentiometer Positions 1, 2, 4, 5, 6, 7, 8 & 9	214
140	Deflections vs Time, Potentiometer Positions 13, 14, 15 & 16	215
141	Deflections vs Time, Potentiometer Positions 17, 19, 21 & 24	216
142	Deflections vs Time, Potentiometer Positions 27 & 28	217
143	Graphic Presentation of Beryllium Rudder Maximum Deflections Under Static Loads	218
144	F-4 Aircraft in Flight with Beryllium Rudder	222
145	Sealing of Rudder Honeycomb Assembly	225
146	Strain Gage Locations for Flight Test Rudder	227
147	Balancing the Flight Test Beryllium Rudder	230
148	Proof Test Set-Up	232

<u>Figure Nr</u>	<u>LIST OF ILLUSTRATIONS (cont'd)</u>	<u>Page</u>
149	Rudder Tension Pad Layout and Proof Test Loads	233
150	Comparison of Rudder Proof Test and Design Limit Loads	235
151	Flight Test Personnel Transporting Rudder to Position for Installation on Aircraft	236
152	Beryllium Rudder Enroute to Aircraft Installation	236
153	Installation of Flight Test Beryllium Rudder	236
154	Beryllium Rudder in Fully Rotated Position	237
155	Maiden Flight Take-Off of F-4 Aircraft With Beryllium Rudder	238
156	Progress of Beryllium Rudder Flight Testing	239
157	Flight Test Data, Steady Yaw, Left Rudder at M=0.5	241
158	Flight Test Data, Steady Yaw, Right Rudder at M=0.5	242
159	Flight Test Data, Steady Yaw, Left Rudder at M=0.8	243
160	Flight Test Data, Steady Yaw, Right Rudder at M=0.8 R	244
161	Flight Test Data for Rolling Pullout	245
162	Flight Test Data, 720° Roll Condition	246
163	Permanent Buckle in Rudder Torque Box Skin	248
164	Location of Maximum-Strain Reading Recorded During Static T-st of Ground Test Beryllium Rudder	250
165	Area of Trailing Edge Cover Skin Having Paint Blisters and Flaking	254
166	Indications Found During Visual Inspection	256

LIST OF TABLES

<u>Table Nr</u>		<u>Page</u>
1	Summary of Beryllium Physical Properties at Room Temperature	10
2	Design Shear Stresses for Bonded Beryllium Lap Joints	24
3	Element Test Program	26
4	Weight Summary for F-4 Beryllium and Aluminum Rudders	53
5	Control Settings for Drilling Beryllium	58
6	Acoustic Fatigue Test Schedule	143
7	Maximum Response Frequency vs Test Time	162
8	Amplitude and Frequency Response of Major Peaks	163
9	Comparison of SPL and Exposure Times for the Test Chamber and "In-Service" Environment	164
10	Beryllium Rudder Maximum Deflections in Inches	213
A-1	Chemical Analysis of Beryllium Sheet for Ground Test Rudder (Reference 1)	267
A-2	Chemical Analysis of Beryllium Sheet for Flight Test Rudder (Reference 2)	267
A-3	Properties of Beryllium Sheet Used for Element Test Specimens and Ground Test Rudder (Reference 1)	268
A-4	Producers Certified Mechanical Properties of Beryllium Sheet Used for Flight Test Rudder (Reference 2)	268

SYMBOLS

A	Area of cross-section
a	Length of the unloaded edge of a panel in uniaxial compression; long dimension of a panel in shear
a	Subscript for accelerated acoustic fatigue test conditions
b	Width of an element; width of a stiffened panel; short dimension of a panel in shear; length of the loaded edge of a panel in uniaxial compression
b _f	Width of stiffener flange element
b _w	Height of stiffener web element
c	Fixity coefficient for columns; distance from neutral axis to extreme fiber; subscript "compression"
cr	Subscript "critical"
D	Diameter
D _m	Damage due to loading conditions
d	depth or height
E	Modulus of elasticity in tension
e	Elongation in percent (this factor being a measure of the ductility of the material and being based on a tension test; unit deformation or strain); eccentricity; minimum distance from a hole center line to edge of sheet
E _c	Modulus of elasticity in compression
F	Allowable stress; Fahrenheit
f	Calculated stress
F _{bru}	Ultimate bearing stress
F _{cc}	Allowable crushing or crippling stress (upper limit of column stress for local failure)

SYMBOLS (cont'd)

F_{cy}	Compressive yield stress at which permanent strain equals 0.002 (from tests of standard specimens)
F_s	Allowable shear stress
$F_{s_{cr}}$	Critical shear stress for buckling of rectangular panels
F_{su}	Ultimate stress in pure shear (average shearing stress over the cross-section)
f_t	Calculated tensile stress
F_{tu}	Ultimate tensile stress (from tests of standard specimen)
F_{ty}	Tensile yield stress at which permanent strain equals 0.002 (from tests of standard specimens)
G	Modulus of rigidity
I	Moment of inertia
J	Polar moment of inertia
K	A constant, generally empirical; thermal conductivity
K_T	Stress concentration factor
ksi	KIPS (1000 pounds) per square inch
M	Applied moment (usually a bending moment)
N	Cycles to failure in fatigue; number of stress reversals required to cause failure at a given level noted by subscript
n	Number of stress reversals at a given level noted by a subscript
P	Applied load, pounds
P_a	Allowable load
psi	Pounds per square inch
R	Radius; ratio of minimum stress to maximum stress; subscript for requirements
S	Stress

SYMBOLS (cont'd)

s	Subscript "shear"; subscript for "in-service" hours in acoustic fatigue analysis
sk	Subscript "skin"
st	Subscript "stiffener"
T	Time
t	Thickness
W	Width of a lug
μ	Poisson's ratio
η	Plasticity reduction factor
α	Negative reciprocal of the slope of the S-N curve plotted on log-log paper

CONVERSION OF U.S. CUSTOMARY UNITS TO SI UNITS

The International System of Units (SI) was adopted by the Eleventh General Conference on Weights and Measures, Paris, October 1960. Conversion factors for the units used in this report are given in the following table:

Quantity	U.S. Customary Units	Conversion Factor (*)	SI Unit
Mass	$\left\{ \begin{array}{l} \text{lb.} \\ \text{oz.} \end{array} \right\}$	$\left\{ \begin{array}{l} 453.6 \\ 28.3 \end{array} \right\}$	grams (g)
Stress	ksi	6.895×10^6	newtons/meter ² (N/m ²)
Length	in.	0.0254	meters (m)
Temperature	(°F+460)	5/9	degrees Kelvin (°K)
Volume	$\left\{ \begin{array}{l} \text{gal.} \\ \text{pint} \end{array} \right\}$	$\left\{ \begin{array}{l} 3.785 \times 10^{-3} \\ 4.732 \times 10^{-4} \end{array} \right\}$	meters ³ (m ³)
Pressure	inch of Mercury	3.377×10^3	newtons/meter ² (N/m ²)
Frequency	cps	1.0	hertz (Hz)
Moment	in-lb	0.113	meter-newtons (m-N)
Moment of Inertia	lb-in ²	0.2926	gram-meters ² (g-m ²)
Velocity	FT/min	5.08×10^{-3}	meter/second
Force	lb.	4.448	newtons (N)

* Multiply value given in U.S. Customary Units by conversion factor to obtain equivalent value in SI Units

Prefixes to indicate multiple of units are as follows:

Prefix	Multiple
mega (M)	10^6
kilo (k)	10^3
deci (d)	10^{-1}
centi (c)	10^{-2}
milli (m)	10^{-3}
micro (μ)	10^{-6}

SECTION I

INTRODUCTION

Beryllium is light, rigid, fairly strong and has good elevated temperature characteristics. It has excellent fatigue properties, can be produced in most if not all the basic mill forms and transformed into structural hardware by conventional secondary fabrication techniques. Failure mode weight analyses of airframes for all types of flight vehicles show beryllium to be outstanding within its temperature range, with weight savings up to 45% over aluminum, 35% over titanium and 41% over stainless steel. Only the advanced composites can theoretically compete with beryllium in producing light weight flight vehicle structures.

Beryllium has one technological shortcoming which, coupled with a controllable toxicity and relatively high costs as compared with the other metals mentioned, has served to delay the development, acceptance and application of beryllium in airframes. Metallurgically, this material does not have sufficient deformation modes for true polycrystalline ductility. Hence, ductility in beryllium is less than and different from that found in more common structural materials. The net result of the low isotropic ductility characteristic of beryllium is a tendency toward brittle fracture under mechanical load conditions and a low impact resistance. Ideally, a load bearing structural material should have sufficient isotropic ductility to permit deformation and resultant redistribution of high intensity stresses regardless of load type while resisting excessive deflection and distortion. While "tough, ductile" materials are preferred for structural

applications, other attributes such as high strength-to-weight and high stiffness-to-weight are often essential to successful airframe design and the materials which provide the latter often do so by sacrificing toughness and/or ductility.

While isotropic ductility with its attendant desirable characteristics is not available in yesterday's or today's wrought beryllium, and there is yet no indication of pending breakthrough to make such a product available for tomorrow, the desirable properties of beryllium offer such unique structural advantage over other metals that reliable, efficient application in airframes is a worthy goal. The development of knowledge to provide efficiency and the demonstration of reliability to establish confidence in any new material system requires design, fabrication and evaluation of hardware. The evaluation phase requires test under simulated and actual operating conditions as well as analysis (theoretical and comparative) of the results of such tests.

In October 1964 the Air Force Flight Dynamics Laboratory paved the way for such a structural beryllium technology development and feasibility demonstration program when they issued a purchase request for an R&D effort "for the advancement of structural beryllium technology through the design, fabrication, test and evaluation of a typical load-carrying aircraft component which demonstrates a potential for increased capability and/or efficiency using this material. The selection, design, fabrication and ground test of the structural component shall be of a thoroughness and quality to qualify the component for flight testing". As a result of competitive bidding, a contract was awarded to the McDonnell Aircraft

Corporation in June 1965 based on their proposal to design and flight test qualify an F-4 beryllium rudder. The details of this design and qualification have been published (Reference 1); however additional tests have been conducted at Wright Patterson Air Force Base and the primary purpose of this report is to describe these tests and the results in order that the reader may become acquainted with the capability of a beryllium structure to carry load even after being severely damaged. For continuity the design and flight qualification tests will be discussed briefly prior to in-depth discussion of the acoustic fatigue endurance test and the residual strength static test which were conducted on this first beryllium rudder. Recognizing that outstanding test results such as achieved with this rudder do not constitute an adequate base for confident acceptance of beryllium for all types of airframe structural components, and that success with one or two test items is inadequate for establishing widespread confidence in our ability to design and fabricate reliable load-carrying structures of this material for applications which subject the structure to high complex stresses, this beryllium rudder has succeeded in demonstrating the potential for beryllium structures beyond simple compressive loads.

Following is a brief resumé of the extremely rough test program to which the original beryllium rudder was subjected (with comments on damage sustained in parenthesis). The first three tests constitute flight test qualification with the fourth originally intended to demonstrate the actual strength of the rudder. These tests were conducted by the contractor, McDonnell Aircraft Corporation (now known as McDonnell Aircraft

Company (MCAIR), McDonnell Douglas Corporation). The last two load tests were conducted by the Air Force Flight Dynamics Laboratory in local facilities to obtain additional data on the load-carrying capability of this rudder. Note that design ultimate load (DUL) is that load to which the structure was designed and is equal to 150% of the design limit load (DLL) which is the maximum load anticipated in actual operational conditions.

Test 1 - A 50,000 cycle fatigue test of upper balance weight support structure. (Aluminum Hi-Shear fastener failed at 28,275 cycles, replaced by steel Hi-Loc and test completed with no further incident.)

Test 2 - A static test to DUL representing the yaw flight condition which produces the full available actuator hinge moment and maximum torque.

Test 3 - A static test to DUL representing the rolling pull-out maneuver which produces the maximum vertical tail bending and deflections and hence the maximum bending and shear in the structure.

Test 4 - A repeat of Test 2 with loads allowed to increase to 167% DUL. (A crack occurred at the forward end of the aft lower closure rib at about 205% DLL but the load did not fall off and was subsequently increased to 250% DLL.)

Test 5 - Acoustic fatigue endurance test in a high intensity noise field representing operational conditions to

about seven normal lives of the rudder. (Failure consisted of a large hole in each of the forward cover skins with extensive cracking and destruction of the connecting rib.)

Test 6 - A residual strength test with loading conditions similar to Test 3 except that a rigid mount was used rather than an F-4 vertical tail and aft fuselage which was used in the first four tests. Failure occurred after 15 seconds at 200% DLL or 133% DUL. (Failure apparently began at the crack previously created in the lower closure rib, continued through the heavily damaged lower section of the forward torque box and continued through the leading edge just above the lower hinge attachment fitting.)

A follow-on contract was awarded to MCAIR in April 1967 for fabrication, instrumentation, flight test and evaluation of a second F-4 beryllium rudder. The flight testing was to be accomplished on a "ride along" basis, meaning that the beryllium rudder would be substituted for a production rudder on an available aircraft with no flight restrictions or control of the operations of the vehicle. The rudder instrumentation was connected to an existing recorder in the chosen vehicle at the time of installation to record loads and response during early flights when maneuvers were performed to impose maximum loads on the rudder. The maiden flight occurred on 14 May 1968 from Lambert St. Louis Municipal Airport when YF-4E number 12200 carried the beryllium rudder aloft for the first time. Flight testing was uneventful

until the tenth flight when the aircraft became roll-yaw coupled during a rolling pullout maneuver, inadvertently exceeding the normal flight envelope of the aircraft. Inspection of the aircraft revealed only a small buckle in one skin of the forward torque box and a review of the data revealed loads of approximately 205% DLL. Flight tests were continued with the contract terminated in August 1969 after 90 flights for a total flight time of 100 hours and 30 minutes. The rudder remained aboard the aircraft and by the end of August 1971 had made 158 flights for a total flight time of 184 hours and 24 minutes.

While the flight history of the F-4 beryllium rudder is not extensive in terms of design life of such aircraft, it does illustrate that primary load-carrying beryllium structures can be used in high performance aircraft. In addition, experience was gained in handling beryllium under multi-mission operating conditions in a variety of atmospheric environments.

SECTION II

RUDDER DESIGN

1. Introduction

The reasons for selection of the F-4 rudder as the airframe component for development of structural beryllium technology and demonstration of feasibility also established the design philosophy of this effort. First, the F-4 rudder is a complete, interchangeable component which can be installed or removed from the aircraft with a minimum of effort. Second, the rudder is a typical sheet-metal assembly incorporating both skin-stringer and full-depth honeycomb core sandwich construction thereby permitting evaluation of a variety of structural and manufacturing techniques within existing technology. Third, the rudder is subjected to reversible loads including elements other than compression with both loads and response data available from the production aluminum counterpart for comparison. Fourth, due to the particular design of the aircraft, the F-4 can fly and land without a rudder so that flight tests can be conducted under fail-safe conditions. Fifth, aircraft were available as flight test beds in the event that a flight test program should evolve from the basic ground test program. Note that none of these reasons for selection of the F-4 rudder deal with beryllium characteristics such as high modulus and low density; however, it was necessary that we have sufficient design knowledge and secondary fabrication skills available to make construction of the selected component practical.

Accordingly, the envelope and support geometry of the beryllium rudders were made virtually identical to that of production aluminum rudders. The structural arrangement of both the production and the beryllium rudders are

similar in that they are two-cell torque boxes supported along their leading edges by four hinges. The forward torque box of each is conventional multi-rib-skin-spar construction while both aft torque box structures are skin-faced honeycomb core with edging members. Both rudder assemblies require balance weights and flutter dampers and were designed to be actuated by a hydraulic power cylinder attached to the rudder torque tube at the lower hinge point. However, within these configuration restrictions and using the same design loads, each rudder was designed for efficient utilization of the applicable construction materials.

2. DESIGN DATA

The beryllium used in developing design data and constructing the rudders was a hot-rolled, stress relieved, ground and etched sheet with a maximum 2.0% BeO content purchased per McDonnell Material Specification MMS-191, reproduced herein in Appendix A. This specification specifies guaranteed minimum mechanical room temperature properties of:

$$F_{t_u} = 70 \text{ KSI (483 mn/m}^2\text{)}$$

$$F_{t_y} = 50 \text{ KSI (345 mn/m}^2\text{)}$$

$$e = 5\% \text{ in 1.0 inch (2.54 cm)}$$

A review of actual material properties of Beryllium sheet used on these programs, tabulated in References 1 and 2 and reproduced in Appendix A, shows that all such sheet exceeded these guaranteed minimum values. Figure 1 gives typical values of F_{t_y} and F_{t_u} vs temperature for beryllium sheet as well as design mechanical property values. The design values were selected by determining the ratio of the guaranteed minimum room temperature value to the typical room temperature value

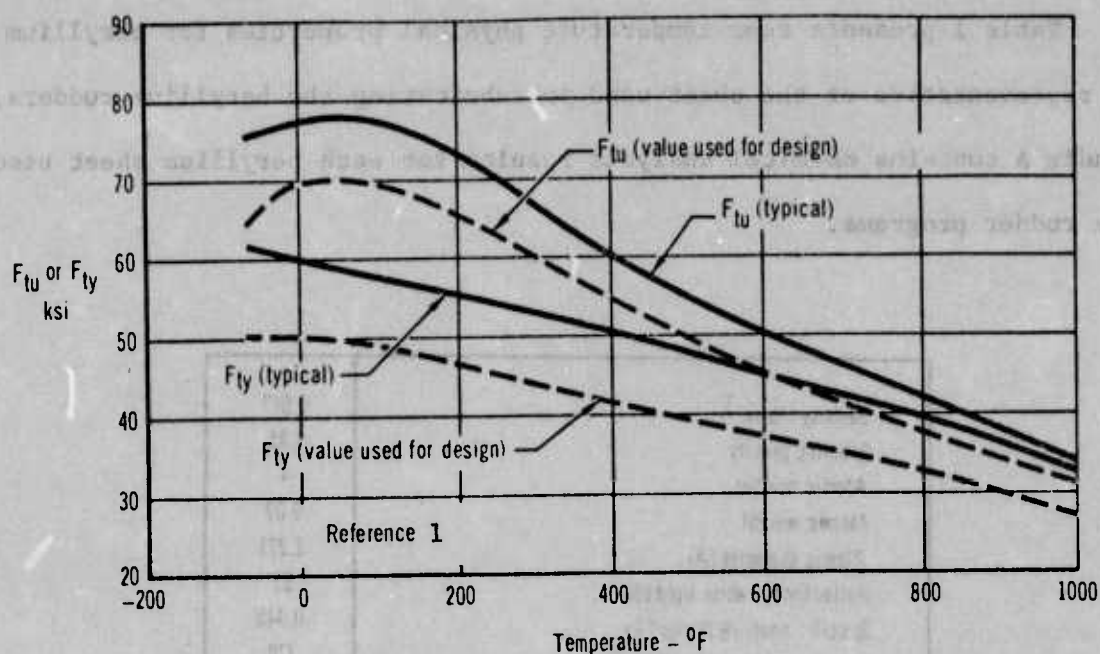


Figure 1 - Effect of Temperature on Tensile Strength of Beryllium Sheet

and reducing typical values by this factor for all temperatures. The resulting minimum values were used in design of the beryllium rudder as an additional safety factor. Figure 2 shows the effect of temperature on F_{bru} and F_{su} .

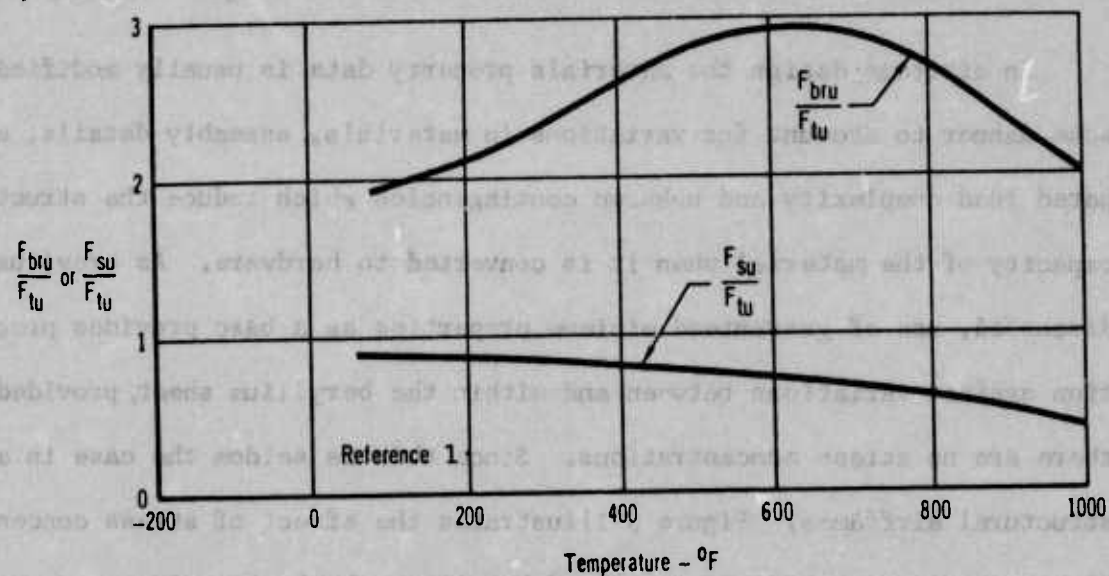


Figure 2 - Effect of Temperature on Bearing and Shear Strength of Beryllium Sheet

Table 1 presents room temperature physical properties for beryllium and is representative of the sheet used in fabricating the beryllium rudders. Appendix A contains chemical analysis results for each beryllium sheet used on the rudder programs.

Density (lb/in. ³)	0.067
Specific gravity	1.85
Atomic number	4
Atomic weight	9.02
Atomic diameter (A)	2.221
Reflectivity, white light (%)	55
Specific heat, (BTU/lb/°F)	0.445
Latent heat of fusion (BTU lb)	470
Melting point (°F)	2340
Thermal conductivity, (BTU/ft. ² /ft/hu)	104
Thermal expansion, room temperature (in. in./°F)	6×10^{-6}
Electrical conductivity (% of copper)	35 to 45
Resistivity (μ ohm-in. ² in.)	1.6

Table 1 - Summary of Beryllium Properties at Room Temperature

In airframe design the materials property data is usually modified in some manner to account for variations in materials, assembly details, anticipated load complexity and unknown contingencies which reduce the structural capacity of the material when it is converted to hardware. As previously discussed, use of guaranteed minimum properties as a base provides protection against variations between and within the beryllium sheet, provided there are no stress concentrations. Since this is seldom the case in actual structural airframes, Figure 3 illustrates the effect of stress concentration on ultimate tensile strength of beryllium sheet at various temperatures. In cases where the notched strength is less than the unnotched strength, the

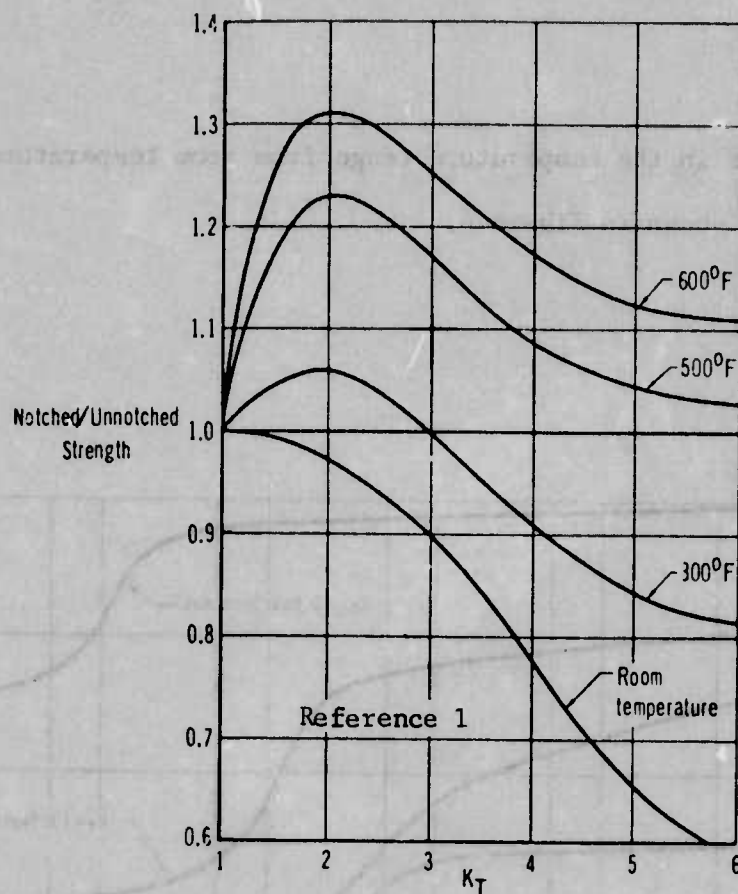


Figure 3 - Effect of Temperature and Stress Concentration on Ultimate Tensile Strength of Beryllium Sheet

former should be used to size tension members having stress concentrations.

For the purpose of the rudder design, fatigue characteristics are very important. MCAIR tests of notched and unnotched tensile fatigue specimens indicated that beryllium has exceptionally good resistance to initiation

of fatigue cracks in the temperature range from room temperature to 500°F (533°K) as shown in Figure 4.

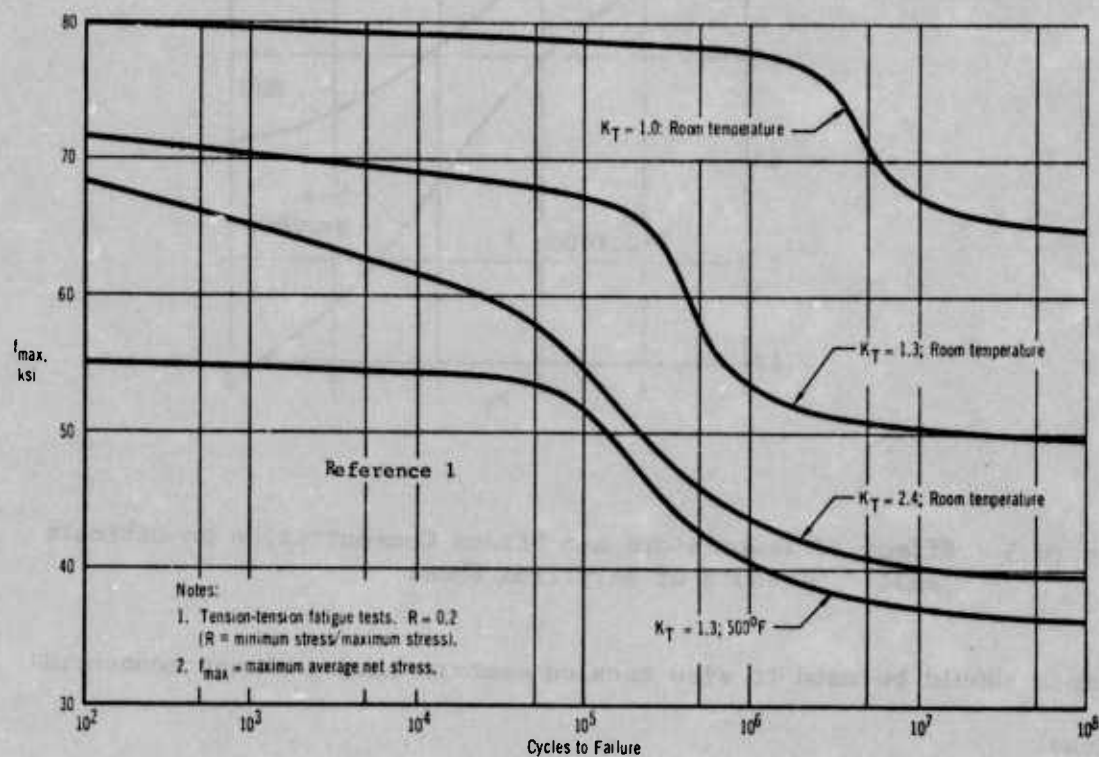


Figure 4 - Fatigue Strength of Hot Rolled, Stress Relieved Ground and Etched Beryllium Sheet.

Reference 1 further reports that joint tests showed that stress concentrations in the form of filled and unfilled fastener holes reduce the static and fatigue strengths of beryllium, and that fatigue strength is improved and static strength not affected by the installation of hole filling

fasteners in beryllium when compared to specimens with empty holes.

Curves were also developed for predicting the initial buckling stress of flat beryllium panels loaded in shear at room temperature with $F_{su} = .8F_{tu}$ assumed on the basis of available beryllium test data. Figure 5 provides these design curves over range from room temperature to 500°F (533°K). Figure 5 also presents a design curve for predicting post-buckled shear strength of flat, unstiffened beryllium panels based on MCAIR test results reported in Reference 1.

Figure 6 shows design curves for predicting the initial compression buckling stress of flat, unstiffened beryllium panels at room temperature and at 500°F (533°K). These curves were developed by the method presented by Gerald and Becker (see Bibliography, NACA TN 3781), and are in agreement, in the elastic range, with similar design curves for beryllium sheet developed by Crawford and Burns (see Bibliography, ASD TR 61-692) developed in 1960 and 1961.

Crippling is another consideration in design of the beryllium rudder. Design curves and analysis methods have been developed for predicting the crippling strength of stiffening members and stiffened flat panels fabricated of beryllium sheet material. Methods which have been previously shown to give accurate strength predictions for beryllium structures in the temperature range from -65°F (219°K) to 500°F (533°K) were used in design of the rudder. The following procedure was used to determine the average crippling stress in the stiffeners ($F_{cc_{st}}$) and the allowable (ultimate) load.

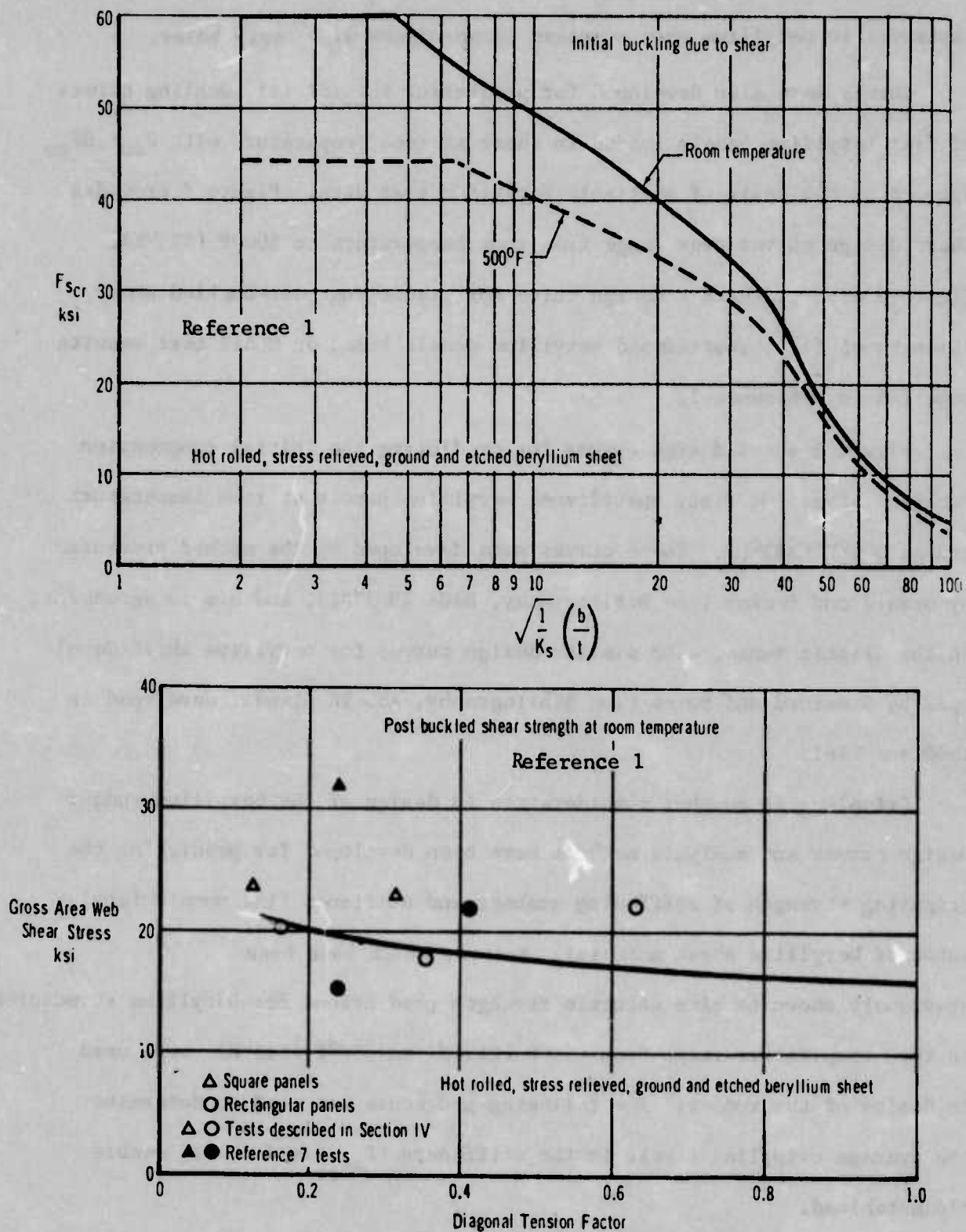


Figure 5 - Design Curves for Initial and Post Buckling Shear Strength of Flat Beryllium Panels

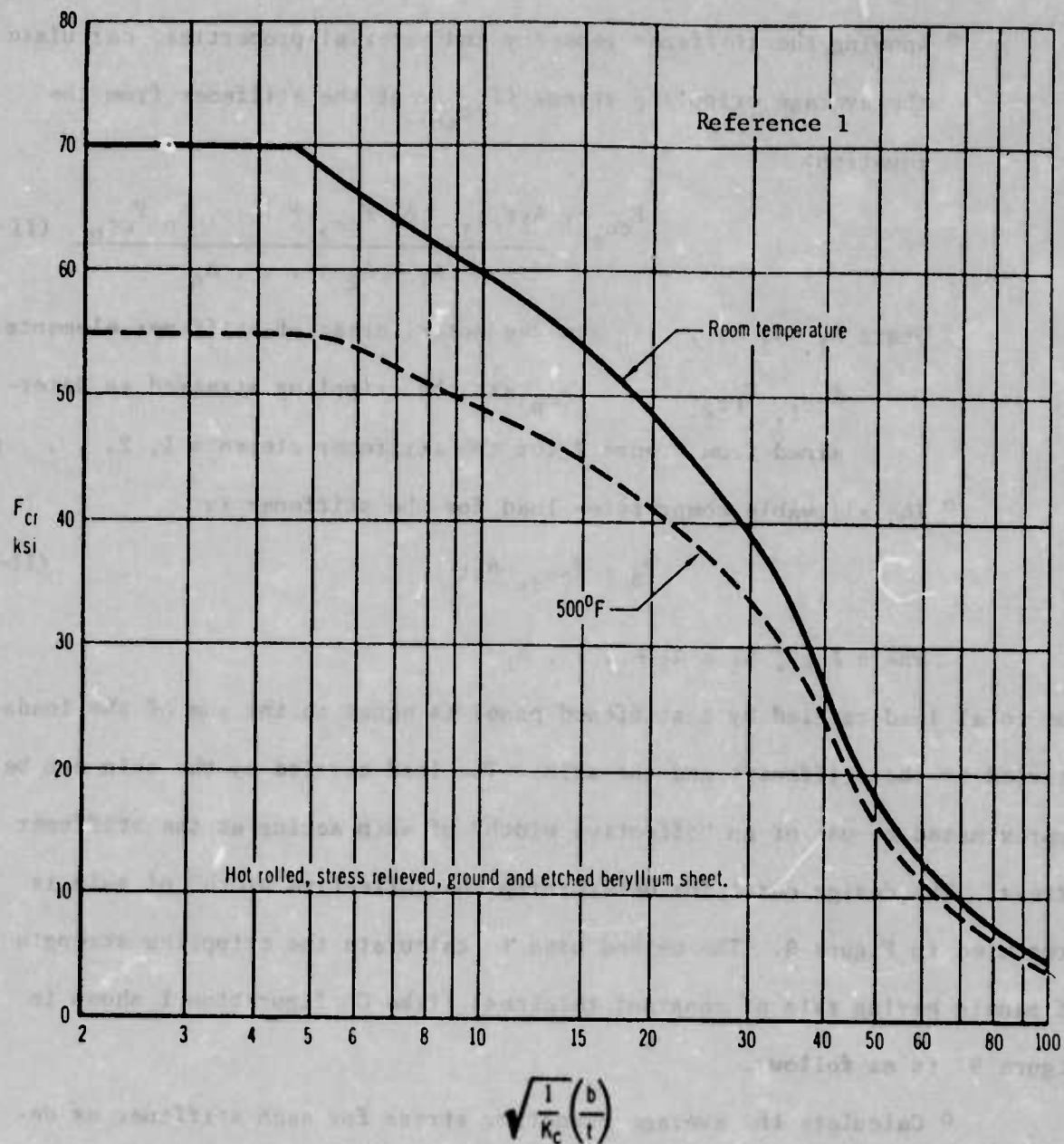


Figure 6 - Design Curves for Initial Compression Buckling Strength of Flat, Unstiffened Beryllium Panels.

- o Knowing the stiffener geometry and material properties, calculate the average crippling stress ($F_{cc_{st}}$) of the stiffener from the equation:

$$F_{cc_{st}} = \frac{A_1 F_{cc1} + A_2 F_{cc2} + \dots + A_n F_{ccn}}{A_1 + A_2 + \dots + A_n} \quad (II-1)$$

Where A_1, A_2, \dots, A_n are the actual areas of stiffener elements.

$F_{cc1}, F_{cc2}, \dots, F_{ccn}$ are the crippling stresses as determined from Figure 7 for the stiffener elements 1, 2, \dots n.

- o The allowable compression load for the stiffener is:

$$P_a = F_{cc_{st}} A_{st} \quad (II-2)$$

Where $A_{st} = A_1 + A_2 + \dots + A_n$

The total load carried by a stiffened panel is equal to the sum of the loads carried by the stiffeners and the skin. The load carried by the skin can be approximated by use of an "effective width" of skin acting at the stiffener stress. The design chart for determining the "effective width" of skin is presented in Figure 8. The method used to calculate the crippling strength of panels having skin of constant thickness (like Configuration I shown in Figure 9) is as follows:

- o Calculate the average crippling stress for each stiffener as described previously.
- o From Figure 8 determine the "effective width" of skin acting at the stiffener stress. With the stiffener stress, F_{cc} , read the value $2W_e/t$. " W_e " is the effective width of skin

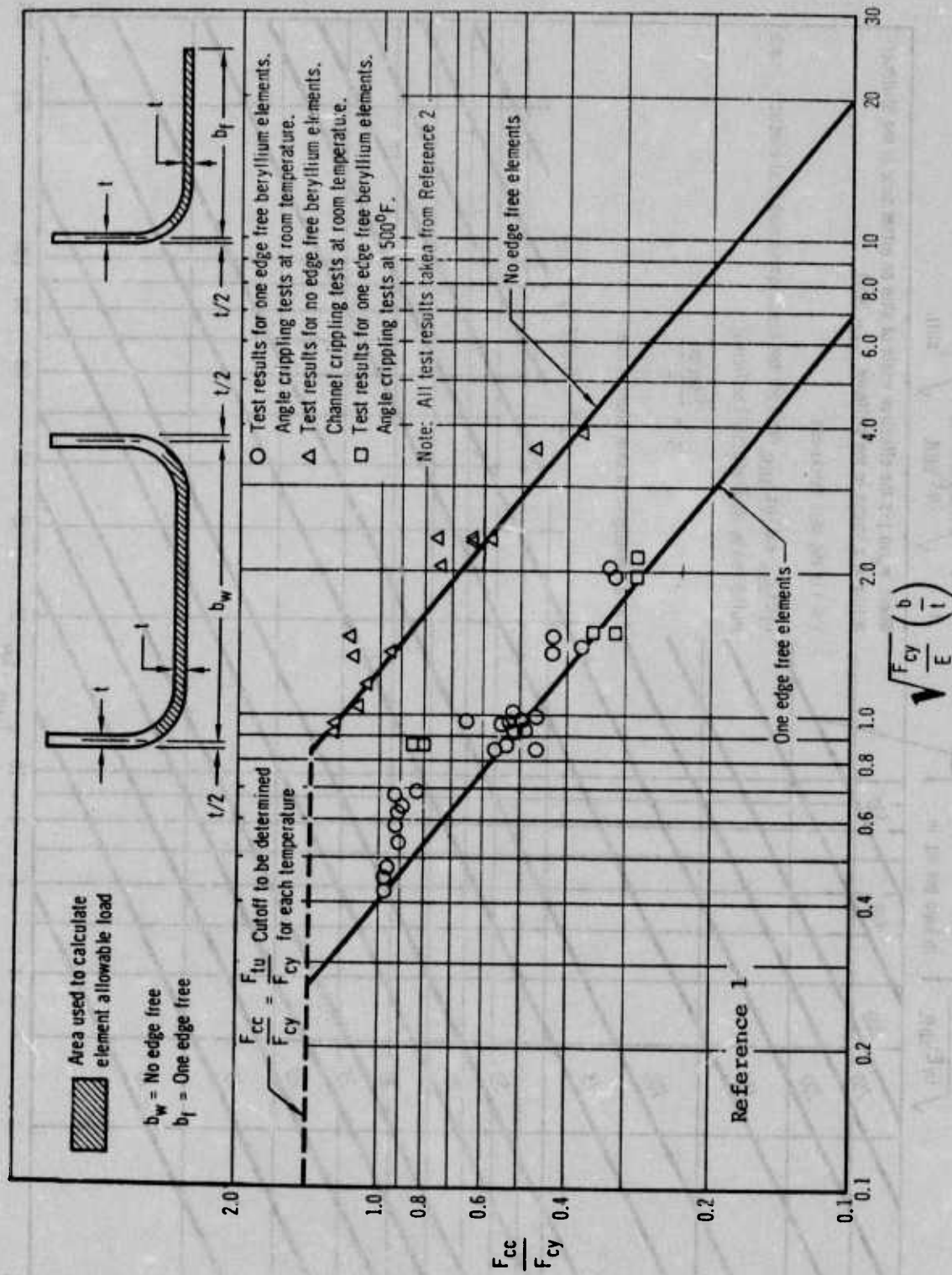


Figure 7- Nondimensional Crippling Design Curves for Beryllium

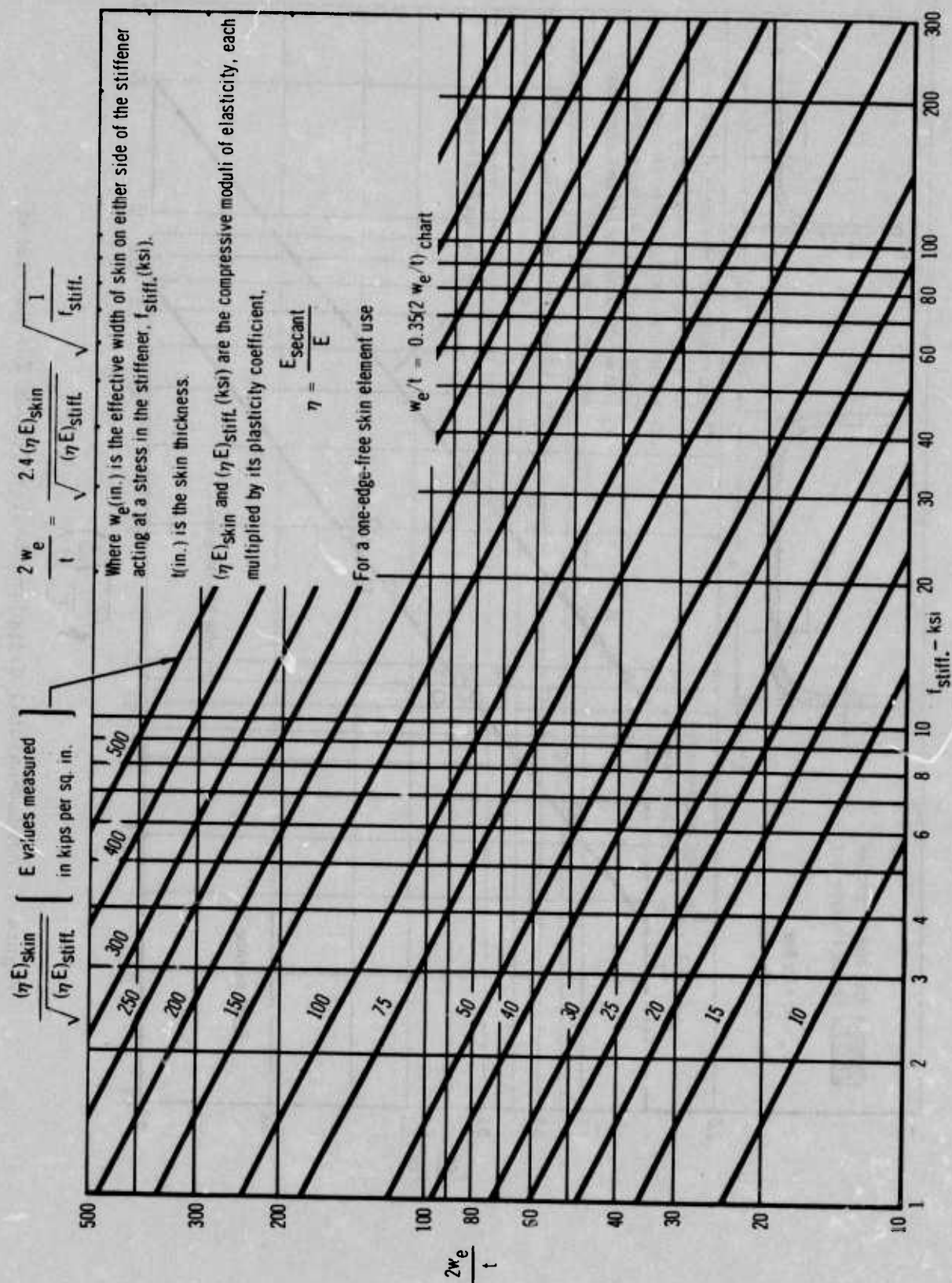


Figure 8- Effective Width of Stiffened Sheet

on either side of the stiffener acting at the same stress as the stiffener. "t" is the skin thickness. If "W_e" is greater than half the stiffener spacing (b) i.e., if effective width overlap, use W_e = b/2.

- ° Calculate the load carried by the effective skin:

$$P_{sk} = F_{ccst} 2W_e t \quad (II-3)$$

- ° The crippling strength of the stiffener and its effective skin is:

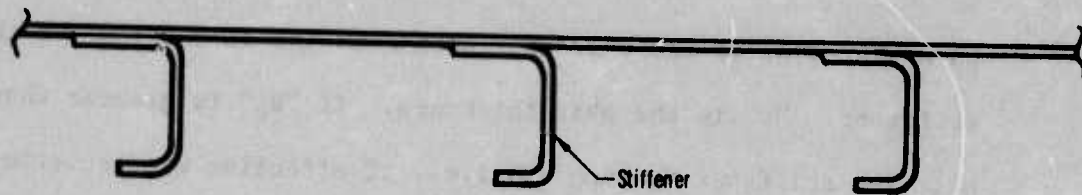
$$P = P_{st} + P_{sk} \quad (II-4)$$

- ° The total load carried by a panel with a number of stiffeners is:

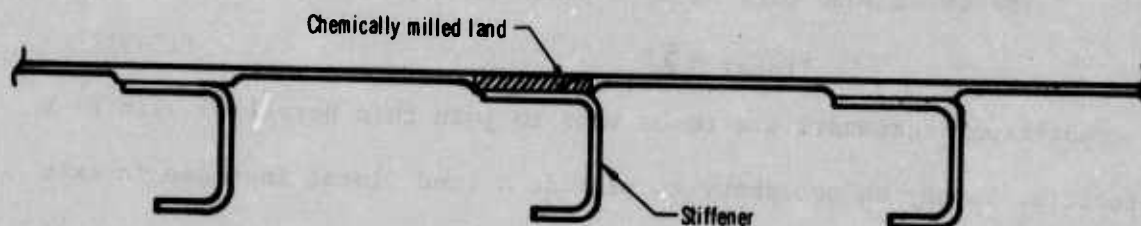
$$P_{total} = \sum P \quad (II-5)$$

Where countersunk fasteners are to be used to join thin Beryllium skin to a substructure, it may be necessary to provide a land (local increase in skin thickness) to avoid the knife-edge effect in the skin at the base of the sink. The land does not necessarily result in a weight penalty since it will carry its share of the load and increase the "effective area" of the skin in compression. The method used to predict the crippling strength of stiffened panels with skin having chem-milled lands (Configuration II in Figure 9) is presented below:

- ° Calculate the stiffener crippling stress and the effective skin width as described previously for panels having constant skin thickness. For panel skins with chem-milled lands, the "effective-width" is measured from the edge of the chem-milled land instead of from the skin-stiffener fastener line.
- ° Calculate the allowable load of the panel assuming the stiffener, the land, and the effective skin are acting at the stiffener crippling stress.



Configuration I
Stiffened panel with constant skin thickness



Configuration II
Stiffened panel with chemically milled lands

Figure 9 - Stiffened Panel Configurations

$$P = F_{ccst} (A_{st} + 2W_{et} + A_{land}) \quad (II-6)$$

° The total load carried by a panel with a number of stringers is:

$$P_{total} = \sum P \quad (II-7)$$

Nondimensional design curves for prediction of the static strength of symmetrically loaded lugs fabricated of Beryllium sheet are presented in Fig-

ure 10. Given the lug geometry and the ultimate tensile strength (F_{tu}) of Beryllium, the designer can predict the allowable lug load from the equation:

$$P_a = \frac{F_{br}}{F_{tu}} (F_{tu}) Dt \quad (II-8)$$

Where $\frac{F_{br}}{F_{tu}}$ is the minimum value read from Figure 10 for $\frac{R}{D}$ or $\frac{W}{D}$.

F_{tu} is the ultimate tensile stress for Beryllium sheet at the temperature considered.

D is the hole diameter.

t is the lug thickness.

Mechanical fastening and adhesive bonding were used for joining the Beryllium rudder structural members. Mechanical fasteners were used to join all members forward of the rear spar and to attach the trailing edge assembly to the forward torque box structure. Adhesive bonding was used to join the trailing edge honeycomb core, face skins, rear spar and closure members.

Special consideration must be given to the geometry of the hole and/or countersink provided for mechanical fasteners. The depth of the countersink for flush fasteners must be at least 0.015 in. (0.381 mm) less than the thickness of the material to avoid a knife edge and subsequent cracking or chipping of the knife edge at the base of the countersink. The resulting minimum thickness at mechanically fastened joints may necessitate extra material in this area which can be readily provided by chem-milling excess material away leaving lands at the joint line such as illustrated in Configuration II of Figure 9. The edge of the hole at the fastener head-to-shank fillet radius must also be chamfered to prevent interference which could produce local dam-

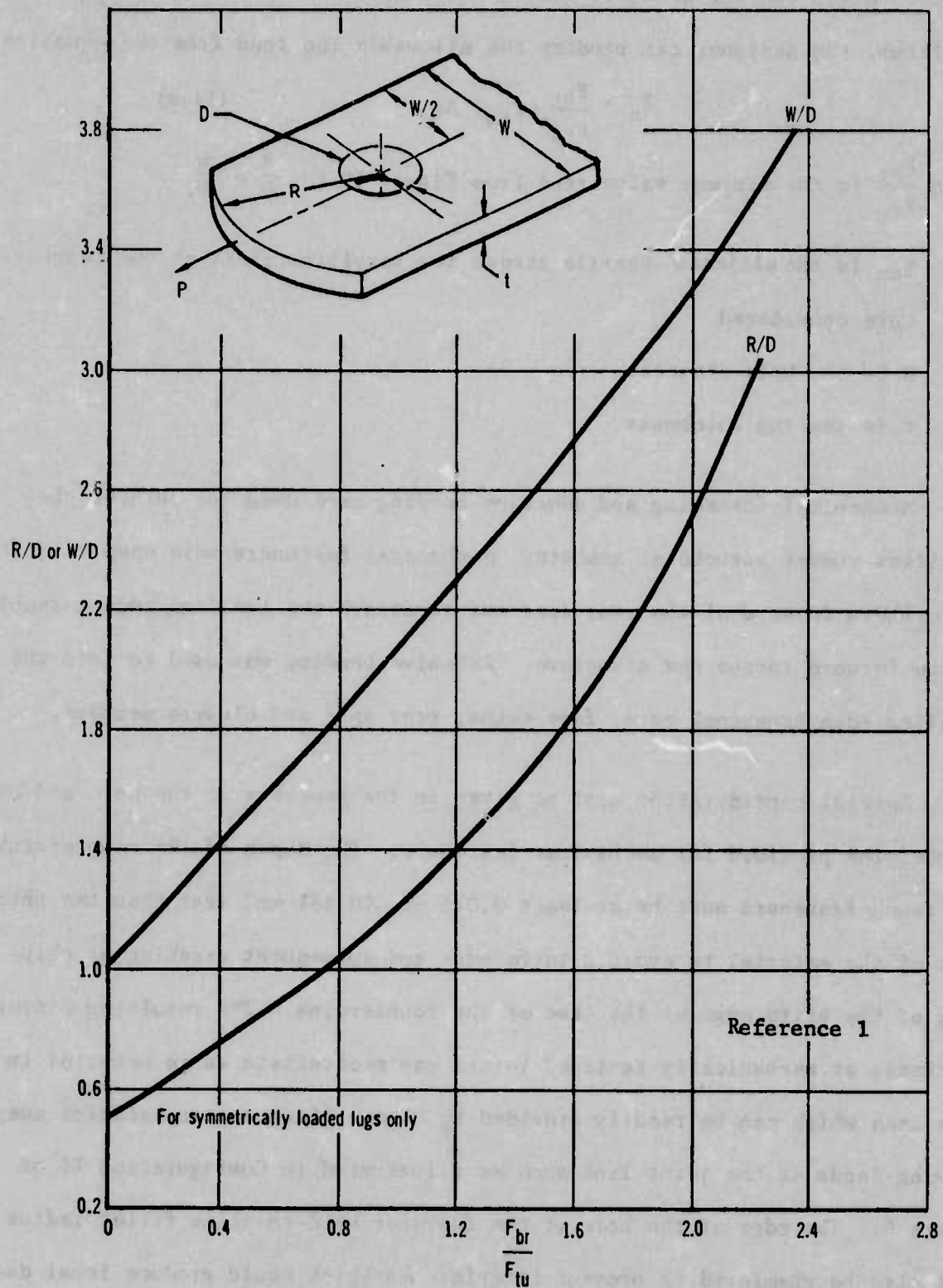


Figure 10- Beryllium Lug Design Chart

age in the beryllium.

Insufficient test data exists for establishing firm design allowables for mechanically fastened Beryllium joints, and the strength of critically loaded joints should be verified by test. The following criteria for computing allowable loads for mechanically fastened Beryllium joints was found to yield conservative strength predictions when compared to available test results.

- ° When fastener shear is critical, use the fastener's minimum guaranteed shear strength.
- ° The ultimate bearing stress of Beryllium sheet is approximately equal to that of 7075-T6 aluminum sheet at room temperature: $F_{bru} \approx 145 \text{ ksi (1000 MN/m}^2\text{)}$. Therefore, when sheet bearing is critical, the Beryllium joint strength is assumed equal to that of an identical 7075-T6 aluminum joint for both protruding head and flush fasteners. To account for the effect of temperature, multiply the room temperature allowable by the ratio of ultimate bearing stress at temperature to ultimate bearing stress at room temperature.
- ° Due to notch sensitivity of Beryllium below 400°F (478°K), joints subjected to tension loads in the plane of the sheet perpendicular to the fastener line may fail at loads less than predicted by above techniques. To avoid a tension failure in the Beryllium sheet between fasteners, the net tension stress should not exceed the notched tensile strength of the material. The maximum net tension stress between fastener holes in the Beryllium sheet should not be allowed to exceed:

$f_{t_{net}} = 50 \text{ ksi (354 MN/m}^2\text{)}$ in joints having no eccentricity

$f_{t_{net}} = 200 \text{ ksi (1379 MN/m}^2\text{)}$ in eccentrically loaded joints

$$\text{where } f_{t_{net}} = \frac{P}{A} + \frac{MC}{I} \quad (\text{II-9})$$

M = Bending moment due to eccentric loading with no joint deflection

A = Net material cross-sectional area between fasteners

These criteria were found to be approximately 10% conservative based on element test results.

Adhesive bonded Beryllium lap shear joints using the FM-61 epoxy adhesive system and the HT-424 epoxy-phenolic adhesive system resulted in bond stresses higher than those obtained in tests of aluminum lap shear specimens bonded with the same adhesive systems. The design lap shear stresses for Beryllium joints bonded with FM-61 and HT-424 adhesive systems are given in Table 2. These design values are 80% of the minimum values obtained in tests.

Adhesive	Temperature (°F)	Design Stress (psi)
FM-61	75	3000
	-65	4300
HT-424	75	3200
	500	1350

Table 2- Design Shear Stresses For Bonded Beryllium Lap Joints

An extensive element test program was conducted to develop design data essential to design of the Beryllium rudder. The objectives of this program

were to verify material properties, obtain design data, and to evaluate certain structural details which were subsequently incorporated into the rudder assembly.

Table 3 presents a summary of the element test program, with a detailed description of each test and the results contained on Reference 1. The results of the fatigue strength tests are plotted in Figure 11 with comparative data for aluminum and titanium. Figure 12 shows the fatigue strength-to-weight efficiency curves for these materials.

3. DESIGN CONSIDERATIONS

In designing the amount of Beryllium utilization in the rudder structure, shown schematically in Figure 13, the primary objective was to save the maximum amount of weight within the limits prescribed by manufacturing state-of-the-art, material availability and reasonable costs. The F-4 rudder is a mass-balanced control surface and all weight saved aft of the hinge line results in additional weight savings due to a corresponding reduction in balance weights. Therefore, every reasonable effort was made to use beryllium structure aft of the hinge line. Exceptions were the honeycomb core, mechanical fasteners, shear clips and trailing edge plastic laminate filler (not shown in the schematic). While no redesign to beryllium was advantageous weight-wise forward of the hingeline, exceptions were made for two areas. The forward torque box cover skin was extended forward to cover the upper balance weight support structure. The lower section of the leading edge skin was converted to Beryllium since it transfers torque into the rudder and contributes significantly to overall torsional stiffness. The detailed drawings of the rudder are shown in Appendix B.

Test	Test Loading	No. of Tests at Temperature			Data Required	Test Results
		-65°F	R.T.	500°F		
Material Acceptance Tests	Tension (Note 1)	—	14	—	F _{tu} , F _{ty} , and e.	F _{tu} = 70.4 - 87.1 ksi F _{ty} = 50.4 - 60.7 ksi e = 9 - 23%
Metal-to-Metal Bond Tests	Shear	1	3	—	Bond Shear Stress (FM-61)	3731 - 3945 psi @ R.T. 5394 psi @ -65°F
	Flatwise Tension	1	3	—	Tension Stress in Bond at Failure (FM-61)	1208 - 1794 psi @ R.T. 1112 psi @ -65°F
Bonded Honeycomb Panel Tests	Flatwise Tension	1	3	—	Tension Stress in Bond at Failure (FM-61)	525 - 551 psi @ R.T. 529 psi @ -65°F
	Core Shear	1	3	—	Shear Stress in Core at Failure	140 - 161 psi @ R.T. 153 psi @ -65°F
	Compression	1	3	—	Compression Stress in Face Skin at Failure	60.7 - 62.0 psi @ R.T. 69.2 psi @ -65°F
	Bond Shear	1	3	—	Shear Stress in Bond at Failure (FM-61)	85 - 147 psi @ R.T. 88 psi @ R.T.
Effect of Stress Concentrations and Interference Fit Fasteners	Tension	—	12	—	Failing Stress	56.0 - 84.0 ksi
	Fatigue	—	23	—	Cycles to Failure	See Fig. 11
Joint Tests	Tension	6	6	—	Joint Failing Load	Total Elastic Stress @ Splice Center 81,500 - 161,400 psi
Panel Shear Tests	Shear	—	7	—	Initial Buckling Stress and Failing Stress	17,833 - 40,656 psi HT-474 Adhesion 16,800 - 18,310 lb @ R.T. 16,030 lb @ -65°F
Spliced Panel Shear Tests	Shear	3	9	—	Joint Shear Strength (Failure Load)	CR7748-4 Rivets 9,580 - 11,230 lb @ R.T. 10,430 lb @ -65°F NAS1620-08 Jo-Bolts 17,510 - 19,600 lb @ R.T. 17,300 lb @ -65°F
Lug Tests	Tension	6	6	6	Lug Strength	F _{br} = 61,800 - 201,000 psi @ R.T.
Tests of Specimens with Corrosion Protec. Finishes	None (Note 3)	—	16	—	Corrosion Rates	None Be Corrosion Pitted after 12 hrs With Selected Protection System, No Corrosion After 500 hrs
	Tension	—	8	—	Effect on Mechanical Properties	No Adverse Effect With Selected Protection System
Stress-Strain Tests	Tension	6	6	6	Stress-Strain Curves	Temp. E (10 ⁶ psi) YS (10 ³ psi) R.T. 41.7 - 47.7 55.0 - 60.0 -65°F 39.0 - 45.0 55.0 - 61.5 500°F 37.0 - 40.0 36.5 - 49.0
	Compression	3	6	3		R.T. 38.0 - 42.8 57.0 - 60.0 -65°F 43.0 - 46.0 57.7 - 60.0 500°F 38.5 - 39.0 45.0 - 50.0
Rudder Composite Section	(Note 2)	—	1	—	(Note 2)	Withstood Loads in Excess of Rudder Ultimate Design Loads.
Crack Repair Eval. Tests	Tension	—	6	—	Failure Mode	Bonded Beryllium Doublers Proved Adequate.

- Notes: 1. Seven each tested in tension in longitudinal and transverse grain directions.
2. Four tests performed: 1) Chordwise bending to limit load, 2) Torsion to limit load, 3) Spanwise bending to 120% limit load, and 4) Combined chordwise bending, spanwise bending and torsion to failure.
3. Specimens were subjected to 5% salt spray for 500 hours.

Table 3 - Element Test Program

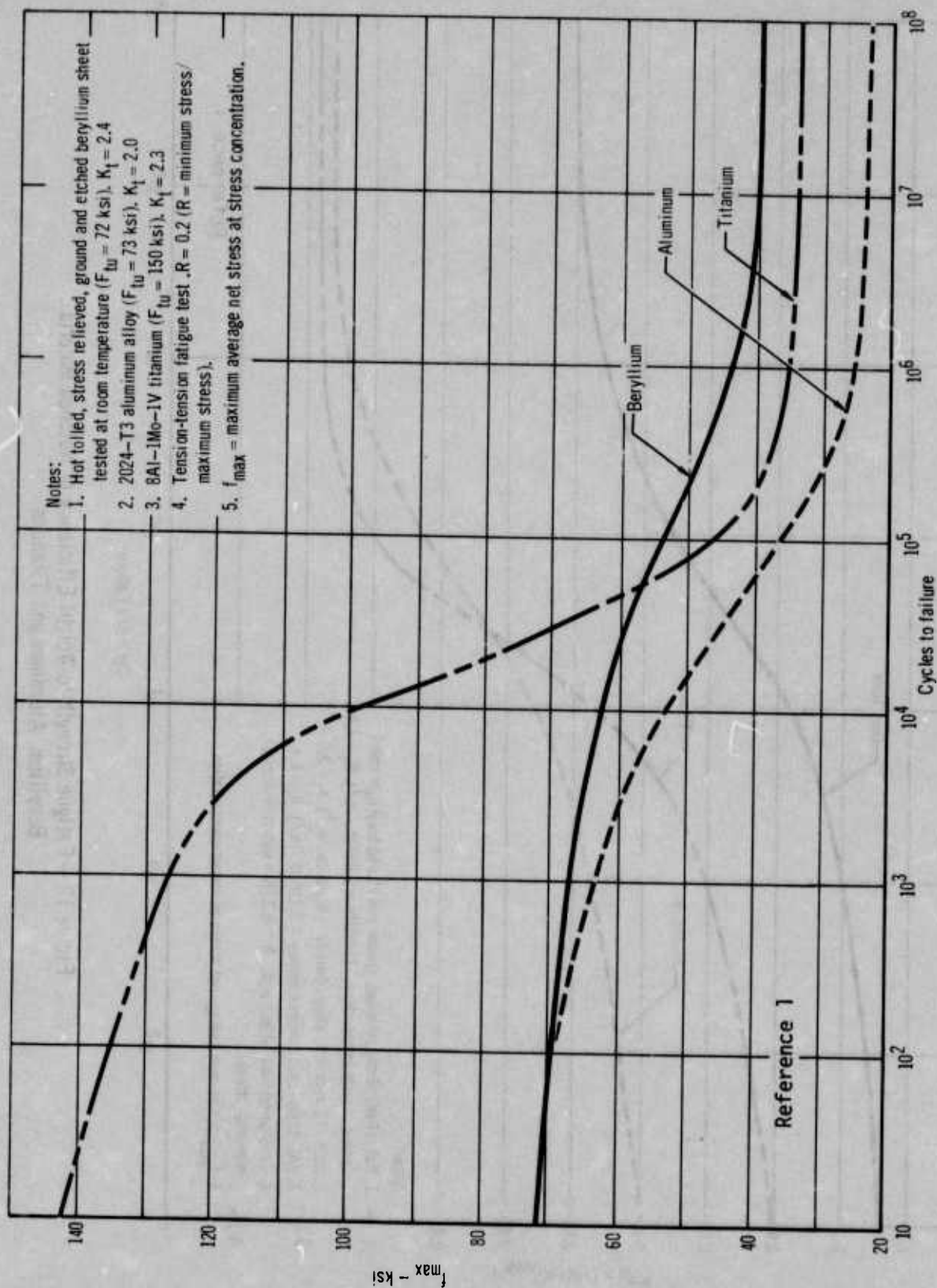


Figure 11 - Fatigue Strength of Notched Sheet: Beryllium, Aluminum and Titanium

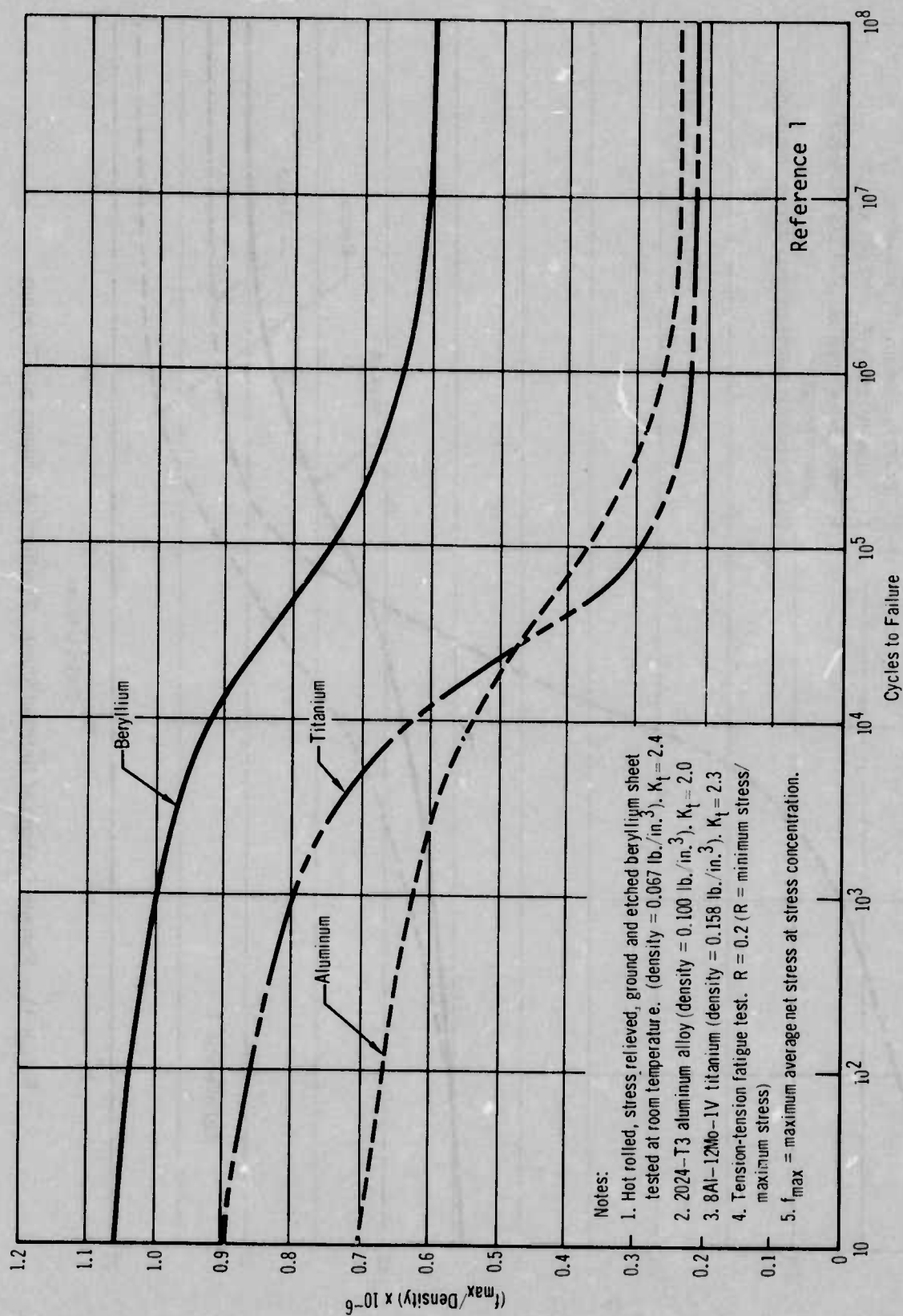


Figure 12 - Fatigue Strength-to-Weight Efficiency of Notched Material:
Beryllium, Aluminum and Titanium

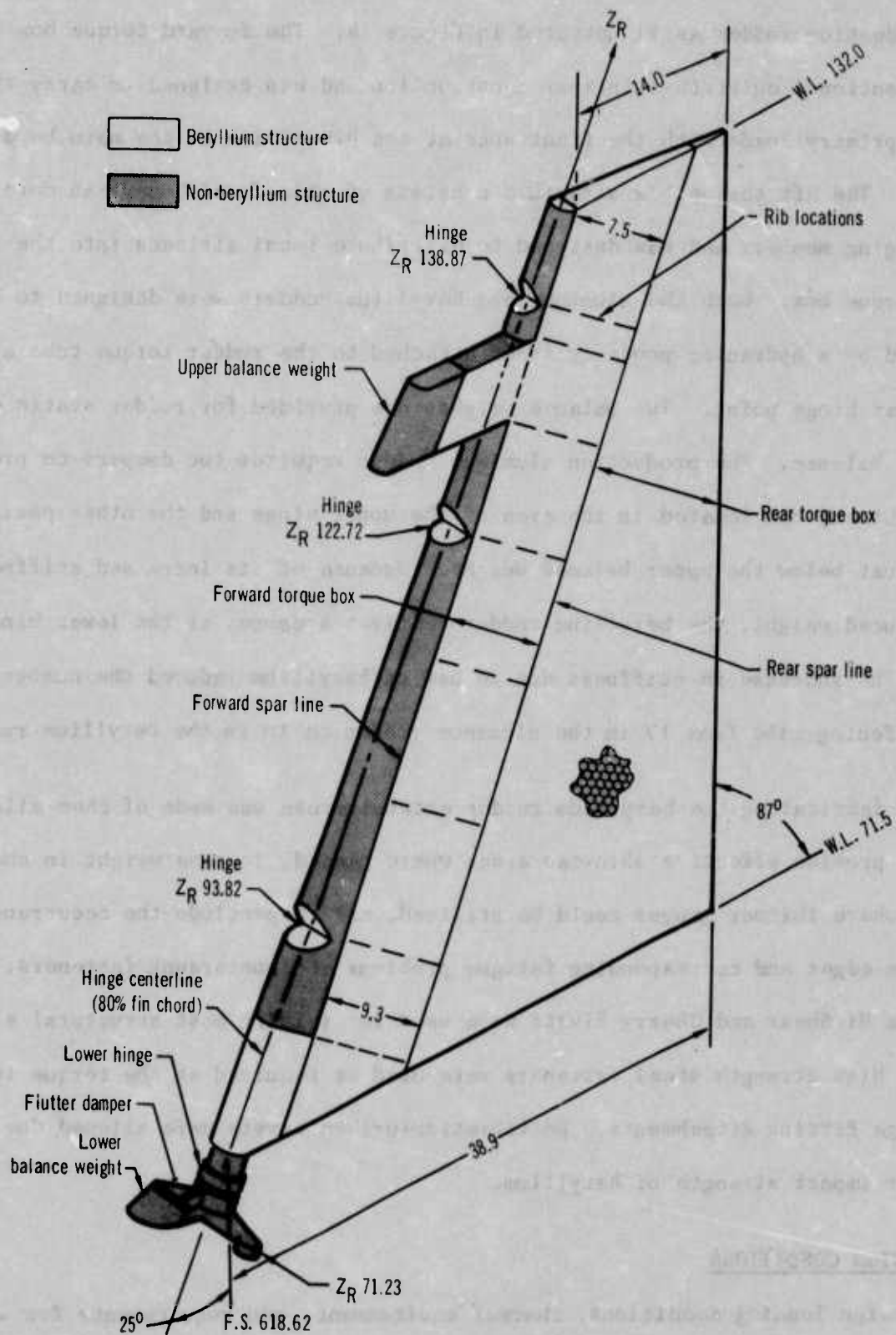


Figure 13 - Beryllium Rudder Structure Schematic

The structural arrangement of the Beryllium rudder is similar to that of the production rudder as illustrated in Figure 14. The forward torque box is of conventional multirib-skin-spar construction and was designed to carry the rudder primary loads with the front spar at the hinge line as the main bending member. The aft torque box structure consists of skin-faced honeycomb core with edging members and was designed to distribute local airloads into the forward torque box. Both the aluminum and beryllium rudders were designed to be actuated by a hydraulic power cylinder attached to the rudder torque tube at the lower hinge point. Two balance weights are provided for rudder static and dynamic balance. The production aluminum rudder requires two dampers to prevent flutter; one located in the area of the upper hinge and the other positioned just below the upper balance weight. Because of its increased stiffness and reduced weight, the beryllium rudder requires a damper at the lower hinge only. The increase in stiffness due to use of beryllium reduced the number of stiffening ribs from 17 in the aluminum rudder to 10 in the beryllium rudder.

In fabricating the beryllium rudder extensive use was made of chem-milling to provide effective skin-cap areas where needed, to save weight in shear panels where thinner gauges could be utilized, and to preclude the occurrence of knife-edges and corresponding fatigue problems at countersunk fasteners. Aluminum Hi-Shear and Cherry Rivets were used for joining most structural elements. High strength steel fasteners were used as required at the torque tube and hinge fitting attachments. No vibration-driven rivets were allowed due to the poor impact strength of beryllium.

4. DESIGN CONDITIONS

Design loading conditions, thermal environment, and requirements for vibration and flutter established for the F-4 aircraft were used in the struc-

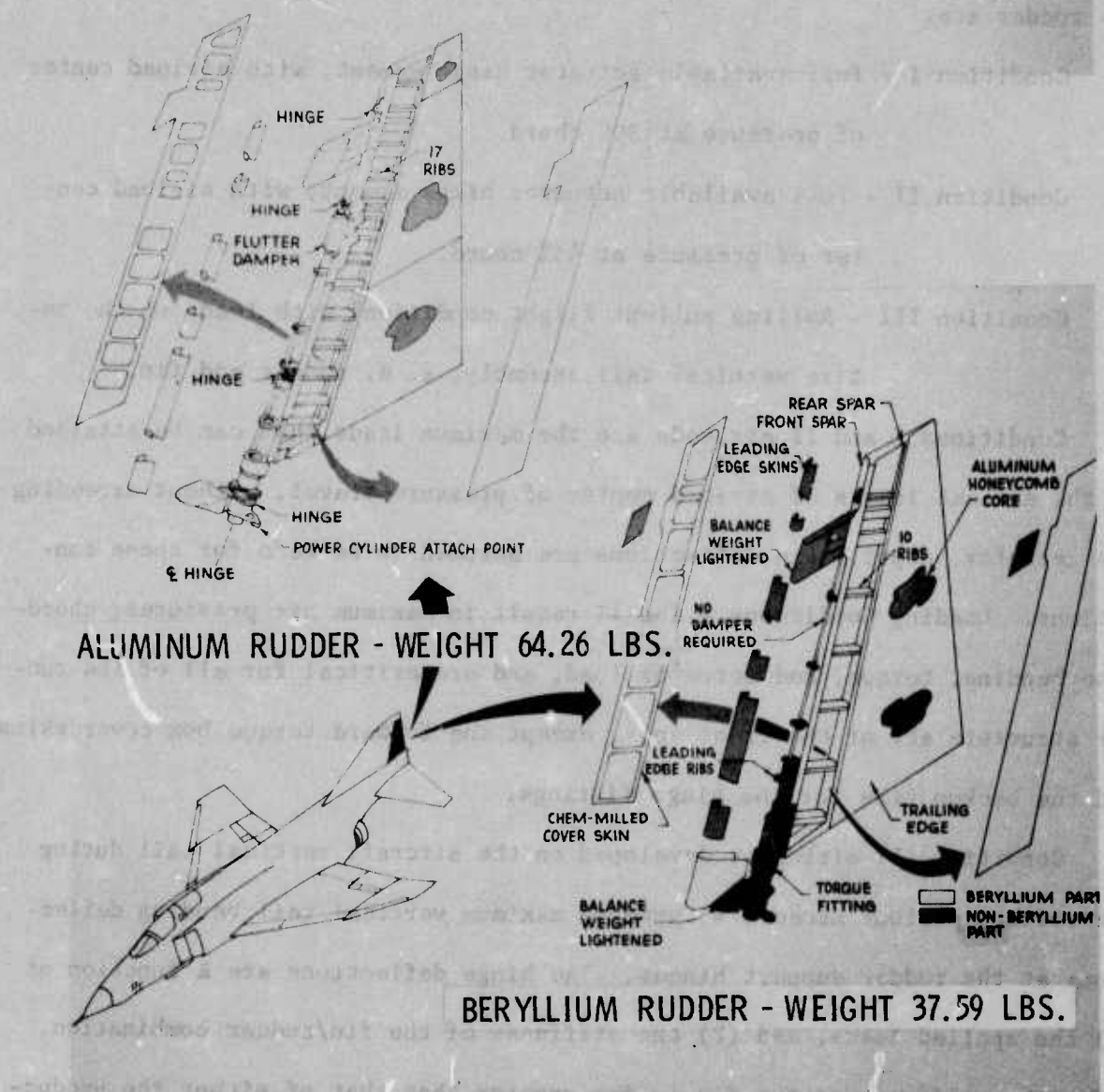


Figure 14 - F-4 Rudder Structural Configurations

tural analysis of the beryllium rudder, and are described below.

Design limit (maximum obtainable in service) loading conditions for the F-4 rudder are:

Condition I - Full available actuator hinge moment, with airload center of pressure at 30% chord.

Condition II - Full available actuator hinge moment, with airload center of pressure at 45% chord.

Condition III - Rolling pullout flight condition, with loads on the entire vertical tail assembly, i. e. rudder and fin.

Conditions I and II airloads are the maximum loads that can be attained at the extreme limits of airload center of pressure travel, without exceeding the actuator output. Fin deflections are assumed to be zero for these conditions. Loading Conditions I and II result in maximum air pressures, chord-wise bending, torque, and actuator load, and are critical for all of the rudder structure aft of the front spar, except the forward torque box cover skins and the backup ribs for the hinge fittings.

Condition III airloads, developed on the aircraft vertical tail during the rolling pullout maneuvers, produce maximum vertical tail bending deflections at the rudder support hinges. The hinge deflections are a function of (1) the applied loads, and (2) the stiffness of the fin/rudder combination. Since the stiffness of the fin is far greater than that of either the production aluminum or beryllium rudders, there is not a great difference in hinge deflection, whichever rudder is installed. These deflections are actually slightly less with the beryllium rudder because it is approximately 6 times as stiff as the aluminum rudder. This increased stiffness, however, results in significantly higher loads in the beryllium rudder than in the aluminum

rudder. Therefore, Condition III loads designed a substantial portion of the Beryllium rudder: rudder hinges, hinge backup ribs front spar, and forward torque box cover skins.

Running airloads on the rudder for the three design conditions are shown in Figure 15. Rudder shear and bending moment diagrams for Conditions I, II, and III are shown in Figures 16, 17, and 18, respectively. Rudder torque about the elastic axis is presented in Figure 19.

The rudder balance weights and their local support structure were designed in compliance with the production aircraft requirements: (1) static side load of ± 100 g's on the balance weight, perpendicular to the aircraft symmetry plane, and (2) 50,000 cycles of fully reversed inertial load of ± 40 g's on the balance weights, perpendicular to the symmetry plane.

The panel flutter criteria used in the design and analysis of the Beryllium rudder are presented in Figure 20. These criteria, as indicated, are based on analytical as well as flight test data. A critical M/q (Mach number/dynamic pressure) ratio of .0985 was determined from the production aircraft speed-altitude diagram. Furthermore, the beryllium rudder was designed to function in a thermal environment identical to that established for the F-4 aircraft production rudder. Normal operating temperatures on the rudder range from -65°F (219°K) to 230°F (383°K) with a transient overspeed condition which could produce short time temperatures up to 270°F (405°K).

5. DESIGN DETAILS

Considerations other than structural geometry, weight and loads enter into the detail design of the Beryllium rudder. These include fabrication and handling characteristics of the material as well as special design factors necessi-

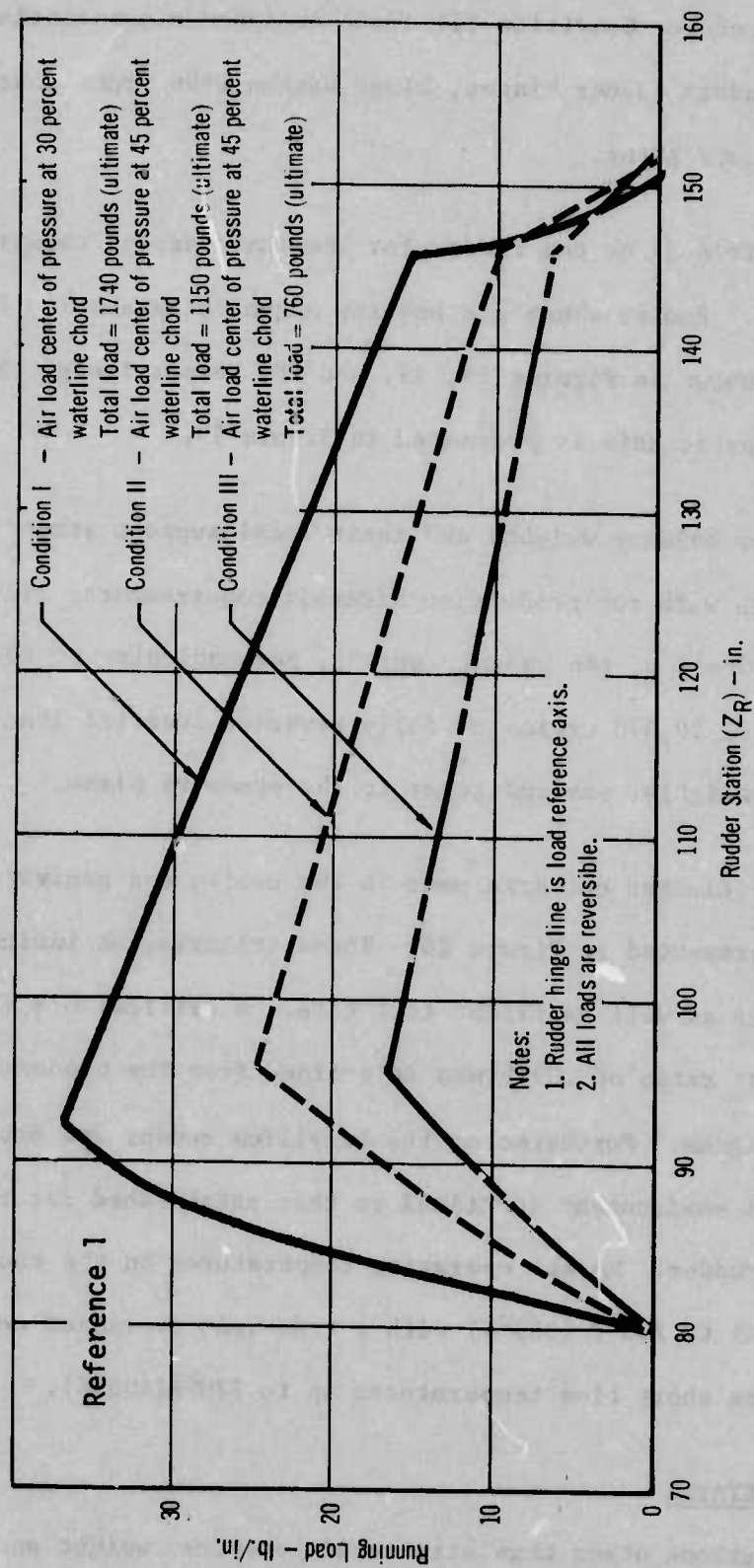


Figure 15 - Ultimate Running Load

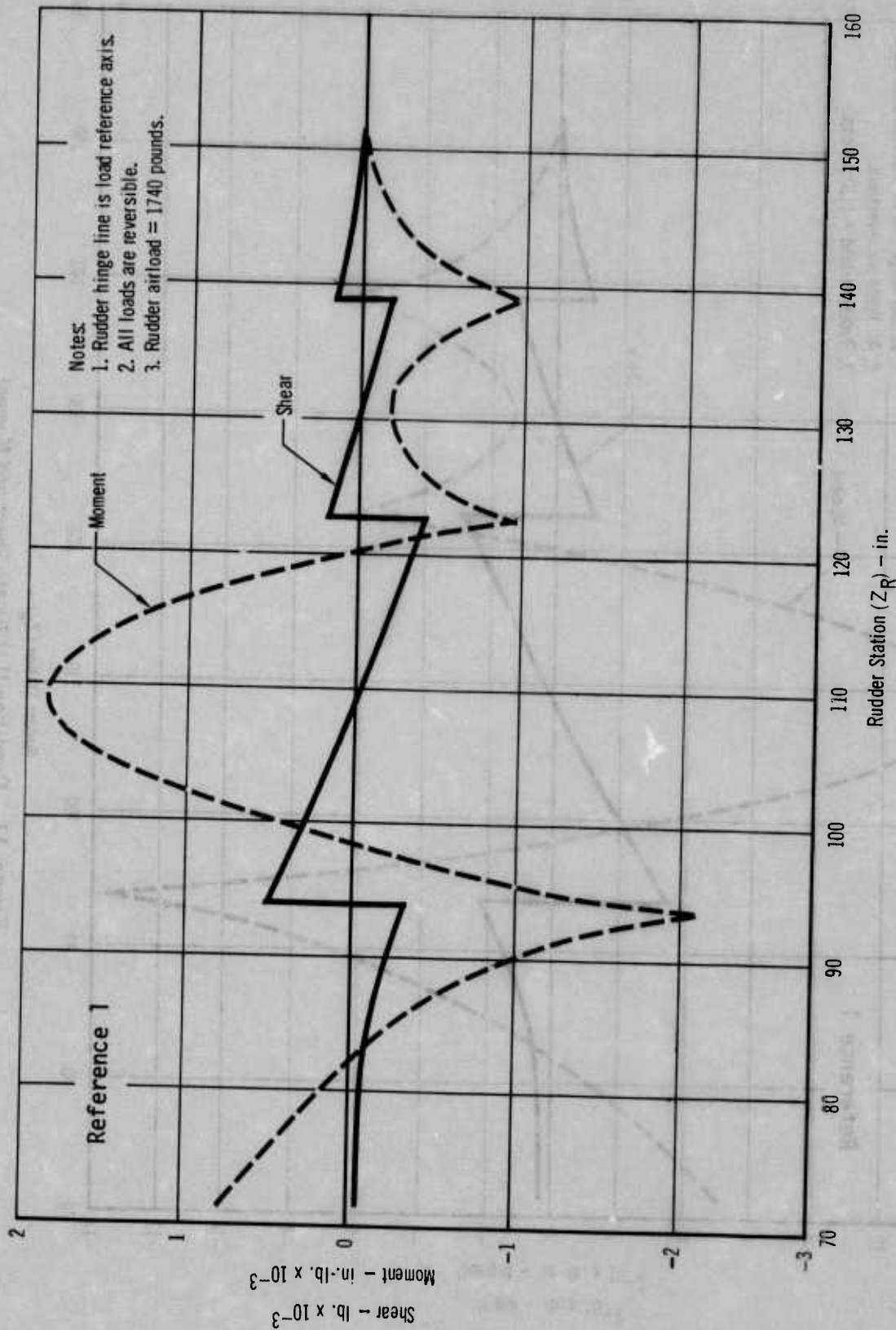


Figure 16 - Condition 1 Ultimate Shear and Moment

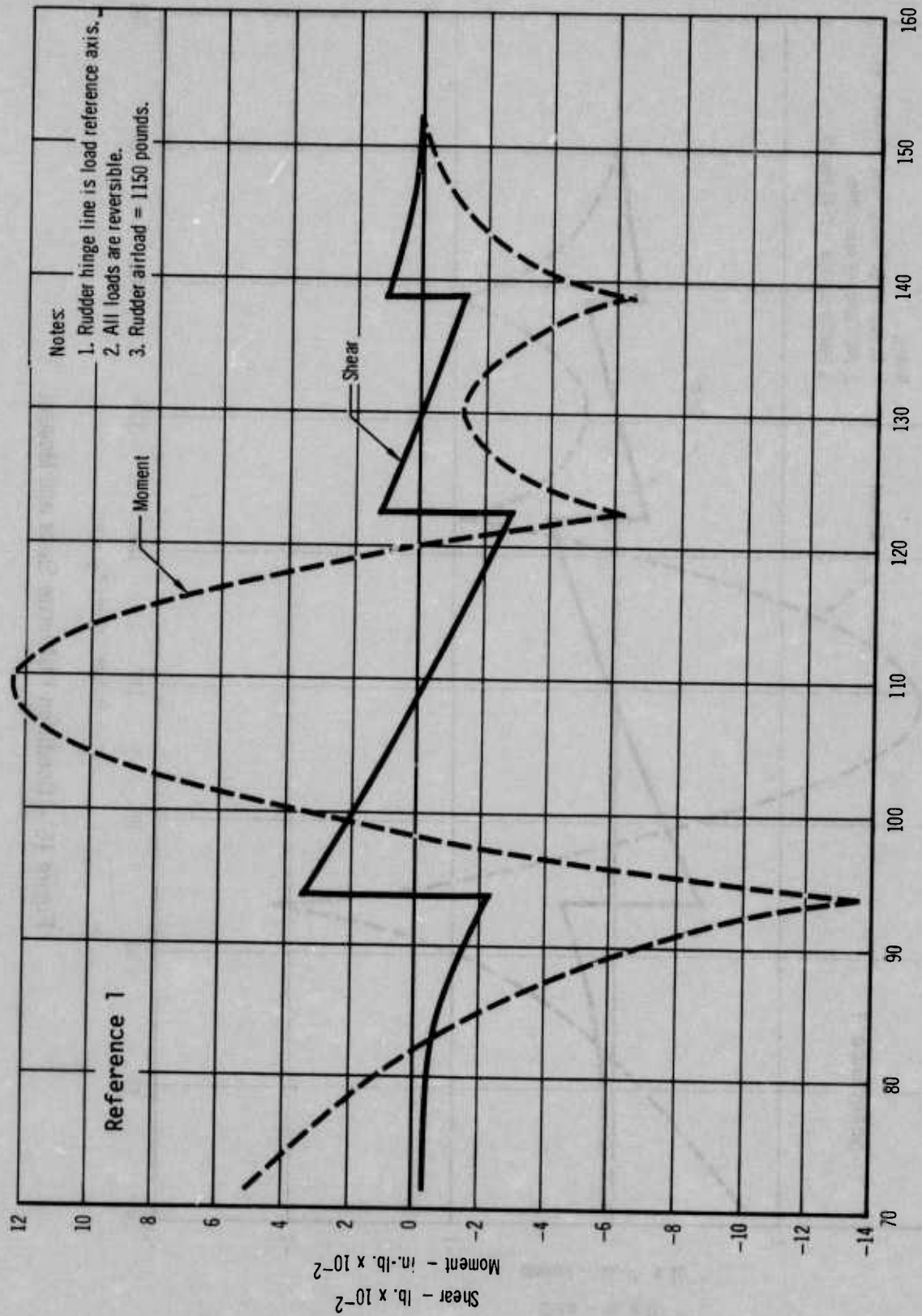


Figure 17 - Condition II Ultimate Shear and Moment

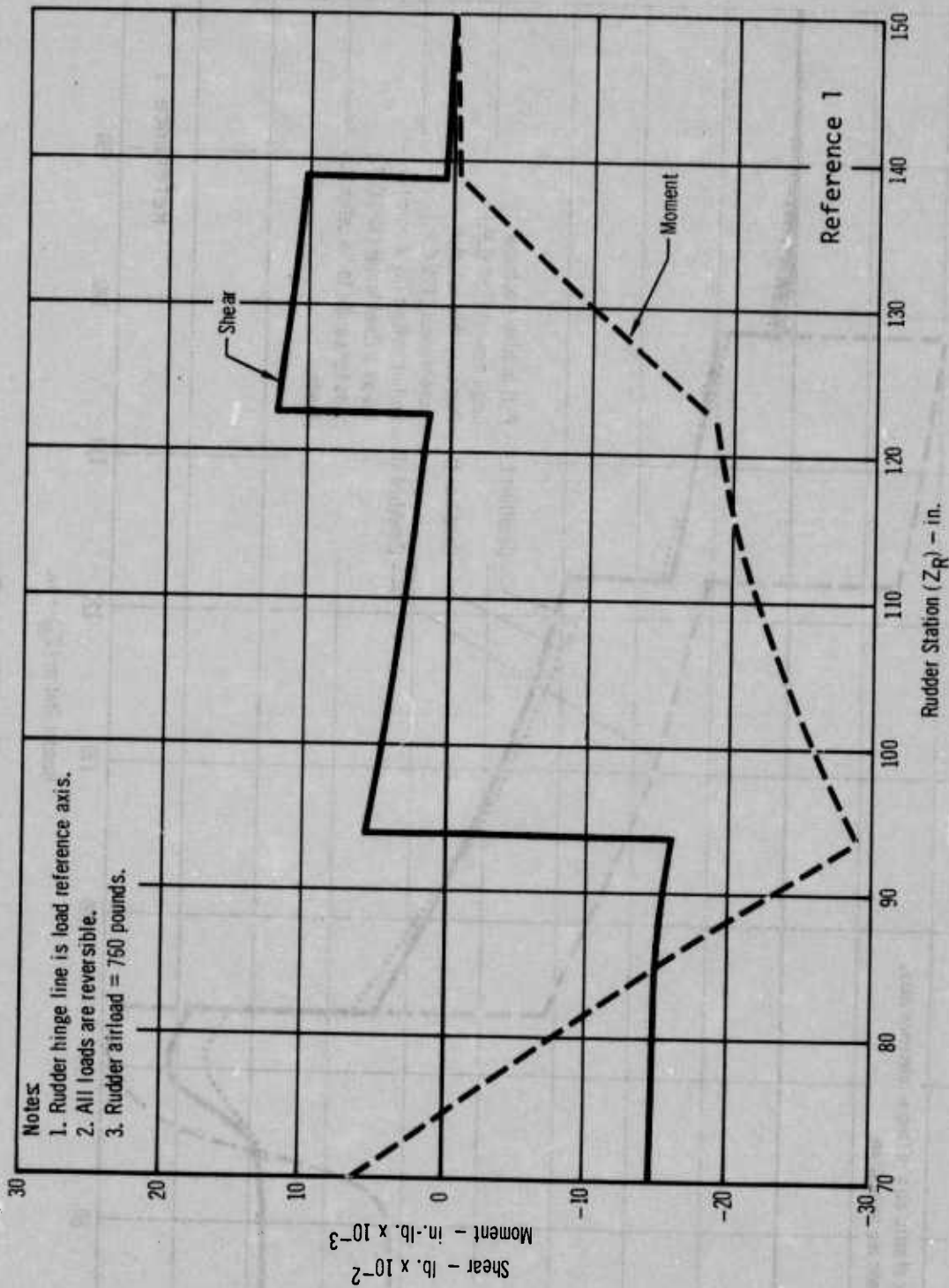


Figure 18 - Condition III Ultimate Shear and Moment

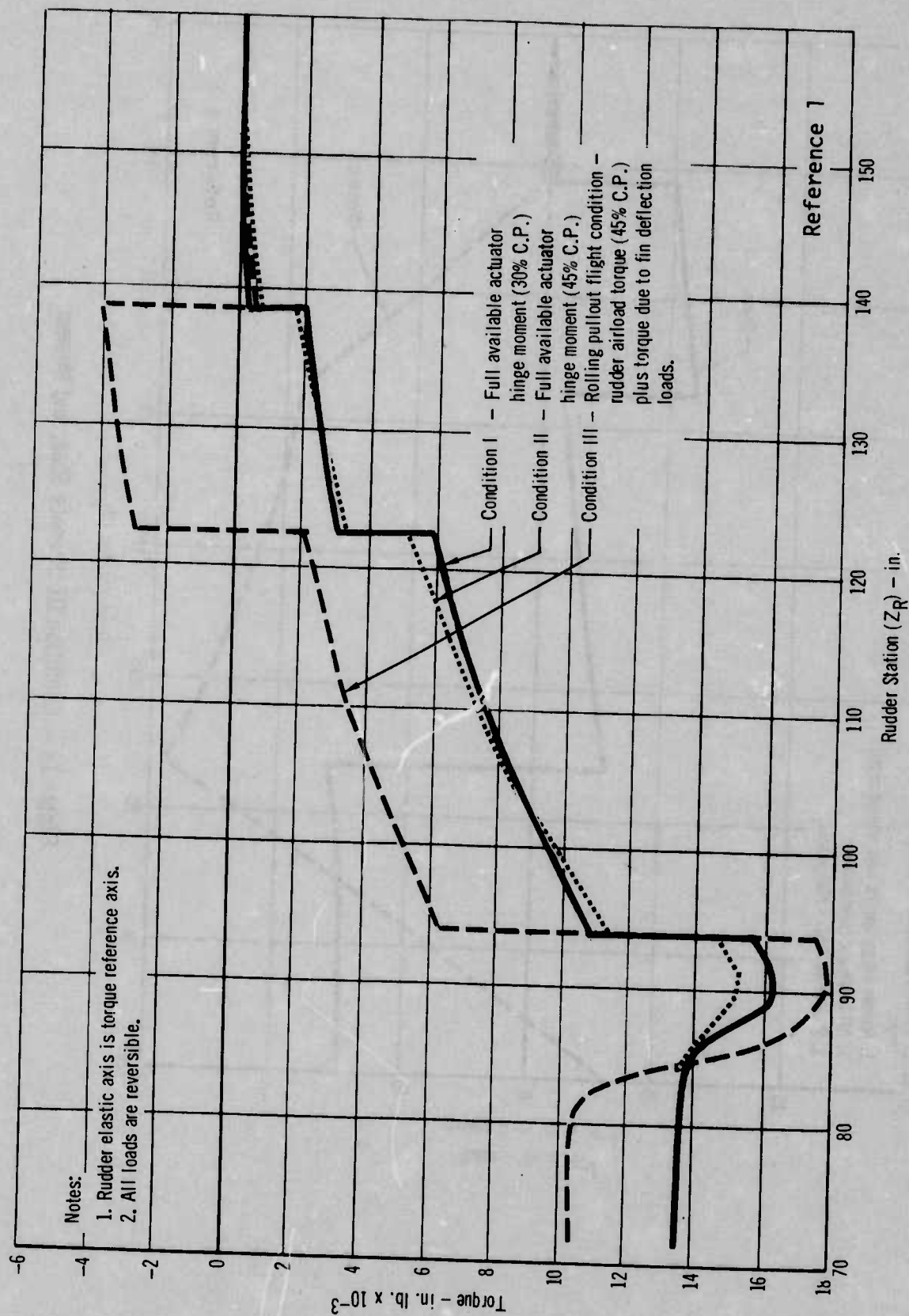


Figure 19 - Ultimate Torque

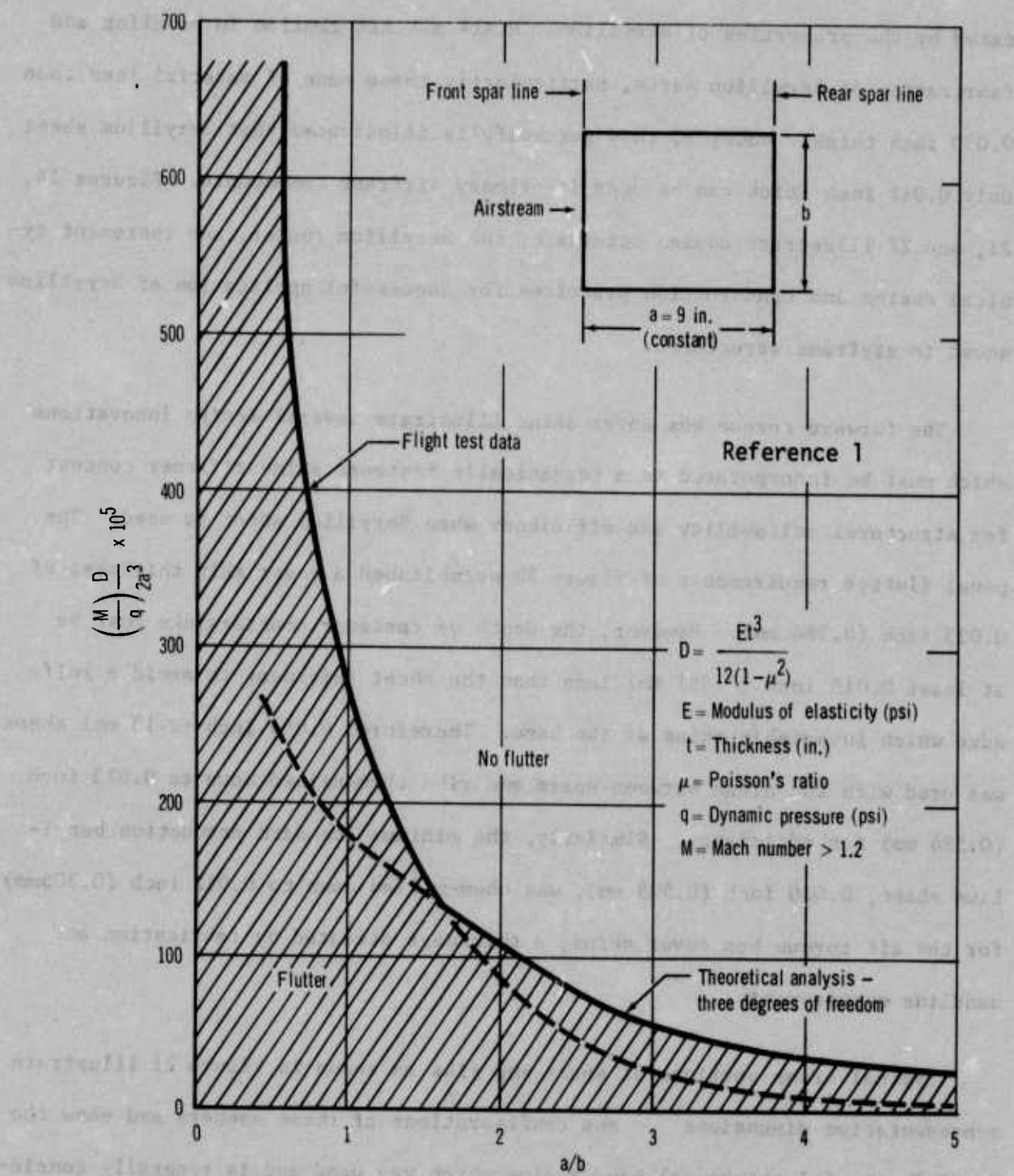


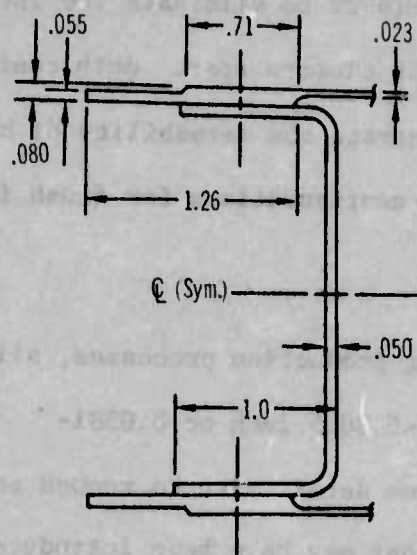
Figure 20 - Panel Flutter Criteria

tated by the properties of Beryllium. MCAIR advises caution in handling and fabrication of Beryllium parts, particularly those made of material less than 0.030 inch thick. However, they successfully illustrated that Beryllium sheet only 0.012 inch thick can be used in primary airframe components. Figures 14, 21, and 22 illustrate design details of the Beryllium rudder, and represent typical design and construction practices for successful application of Beryllium sheet to airframe structures.

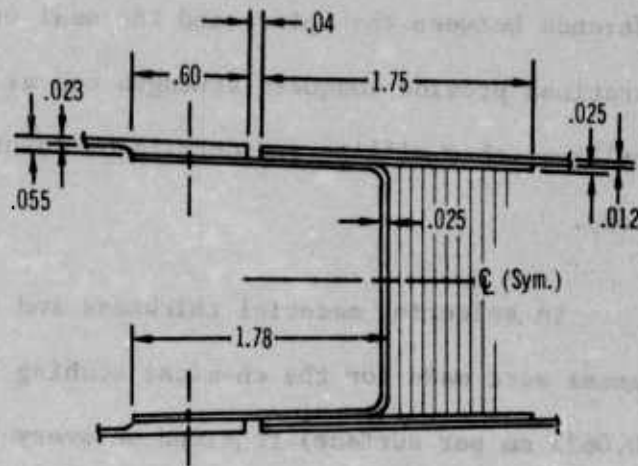
The forward torque box cover skins illustrate several design innovations which must be incorporated in a mechanically fastened skin-stiffener concept for structural reliability and efficiency when Beryllium sheet is used. The panel flutter requirements of Figure 20 established a cover skin thickness of 0.023 inch (0.584 mm). However, the depth of fastener countersinks must be at least 0.015 inch (0.381 mm) less than the sheet thickness to avoid a knife edge which invariably chips at the base. Therefore, 0.084 inch (2.13 mm) sheet was used with the areas between spars and ribs chem-milled down to 0.023 inch (0.584 mm) for efficiency. Similarly, the minimum standard production beryllium sheet, 0.020 inch (0.508 mm), was chem-milled down to 0.012 inch (0.305mm) for the aft torque box cover skins, a thickness dictated by fabrication and handling requirements.

Typical cross sections of spars and ribs as shown in Figure 21 illustrate representative dimensions and configurations of these members and show the 5t (5 X material thickness) bend radius which was used and is generally considered a minimum for forming hot rolled Beryllium sheet. Two of the ribs were formed with joggled flanges with the joggle length ten times its depth.

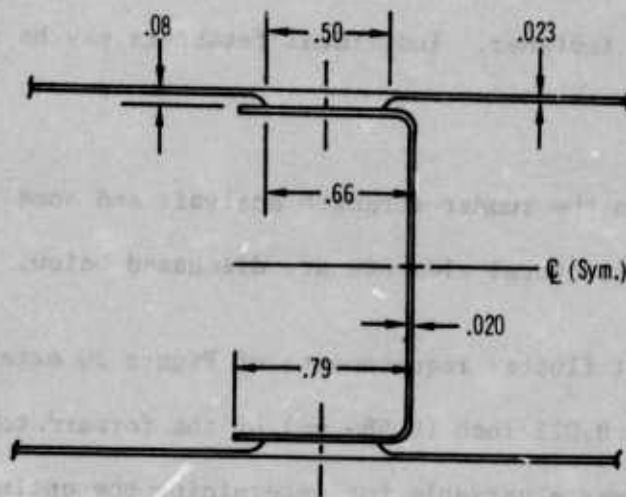
The Beryllium rudder leading edge skin splice for the lower edge was mod-



Typical section of forward spar



Typical section of rear spar



Typical section of rib

Figure 21 - Beryllium Rudder Rib and Spar Cross-Sections

ified for the flight test rudder as shown in Figure 22 to eliminate the interference between the splice and the seal on the fin closure spar. Both configurations provide adequate strength and also illustrate the formability of beryllium, chem-milling and details on countersink configurations for flush fasteners.

In selecting material thickness and planning production processes, allowances were made for the chemical etching (0.0015-0.0025 inch or 0.0381-0.0635 mm per surface) required on every beryllium detail part to remove any microscopic surface cracks or mechanical twins that may have been introduced during machining. Alignment of fastener holes must be precise and the actual hole size of adjacent members should be identical so that the fastener will fit snugly in both members and provide an even distribution of load across the diameter of the fastener. Individual fasteners may be selected by fit.

6. DESIGN ANALYSIS

The approach to the rudder strength analysis and some pertinent results relative to major structural elements are discussed below.

While the panel flutter requirements of Figure 20 established the chem-milled thickness of 0.023 inch (0.584 mm) of the forward torque box cover skins, rib spacing was a variable for determining the optimum panel configuration. A plot of skin thickness versus rib spacing is shown in Figure 23. Using a constant panel length of 9 inches (23 cm) reflecting the approximate chordwise distance between the forward and the aft spars, a maximum rib spacing of 9.6 inches (24.4 cm) was selected. Fabrication and handling requirements dictated the bonded honeycomb cover skin thickness of 0.012 inch (0.305 mm) used on the aft torque box.

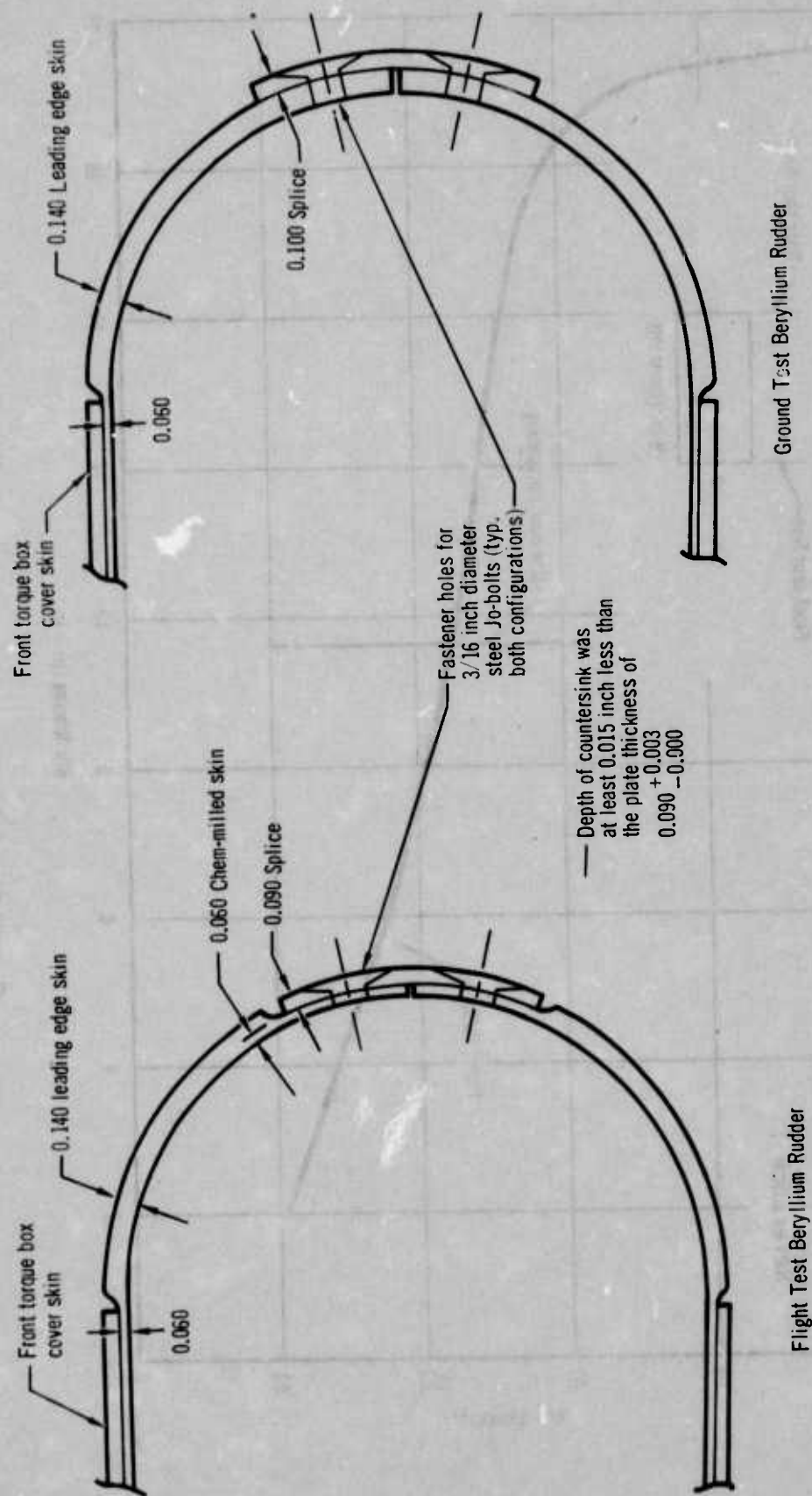


Figure 22- Beryllium Rudder Leading Edge Skin Splice Configurations

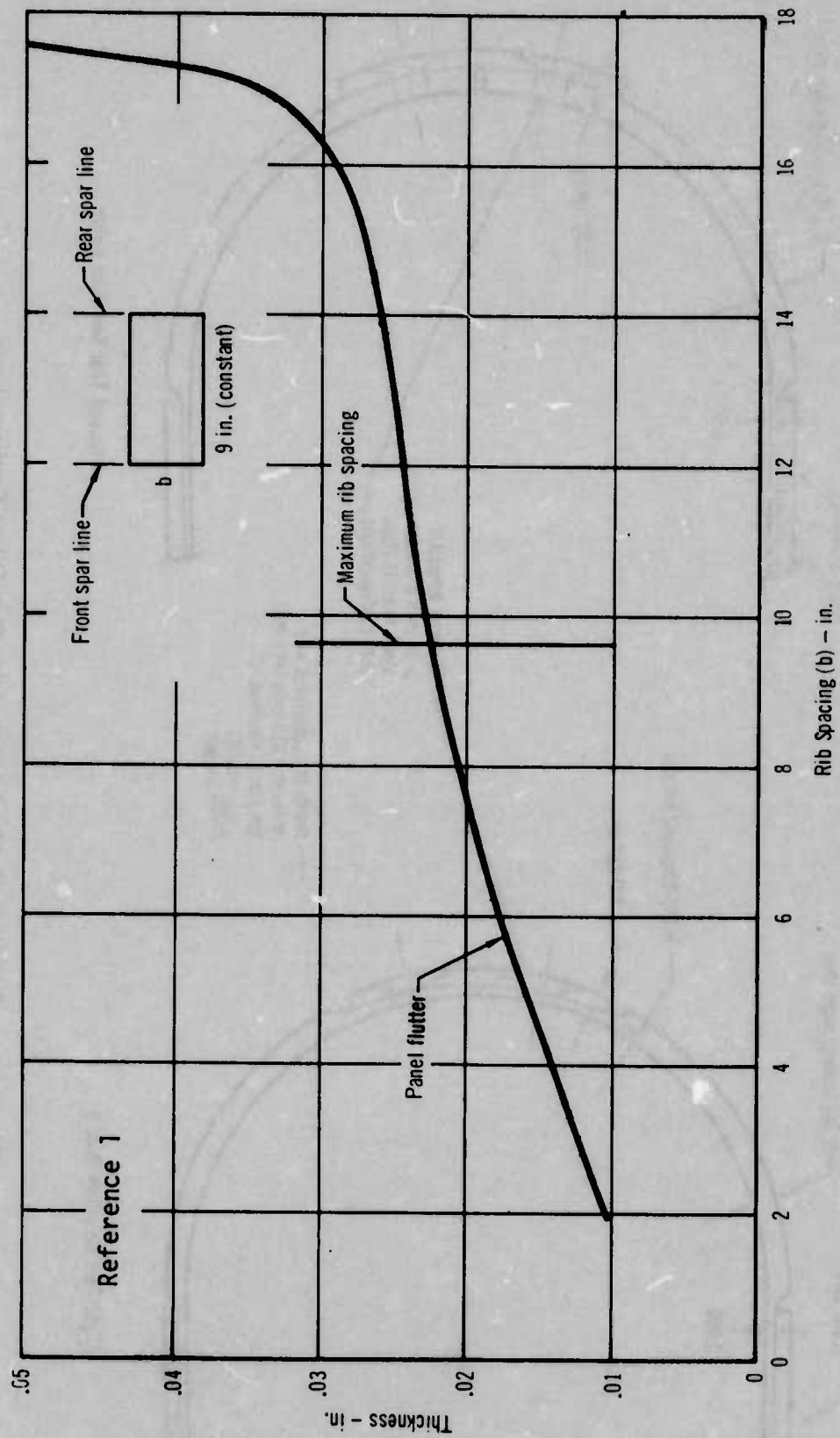


Figure 23 - Cover Skin Thickness Requirements

The maximum shear flow in the rudder skins as illustrated in Figure 24 is the result of the rudder torque presented in Figure 19. The relative stiffness of the two torque boxes defines the percent of total torque in each. The panel thickness required to preclude flutter provided more than adequate shear post buckling strength.

The forward spar was analyzed conservatively as resisting all spanwise bending imparted to the rudder by the most severe bending moments under Loading Condition III previously described and shown in Figure 18. Material gages were established by crippling strength requirements of the spar caps. Allowable crippling stresses were determined using the non-dimensional crippling curves for Beryllium presented in Figure 7. Rear spar thickness was dictated by strength requirements for transferring trailing edge loads into the forward torque box. The spar webs were analyzed for maximum shears and shown to be shear resistant. Bearing stresses were checked at the fastener locations of the hinge support fittings.

Ribs in the forward torque box are located at the upper balance weight attachment, and at intermediate positions as required to prevent panel flutter. A cross-section at a rib is shown in Figure 21. The two upper balance weight ribs were analyzed for redistributing the balance weight inertial loads into the forward torque box with 60 percent of the total load applied to the lower rib and 40 percent to the upper to account for balance weight sweepback relative to the front spar. The ribs at the upper three hinges were analyzed for the hinge loads of Condition III. The two drive ribs at the lower portion of the rudder were analyzed for transmitting torque between the rudder and the torque tube.

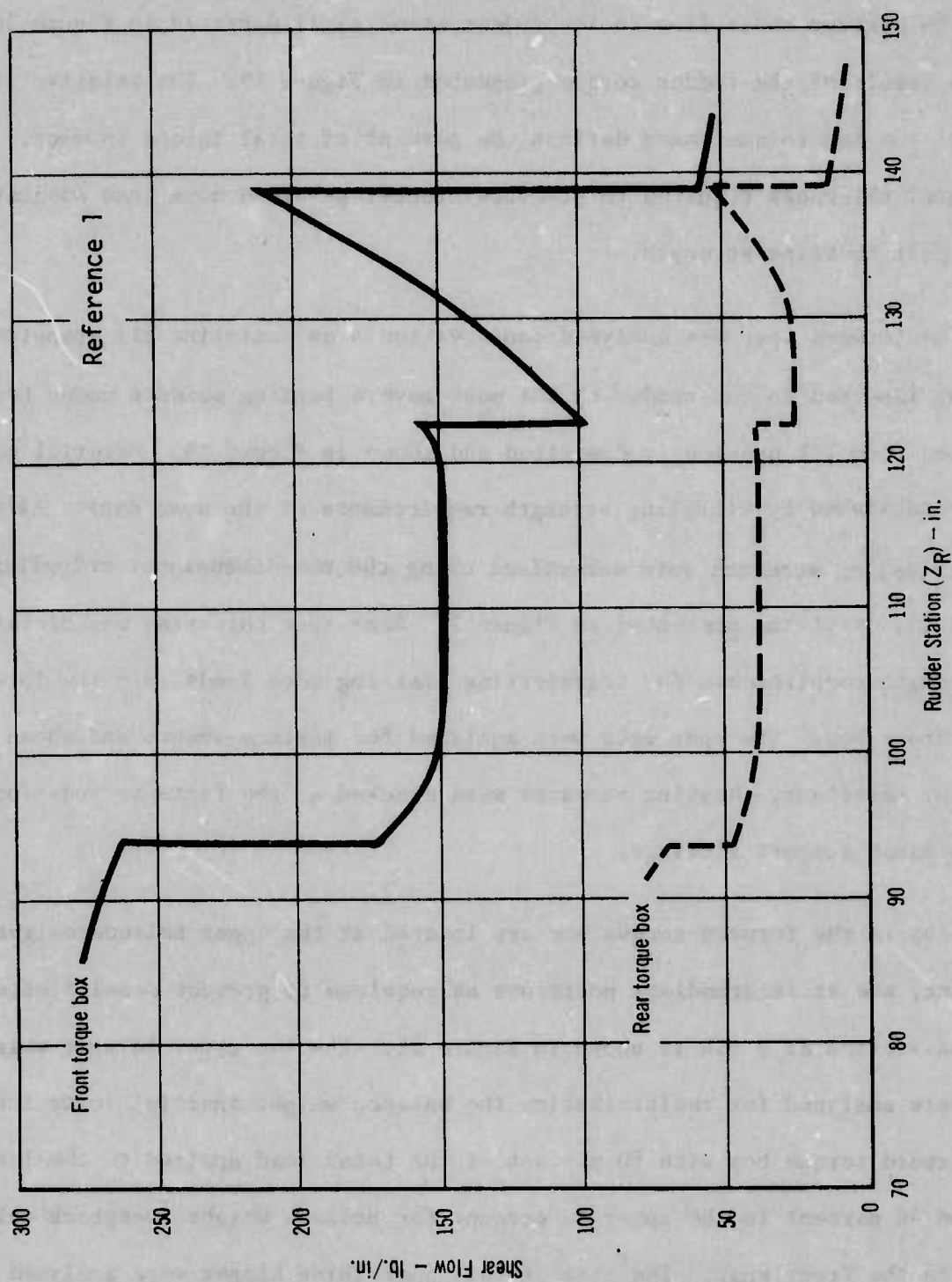


Figure 24 - Ultimate Shear Flows

In addition, all ribs were analyzed for reacting cover skin airloads. The honeycomb trailing edge structure was assumed to act as a cantilever at the aft spar; thus, airload-induced moment and shear forces along the spar length are reacted at the forward torque box ribs and skins. Furthermore, an analysis was made to establish thermal stresses in the rudder and the relationship between thermal and mechanical stresses. The maximum thermal stresses were found not to occur at the same time as the maximum flight loads.

Bending and torsional stiffnesses of both the beryllium and aluminum rudders are presented in Figure 25. The maximum bending stiffness of the beryllium rudder is 230% that of the aluminum rudder while the maximum torsional stiffness of the Beryllium rudder is 620% that of the aluminum rudder. As noted in Section II.4, the increased bending stiffness of the Beryllium rudder results in higher loads within this rudder under Condition III airloads than in production aluminum rudder. The Beryllium rudder is, however, designed to withstand these higher loads.

An analysis of the structural dynamic characteristics of the Beryllium rudder and of the fin with the Beryllium rudder installed was conducted to establish: (1) the influence of the Beryllium rudder on fin stability and (2) the need for rudder dampers to prevent transonic rudder buzz. The analysis showed that (1) fin stability is slightly improved and (2) the upper rudder damper on the production aluminum rudder is not required on the Beryllium rudder. The frequency separation is more favorable for the Beryllium rudder design than for the aluminum rudder design as shown below.

<u>MODE</u>	<u>ALUMINUM DESIGN</u>	<u>BERYLLIUM DESIGN</u>
Fin Bending	19 cps (Hz)	19 cps (Hz)
Rudder Rotation	27 cps (Hz)	42 cps (Hz)

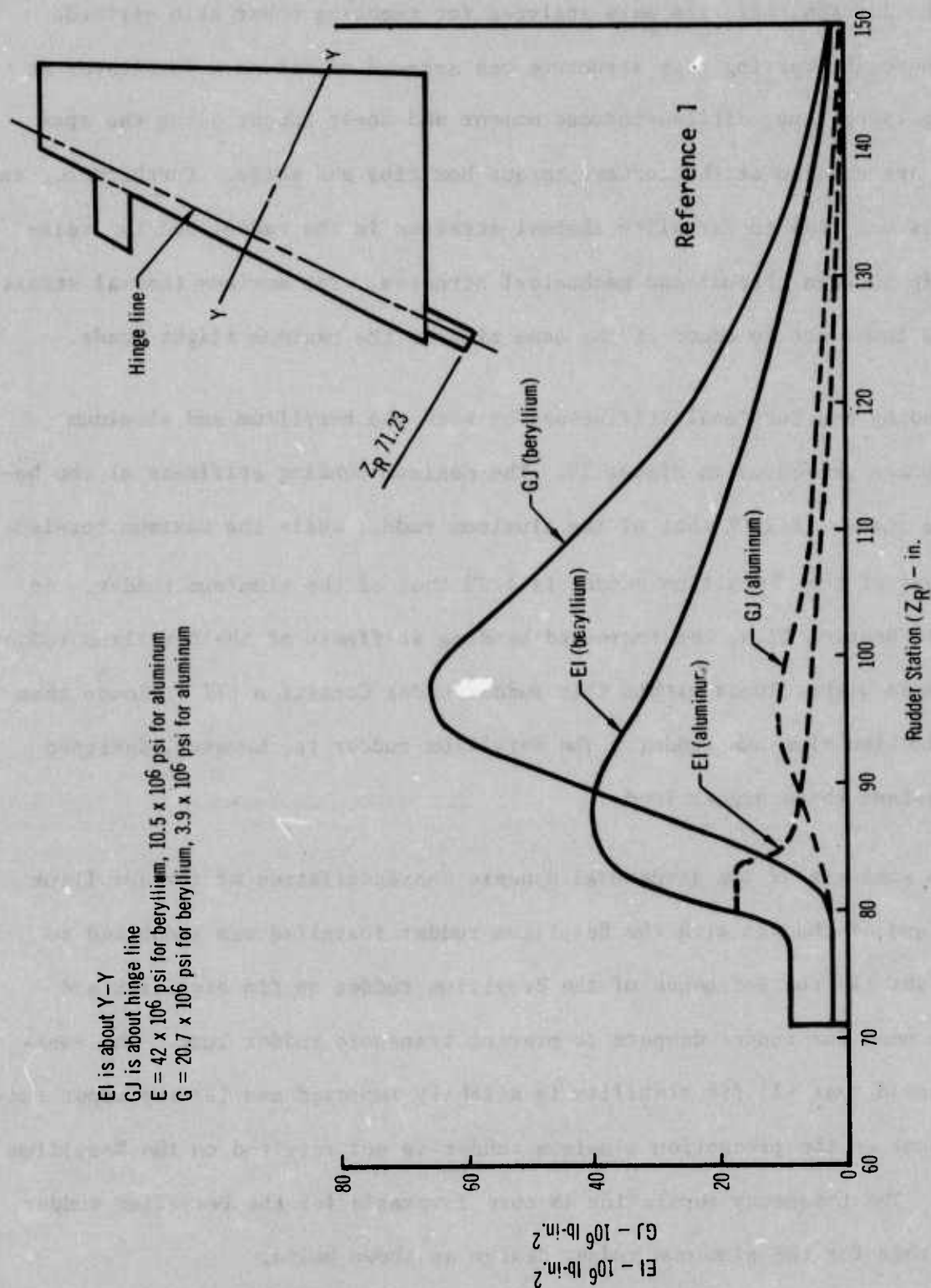


Figure 25 - Rudder Bending and Torsional Stiffnesses

Fin Torsion	39 cps (Hz)	40 cps (Hz)
Rudder Torsion	40 cps (Hz)	110 cps (Hz)

The modes which could couple to reduce the speed at which flutter occurs or increase the response amplitude are: (1) Fin Bending and Fin Torsion, (2) Fin Bending and Rudder Rotation, (3) Fin Torsion and Rudder Torsion, and (4) Fin Torsion and Rudder Rotation. The frequency separation in the first three was found to be more favorable for the Beryllium rudder. Condition (4) type flutter is prevented by the lower rudder damper. Figure 26 shows that the lower damper provides adequate stability for all values of effective stiffness to prevent transonic buzz problems in the Beryllium rudder.

A stability analysis of the F-4 rudder power cylinder with the appropriate rudder installed shows the relative stability of the Beryllium rudder system as compared to the production aluminum rudder. Figure 27 illustrates the relative stability with the aluminum rudder requiring 1.12% external damping whereas the Beryllium rudder requires only 0.88%. This is due mainly to the decrease in inertia about the hinge line of the Beryllium rudder which increases the rotational natural frequency (ω_r) of the rudder from 17.4 cps (Hz) to 21.1 cps (Hz).

The increased stiffness of the Beryllium rudder has a direct effect on YAW damper operation since there is less lost motion due to surface distortion at high speed. The net effect is an increase in gain at higher speeds and an attendant 40% increase in aircraft damping.

7. RUDDER MASS BALANCE

The required balance conditions for the Beryllium rudder were established

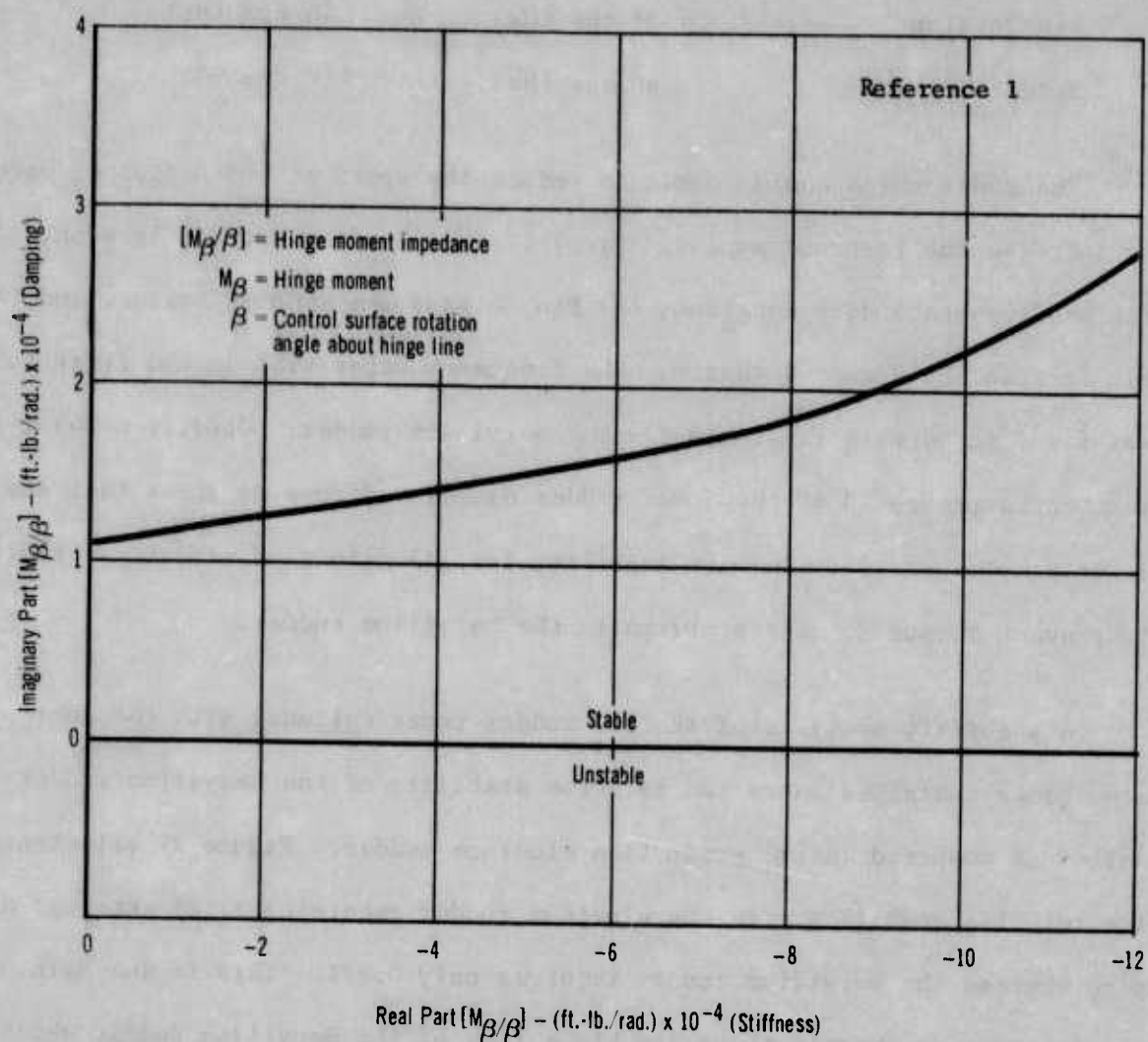


Figure 26 - Stability of Rudder With Upper Damper Removed

to decouple dynamically the rudder motion from that of the fin. The equipment used to mass balance the Beryllium rudders is similar to that used to balance production aluminum rudders. The procedures were similar with some adjustments made for the flight test rudder to achieve good agreement with measured inertia properties. The final balance condition of the ground test Beryllium rudder was established as 10.63 in.-lbs. (1.2 m-N) over-balance (nose heavy) about the hinge line. The final weights of the upper and lower

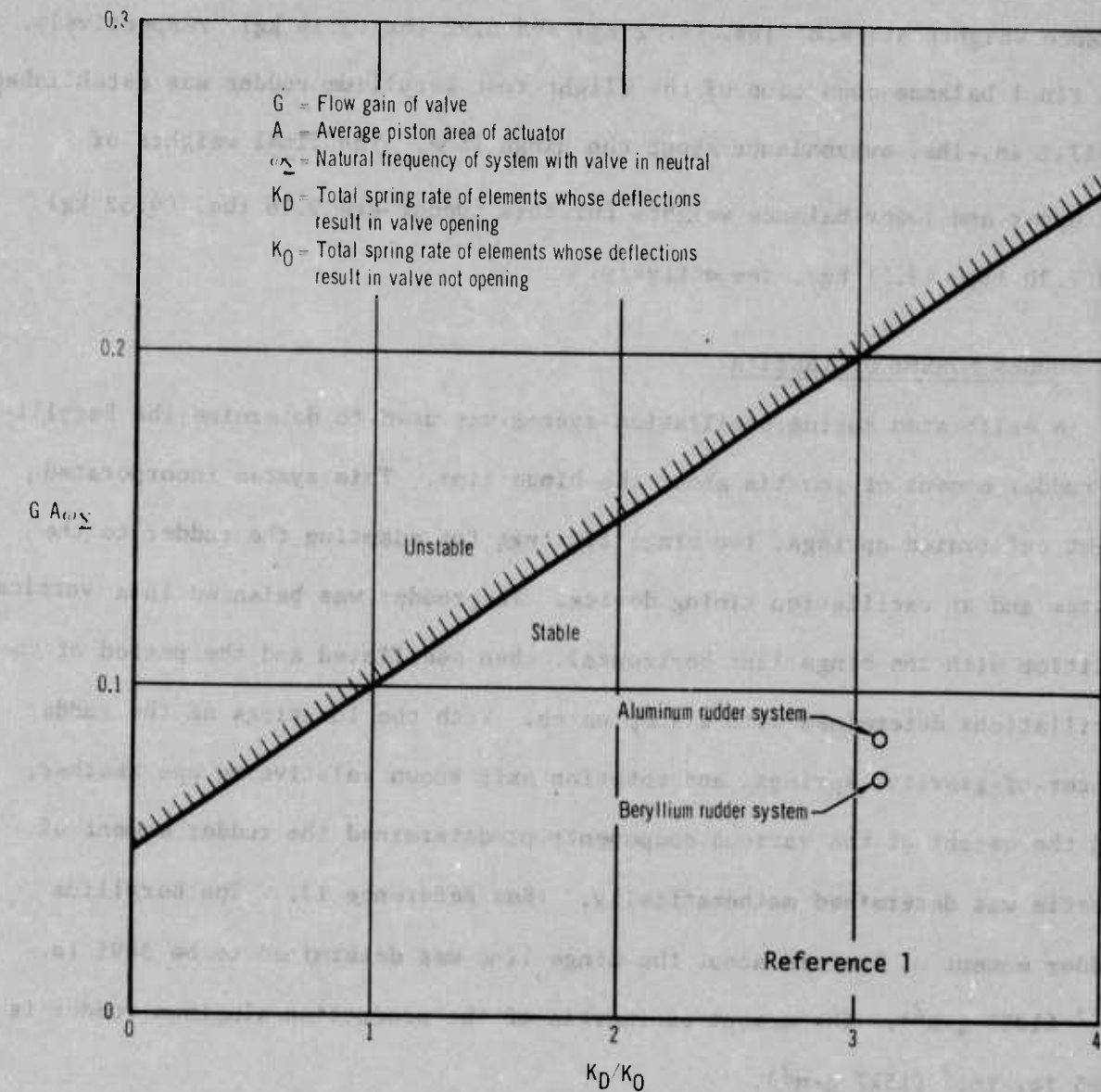


Figure 27 – Beryllium Rudder Power Cylinder Stability

balance weights are 8.87 lbs. (4.02 kg) and 6.92 lbs (3.14 kg), respectively. The final balance condition of the flight test beryllium rudder was established as 17.1 in.-lbs. overbalance about the hinge line. The final weights of the upper and lower balance weights for this rudder are 9.96 lbs. (4.52 kg) and 7.30 lbs. (3.31 kg), respectively.

8. RUDDER MOMENT OF INERTIA

A calibrated spring oscillation system was used to determine the Beryllium rudder moment of inertia about the hinge line. This system incorporated eight calibrated springs, two hinge fittings for adapting the rudder to the system and an oscillation timing device. The rudder was balanced in a vertical position with the hinge line horizontal, then oscillated and the period of the oscillations determined with a stop watch. With the locations of the rudder center-of-gravity, springs, and rotation axis known relative to one another, and the weight of the various components predetermined the rudder moment of inertia was determined mathematically, (See Reference 1). The Beryllium rudder moment of inertia about the hinge line was determined to be 3491 lb.-in.² (1021 g-m²). The moment of inertia of the production aluminum rudder is 5185 lb.-in.² (1517 g-m²).

9. RUDDER WEIGHT

Table 4 provides a weight breakdown of both the Beryllium rudders and the production aluminum rudders. As shown, the primary structure weights of the two Beryllium rudders are nearly equal with the flight test rudder being 0.23 pounds (0.104 kg) lighter. Even the heavier Beryllium primary structure provides a weight savings of 30% over the aluminum primary structure. The total weight of the flight test rudder is 4.47 lbs. (2.02 kg) greater than

the ground test rudder as the result of the addition of sealant and paint to prevent corrosion, internal instrumentation required for tests, and the increase in balance weights required to offset this additional weight aft of the rudder hinge line. Both beryllium rudders profit from elimination of the upper flutter damper as well as the reduced balance weight requirements. The total weight saved as the result of berylliumizing the F-4 rudder is 41.5% for the ground test rudder and 34.6% for the flight rudder.

Item	Weights - Pounds (Kgs)		
	Flight Test Beryllium Rudder	Ground Test Beryllium Rudder	Production Aluminum Rudder
Front torque box assy.	11.19 (5.08)	11.06 (5.02)	16.74 (7.59)
Trailing edge assy.	6.20 (2.81)	6.39 (2.90)	10.23 (4.64)
Lower balance weight attachment assy.	4.18 (1.90)	4.35 (1.97)	4.26 (1.93)
External paint and sealant	1.28 (0.58)	0	1.23 (0.56)
Balance weights	17.26 (7.83)	15.79 (7.16)	23.90 (10.84)
Upper damper	0	0	7.90 (3.58)
Instrumentation	1.95 (0.88)	0	0
Total rudder weight	42.06 (19.08)	37.59 (17.05)	64.26 (29.14)

Table 4 - Weight Summary for F-4 Beryllium and Aluminum Rudders

SECTION III

RUDDER FABRICATION AND ASSEMBLY

1. Introduction

The purpose of this section is to acquaint the reader in general with the various processes and techniques used to produce the F-4 Beryllium rudders. The serious student of Beryllium hardware production techniques should read Reference 1 plus appropriate documents from the bibliography which provide very detailed information on equipment and procedures for producing reliable structures of Beryllium. All fabrication of the Beryllium rudders was accomplished at the McDonnell Douglas Corporation facilities in St. Louis, Missouri, which includes a specially equipped beryllium fabrication facility. Beryllium is hard, notch sensitive, relatively brittle and presents a toxic hazard; all of which contributes to limitation, or requires modification, of fabrication processes which can be used in the production of beryllium hardware. However, experience has shown that most fabrication processes can be satisfactorily used in Beryllium hardware fabrication with proper design and/or selection of tooling and adequate care in performing the actual operation. Secondary fabrication processes used in production of the Beryllium rudders include sawing, machining, drilling, countersinking, forming, chemical milling, adhesive bonding, installing mechanical fasteners, non-destructive inspection and assembly.

2. GENERAL SHOP PRACTICES

Beryllium and its compounds present a toxic hazard in that they are capable of inducing acute or chronic pathological changes in a number of human tissues.

Involved are the skin, eye, lungs and respiratory tract, and other internal structures. The exposure to airborne particles is more likely to occur during processing of material and fabrication of hardware. Adequate safety measures have been developed and published. The key is an air exhaust system, or equivalent, for collection of Beryllium dust wherever sawing, grinding, sanding or machining operations are performed. Such a facility using standard industrial hygiene procedures was used at MCAIR for fabrication of the Beryllium rudders.

The limited short transverse ductility creates a need for care in the handling and fabrication of Beryllium parts, particularly those made of material less than 0.030 inch (0.76 mm) thick. During manufacture of the Beryllium rudders several Beryllium parts were broken or cracked, and every one of these parts was less than 0.030 (0.76 mm) inch thick. Thicker material is much less susceptible to damage from mishandling and more tolerant to variations in manufacturing techniques.

The parts and the work surface should be kept clean since a foreign object between mating surfaces can create a high local bearing stress during fabrication resulting in part breakage. The use of scribe lines on Beryllium cannot be tolerated. Similarly, sharp objects such as metal chips capable of scratching the Beryllium should be kept clear since such surface defects are known to reduce strength and ductility.

3. SAWING BERYLLIUM

Sawing Beryllium sheet was accomplished with a DoAll Band saw using a

blade speed of 552 feet per minute (2.80 meter/second) and feeding by hand. The material being sawed must remain in direct contact with the saw table at the blade throughout the operation to reduce vibration and chatter. For large sheets a foot-like support was added to the saw table against which the sheet rested solidly to minimize vibration and chatter. Since there may be some chipping and microcracking along the sawed edge, approximately 1/8 inch excess material was allowed on the sawed edge for clean-up by finish machining. Only four parts of over three hundred produced for the Reference 1 program cracked during sawing.

4. MACHINING BERYLLIUM

All Beryllium part blanks were reduced to finished dimensions by machining on a vertical milling machine. The use of adequate support along with a special square end master mill cutter, relatively low feed and cutter speed rates, and small depths of cut ranging from 0.050 inch (1.25 mm) to 0.001 inch (0.025 mm) for the last cut resulted in successful machining of the Beryllium parts. Stack milling of 3 to 6 parts resulted in a considerable reduction of machining time where possible. Figure 28 shows tools used to machine, drill and counter-sink Beryllium

5. DRILLING BERYLLIUM

Drilling defects which are cause for Beryllium part rejection are: (1) delaminations, (2) spalling and (3) cracking. Special equipment, tools and procedures are required to consistently drill good holes in Beryllium. The Tornetic driller provides positive control of torque and speed to remove material at the most efficient rate. Special carbide drills such as shown in Figure 28 permit clean, accurate removal of material so long as they remain sharp and the point is not rounded. Care to prevent the work piece from moving

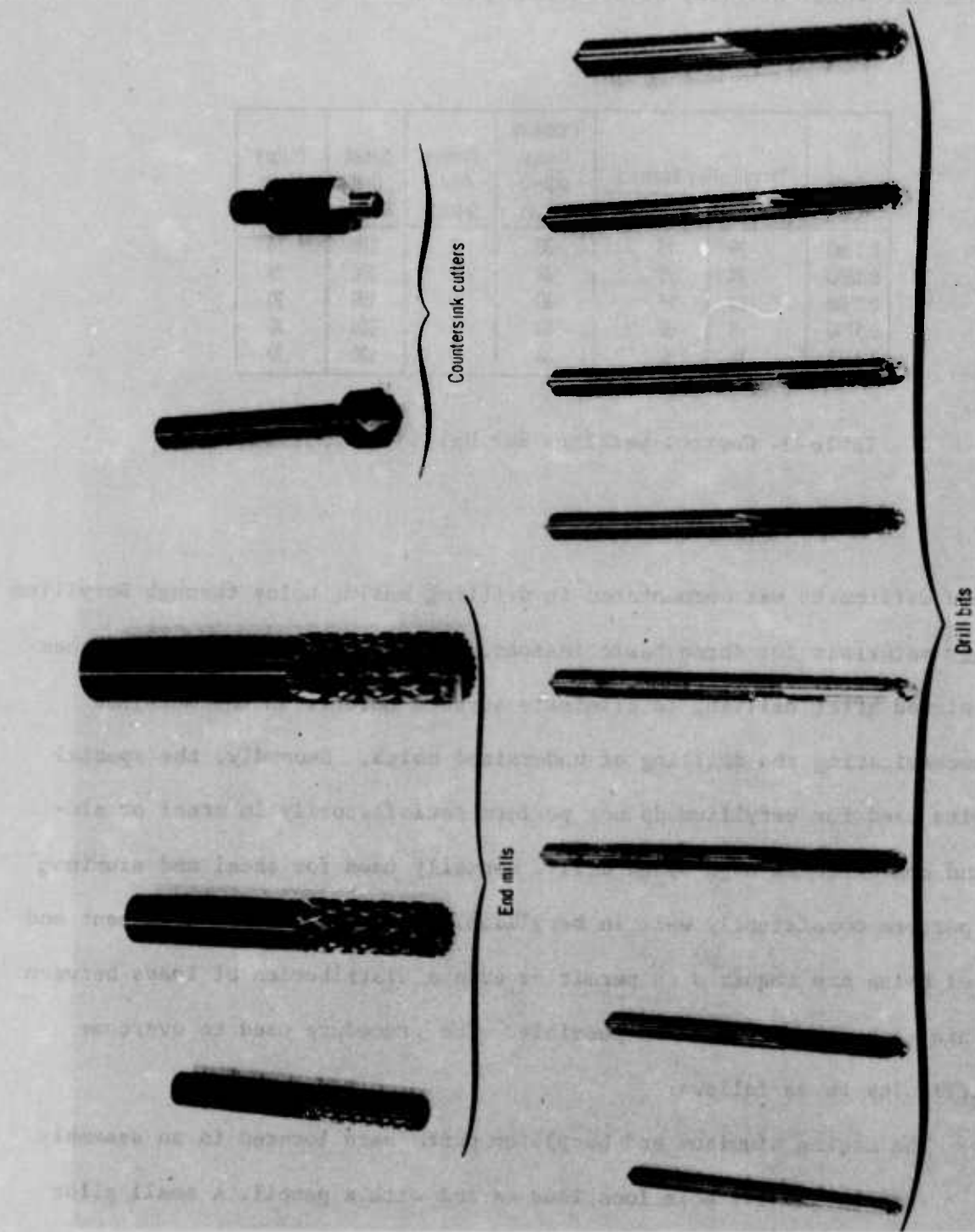


Figure 28 - Tools Used to Machine, Drill and Countersink Beryllium

during drilling along with control of speed and feed as indicated in Table 5 permitted successful drilling of Beryllium parts.

Drill Dia.	Drive Pulley Numbers		Pressure Gauge Setting (psig)	Torque Dial Setting	Speed Dial Setting	Torque Meter Reading
	Motor	Spindle				
0.1250	29	24	30	20	100	10
0.1890	24	29	30	20	100	20
0.2500	24	29	30	20	100	20
0.3750	16	36	30	40	100	20
0.4375	16	36	30	40	100	20

Table 5- Control Settings For Drilling Beryllium

Some difficulty was encountered in drilling mating holes through Beryllium and other materials for three basic reasons. First, Beryllium has to be chemically etched after drilling to eliminate surface defects on the machined edges necessitating the drilling of undersized holes. Secondly, the special drill bits used for beryllium do not perform satisfactorily in steel or aluminum and conventional high speed drills normally used for steel and aluminum do not perform consistently well in beryllium. Thirdly, precise alignment and sizing of holes are required to permit as even a distribution of loads between and within each fastener hole as possible. The procedure used to overcome this difficulty is as follows:

The mating aluminum and beryllium parts were located in an assembly fixture and all hole locations marked with a pencil. A small pilot

hole was drilled through all parts using a conventional carbide twist drill in a portable air motor on the Tornetic driller. The pilot hole was drilled small enough ($1/2$ the final hole size) so that any defect introduced in the Beryllium would be removed in final drilling and etching. After all fastener holes were pilot drilled, the parts were disassembled and the holes in the aluminum parts were conventionally drilled to final size. The holes in the beryllium were then drilled to full size (less allowance for chemical etching) using the special equipment and procedures described previously.

Yet spalling occurred at a number of beryllium holes and rough edges were removed by hand sanding with 180-400 emery paper or redrilled oversize to remove the spalled area prior to final etching. In the latter case an oversized repair fastener was used. No parts were rejected because of defective holes.

Less difficulty was experienced with drilling holes when mating beryllium parts, with fewer than 2% of such holes found defective. The only real problem was cracking believed to have resulted from the lack of adequate backup during drilling.

Although spalling was always immediately evident, delaminations were usually not evident until after chemical etch. When redrilling for a repair fastener after final etch, it was necessary to locally etch the redrilled hole using a felt rod or 'Q'-Tip. Such a salvage procedure leave the hole oversize and out of round and is not suitable for highly loaded joints where all fasteners must be fully effective to develop the joint strength.

6. COUNTERSINKING BERYLLIUM

Countersink recesses in Beryllium for flush fasteners were machined using a conventional stop countersink with a carbide cutter such as shown in Figure 28. The machining was accomplished by hand feed in a drill press with a cutter speed of 1115 rpm. A piloted backup was used to avoid dimpling. Approximately 50 countersink recesses for 5/32 or 3/16 flush fasteners could be machined before the cutter had to be sharpened. As discussed in Section II.2, the depth of countersink for flush fasteners must be at least 0.015 inch (0.381 mm) less than the thickness of the material to avoid a knife edge at the base of the countersink. In addition, the edge of the hole at the fastener head-to-shank fillet radius must also be chamfered to prevent interference which can damage the Beryllium or prevent seating of the fastener. Such chamfering can be done with a 45° micrometer stop countersink prior to final etch.

7. FORMING BERYLLIUM

Forming was accomplished in a 500 ton hydraulic press with electrically heated platens used to heat the forming dies to the desired $1325^{\circ} \pm 25^{\circ}\text{F}$ ($990^{\circ} \pm 14^{\circ}\text{K}$) temperature. Temporary tooling of machined H-13 steel mated dies were used for Beryllium forming. Two of the rudder ribs were formed with jogged flanges, with no modification to the forming procedure, using dies with jogged faces. Joggle length was ten times joggle depth.

In addition to temperature, critical factors for forming Beryllium are the minimum bend radius of $5t$ (5 times material thickness) and the forming rate no greater than 0.15 inch per minute (3.81 mm/minute). No spring back allowance was made and a dwell time of 15 minutes with the die closed was

allowed to accomplish stress relief. After forming larger parts and turning off the heating elements, the parts were allowed to cool in the die to prevent distortion and warpage. Parts less than 12 inches (30.5 cm) were removed from the die immediately after stress relief and allowed to air cool without excessive distortion. Oxidation of the Beryllium which occurred during forming was removed by liquid honing with a slurry containing Burr-Al-220 aluminum oxide abrasive at an air pressure of 60-80 psi (413,000-551,000 N/m²).

8. CHEMICAL MILLING BERYLLIUM

A 10% sulfuric acid (by volume) solution was used for chemical milling and etching of all Beryllium parts for this program. With a metal removal rate of 0.008 inch per minute (0.203 mm/minute) and a maximum metal removal from a surface by chemical milling of 0.080 inch (2.03 mm) the specified tolerance of 0.001 inch (0.025 mm) was achieved in all cases. Chemical etching 0.0015-0.0025 inch (0.038-0.063 mm) per surface was required on every Beryllium surface to remove any microscopic surface cracks or mechanical twins that may have been introduced during machining.

9. JOINING BERYLLIUM

The key to successfully joining Beryllium to itself or to other materials is the minimization of localized high stresses and a relatively even distribution of stress throughout the joint. Both adhesively bonded and mechanically fastened joints were used extensively in fabricating the Beryllium rudders. Design of such joints is discussed in Section II.2, and hole preparation for mechanical joints discussed in Sections III.5 and III.6 above. This section will highlight those production steps necessary to accomplish satisfactory adhesively bonded and mechanically fastened joints as practiced in fabrication

of the F-4 Beryllium rudders.

a. ADHESIVE BONDING

Bonding materials and procedures used for Beryllium are essentially the same as used to bond aluminum. The honeycomb aft torque box is a relatively complex structure which was bonded with FM-61 adhesive, a nitrile phenolic/epoxy film. Figure 29 shows the structural details of this assembly. The face skins, doublers and edging members are Beryllium. The non-perforated honeycomb core is 5052-H39 aluminum with 1/4 inch cell size and 0.001 inch foil thickness, the same as used on the production rudder.

Bonding should occur within 24 hours after final chemical etch providing the parts are protected from contamination during this time. Otherwise, a light chemical etch to remove 0.0005 inch (0.0013 mm) from the surface is adequate for cleaning the Beryllium prior to bonding. After cleaning, all surfaces to be bonded except the honeycomb core were treated with an epoxy resin primer (coupling agent, air dried for 30 minutes, and oven dried at 230°-240°F (384°-389°K)). The parts were then assembled on a contoured base with the FM-61 adhesive film between all faying surfaces. The assembly was then placed in a vacuum bag and compressed when the bag pressure was reduced to approximately 10 inches of mercury (33,770 N/m²). While maintaining the vacuum condition, the assembly was placed in an autoclave. Autoclave pressure was increased to approximately 25 psig (172,500 N/m²) and the vacuum bag vented to atmospheric pressure. Temperature in the autoclave was raised to 330°-345°F (438°-447°K) and maintained for one hour before the assembly was allowed to cool while autoclave pressure was maintained.

b. MECHANICAL FASTENERS

The foremost consideration in selection of mechanical fasteners

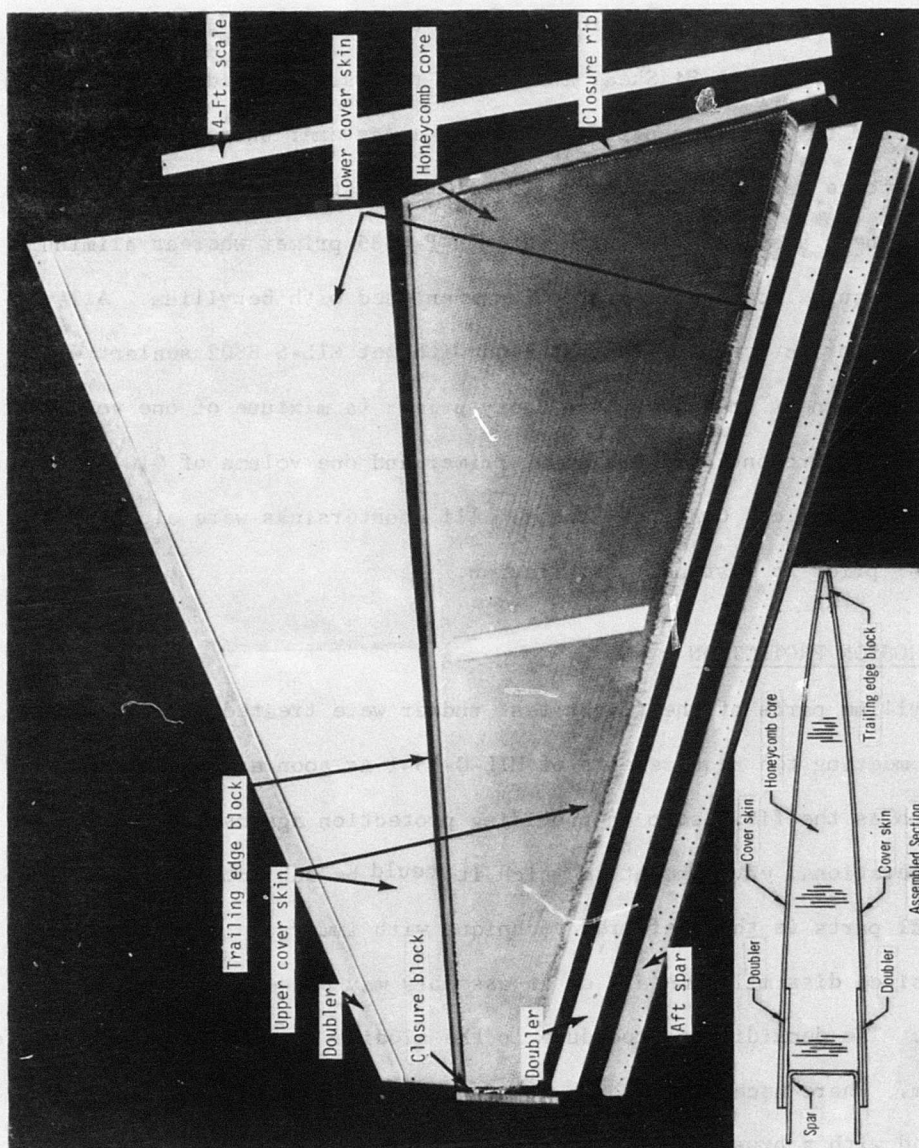


Figure 29- Rudder Trailing Edge Assembly Structural Details

for the Beryllium rudder was that no vibration driven fasteners were to be used in the structure. Over 700 mechanical fasteners were installed in each rudder including Hi Shear rivets, Hi Loks, Jo Bolts and Cherry rivets. Figure 30 shows the front torque box detail parts which were assembled entirely with mechanical fasteners. In addition, the aft torque box was joined to this forward torque box with Hi Shear and Cherry rivets. Individual fasteners were selected to insure proper fit: i. e. the fastener snugly filled the holes yet force was not required to insert the fastener. On interior surfaces, steel fasteners are installed with wet MIL-P-8585 primer whereas aluminum fasteners require no organic protection when used with Beryllium. All permanent exterior fasteners were installed with wet MIL-S-8802 sealant with removable fasteners coated with an epoxy primer (a mixture of one volume of 515-006 Super Koropon Fluid Resistant Primer and one volume of 910-117 Activator-DeSoto Chemical Coatings, Inc.). All countersinks were alodined per MIL-C-5541 prior to fastener installation.

10. CORROSION PROTECTION

Beryllium parts of the flight test rudder were treated with an alodine solution meeting the requirements of MIL-C-5541 as soon as possible after final etch as the first step in providing protection against the corrosive saline operational environment to which it could be subjected. Immersion of individual parts is the preferred technique with immersion of assemblies avoided since dissimilar metals on an assembly may cause corrosion when in solution. The deoxidizing procedure in the alodine process is prohibited for Beryllium. Where necessary, touch-up of inorganic treated Beryllium was accomplished with a brush applied alodine solution per MIL-C-5541. Aluminum metals in this assembly were also treated with the Alodine solution.

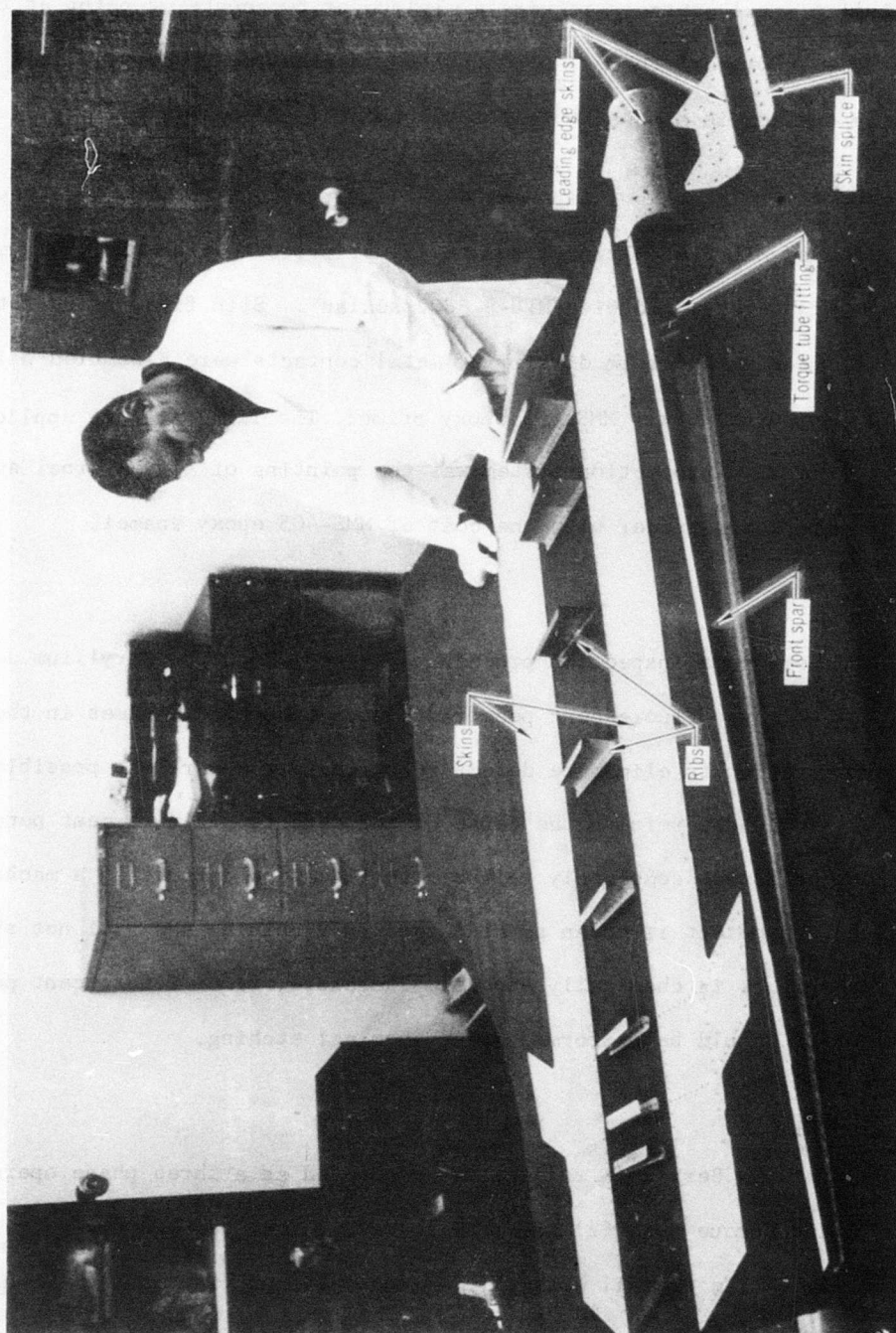


Figure 30 - Rudder Front Torque Box Beryllium Detail Parts

Dissimilar metal contacts require a minimum of two coats of paint at the faying surface. However, the use of MIL-S-8802 sealant at the dissimilar metal faying surface is a substitute for the paint requirement.

Those Beryllium areas not exposed to the exterior environment were coated with two coats of MIL-P-8585 zinc chromate primer prior to assembly. All mold line butt joints were sealed with MIL-S-8802 sealant. Slip fits, press fits and threaded inserts that form dissimilar metal contacts were assembled using wet MIL-P-8585 primer or wet MMS-405 epoxy primer. The final step in application of the corrosion protection system was the painting of all external surfaces of the completed rudder with one coat of MMS-405 epoxy enamel.

11. INSPECTION

Standard aerospace inspection procedures were used on the Beryllium detail parts and assemblies. Fluorescent penetrant inspected several times in the course of fabrication to eliminate defective parts at the earliest possible time, and to aid in determining the cause of the defects. Fluorescent penetrant inspection is not completely reliable for locating defects on a machined surface since the defect is often smeared over in machining and will not show up until the surface is chemically etched. Therefore, final fluorescent penetrant inspection should be performed after chemical etching.

12. RUDDER ASSEMBLY

Assembly of the Beryllium rudders was conducted as a three phase operation: (1) assemble aft torque box, (2) assemble forward torque box and (3) mate the two assemblies. While overall assembly was accomplished with what was considered minor difficulty, there were problems including damaged parts which re-

quired repair or replacement. The nature of such damage will be discussed for both the ground and flight test Beryllium rudders along with a brief description of the corrective action taken for each. The reader interested in more specific details on extent of damage, detailed repair procedures and/or tests conducted to verify the reliability of the repair should consult References 1 and 2. Suffice it to say here that the Beryllium rudders are not perfect examples of production infallability, but are examples of realistic hardware on which production difficulties have arisen and been overcome by parts replacement or repair as required. The reliability of the repair techniques used are best illustrated by demonstrated structural integrity of the completed assemblies under simulated and actual flight test conditions.

After fabrication, excluding drilling of fastener holes, the detail rudder parts were assembled in the assembly fixture using clamps as shown in Figure 31. This was accomplished to determine the need for any final machining or shimming to insure proper fit of the various parts and to locate and pilot drill fastener holes. After disassembly, the fastener holes and countersinks were drilled to size, less allowance for final etch of the Beryllium parts. Following this drilling operation all Beryllium parts underwent chemical etching and fluorescent penetrant inspection. Four cracked members (2 ribs and 2 doublers) uncovered in this inspection were replaced.

After inspection of the various parts, the aluminum honeycomb core, Beryllium skins, aft spar and edging members shown in Figure 29 were cleaned and bonded together as previously discussed in Section III.9.a to produce the trailing edge assembly shown in Figure 32. Upon completion of the bonding of the ground test rudder trailing edge assembly a crack was discovered in the

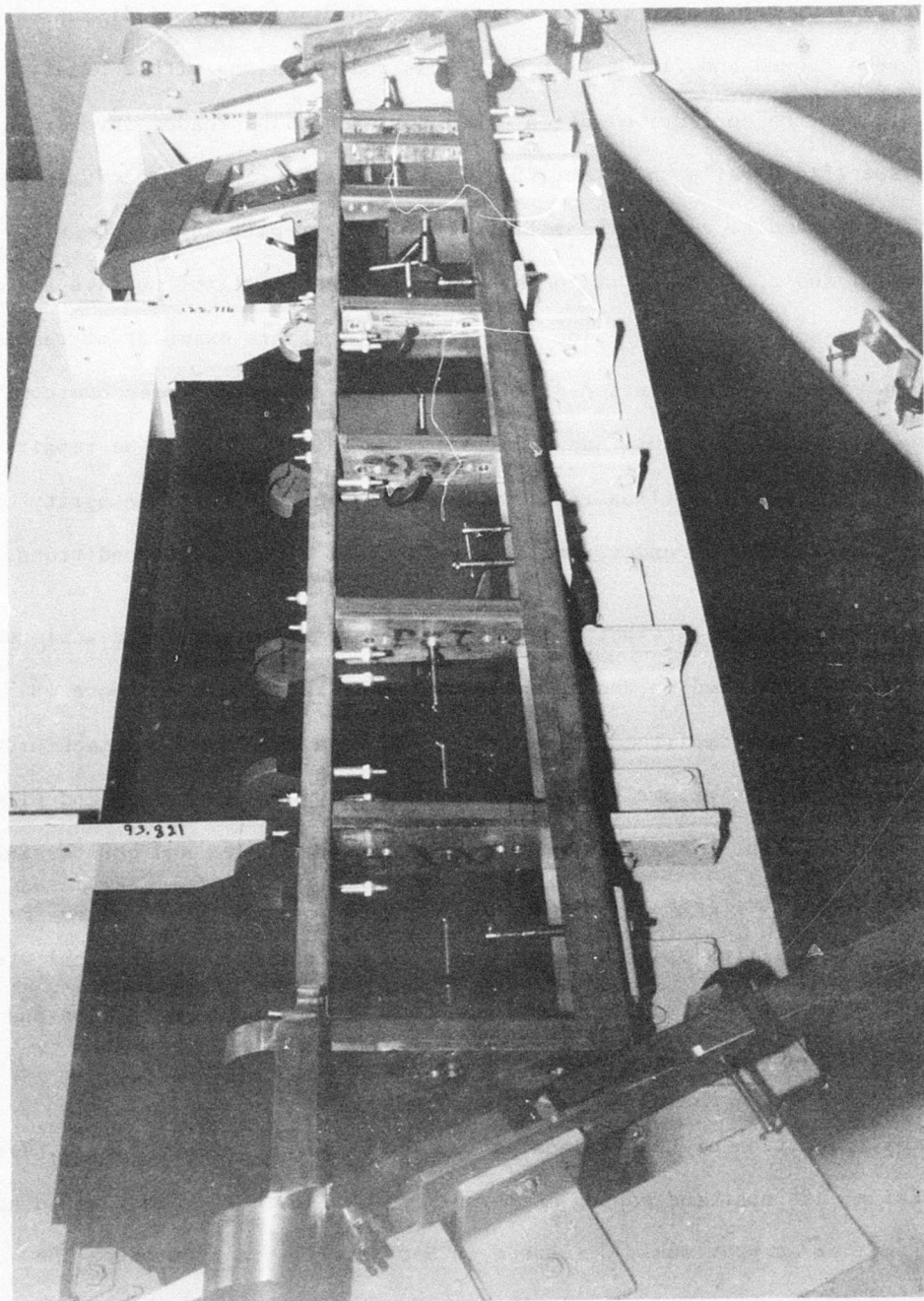


Figure 31 - Pre-Fit Assembly of Beryllium Rudder In Assembly Fixture

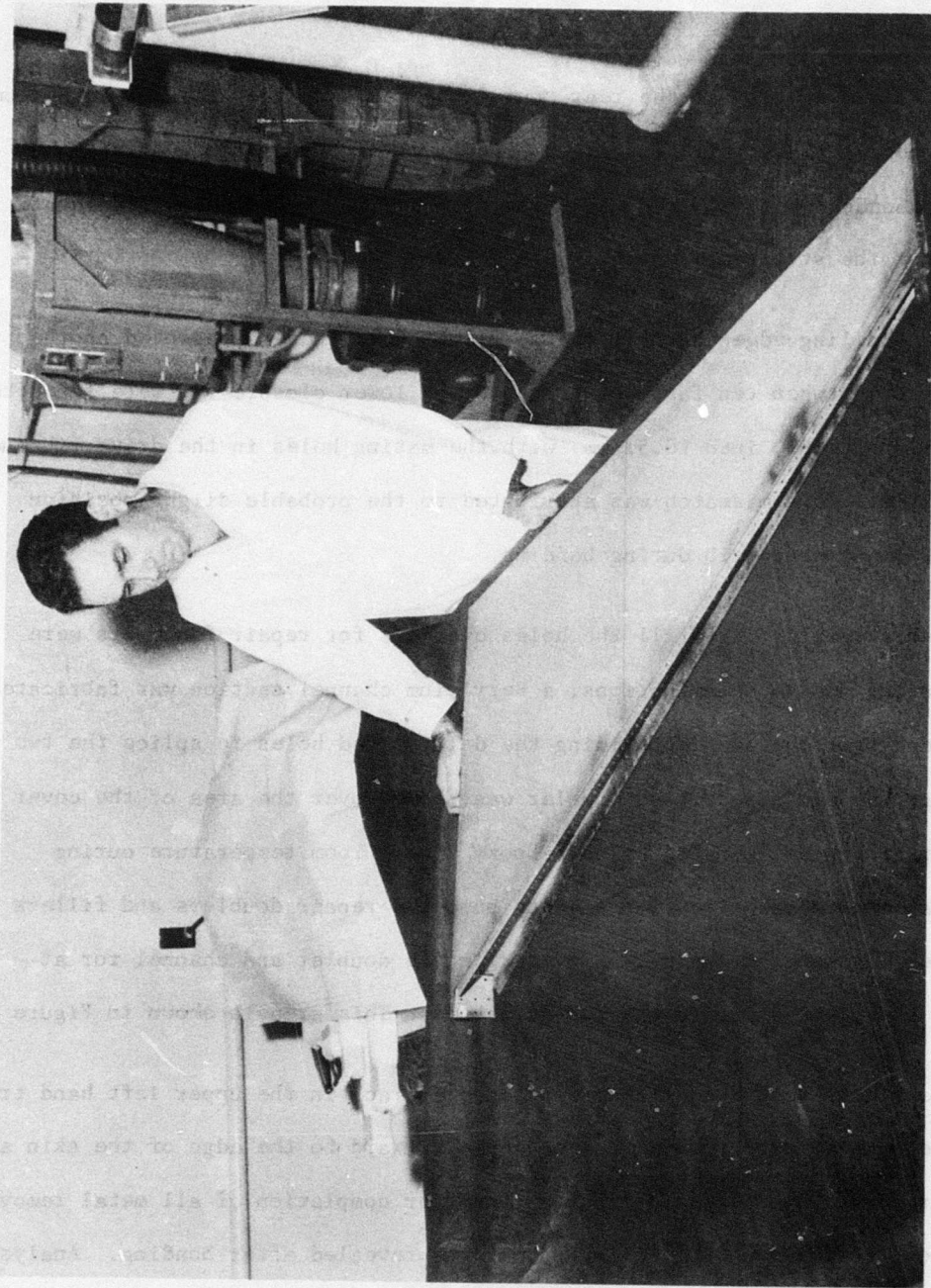


Figure 32 - Beryllium Rudder Bonded Trailing Edge Assembly

upper right cover skin at the rear spar. The cause of the crack could not be determined. Because this area of the rudder is lightly loaded, an external doubler bonded over the area of the skin containing the crack was adequate to restore the structural integrity of the assembly.

The trailing edge assembly of the flight test rudder presented another repair problem when ten fastener holes in the lower closure rib were found to be misaligned 0.020 inch (0.51 mm) with the mating holes in the drive rib and cover skins. This mismatch was attributed to the probable slight position shift of the closure rib during bonding.

When attempts to redrill the holes oversize for repair fasteners were unsuccessful due to delaminations, a Beryllium channel section was fabricated and bonded over the area containing the delaminated holes to splice the two ribs together and a Beryllium doubler was bonded over the area of the cover skin containing delaminated holes. Epoxy 934, a room temperature curing epoxy paste-type adhesive, was used to bond the repair doublers and fillers in place. Fastener holes were provided in the doubler and channel for attaching the cover skins to the sub-structure. This area is shown in Figure 33.

The flight test rudder also developed a crack in the upper left hand trailing edge skin running from a fastener hole forward to the edge of the skin at the rear spar. Dye penetrant inspection after completion of all metal removal operations revealed no such flaw, but it was revealed after bonding. Analysis indicated that this skin is not critically loaded, the skin is bonded with a doubler to the rear spar in the area of the crack, and the crack terminates in the drilled hole which precludes its propagation beyond that point. Accordingly, the skin was considered acceptable for use in the rudder assembly. No evidence of extension of this crack has been reported to date.

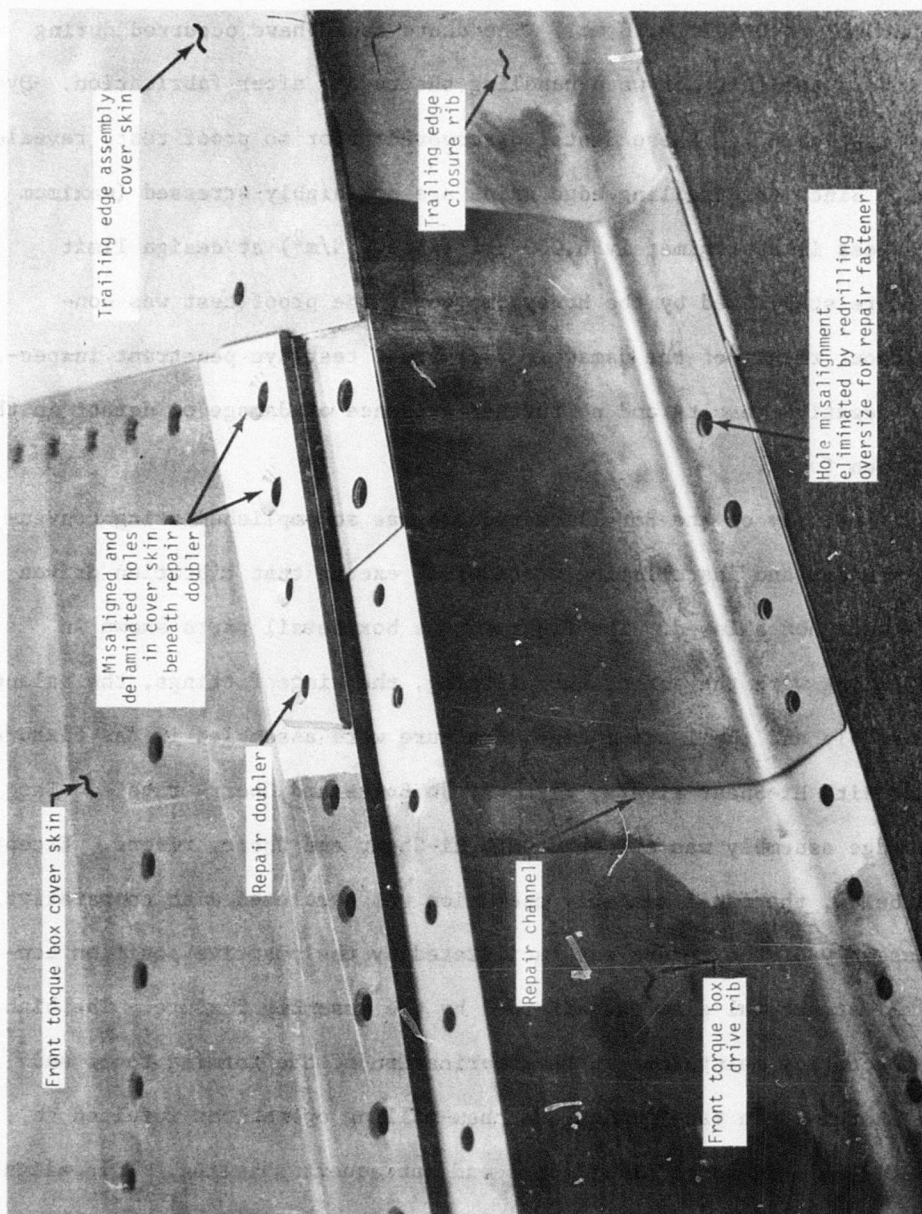


Figure 33 - Repair of Lower Closure Rib

Six small dents were found in the trailing edge cover skins of the flight test rudder, three on each side. These dents range in depth from 0.0015 inch (0.038 mm) to 0.007 (0.18 mm). The dents could have occurred during fabrication of the skins or when handling the rudder after fabrication. Dye penetrant inspection of these dents, discovered prior to proof test, revealed no cracks. Since the trailing edge skins are not highly stressed (maximum tensile stress is approximately 6,000 psi (41,300 N/m²) at design limit load) and are stabilized by the honeycomb core, the proof test was conducted without repair of the damage. Post proof test dye penetrant inspection gave negative results and no further evidence of damage or defect in this area has been found.

Final assembly of the Beryllium rudders was accomplished using conventional fasteners and installation procedures, except that vibration driven fasteners were not allowed. The front torque box detail parts shown in Figure 30 along with the torque tube fitting, the hinge fittings, the balance weight assembly and the leading edge structure were assembled in the fixture and joined with Hi-Shear rivets, Hi-Loks, Jo Bolts and Cherry rivets. The trailing edge assembly was attached with Hi-Shear and Cherry rivets. Except as noted below, the final assembly operation was completed with comparative ease. Assembly of the rudder was facilitated by the positive position control of all structural elements afforded by the assembly fixture. The high degree of accuracy maintained in the fabrication of the forming tools and the care exercised in the forming and chem-milling operations resulted in relatively little mismatching of parts and subsequent shimming. Hole alignment and subsequent fastener installation was accomplished with relatively little difficulty through use of the assembly fixture. Final assembly of the beryllium rudder in this fixture is shown in Figure 34.

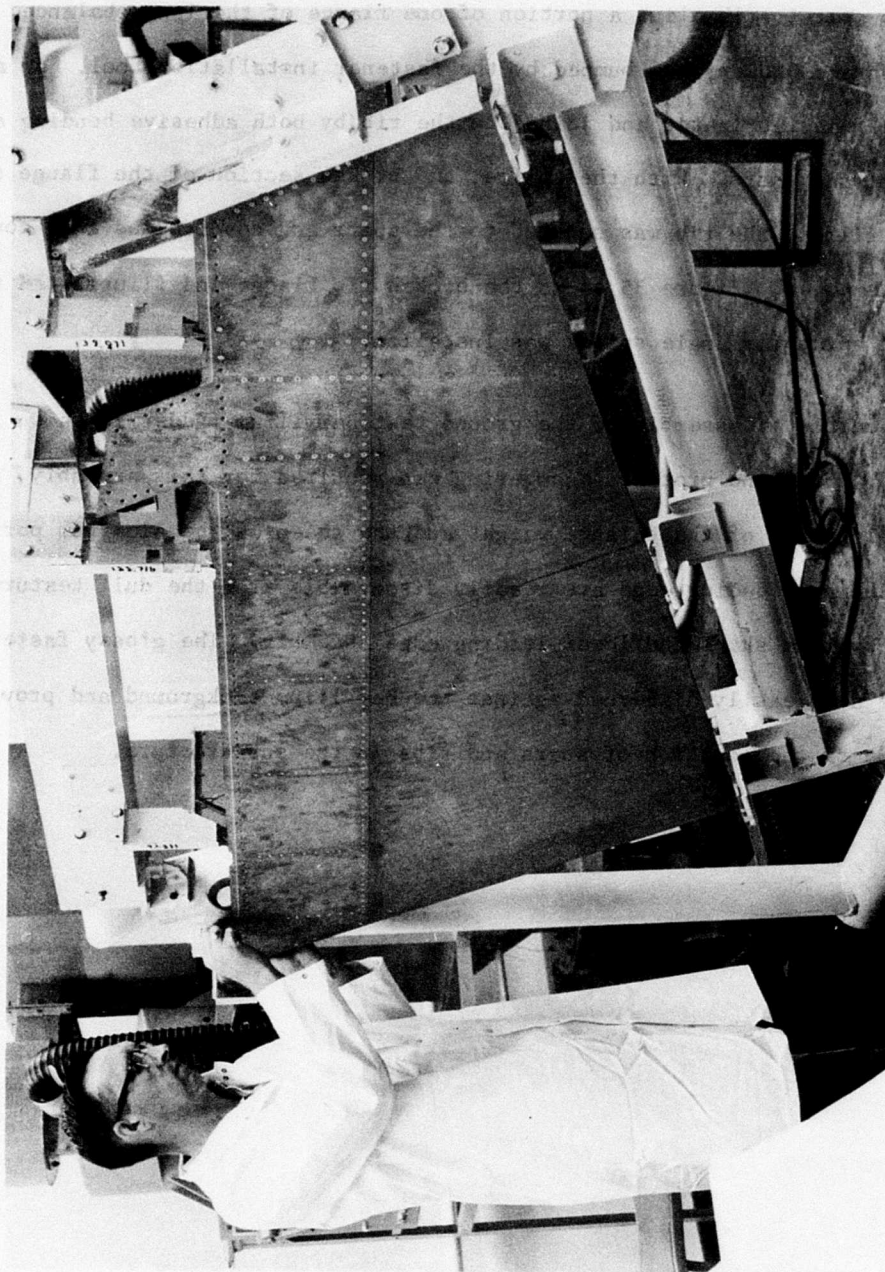


Figure 34 - Final Assembly of Beryllium Rudder

During assembly of the ground test rudder, while installing fasteners in the front spar-to-rib clip, a portion of one flange of the lower balance weight rib was broken when bumped by the fastener installation tool. An angle splice was fabricated and joined to the rib by both adhesive bonding and mechanical fasteners. With the splice, and broken section of the flange serving as a filler, the rib was secured to the spars and cover skins in a conventional manner. Figure 35 shows the broken rib flange and illustrated the manner in which the angle splice was installed.

The completed assembly of the ground test Beryllium rudder is shown in Figure 36. Since no protective covering was required for this assembly, the darker coloration of the balance weight and the sheen of the aluminum portion of the aluminum leading edge are readily discernible from the dull texture of the Beryllium skins and lower leading edge assembly. The glossy fastener heads are also easily discerned against the Beryllium background and provide an outline of the location of spars and ribs in the substructure.

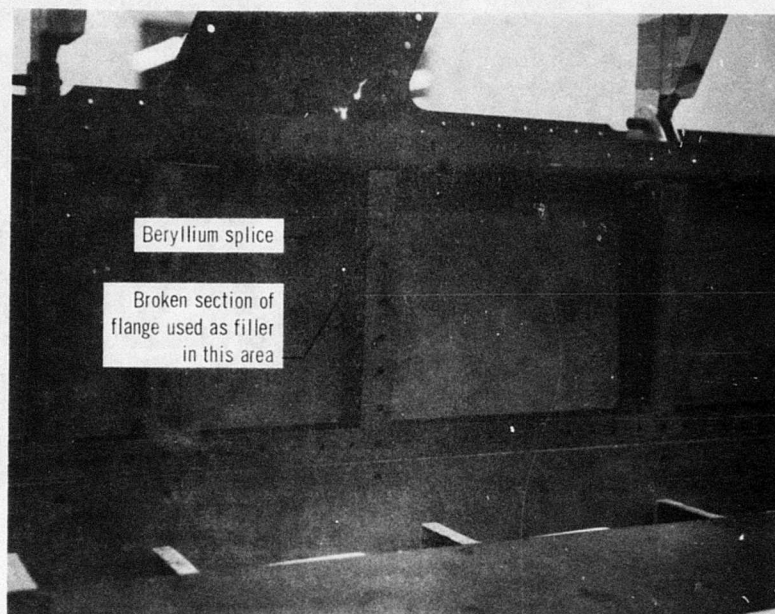
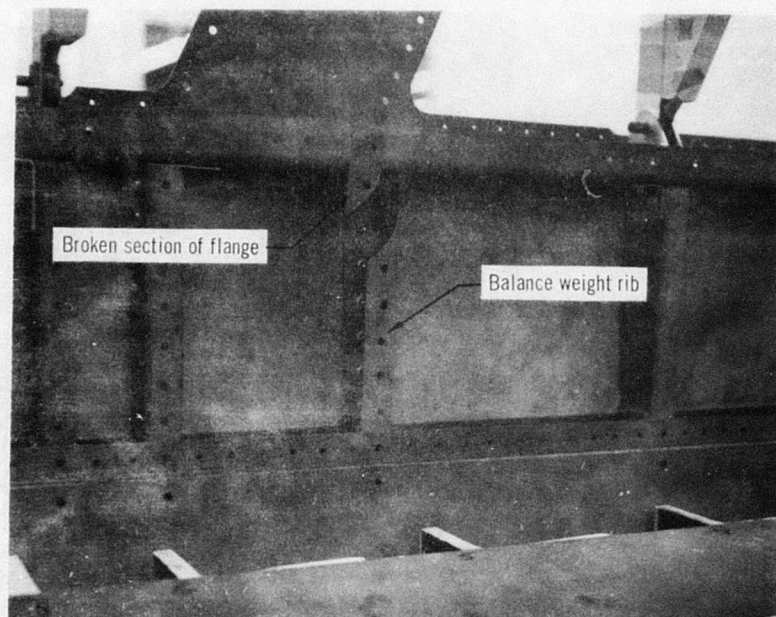


Figure 35 - Beryllium Rib with Broken Flange and Repair Splice

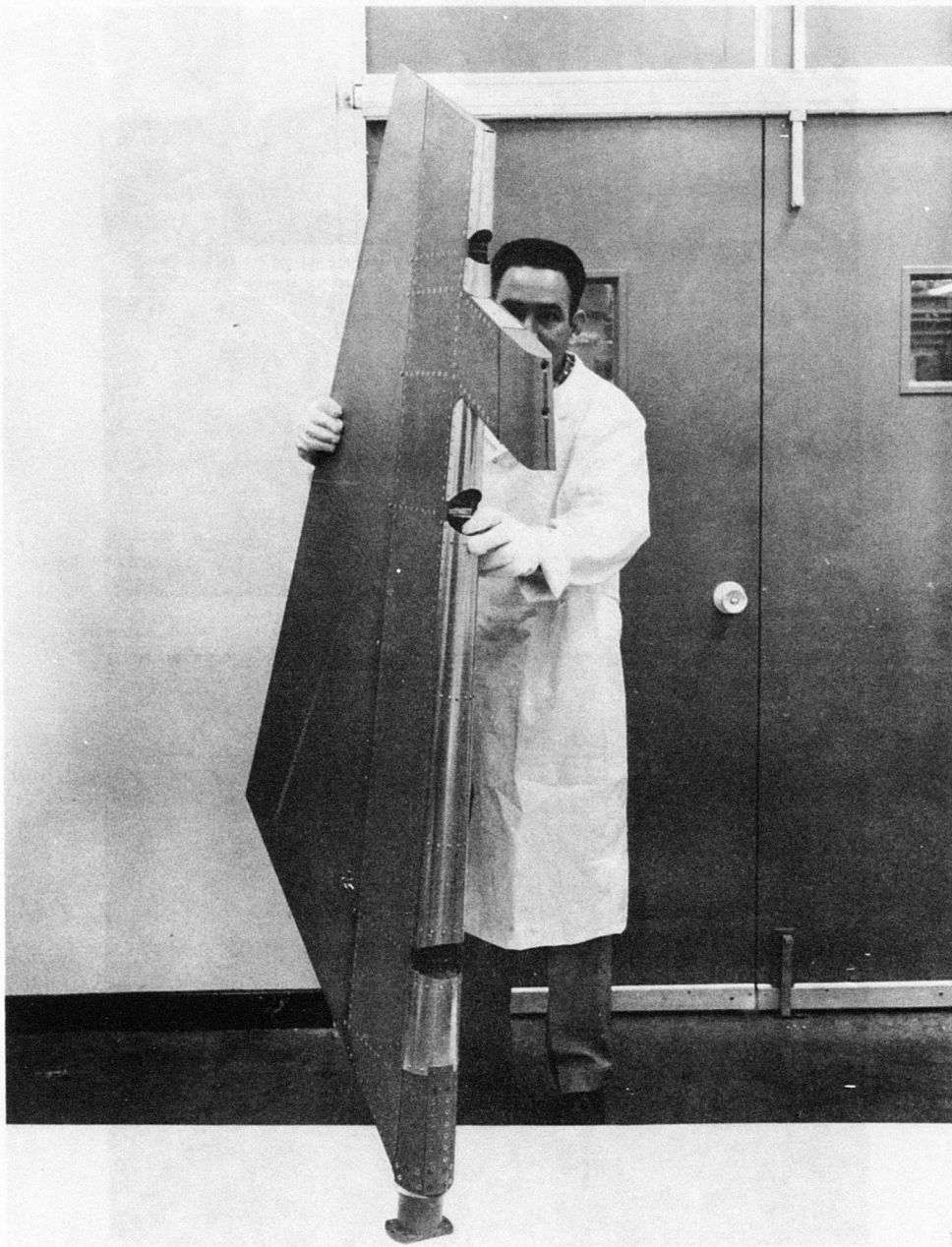


Figure 36 - Completed Beryllium Rudder Assembly

SECTION IV

FLIGHT QUALIFICATION TESTS

1. Introduction

The objective of the Beryllium rudder ground test program was to substantiate the structural integrity of the rudder assembly and qualify it for flight testing on the F-4 aircraft. Test conditions duplicated as nearly as practical the design loading conditions discussed in Section II including interaction between the rudder and the vertical fin-aft fuselage assembly. Prior to conducting tests on the assembled rudders, the mass balance was established and the moment of inertia was determined as discussed in Section II. Four ground tests were conducted by MCAIR, the first three to qualify the rudder design for flight test and the fourth to determine the actual static strength of the rudder. These tests are summarized below in chronological order.

° Test 1 was a fatigue test of the upper balance weight support structure. Mounted on a vertical fin-aft fuselage assembly, the rudder was subjected to 50,000 cycles of ± 40 g's inertial load on the upper balance weight perpendicular to the symmetry plane of the aircraft. One of the four aluminum Hi-Shear fasteners used for attaching the hinge fittings to the front spar flanges at hinge position $Z_R = 122.72$ failed at 28,275 cycles but no other damage occurred. The failed rivet was replaced with a steel Hi-Lok fastener and the required 50,000 cycles were attained with no further incident. A post test inspection did not reveal any damage to the Beryllium rudder assembly. After completion of this test the other three Hi-Shear fasteners in this area were replaced by Hi-Lok fasteners.

° Test 2 was a rudder design ultimate static test to Condition I loads, in which the rudder was subjected to 150% of maximum airload with the center of pressure at 30% chord, which produces the maximum torque that the rudder structure can sustain without overpowering the rudder actuator. This test represents the YAW flight condition and was completed with no apparent damage to the rudder.

° Test 3 was a design ultimate static test to Condition III loads, in which the rudder and vertical fin were subjected to 150% of maximum total load on the vertical tail, producing the maximum vertical tail bending and deflections and hence the maximum bending and shear in the rudder due to the compatibility between the rudder and fin structures. This test was completed with no apparent structural damage and the Beryllium rudder configuration was considered qualified for flight.

° Test 4 was a repeat of Test 2 except that the loads were allowed to increase beyond the 150% design limit load (DLL) condition to provide a direct comparison with the production aluminum rudder configuration which had previously sustained 225% DLL under this condition. This test was planned as an ultimate strength test and after approximately 205% DLL had been applied a crack appeared at the forward end of the lower closure rib. However, the load did not fall off and it was subsequently increased to 250% DLL (167% ultimate) and held for 30 seconds with no further visible damage. Test series was terminated in favor of other more useful tests.

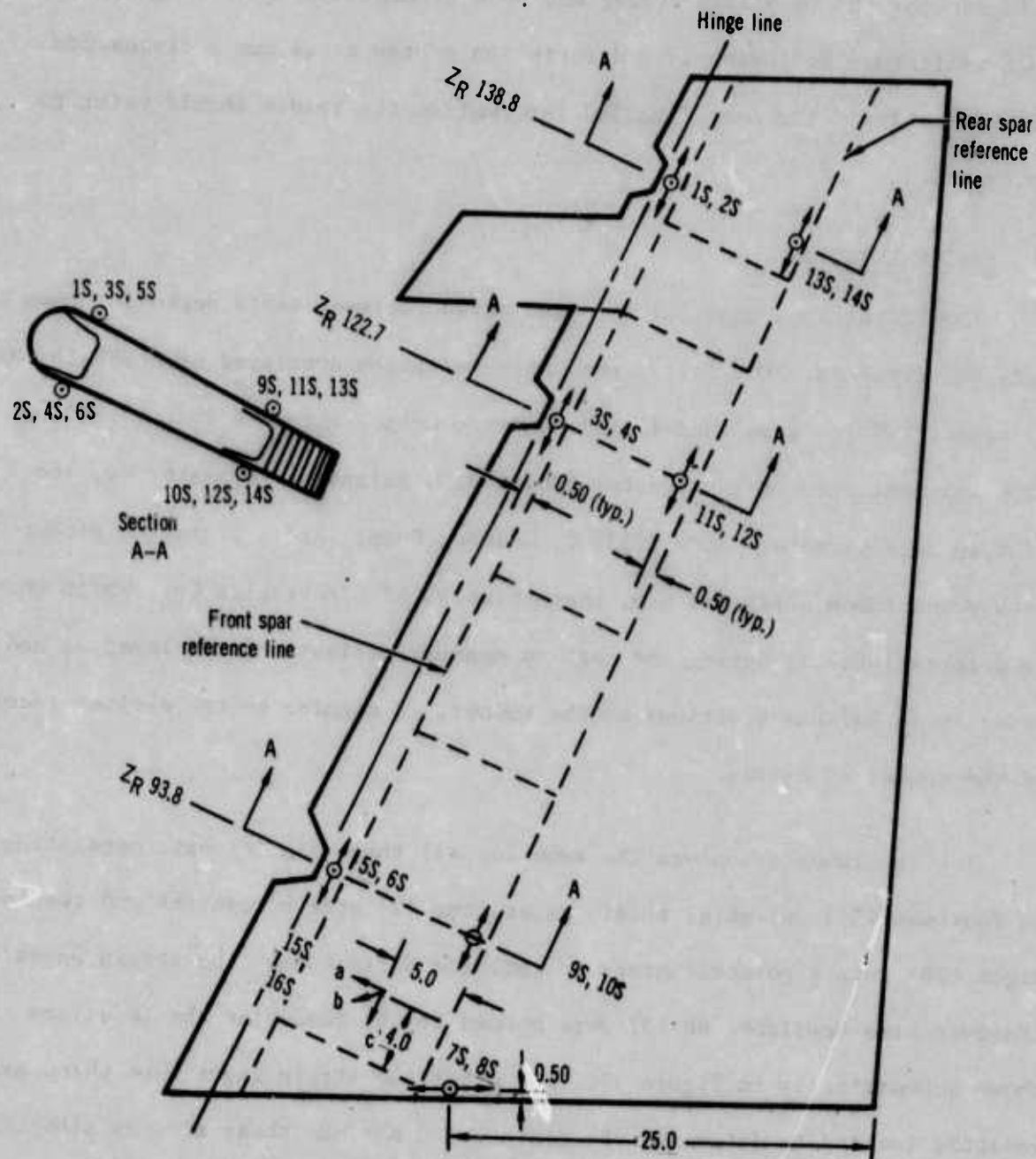
At the conclusion of this test series, which was more stringent than the one undergone by the production aluminum rudder, the structural

integrity of the beryllium rudder had been demonstrated and all goals had been realized. Following is a description of the tests and a discussion of the results. For more detailed information the reader should refer to Reference 1.

2. INSTRUMENTATION

The actual instrumentation in use varied between tests depending upon the data requirements. For Test 1 the instrumentation consisted of a 500 lb (2224 N) capacity force gage (Model 2103, Endevco Corp.) attached to the loading link and monitored on a voltmeter (Model 320, Balantine Laboratories, Inc.) plus an accelerometer (Model 2235 C, Endevco Corp.) and a vibration pickup with meter (Models 115 and M-6, respectively, MB Electronics Co.) which were used intermittently during the test to measure deflection, acceleration and velocity at various positions on the rudder. A counter on the exciter recorded the number of cycles.

The instrumentation was the same for all three static tests consisting of fourteen (14) uni-axial strain gages, two (2) strain rosettes and twenty-eight (28) rotary potentiometers to indicate deflection. The strain gages (Baldwin-Lima-Hamilton, AD-13) were bonded to the rudder at the locations shown schematically in Figure 37. The other two strain gages were three axis rosettes located to determine the maximum and minimum shear strains plus the angle of principal strain in the forward cover skins near the rudder actuator. The rotary potentiometers (deflection indicators) were mounted on a fixed frame and connected with the rudder at points as indicated on Figure 38. Details of this installation can be seen in Figure 39. Test data was recorded with the McDonnell Central Data Acquisition System.



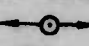
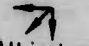
- Notes: 1. Instrumentation installed on both sides of rudder at locations indicated.
 2.  indicates axis of strain gages.
 indicates strain rosette.
 3. All instrumentation installed on rudder external surfaces.

Figure 37 - Beryllium Rudder Strain Gage Locations

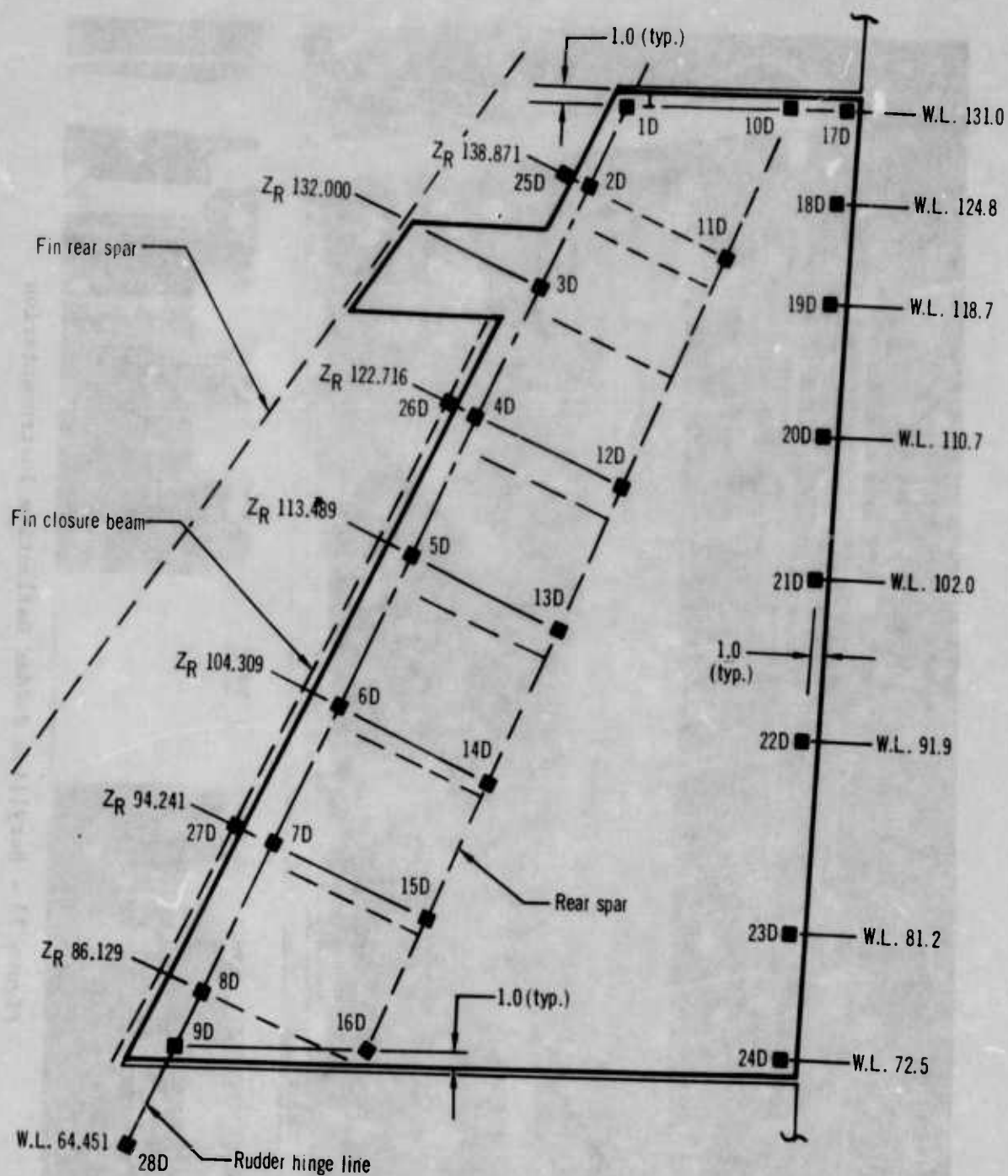


Figure 38 - Beryllium Rudder Deflection Point Locations

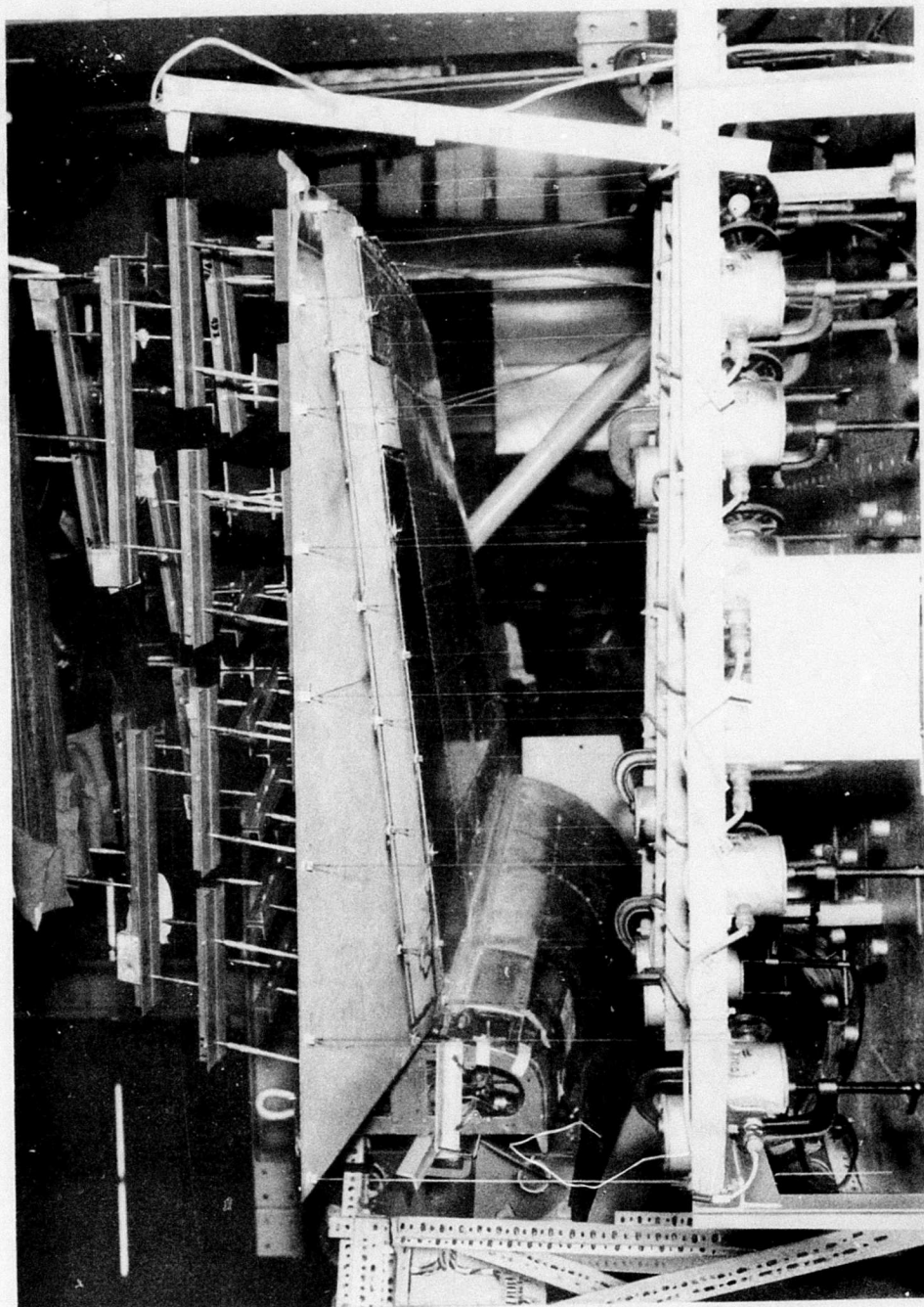


Figure 39 - Beryllium Rudder Deflection Instrumentation

3. TEST 1- FATIGUE TEST OF UPPER BALANCE WEIGHT SUPPORT STRUCTURE

The objective of this test was to demonstrate the structural integrity of the upper balance weight support structure for repeated inertial loading in accordance with the requirements set forth in Section II. The lower balance weight support structure is identical to the one previously qualified for production rudders and therefore did not require testing.

The set-up for the fatigue test is shown in Figure 40. The rudder was installed in a vertical fin-aft fuselage assembly with the fin in a horizontal position. Rudder hinge points were connected as in a normal service installation. The fuselage section was bolted to a fixed support at its forward end (fuselage station 515.00). Actuator backup stiffness was simulated by a torsion spring bolted to a support fixture and connected to the control horn attachment of the rudder. The exciter was connected by a loading link to the balance weight by bolting through a 1/4 inch (6.35 mm) hole drilled through the balance weight's center of gravity. To reduce inertial loads in the fin, it was restrained during the test with lead weights and a link attached to the tip of the fin and the platform supporting the exciter. The tension pads shown in Figure 40 had been installed for subsequent use in static testing the rudder, but were not used in the fatigue test.

A 5 cps (H_z) sinusoidal force, perpendicular to the symmetry plane of the aircraft and equal to 40 g's peak load, was applied to the rudder structure at the balance weight center of gravity. This force was applied for 50,000 cycles and was equal to 40 times 8.87 lbs. (4.02 kg) of balance weight; force=355 lbs (1579 N). The counter for recording the number of cycles was not activated until this peak load was reached as indicated by the force gage.

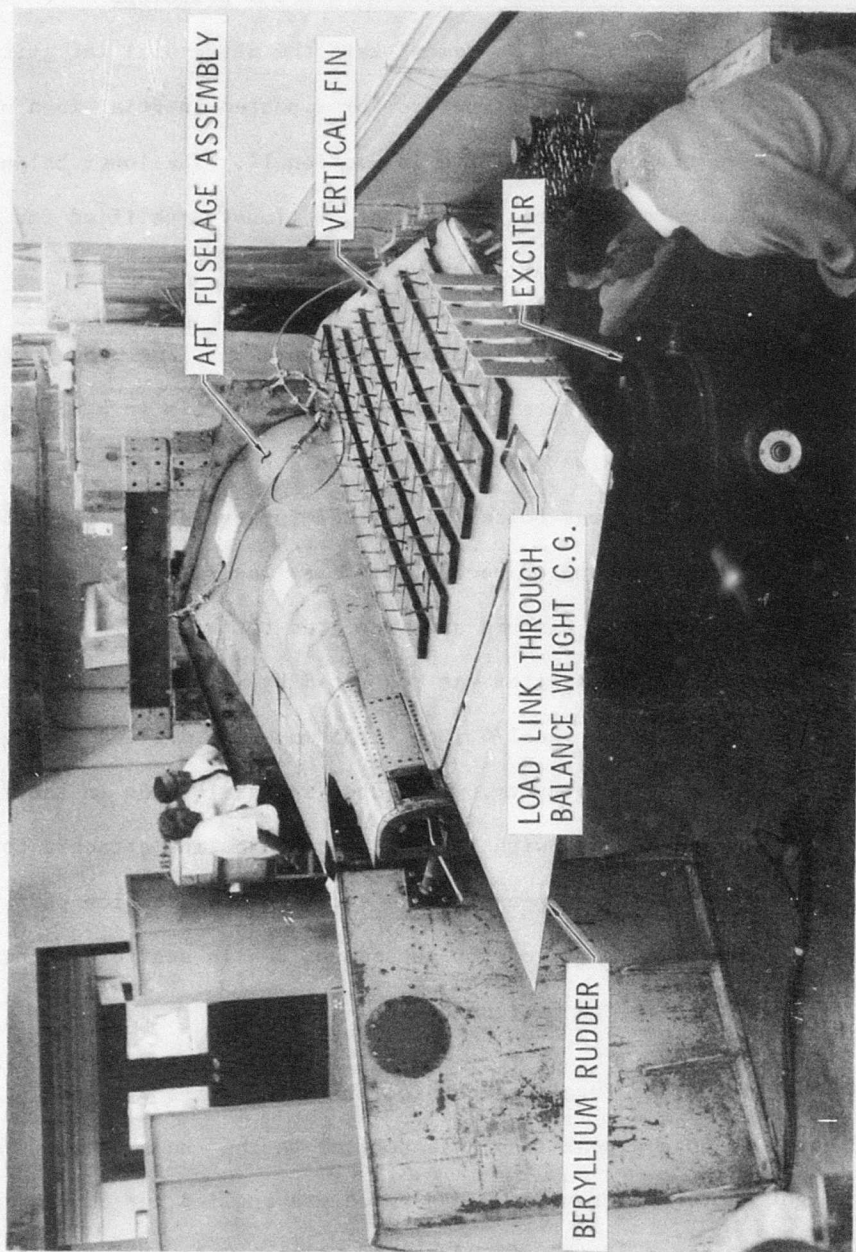


Figure 40 - Setup for Balance Weight Support Structure Fatigue Test

A loud sharp noise was heard and testing was immediately halted at 28,275 cycles. Examination showed the rudder structure to be unharmed except for failure of one of four aluminum Hi-Shear rivets used to attach the hinge fitting to the rudder spar flanges at station $Z_r=122.72$ (see Figure 13 for location). The fracture at a section in the collar retention groove probably resulted from the prying action of the test load which was reacted at that hinge. The failed rivet was replaced with a steel Hi Lok threaded fastener and testing was continued: the other three Hi Shear rivets at this hinge were similarly replaced after the test was completed. The required 50,000 cycles were attained with no further incident. A post-test inspection did not reveal any damage to the Beryllium rudder assembly.

4. TEST 2- RUDDER ULTIMATE STATIC TEST WITH MAXIMUM AIRLOAD AT 30% CHORD

The objective of this test was to demonstrate the structural integrity of the rudder structure under airloads producing the full available actuator hinge moment with the airloads center of pressure at 30% chord. The test loads simulated the loads of Design Condition I, described in Section II, and were carried to ultimate (150% of limit). Loading conditions are critical for all of the rudder structure aft of the front spar, except the forward torque box cover skins and the backup ribs for the hinge fittings.

The test set-up for this and the following two static test described in this section is shown in Figure 41. The installation of the rudder onto the vertical fin-aft fuselage assembly remained the same as for the fatigue test, except that a fixed length jig assembly simulating the actuator was installed between the rudder and fuselage to maintain the rudder in neutral position during the test. The aft fuselage assembly was cantilevered from a fixture, shown in Figure 42 at fuselage station 515.00. Neoprene rubber tension pads

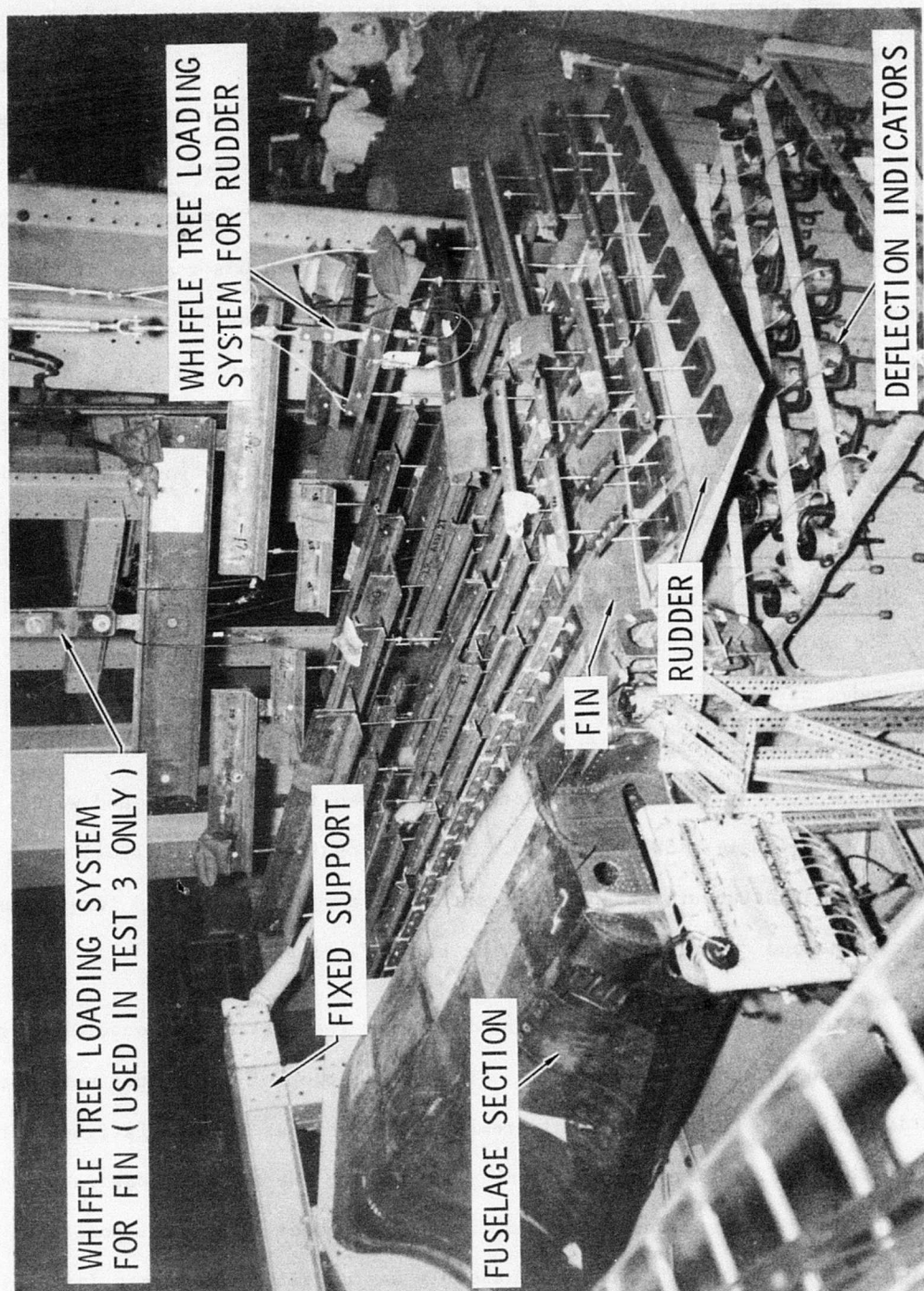


Figure 41 - Setup for Static Tests of Beryllium Rudder

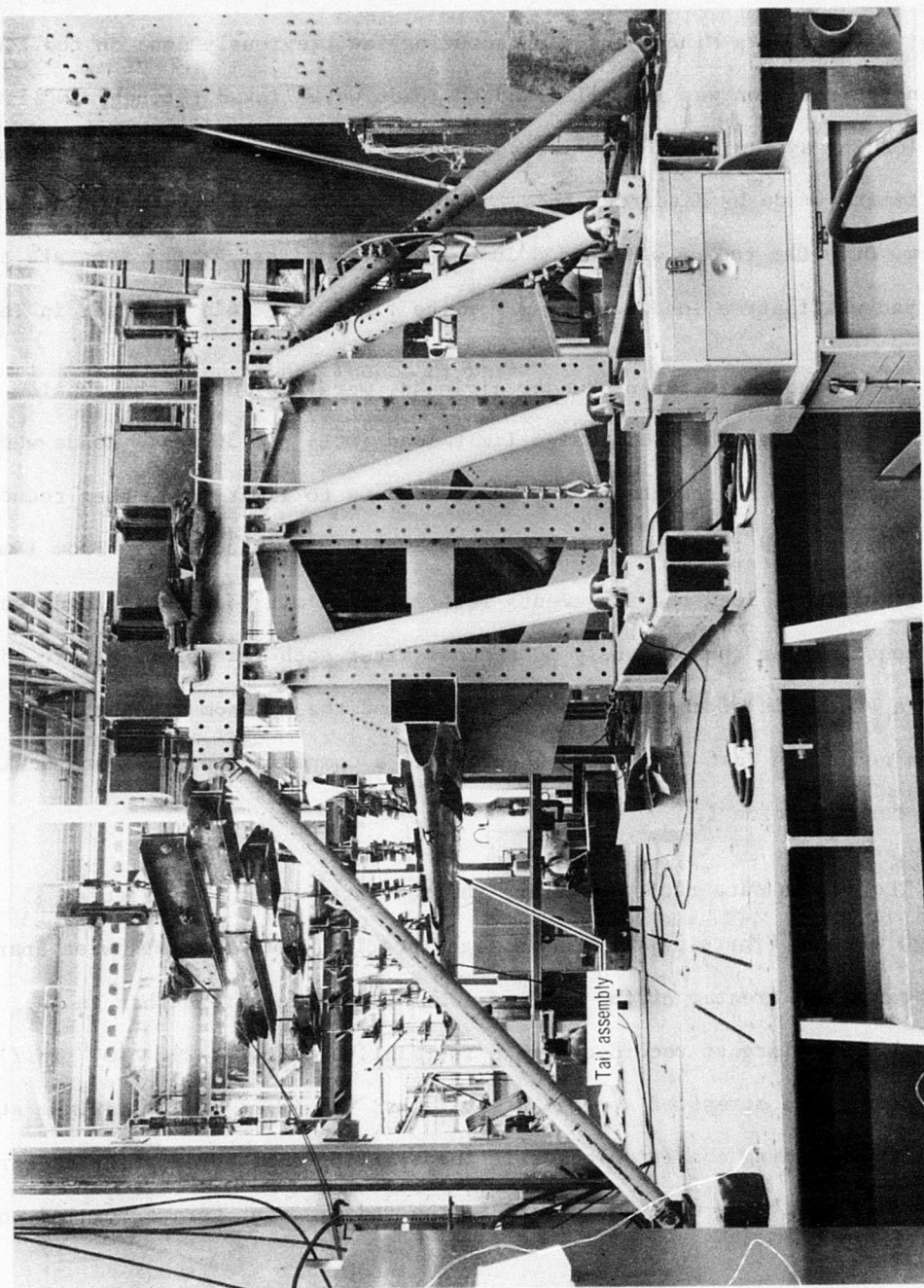


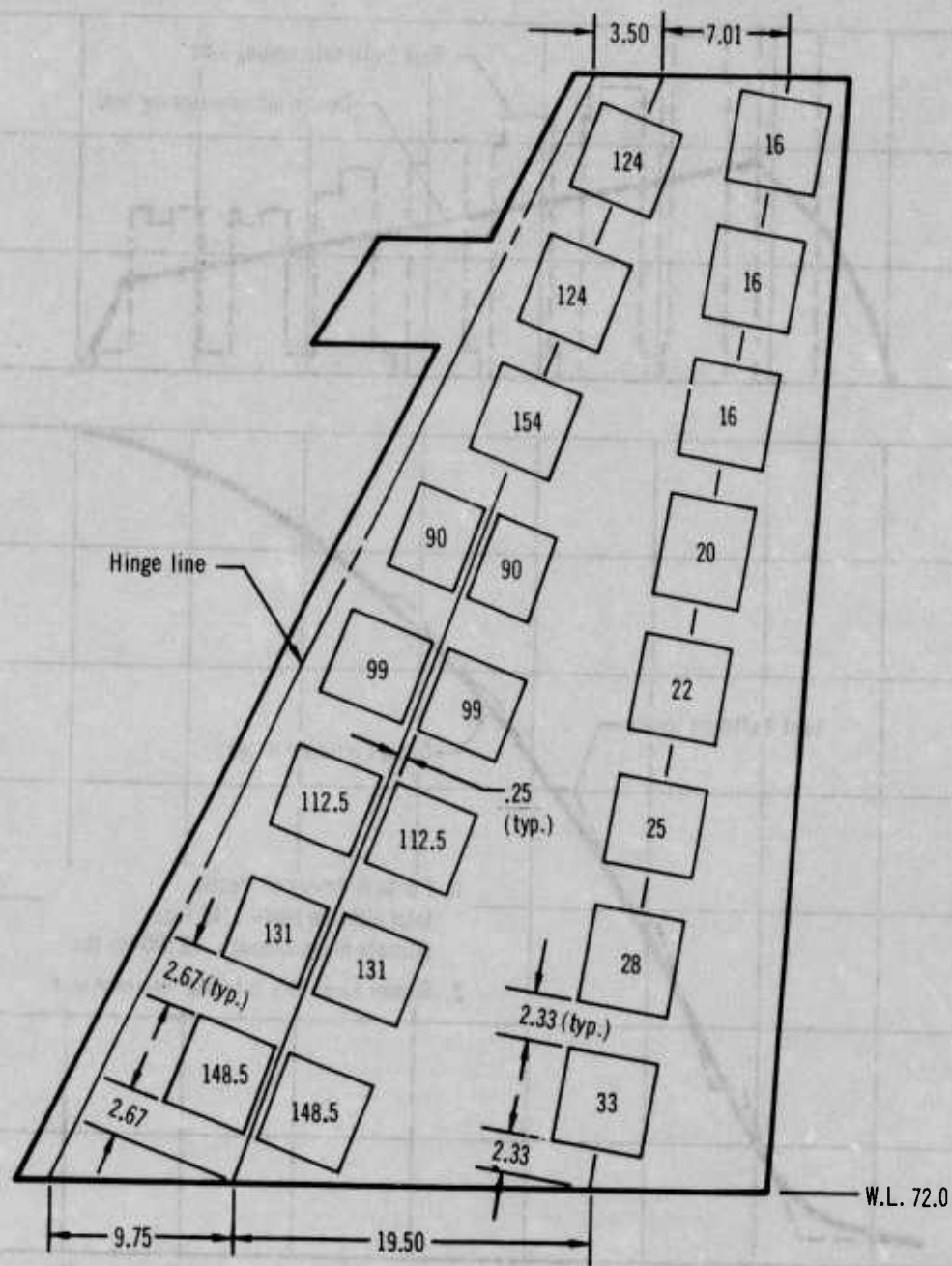
Figure 42 - Aft Fuselage Support Fixture for Beryllium Rudder Static Tests

for applying test loads were bonded to the surface of the rudder using EC1300 adhesive (Minnesota Mining and Manufacturing) as previously done on the fin. All instrumentation was installed and the pads were linked through a whiffle-tree loading system to a hydraulic actuator. Loads were controlled by load programmers (made by Research, Inc.) through a calibrated strain link-feedback system. Only the rudder was loaded in this test and Test 4; the separate tension pad-whiffletree loading system for the fin (Figure 41) was used in Test 3.

Test loads, simulating rudder airloads, were applied to the tension pads at a maximum rate of 20% of design limit load (DDL) per 30 sec. Loads were first applied in increments of 20% limit load up to limit load, then reduced to 20% limit, and finally increased to 150% of limit (ultimate). From limit load to ultimate load the increments were 10% of limit load. All loads were held constant for approximately 30 seconds after each increment. Figure 43 shows a schematic of the tension pad layout and the maximum loads applied to the rudder in Test 2. Figure 44 presents a comparison of test and design loads for Condition I.

The strain data recorded during the test are shown in Figures 45 through 47. See Figure 37 for strain gage location. Note that spanwise spar cap strains are greater at the mid and lower rudder locations than in the upper areas, but the largest recorded strain is relatively low at 290×10^{-6} in./in. (equivalent to a stress of approximately 12 ksi (83 MN/m²)). The maximum stresses for this loading condition occur in the trailing edge cover skins as a result of the airloads being carried forward to the rudder front torque box and in the torque tube.

Deflection data are presented in Figures 48 through 51. Figure 38 shows



- Notes:
1. ☐ indicates tension pad and load in pounds.
 2. All tension pads were 5 inches x 5 inches except two pads with 90 lb. loads. These pads were 4 inches x 5 inches.
 3. Ultimate load = 1,740 lbs. Ultimate hinge moment = 13,500 in.-lbs. Center of pressure at 30% chord.

Figure 43 - Rudder Tension Pad Layout and Ultimate Loads for Test 2

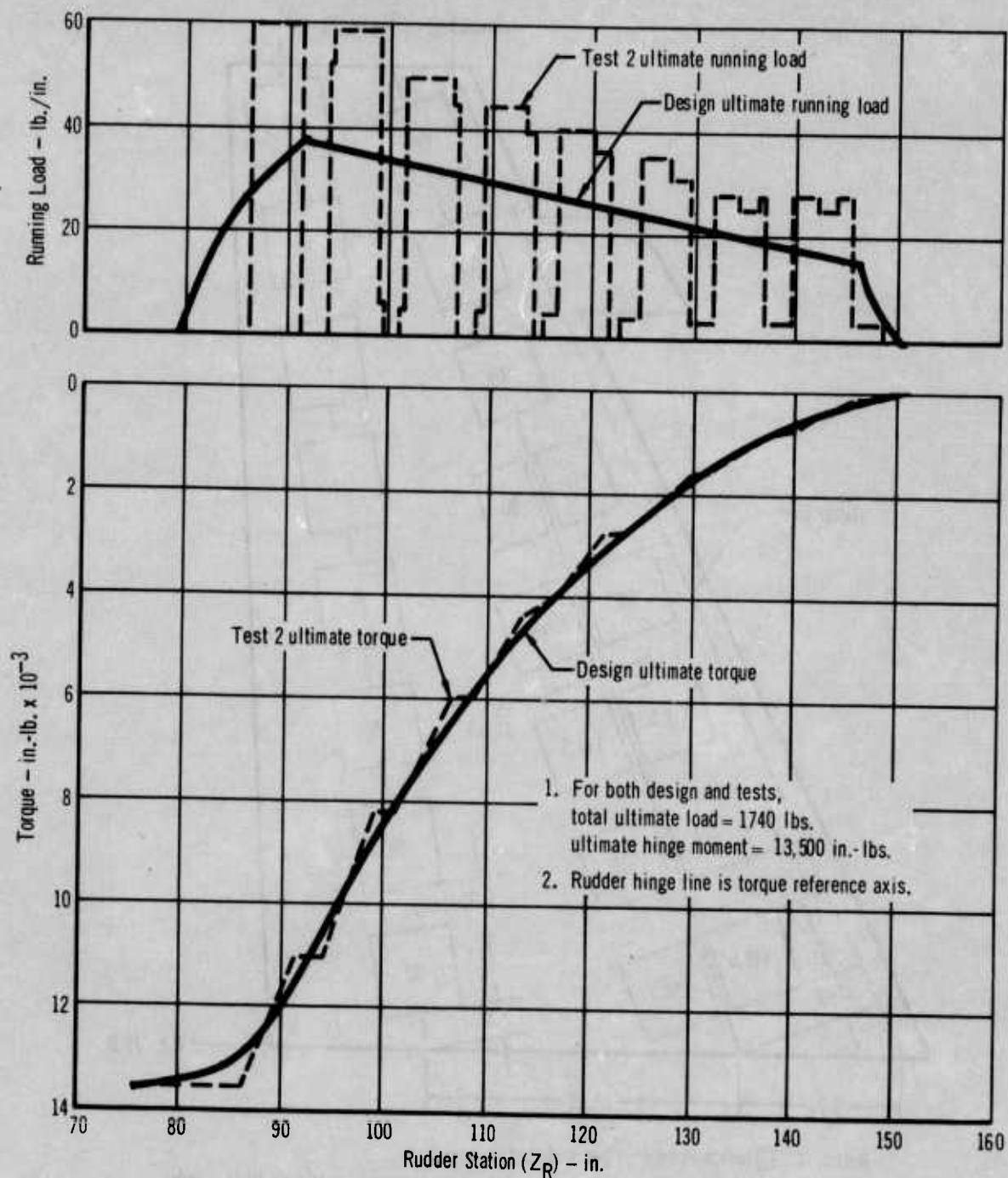


Figure 44 - Comparison of Test and Design Loads: Design Condition I

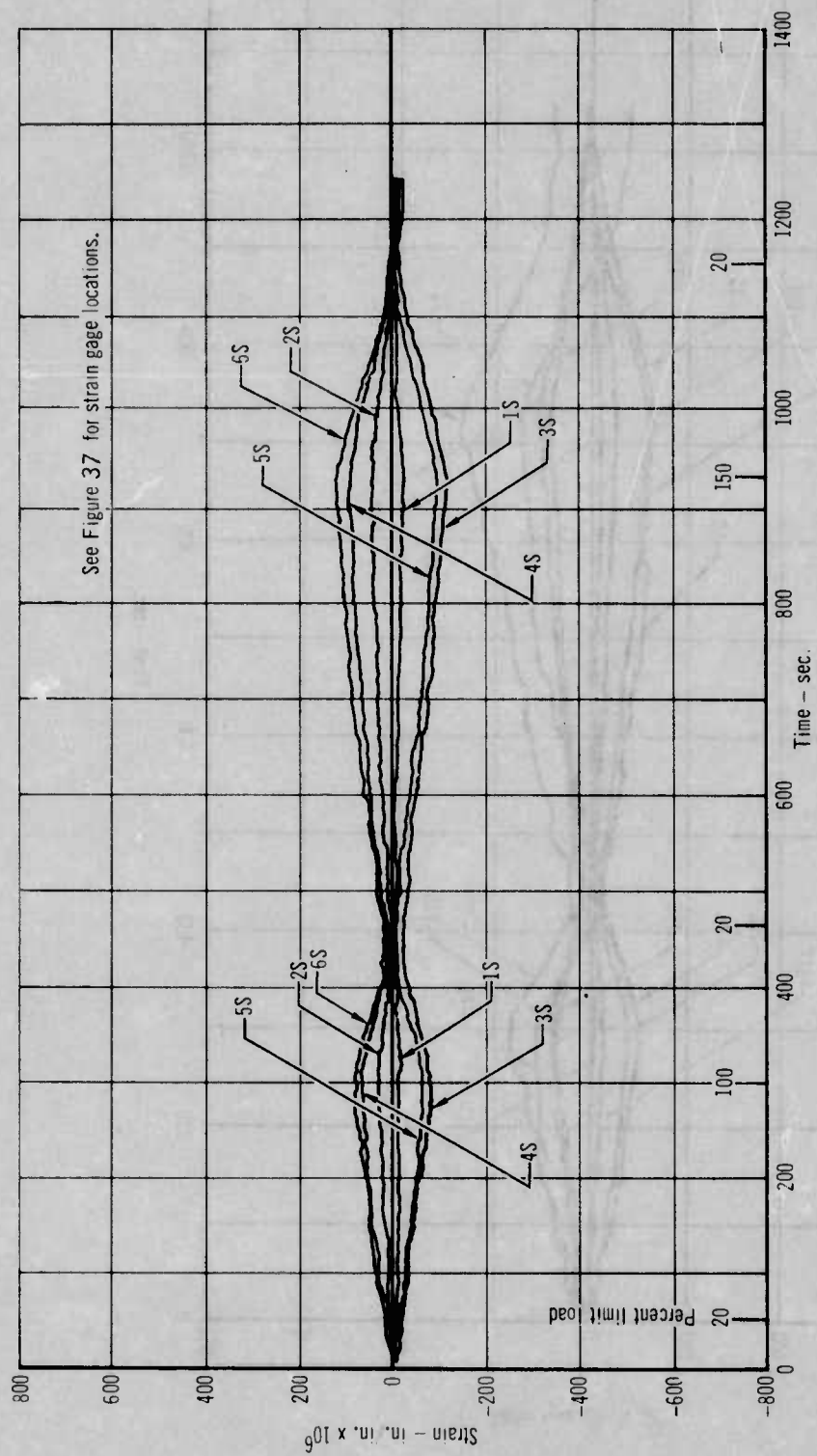


Figure 45 - Beryllium Rudder Front Spar Strains: Test 2

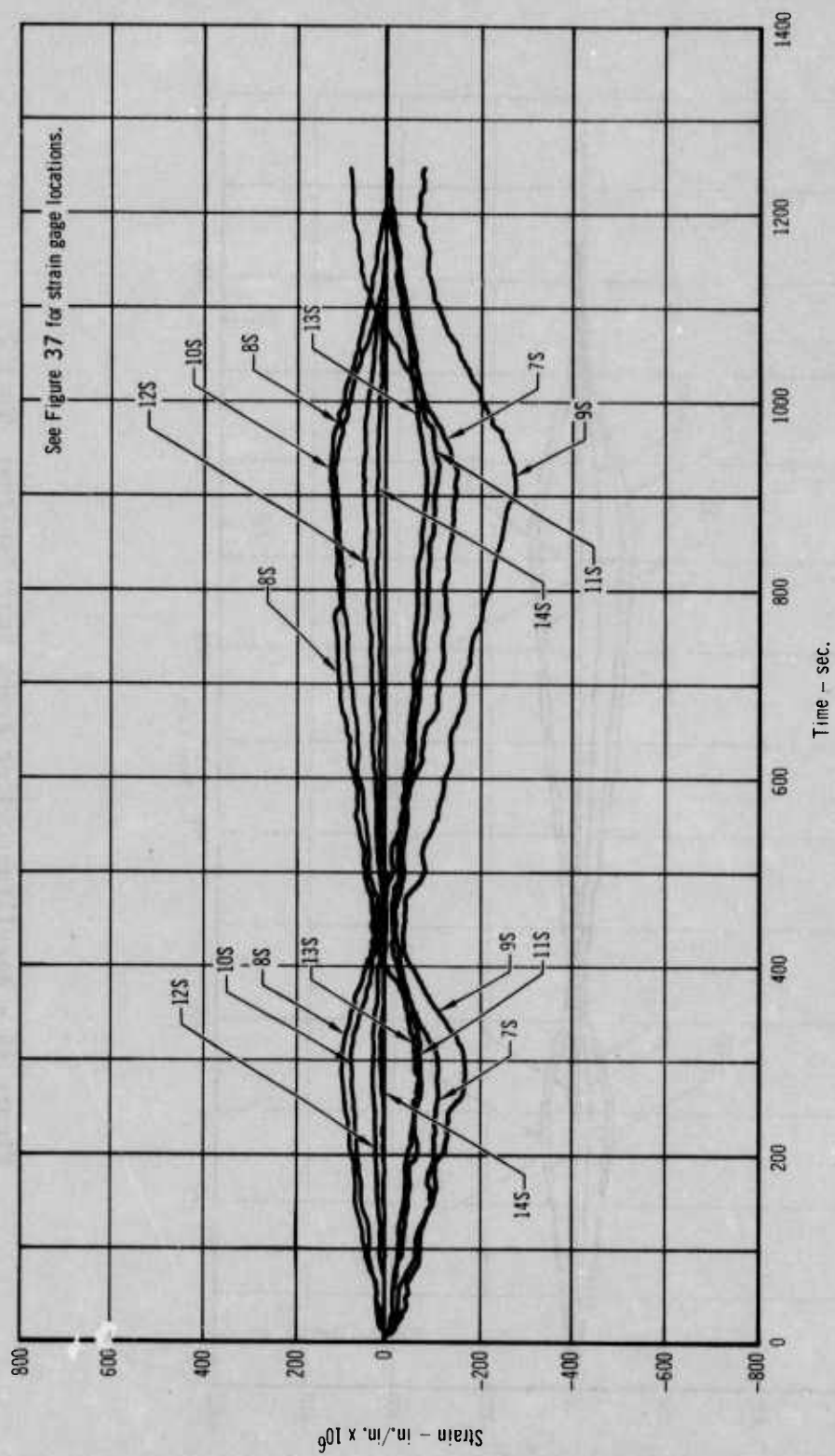


Figure 46 - Rear Spar and Trailing Edge Strains: Test 2

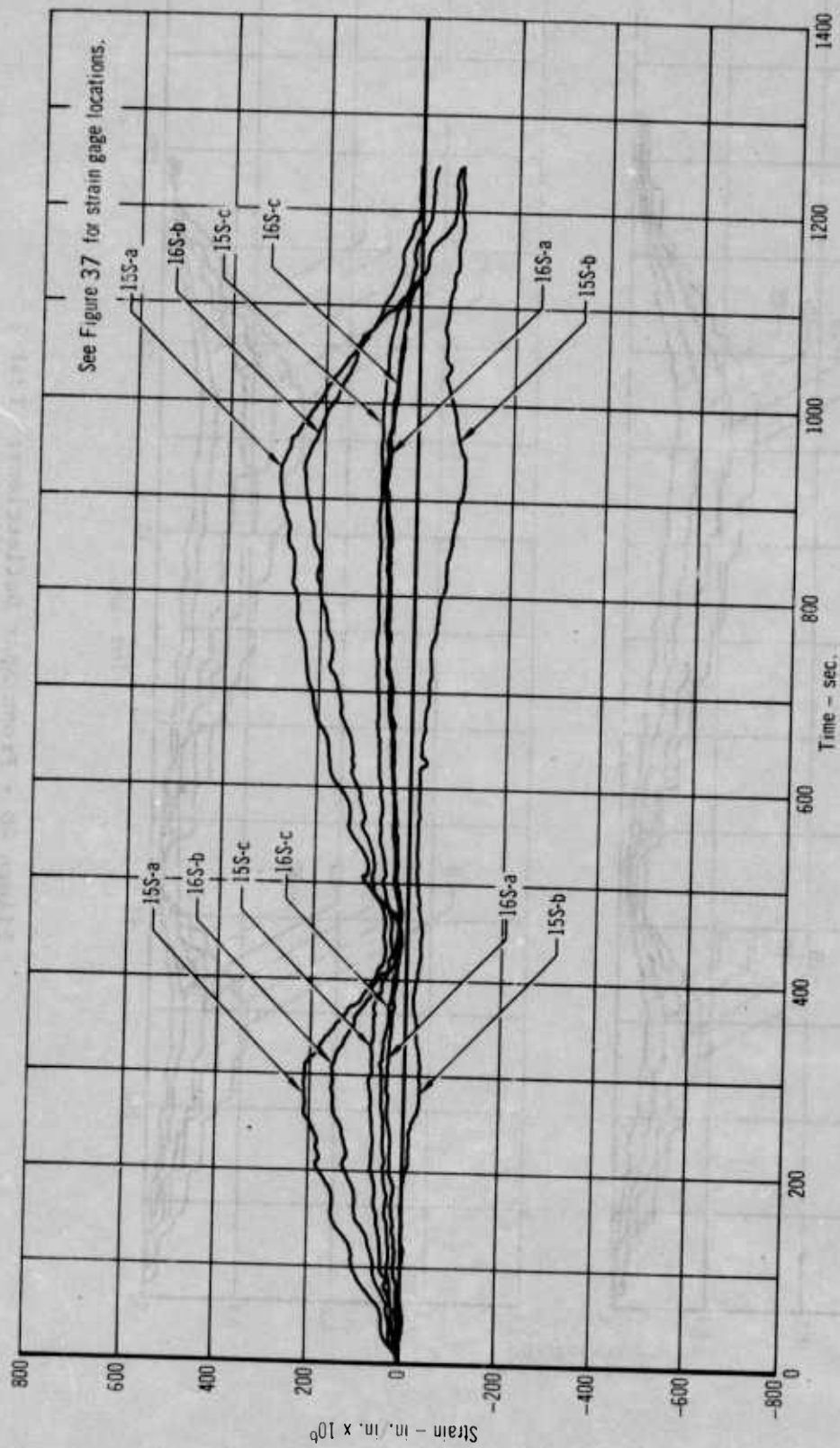


Figure 47 - Forward Cover Skin Strains: Test 2

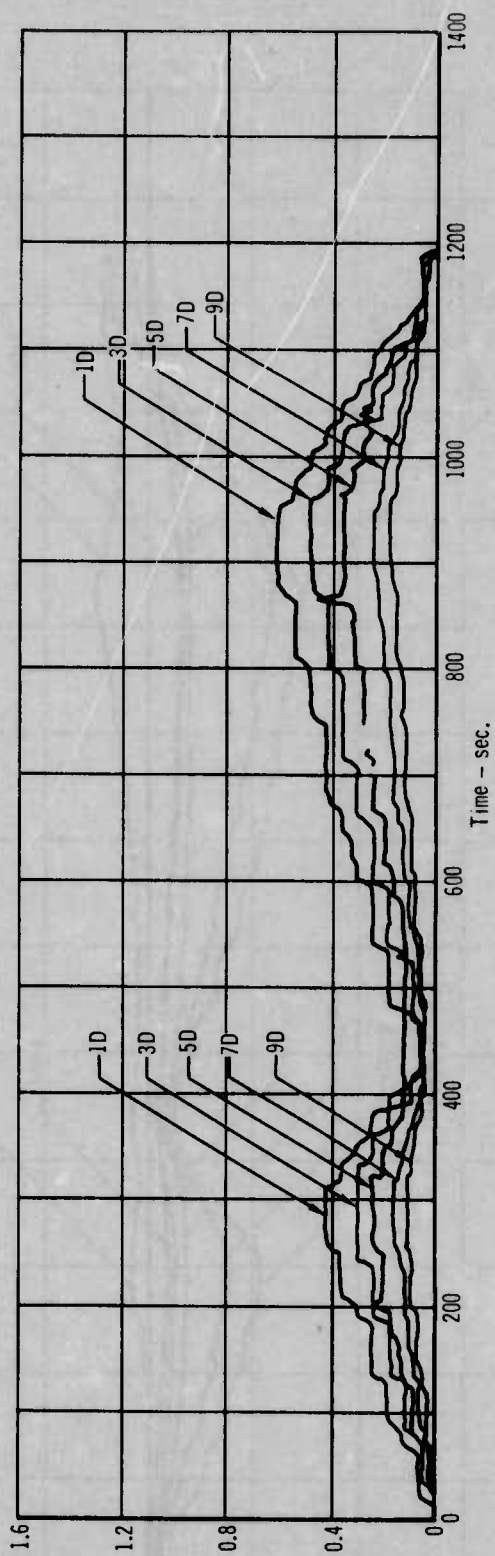
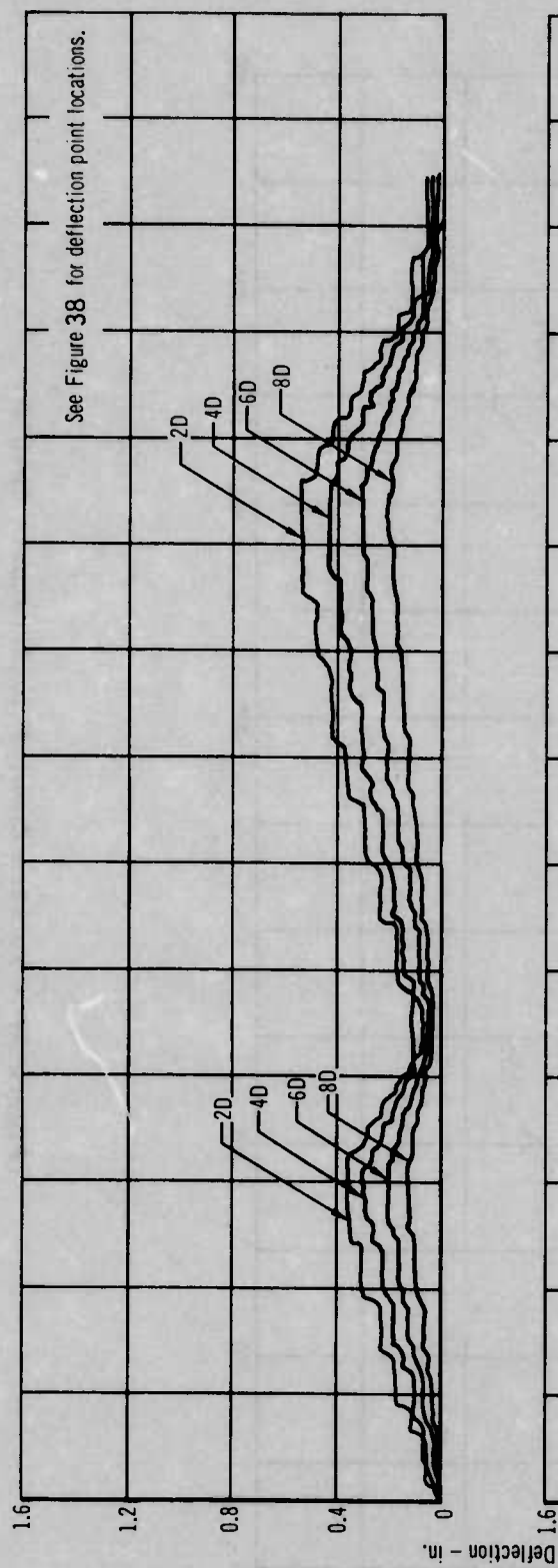


Figure 48 - Front Spar Deflections: Test 2

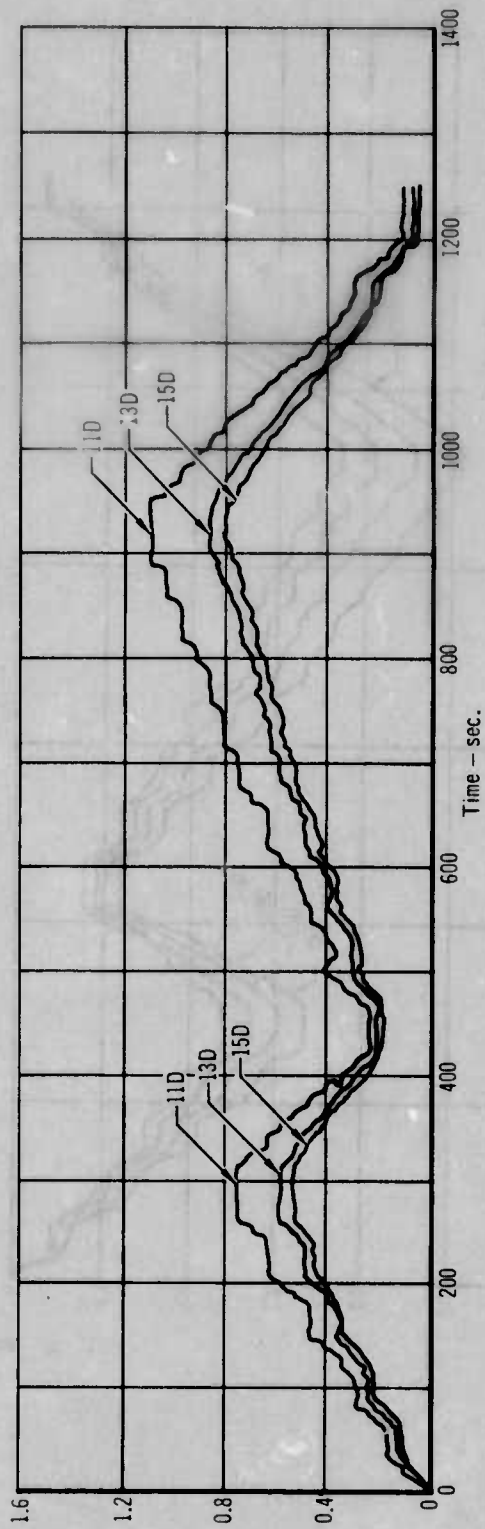
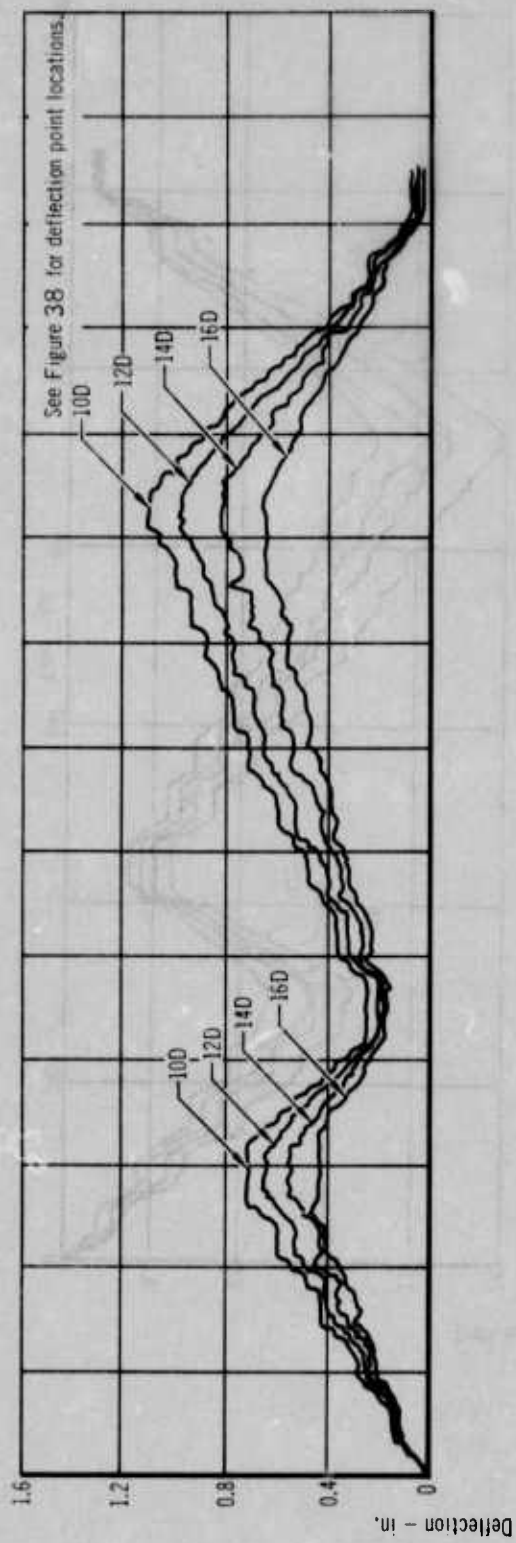


Figure 49 - Rear Spar Deflections: Test 2

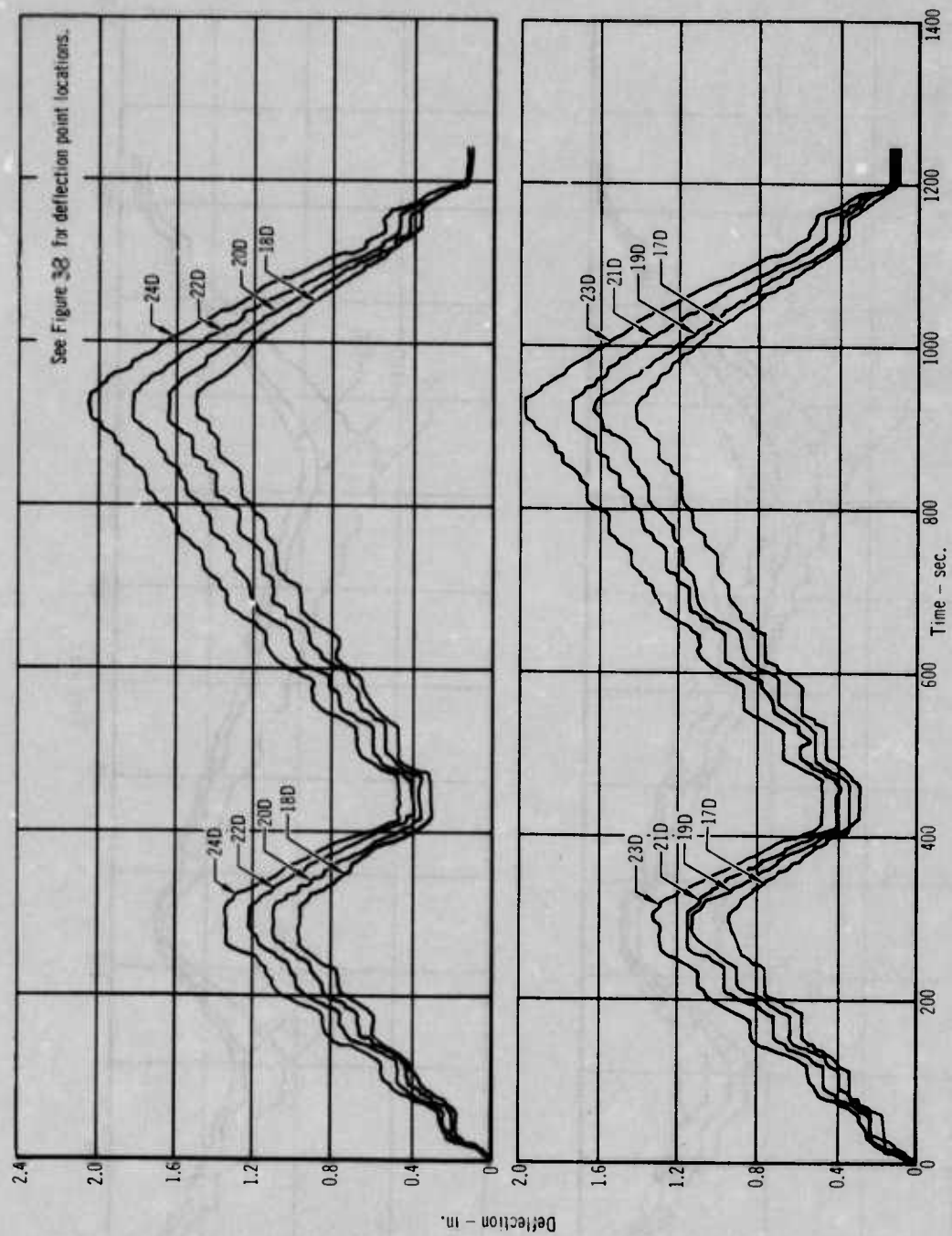


Figure 50 - Trailing Edge Deflections: Test 2

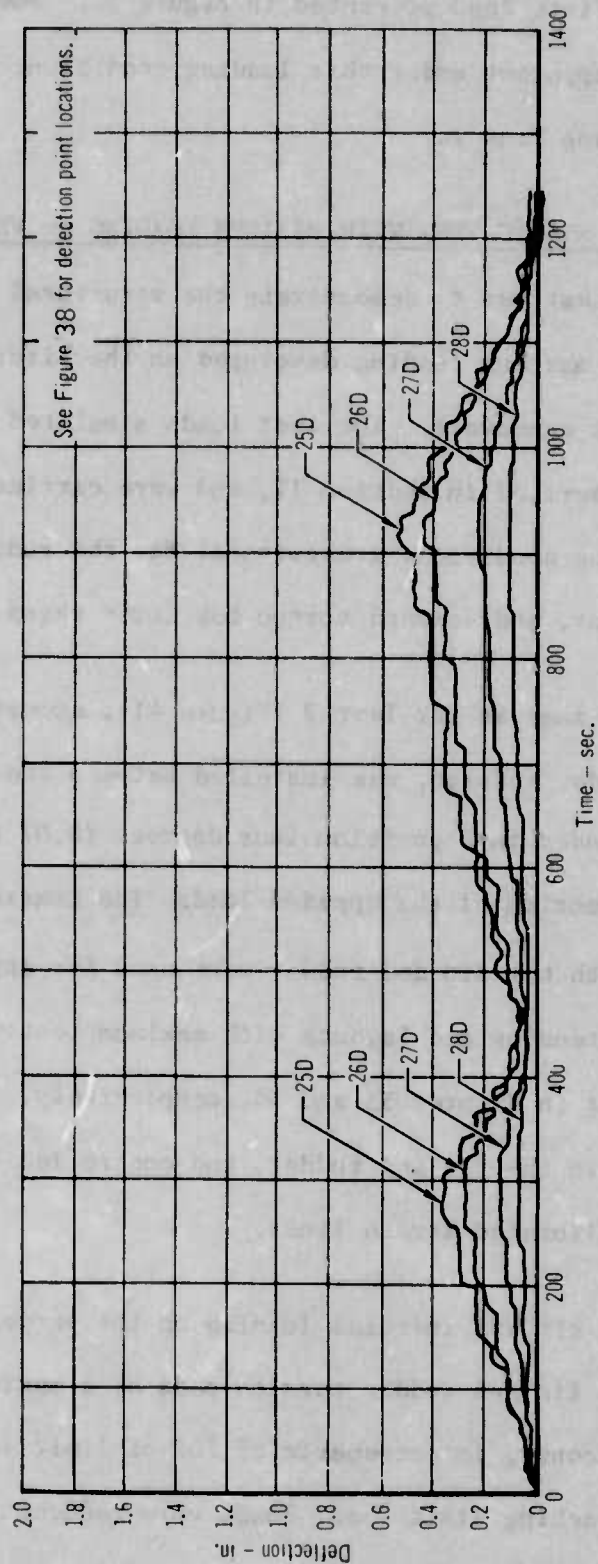


Figure 51 - Hinge Deflections: Test 2

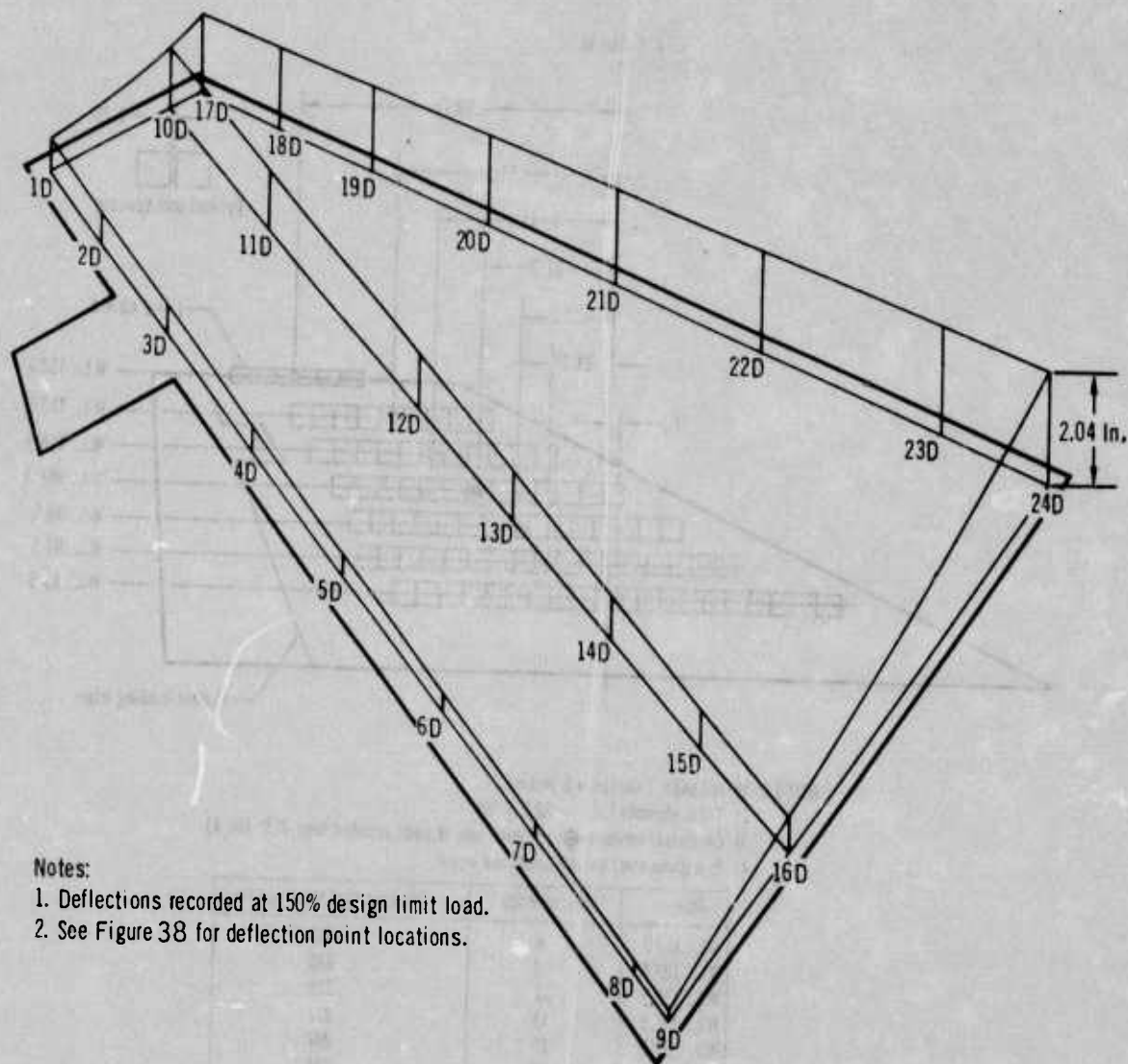
the location of the various deflection points, with a schematic of the rudder deflections at 150% design limit load presented in Figure 52. Some twisting of the Beryllium rudder is apparent under this loading condition. There was no damage to the rudder during Test 2.

5. TEST 3- RUDDER ULTIMATE STATIC TEST WITH MAXIMUM LOADING on VERTICAL TAIL

The objective of this test was to demonstrate the structural integrity of the rudder assembly for the maximum loading developed on the aircraft vertical tail during rolling pull-out maneuvers. The test loads simulated the loads of Design Condition III, described in Section II, and were carried to ultimate (150% design limit). Loading conditions are critical for the rudder hinges, hinge backup ribs, front spar, and forward torque box cover skins.

The test set-up is the same as for Test 2 (Figure 41), except that a jig assembly simulating the rudder actuator was installed between the rudder and fuselage to maintain the rudder in a position four degrees (0.07 radians) from the neutral axis in the direction of the applied loads. The tension pad-whiffle-tree loading systems for both the fin and rudder were used for applying the test loads. Schematics of tension pad layouts with maximum test loads are shown for the fin and rudder in Figures 53 and 54, respectively. Loading was applied simultaneously to the fin and rudder, and controlled by programmers in conjunction with calibrated strain links.

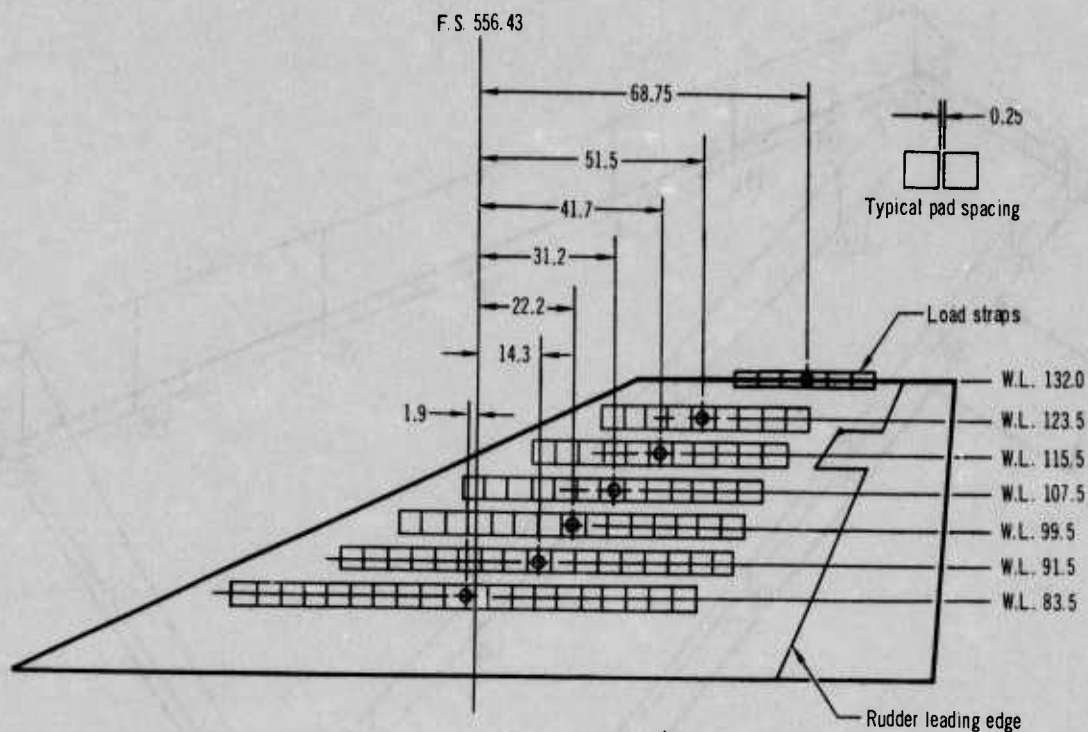
Test loads, simulating air and inertial loading on the vertical tail assembly, were applied to the fin and rudder tension pads at a maximum rate of 20% of limit load per 30 seconds, in increments of 20% of limit load, up to limit load. After first reaching limit load, loads were reduced to 20% limit then increased to 150% limit (ultimate). From limit load to ultimate load



Notes:

1. Deflections recorded at 150% design limit load.
2. See Figure 38 for deflection point locations.

Figure 52 - Rudder Deflections: Design Condition I

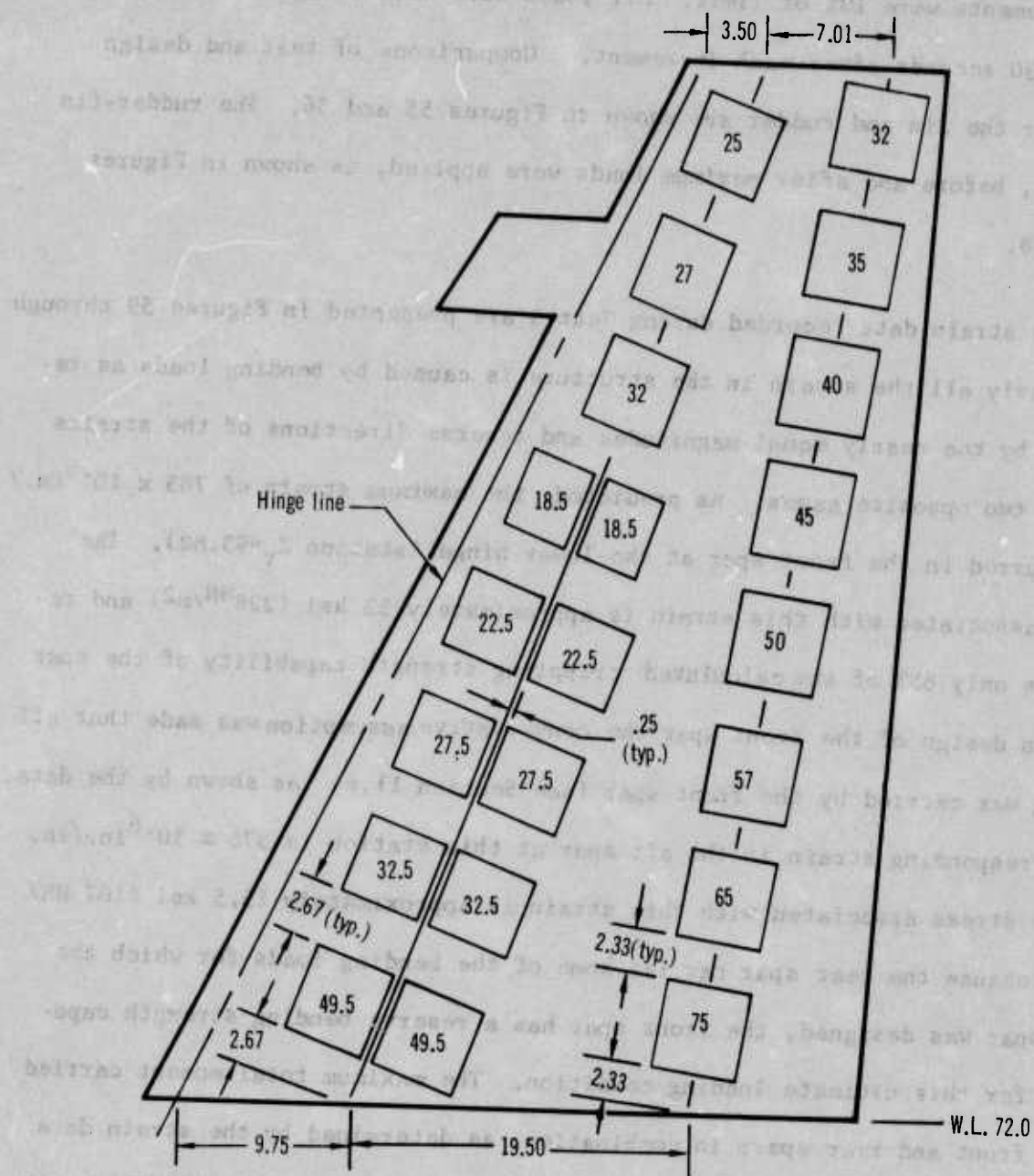


- NOTES: 1) All pads 5 inches x 5 inches.
 2) Total ultimate load = 22,213 lbs.
 3) Geometric center (⊕) of each row of pads located from F.S. 556.43
 4) In a given row, all pad loads are equal.

Row	No. of Pads	Ultimate test load/pad (lb.)
W.L. 132.0	6	485
W.L. 123.5	9	248
W.L. 115.5	11	229
W.L. 107.5	13	217
W.L. 99.5	15	207
W.L. 91.5	17	198
W.L. 83.5	20	263

- 5) Vertical fin test loads were applied in conjunction with and in the same direction as the rudder loads shown in Figure 54.
 6) Vertical fin design and test loads are compared in Figure 55.

Figure 53 - Vertical Fin Tension Pad Layout and Ultimate Loads for Test 3



- Notes: 1. □ indicates tension pad and load in pounds.
 2. All tension pads were 5 inches x 5 inches, except two pads with 18.5 lb. loads. These pads were 4 inches x 5 inches.
 3. Ultimate load = 784 lb. Ultimate hinge moment = 10,260 in.-lb. Center of pressure at 45% chord.
 4. These loads were applied in conjunction with and in the same direction as the vertical fin loads shown in Figure 53.

Figure 54 - Rudder Tension Pad Layout and Ultimate Loads for Test 3

the increments were 10% of limit. All loads were held constant for approximately 30 seconds after each increment. Comparisons of test and design loads for the fin and rudder are shown in Figures 55 and 56. The rudder-fin assembly, before and after maximum loads were applied, is shown in Figures 57 and 58.

The strain data recorded during Test 3 are presented in Figures 59 through 61. Nearly all the strain in the structure is caused by bending loads as reflected by the nearly equal magnitudes and reverse directions of the strains for any two opposite gages. As predicted, the maximum strain of 785×10^{-6} in./in. occurred in the front spar at the lower hinge (station $Z_r=93.82$). The stress associated with this strain is approximately 33 ksi (228 MN/m^2) and represents only 65% of the calculated crippling strength capability of the spar cap. In design of the front spar the conservative assumption was made that all bending was carried by the front spar (see Section II.6) As shown by the data, the corresponding strain in the aft spar at this station is 370×10^{-6} in./in. and the stress associated with this strain is approximately 15.5 ksi (107 MN/m^2). Because the rear spar carries some of the bending loads for which the front spar was designed, the front spar has a reserve bending strength capability for this ultimate loading condition. The maximum total moment carried by the front and rear spars in combination, as determined by the strain data and the physical characteristics of the spars, is approximately 24,000 in.-lbs. (2712 m-N). This is in reasonable agreement with maximum ultimate design moment of 28,000 in.-lbs. (3164 m-N) presented in Figure 18 and indicates a degree of conservatism in the analysis.

The deflection data recorded during this test are presented in Figures 62 through 65. Figure 66 presents a schematic of the rudder with maximum recorded

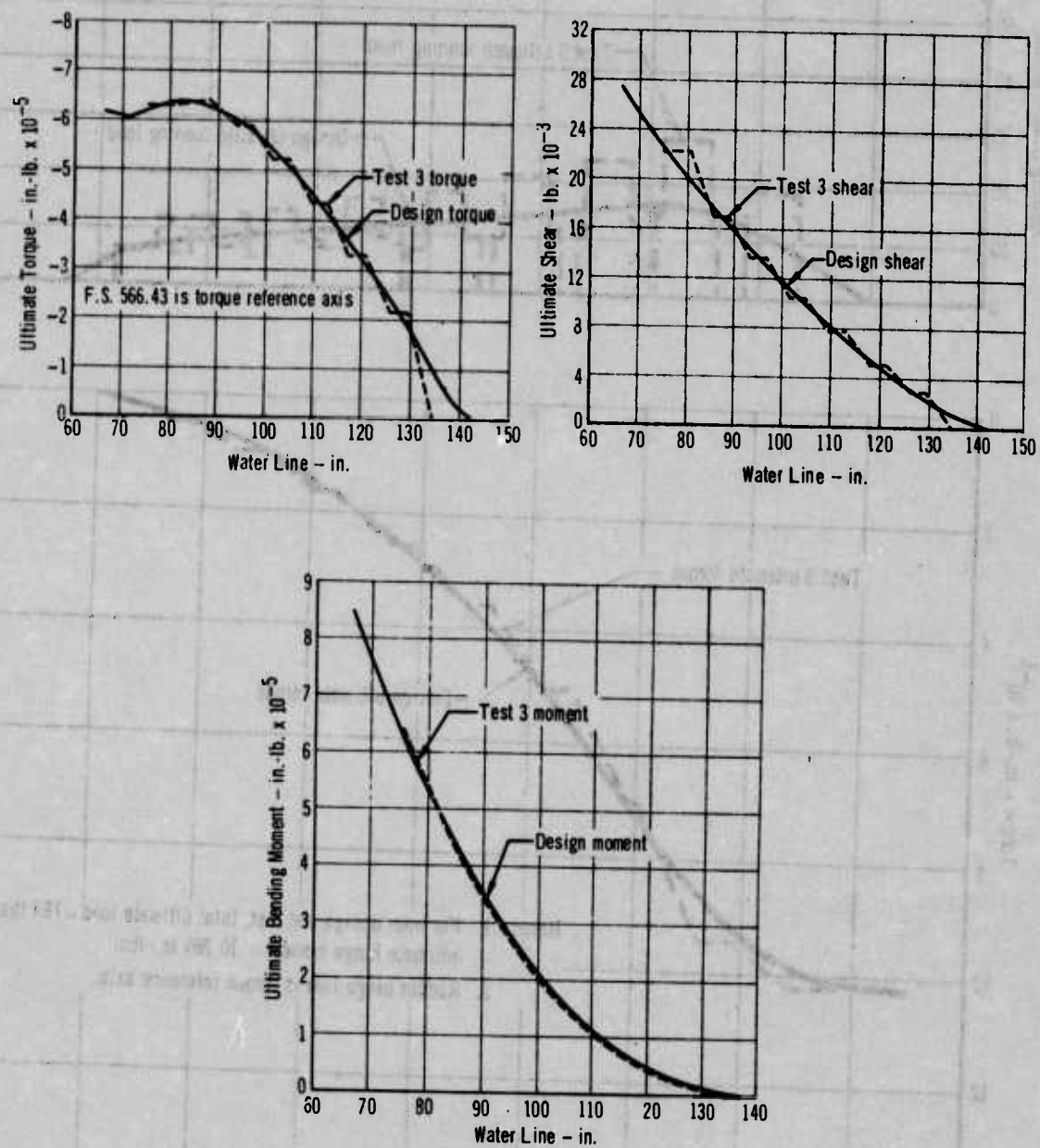


Figure 55 - Comparison of Fin Test and Design Loads: Design Condition III

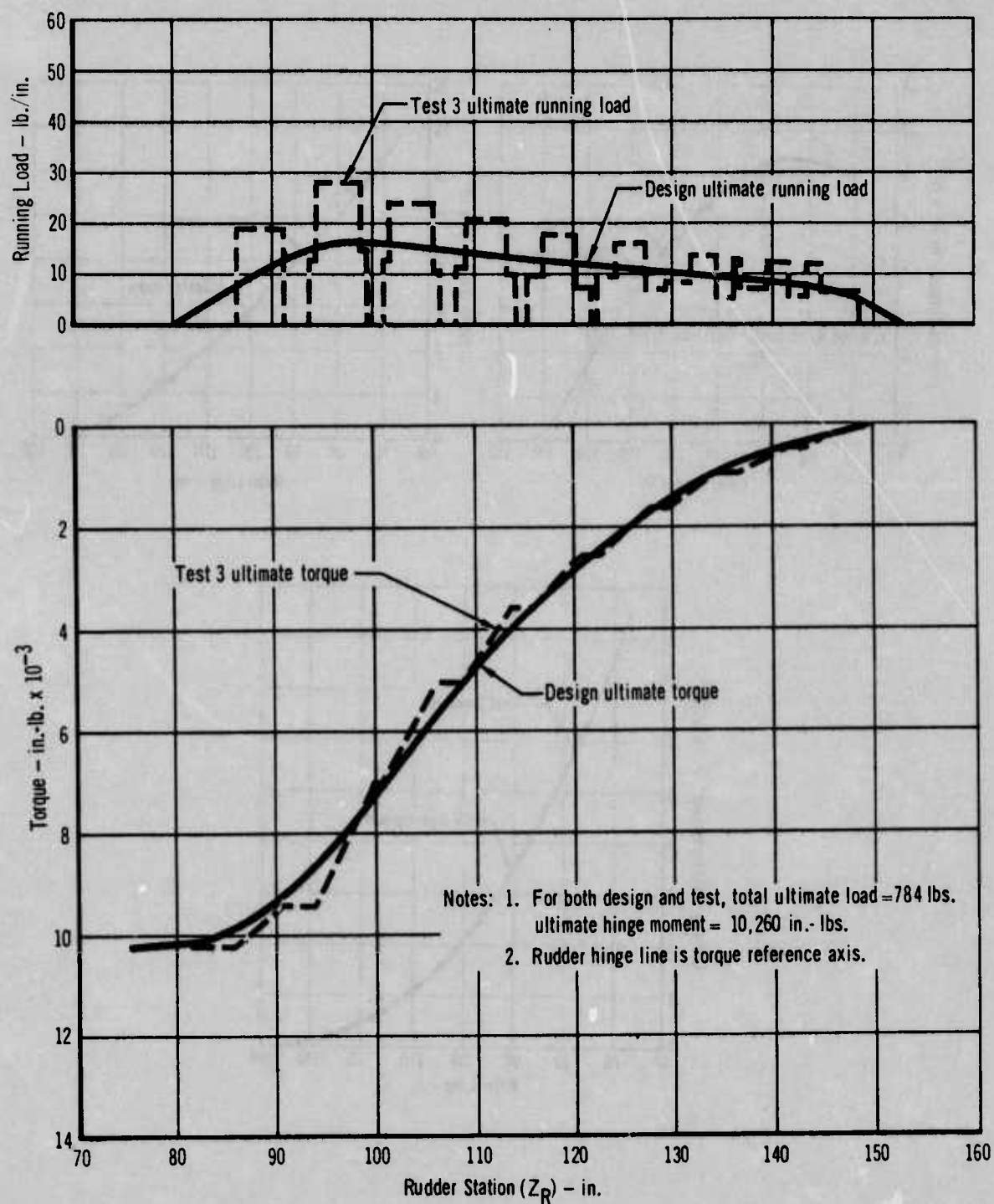


Figure 56 - Comparison of Rudder Test and Design
 Loads: Design Condition III

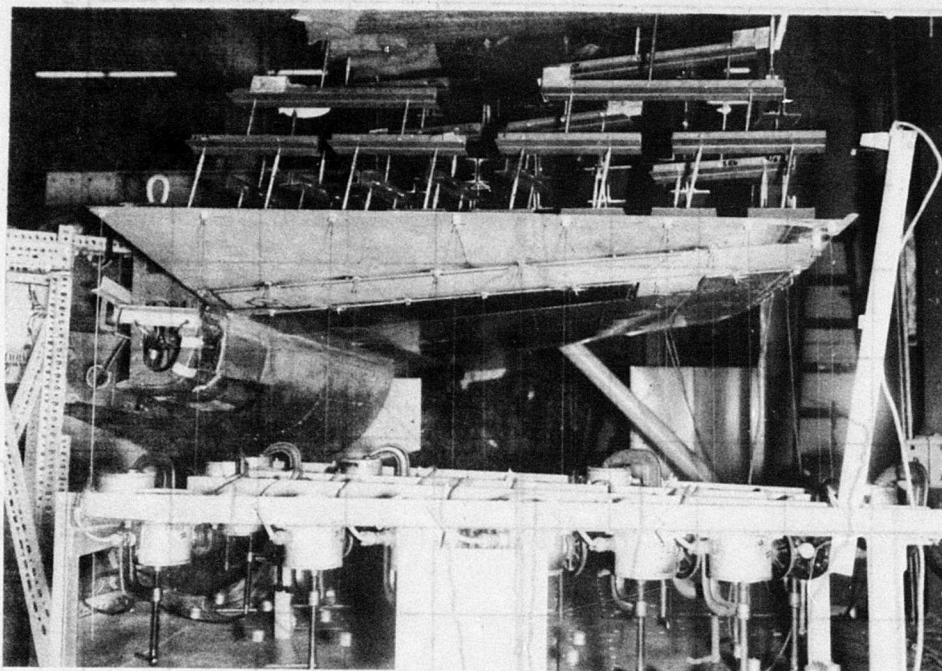


Figure 57 - F-4 Fin and Beryllium Rudder Prior to Loading

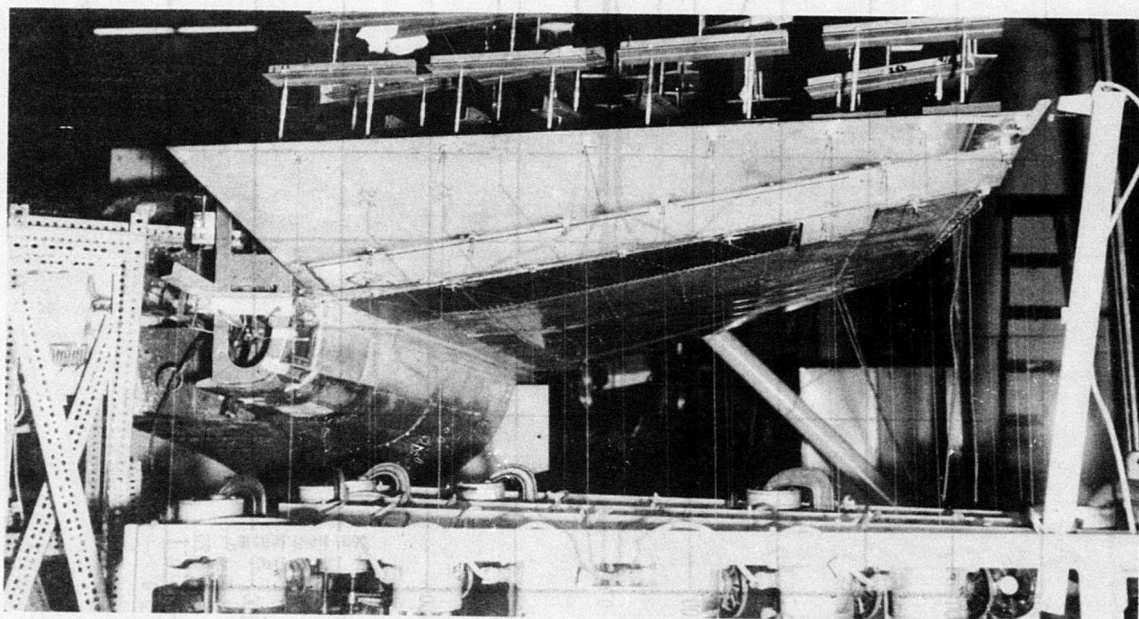


Figure 58 - F-4 Fin and Beryllium Rudder with Condition III Ultimate Loads Applied

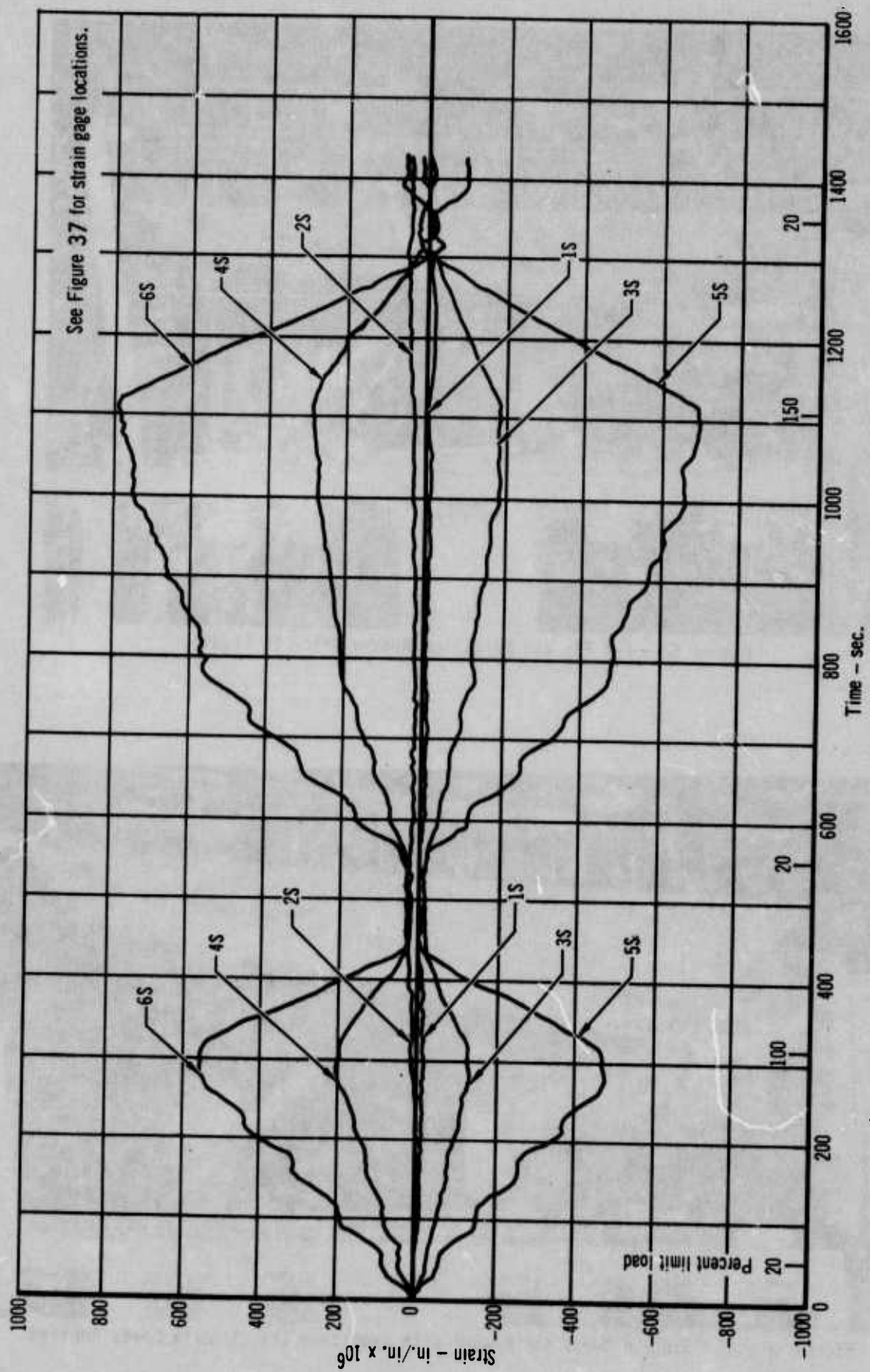


Figure 59 - Front Spar Strains: Test 3

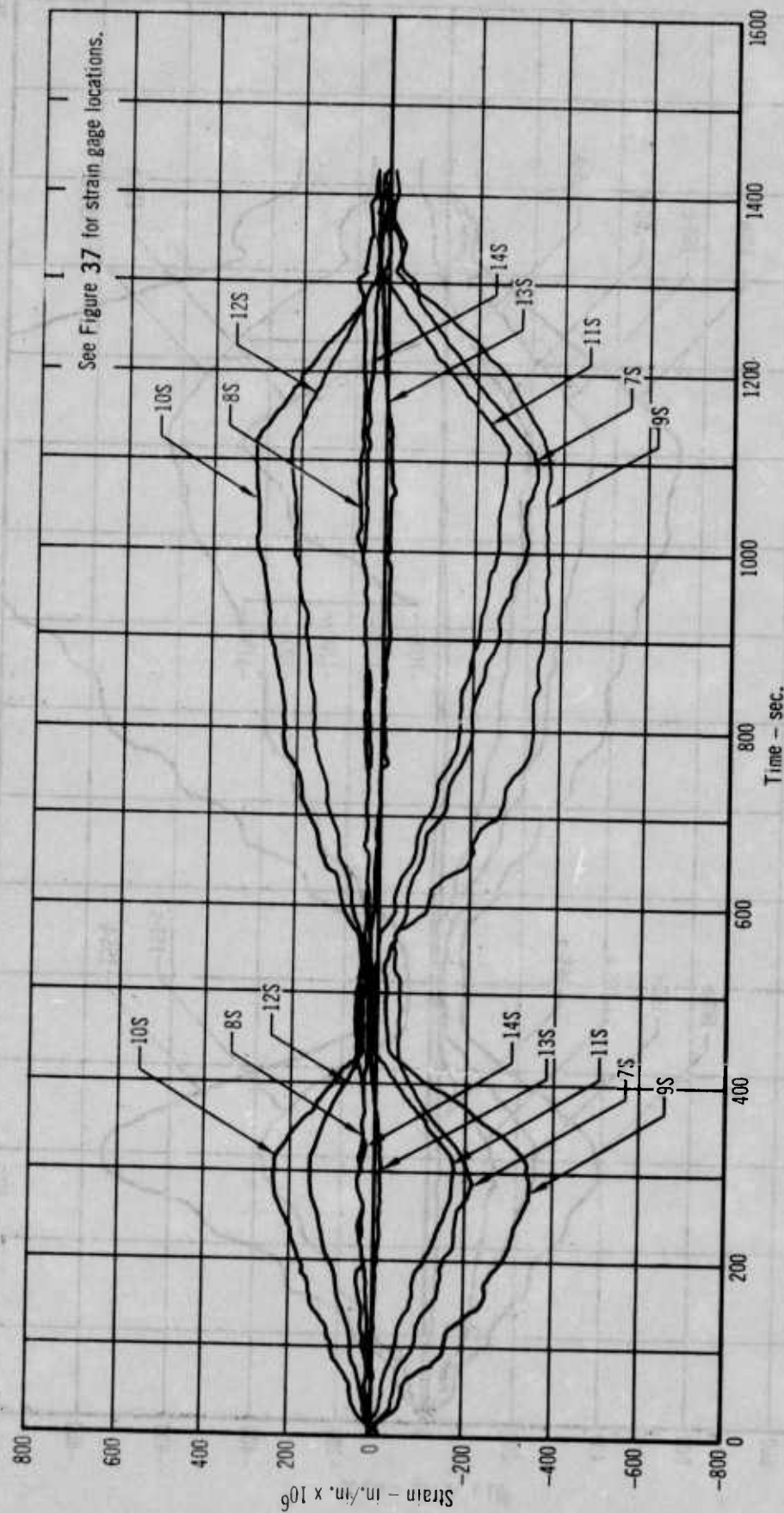


Figure 60 - Rear Spar and Trailing Edge Strains: Test 3

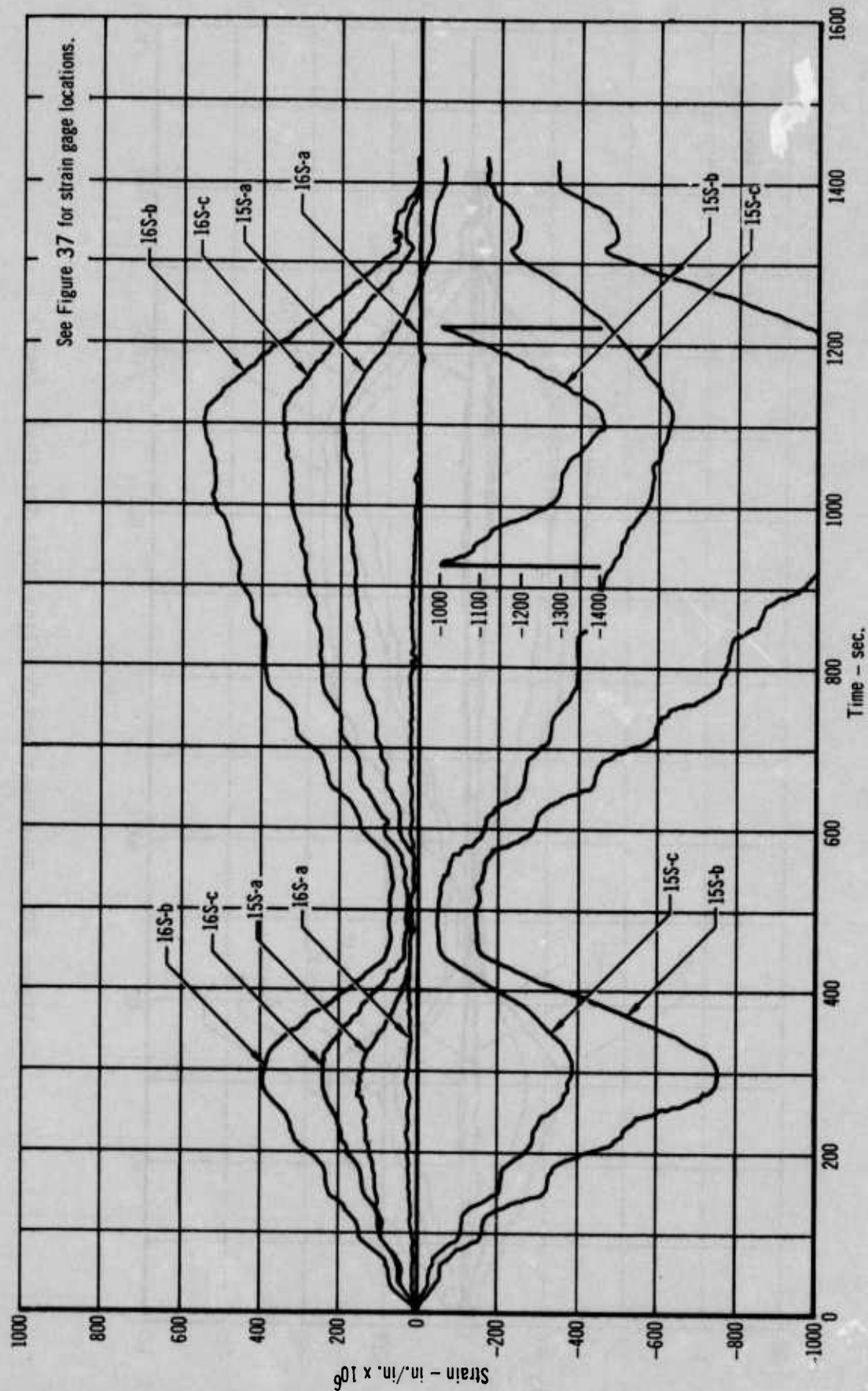


Figure 61 - Forward Cover Skin Strains: Test 3

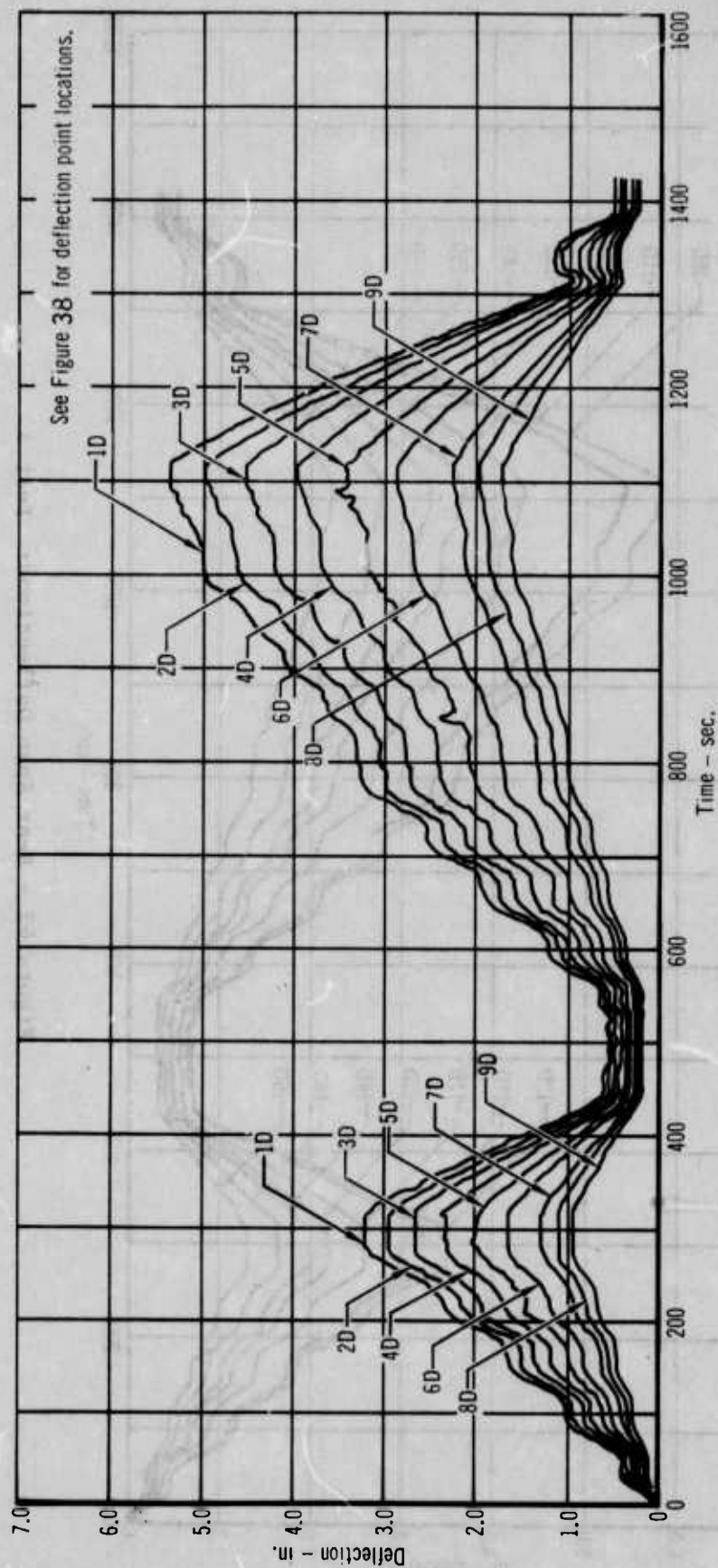


Figure 62 - Front Spar Deflections: Test 3

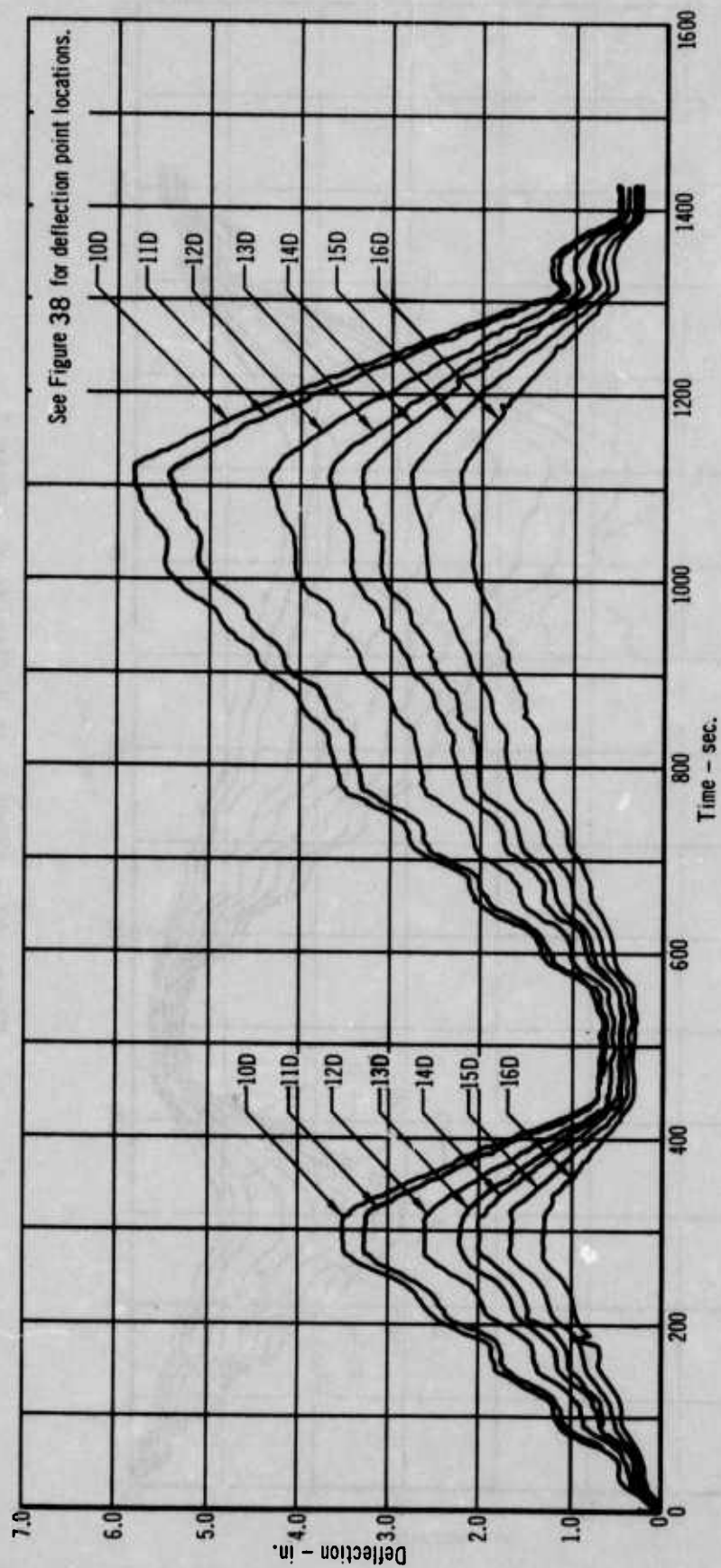


Figure 63 - Rear Spar Deflections: Test 3

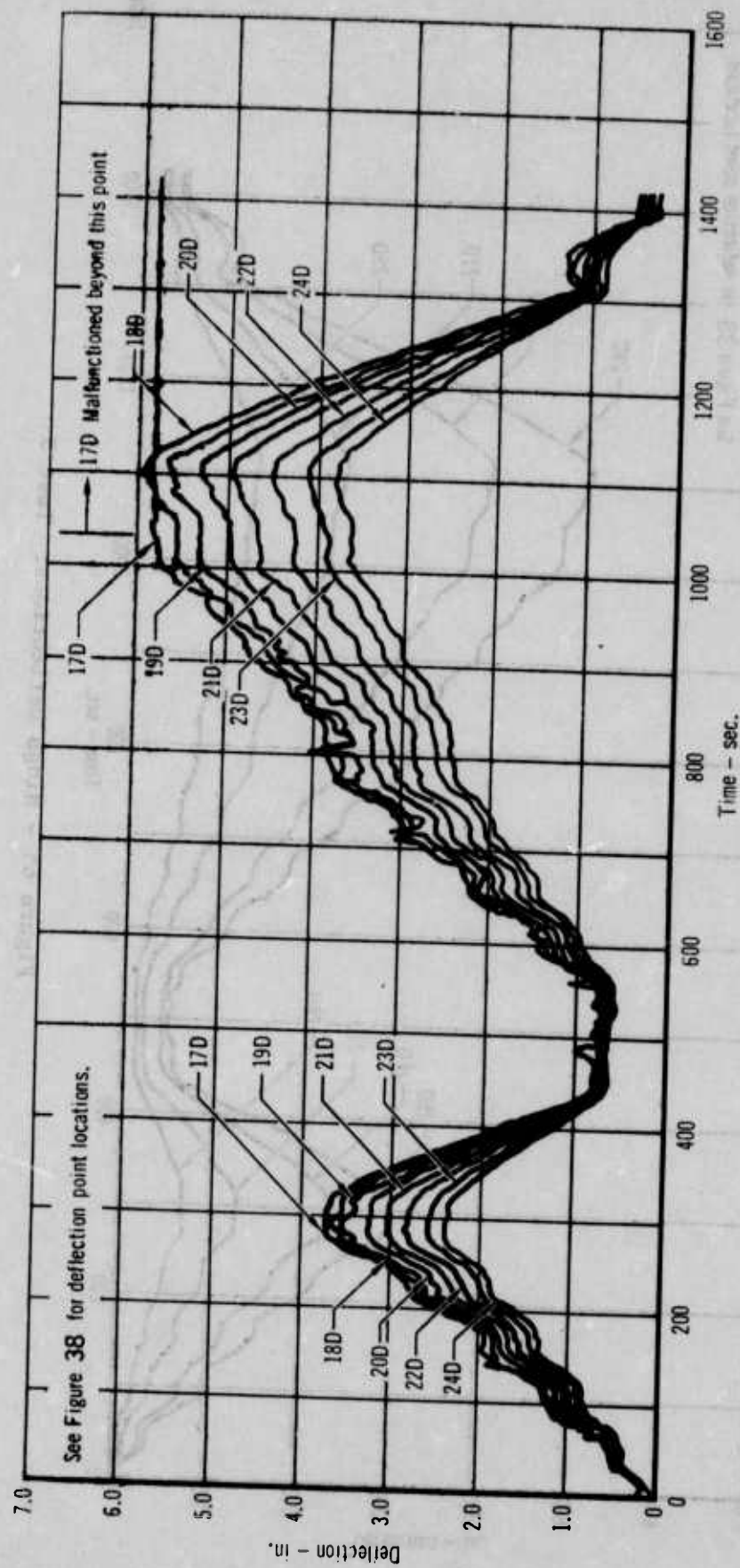


Figure 64 - Trailing Edge Deflections: Test 3

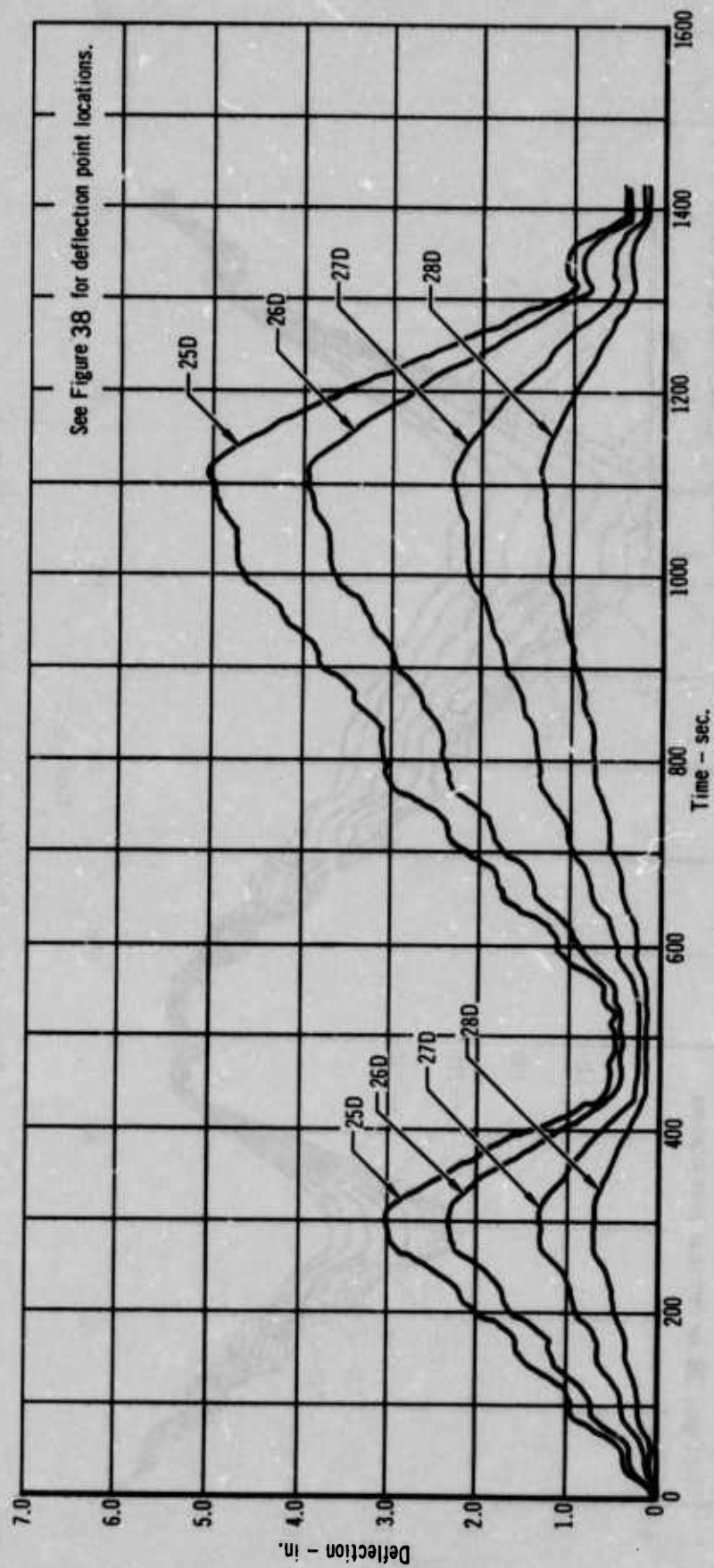
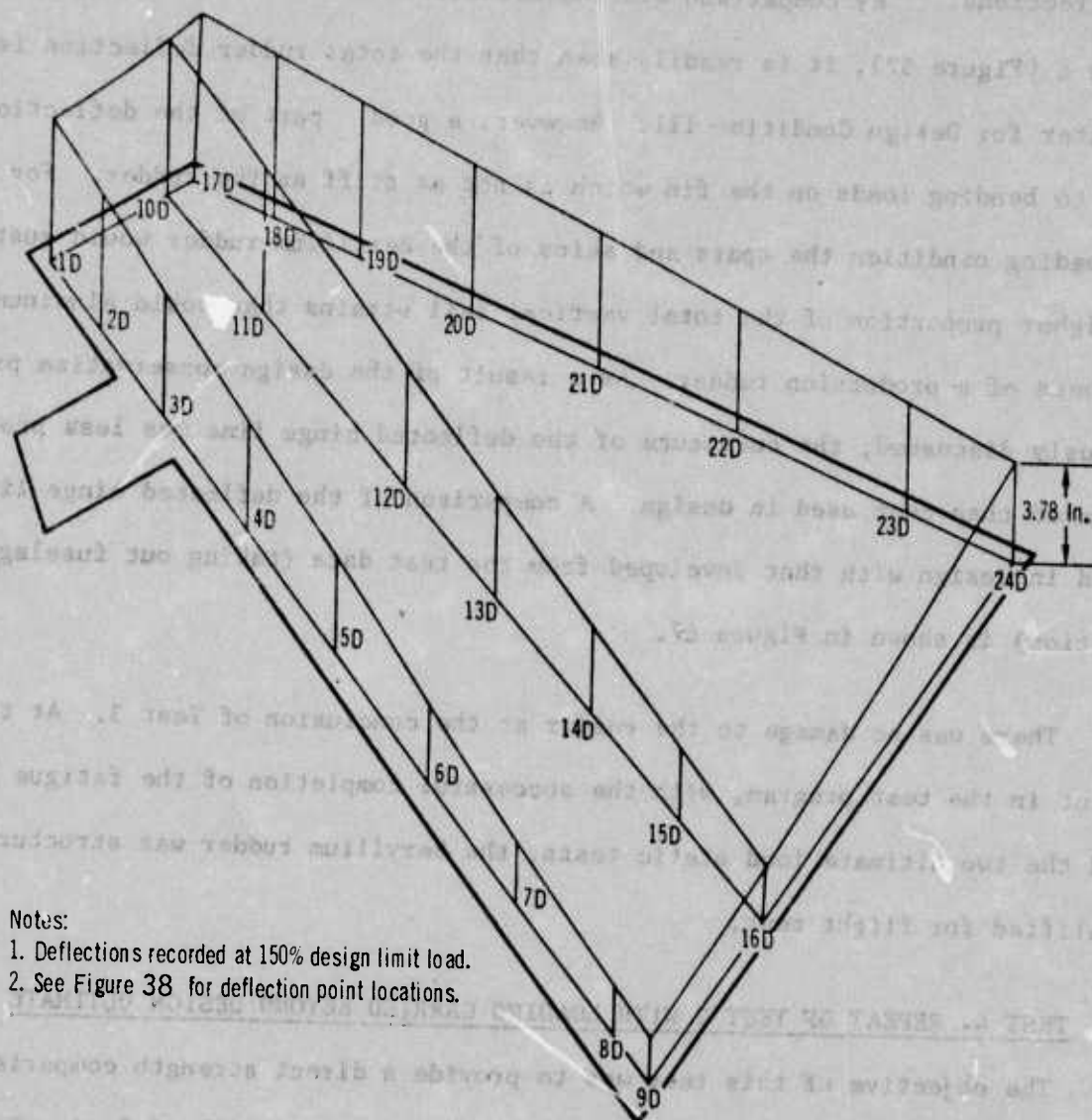


Figure 65 - Hinge Deflections: Test 3



Notes:

1. Deflections recorded at 150% design limit load.
2. See Figure 38 for deflection point locations.

Figure 66 - Rudder Deflections: Design Condition III

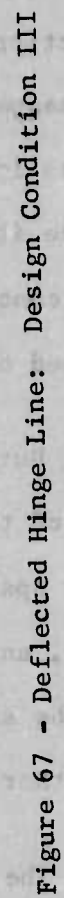
deflections. By comparison with the deflection schematic for Design Condition I (Figure 52), it is readily seen that the total rudder deflection is greater for Design Condition III. However, a good part of the deflection is due to bending loads on the fin which is not as stiff as the rudder. For such a loading condition the spars and skins of the Beryllium rudder would sustain a higher proportion of the total vertical tail strains than would aluminum members of a production rudder. As a result of the design conservatism previously discussed, the curvature of the deflected hinge line was less pronounced than that used in design. A comparison of the deflected hinge line used in design with that developed from the test data (taking out fuselage station) is shown in Figure 67.

There was no damage to the rudder at the conclusion of Test 3. At this point in the test program, with the successful completion of the fatigue test and the two ultimate load static tests, the Beryllium rudder was structurally qualified for flight test.

6. TEST 4- REPEAT OF TEST 2 WITH LOADING CARRIED BEYOND DESIGN ULTIMATE

The objective of this test was to provide a direct strength comparison with the production aluminum rudder which had sustained 225% of Design Condition I limit load without catastrophic failure. In Test 4, therefore, the beryllium rudder was subjected to Design Condition I loading in a manner identical to that described for Test 2, except that loads were increased incrementally beyond ultimate (150% of limit).

Test loads were applied to the rudder only at a maximum rate of 20% of limit load per 30 seconds, in increments of 20% of limit load, up to limit load. From this point to conclusion of the test, loads were applied in incre-



ments of 10% of limit load. Loads were held for approximately 30 seconds after each load increment.

While loads on the rudder were being increased from 200% DLL to 210% DLL, a sharp noise was heard. However the loads did not fall off and a visual inspection during the hold at 210% DLL failed to reveal any damage to the rudder. Consequently, testing continued until the rudder had sustained 250% DLL (1.67 times loads shown in Figure 43) for 30 seconds. Testing was then discontinued since it was felt testing beyond this point would be of little significance at the conclusion of an already successful test program. Further, it was believed other more productive tests may be conducted on the beryllium rudder.

During the post-test examination, a small crack was discovered in the web of the trailing edge lower closure rib of the front torque box at the rear spar line. As shown in Figure 68, the crack passed through a fastener hole, an area of high stress concentration. The crack very likely was caused by the shear load transferred from the trailing edge assembly at the rib joint. No other damage to the rudder was found.

The strain data recorded during Test 4 are shown in Figures 69 through 71. Note the reaction of strain gages 75 and 85 (Figure 70), approximately 760 seconds after the start of testing. The time corresponds to the occurrence of noise at approximately 205% DLL applied to the rudder. These gages are located adjacent to the area of the cracked web on the outer surface of the rib caps. The sudden change in recorded strain confirms the crack occurrence at this load level. Following this surge, the strains recorded by these two gages resumed the pattern of other appropriate recorded strains as loading increased to 250% DLL and was removed upon termination of the test.

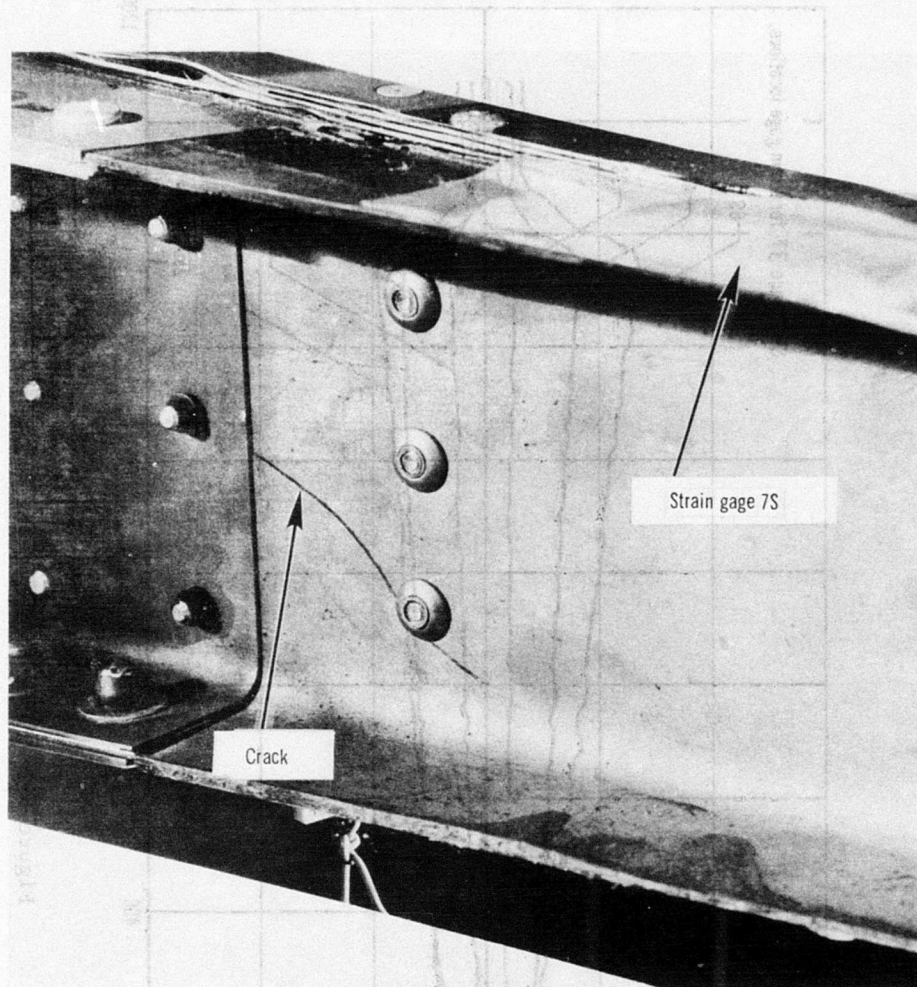


Figure 68 - Crack in Trailing Edge Lower Closure Rib of Beryllium Rudder

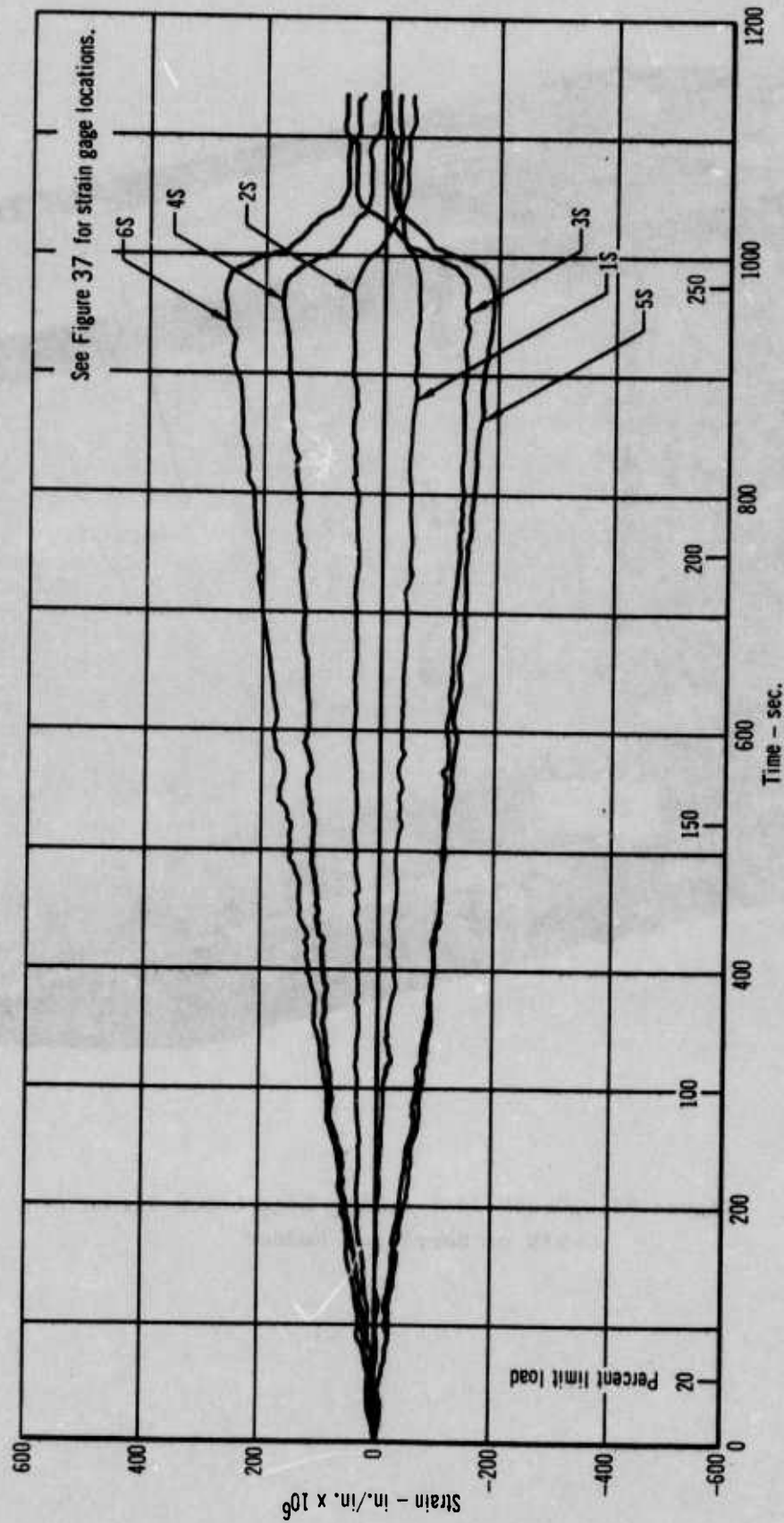


Figure 69 - Front Spar Strains: Test 4

ALBANY, N.Y. - POLARIS CORP. 25TH STREET 10000

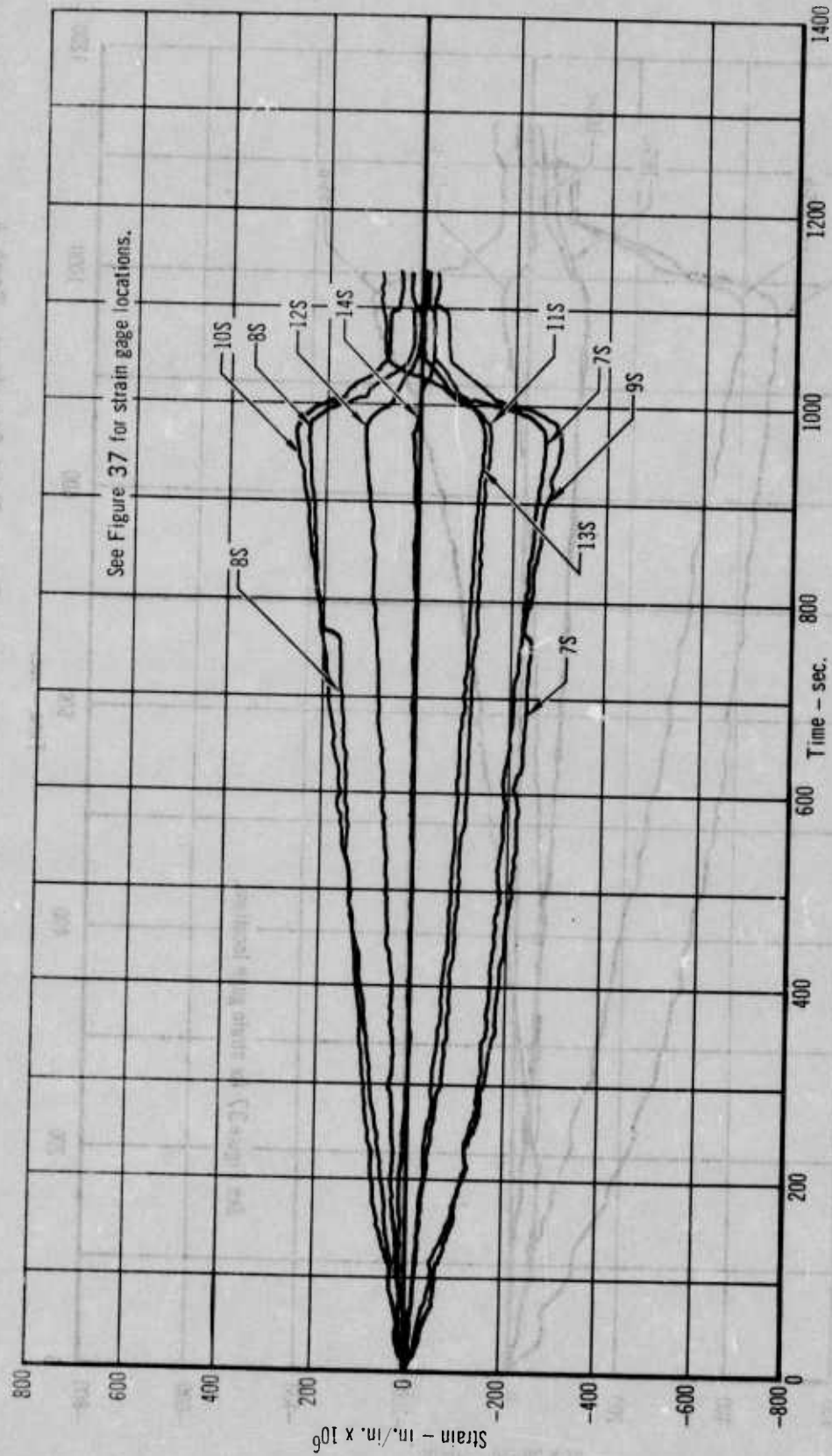


Figure 70 - Rear Spar and Trailing Edge Strains: Test 4

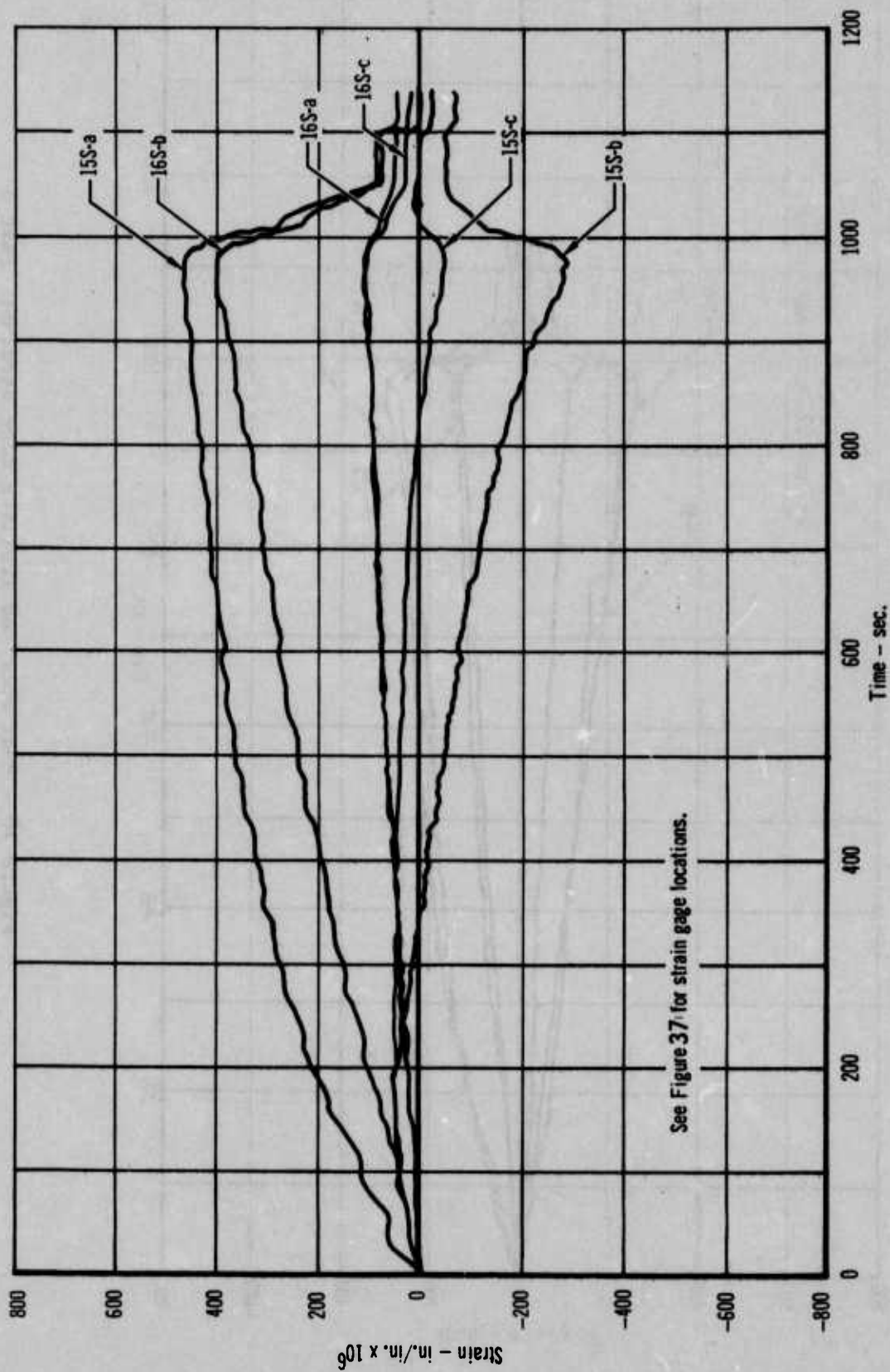


Figure 71 - Forward Cover Skin Strains: Test 4

Deflection data for this test are shown in Figures 72 through 75. The load-deflection relationships are as expected with no unusual occurrences. Figure 76 presents a schematic of the rudder with maximum recorded deflections at 250% DLL for Design Condition I. These deflections are approximately twice those recorded at 150% DLL (Design Ultimate) along the front spar and only about 1.82 and 1.75 times as great at the rear spar and trailing edge, respectively.

The ability of the beryllium rudder to sustain 250% of Design Condition I limit load without catastrophic failure demonstrates a strength capability for this condition which compares favorably with that demonstrated for the production aluminum rudder. Moreover the beryllium rudder sustained this load after being fatigue tested and twice static tested to design ultimate loads - and with a damaged primary structural member - in a ground test program more stringent than any undergone by its aluminum counterpart.

7. EPILOGUE

At the termination of the planned test program in January 1967, the rudder was removed from the test facility, and all tension pads and instrumentation were removed from the rudder. The bare rudder was then shipped to the Air Force Flight Dynamics Laboratory at Wright-Patterson Air Force Base. During the next nine months the rudder was placed on display at WPAFB and in Washington D. C. on several occasions where it was handled and mishandled by various people. While construction of a Beryllium flight test rudder continued, further ground tests were planned for this rudder.

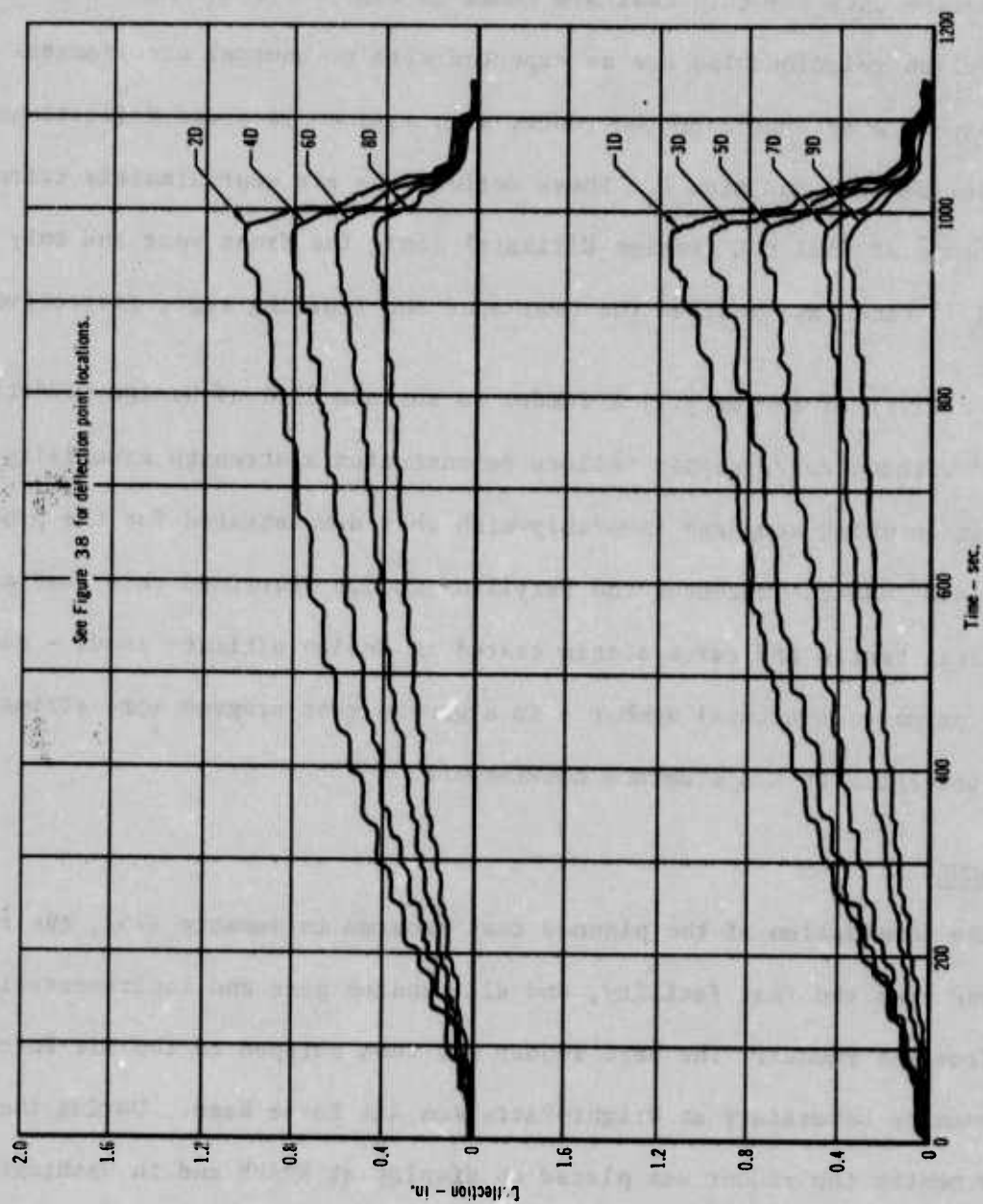


Figure 72 - Front Spar Deflections: Test 4

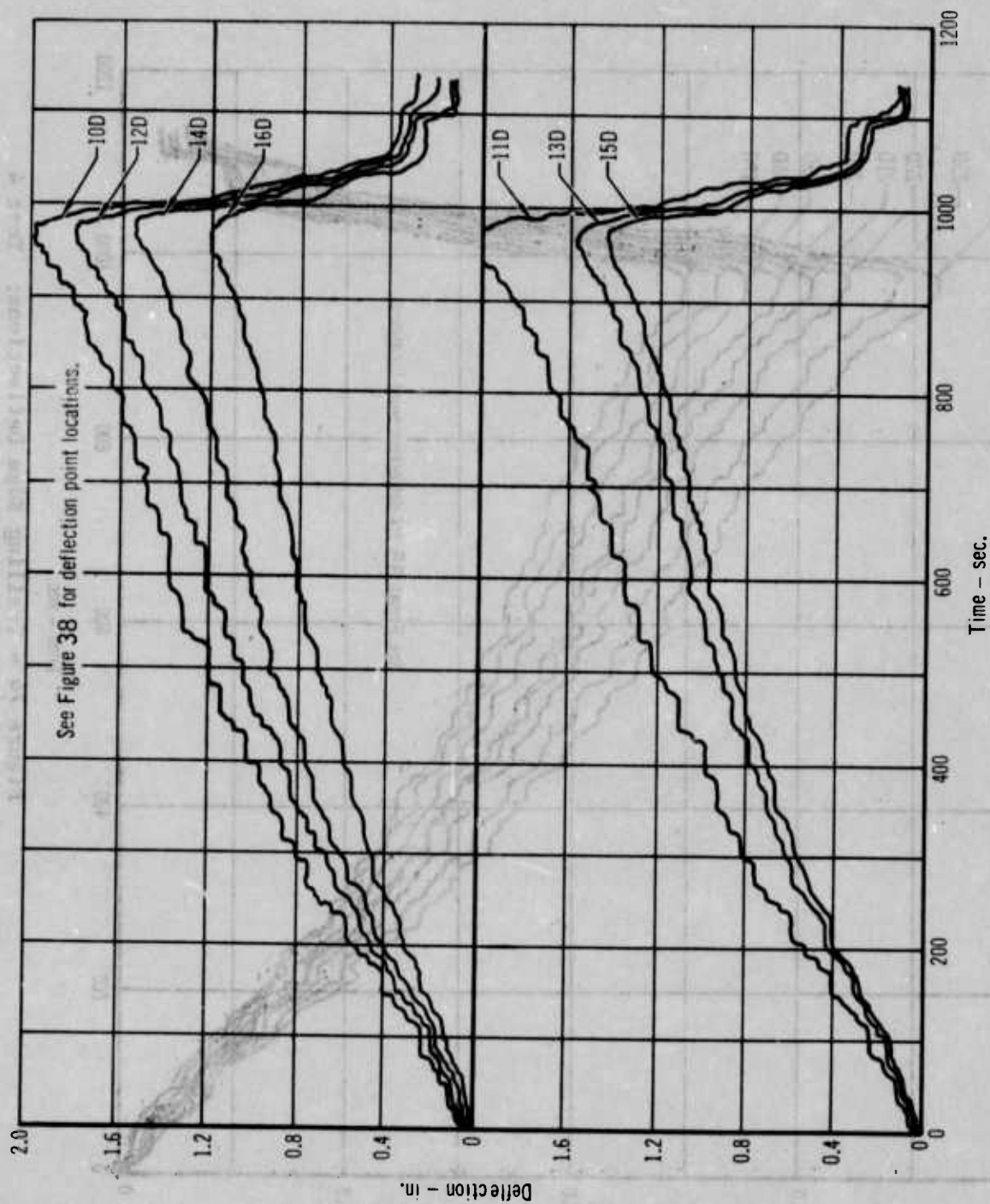


Figure 73 - Rear Spar Deflections: Test 4

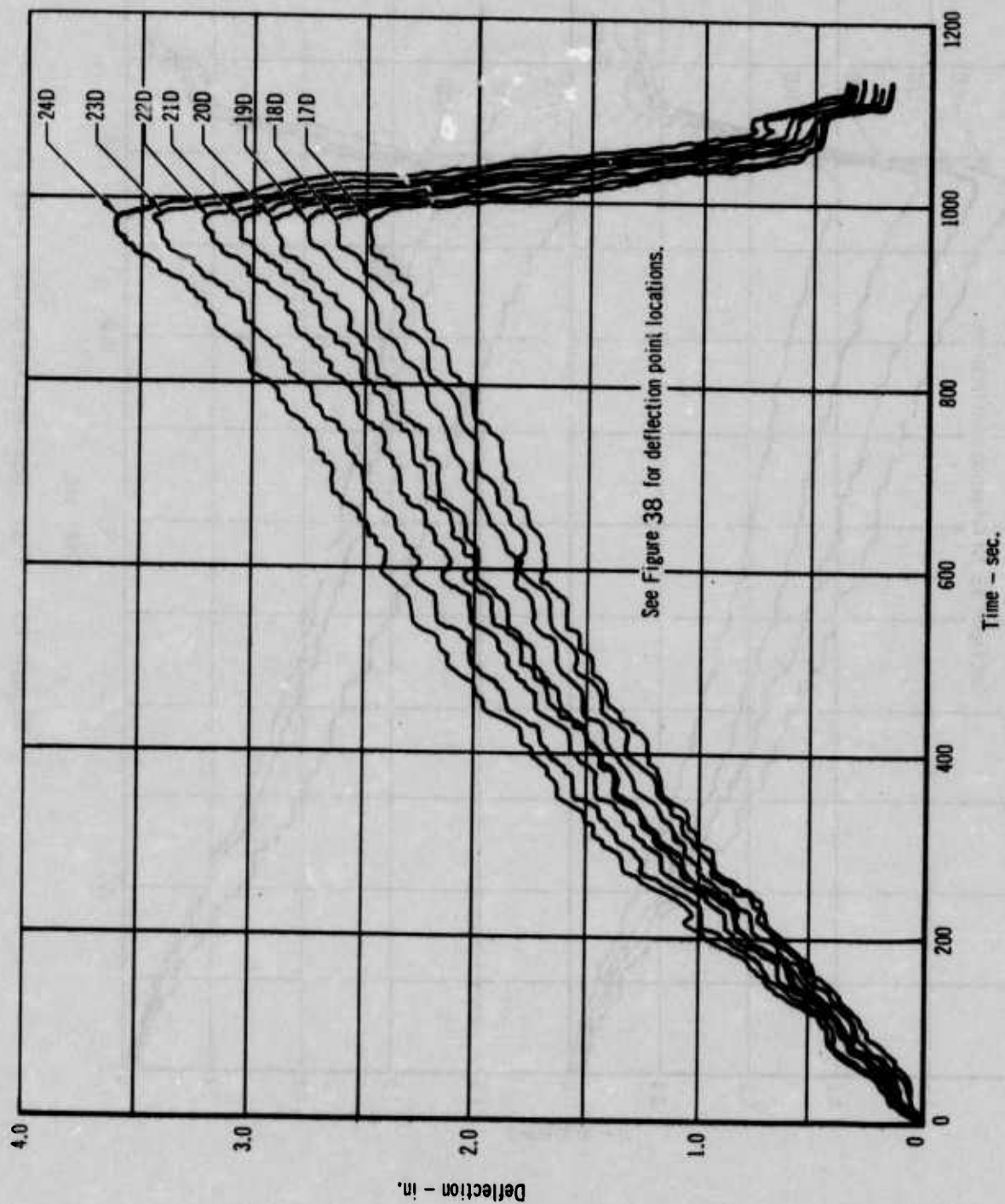


Figure 74 - Trailing Edge Deflections: Test 4

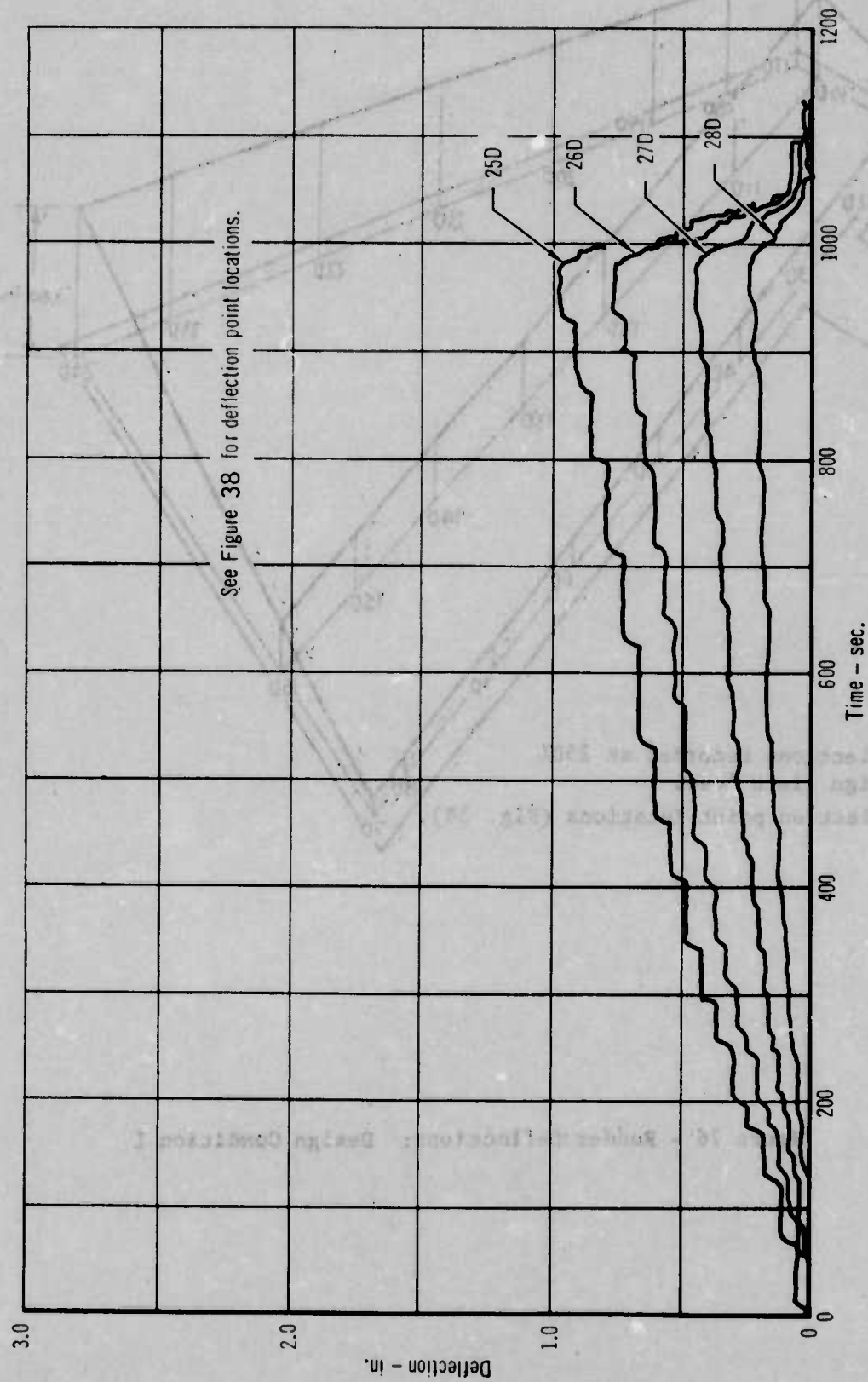
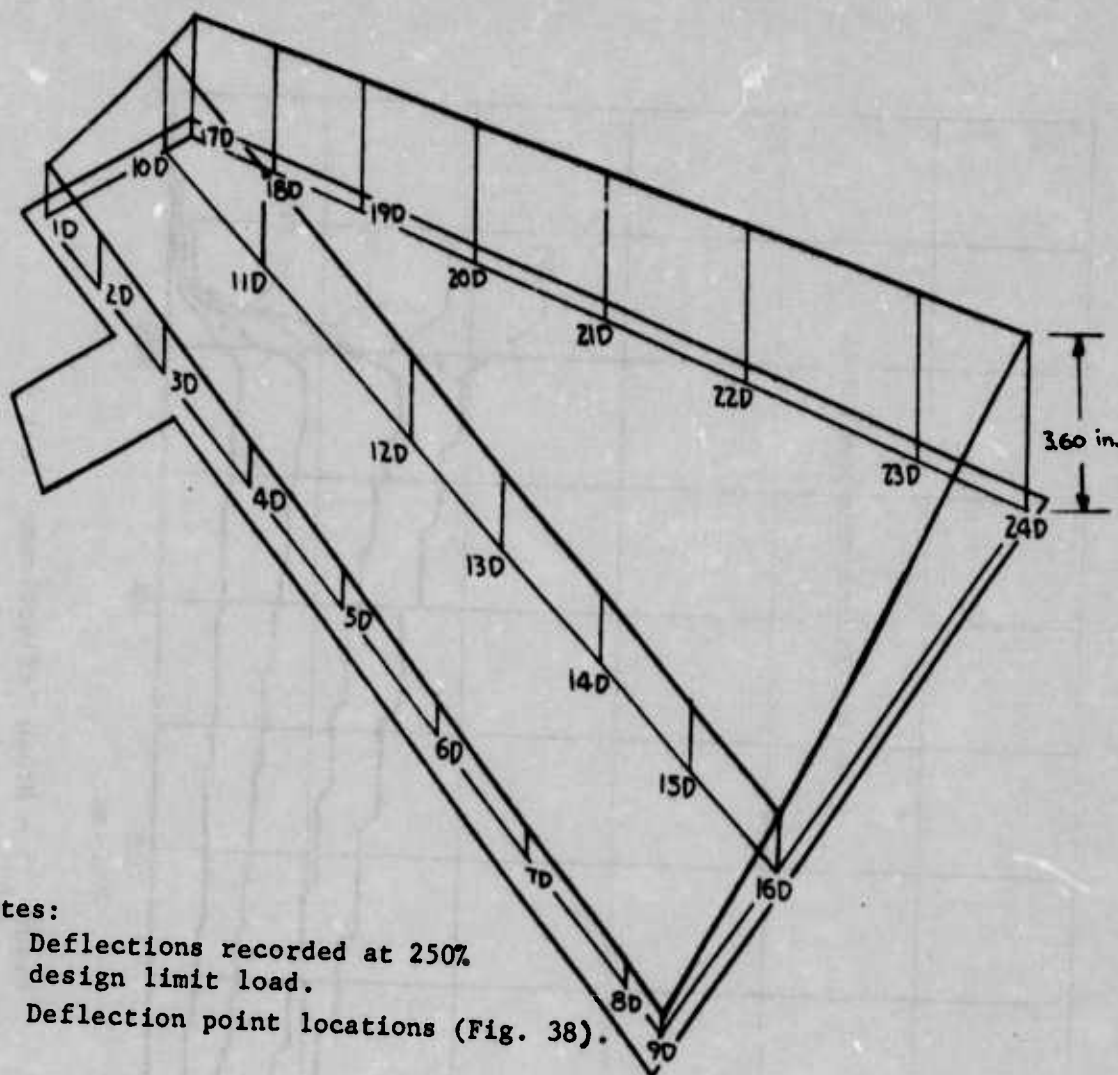


Figure 75 - Hinge Deflections: Test 4



Notes:

1. Deflections recorded at 250% design limit load.
2. Deflection point locations (Fig. 38).

Figure 76 - Rudder Deflections: Design Condition I

SECTION V

ACOUSTIC FATIGUE ENDURANCE TEST

1. Introduction

In November 1967 an acoustic fatigue test was initiated to determine the susceptibility of the F-4 beryllium rudder to high intensity noise. The tests were to determine the frequency and stress response of the rudder and estimate its fatigue life. According to Miner's rule some fatigue damage had occurred in the material during the previous fatigue and static tests, but sufficient stress data on the ribs and skins was not available to predict the degree of damage. However, a test program discussed in detail in Reference 3 was conducted until fatigue failure occurred and interpretation of the data revealed the rudder withstood a total acoustic test time equivalent to about seven normal lives of the rudder.

Prior to and at intervals during the acoustic fatigue test, the Air Force Materials Laboratory made radiographic (X-ray) inspections of the rudder to locate and record internal damage growth. The details of this investigation will be discussed in Section VI; however, reference to the results of particular radiographic examinations will be made at appropriate points in this section to provide continuity.

2. Description of Test Facility and Instrumentation

Test 5 was conducted by the AFFDL Vehicle Dynamics Division in their Wide Band Test Facility, Figure 77. This facility is constructed

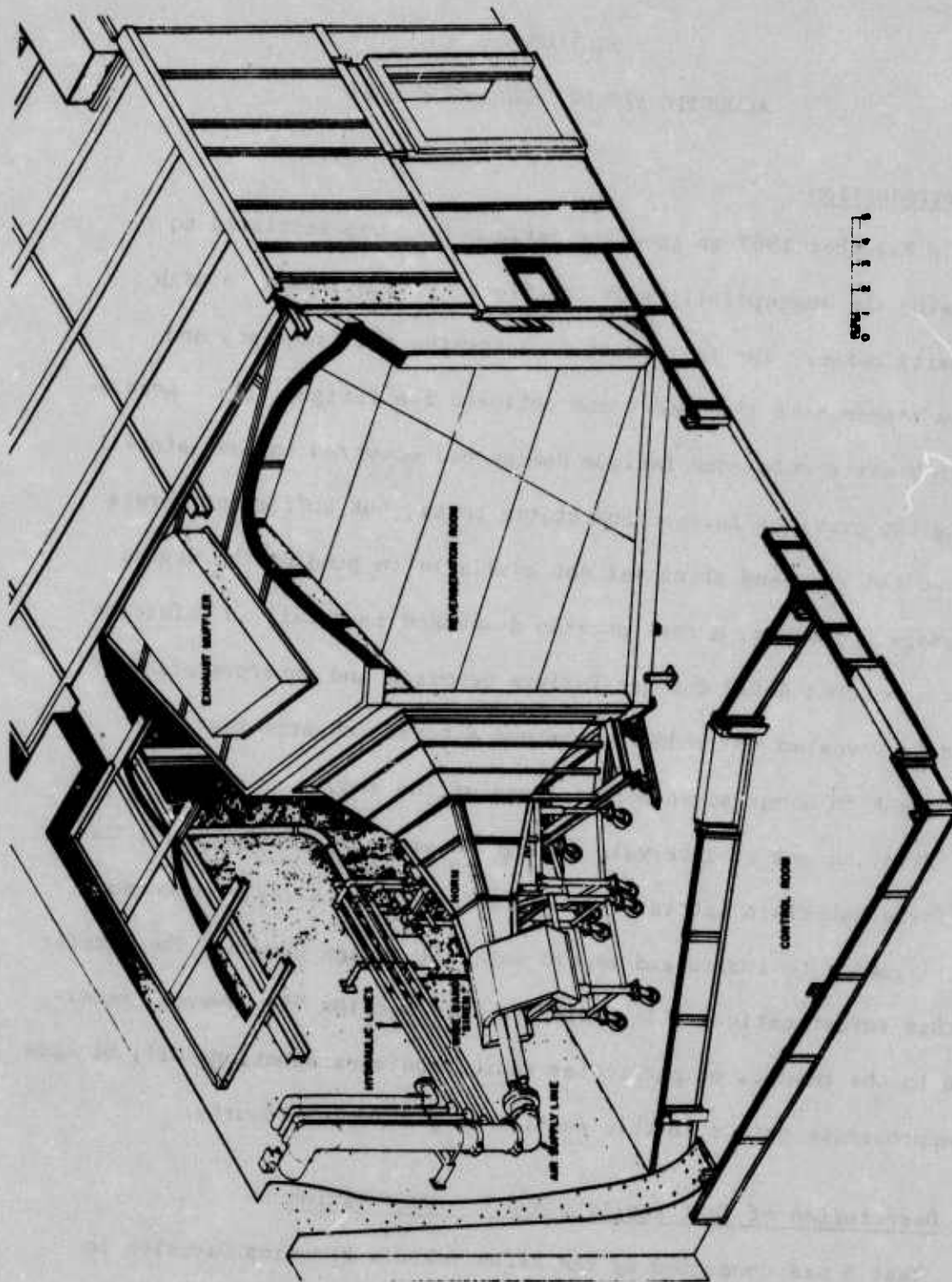


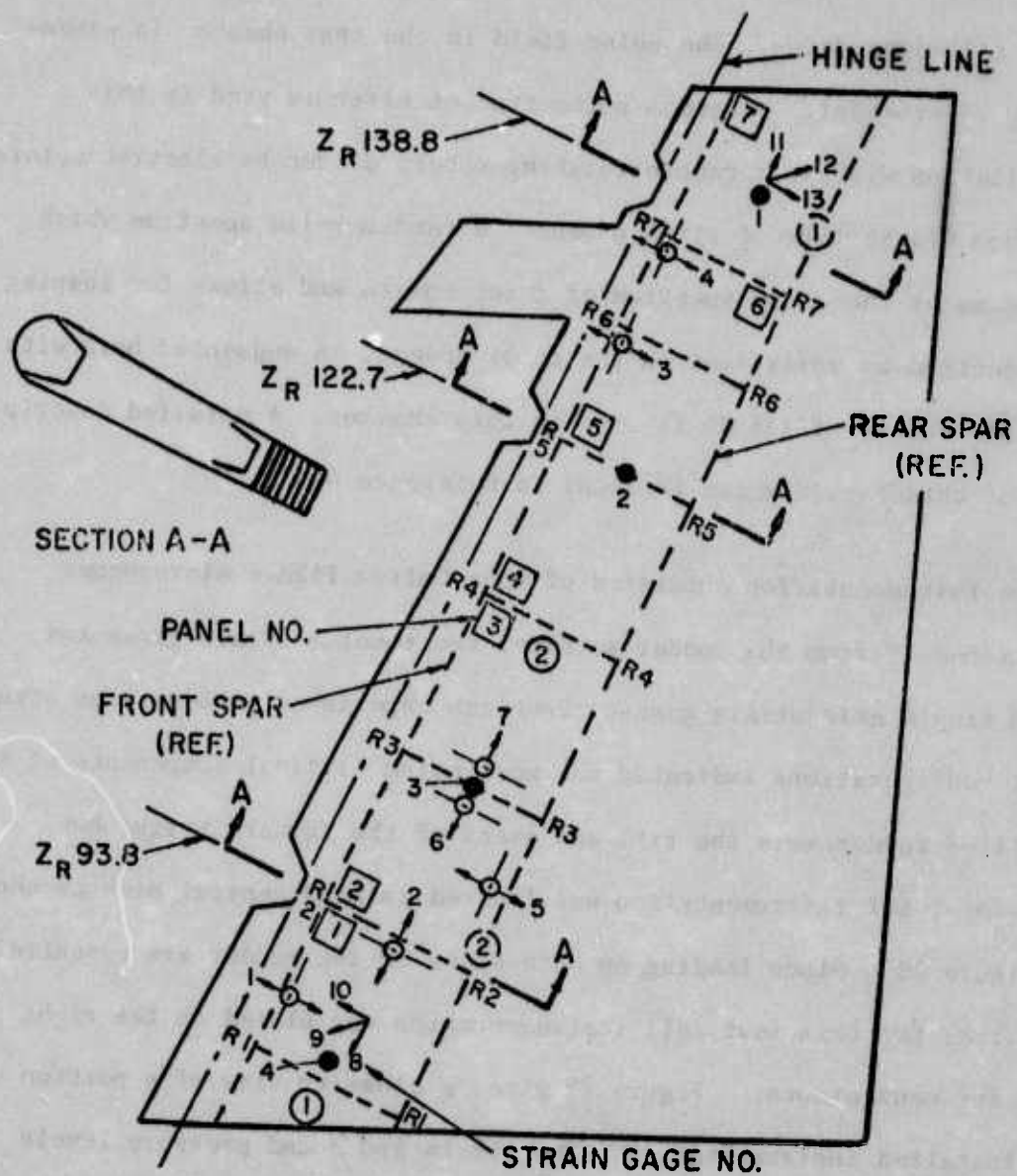
Figure 77- Wide Band Test Facility

from composite panels fabricated of steel sheets separated by fiberglass filled cavities. The noise field in the test chamber is essentially reverberant. A random-noise type of siren is used in this installation with four counterrotating rotors driven by electric motors. This von Gierke type of siren produces a random noise spectrum which approximates the sound spectrum of a jet engine and allows for shaping the spectrum by variations in the rotor speeds. A segmented horn with variable cutoff of 156 db is used in this chamber. A detailed description of this facility can be found in Reference 4.

The instrumentation consisted of four Gulton P42M-6 microphones positioned 4" from the rudder surface, two rosette strain gages and seven single axis strain gages. Previous experience with various structural configurations indicated the most noise critical components of the beryllium rudder were the ribs and skins of the forward torque box. Therefore, all instrumentation was located in this general area as shown in Figure 78. Since loading on both sides of the rudder are essentially identical for this test, all instrumentation was placed on the right side for convenience. Figure 79 gives a close-up view of a portion of the installed instrumentation. The strain and sound pressure levels were recorded on a 14-channel tape recorder. The data were analyzed with octave, 1/3 octave and 10 Hz bandwidth filters and recorded on level recorders and X-Y plotters.

3. Measured Noise Levels on the Rudder of the F-4 Aircraft

The results of two independent measurements of the actual noise level on operational F-4 rudders were available for use in determining the acoustic loads to be applied during acoustic fatigue test of the



1. $\leftarrow \bigcirc \rightarrow$ indicates axis of strain gages.
 $\nearrow \searrow$ indicates strain gage rosette.
2. All instrumentation on rudder external surfaces.
3. \bigcirc AFFDL microphone positions for field measurements.
4. \bigcirc McDonnell Douglas Corp. microphone positions for field measurements.
5. \bullet microphone positions for facility tests.

Figure 78- Beryllium Rudder Strain Gage and Microphone Locations

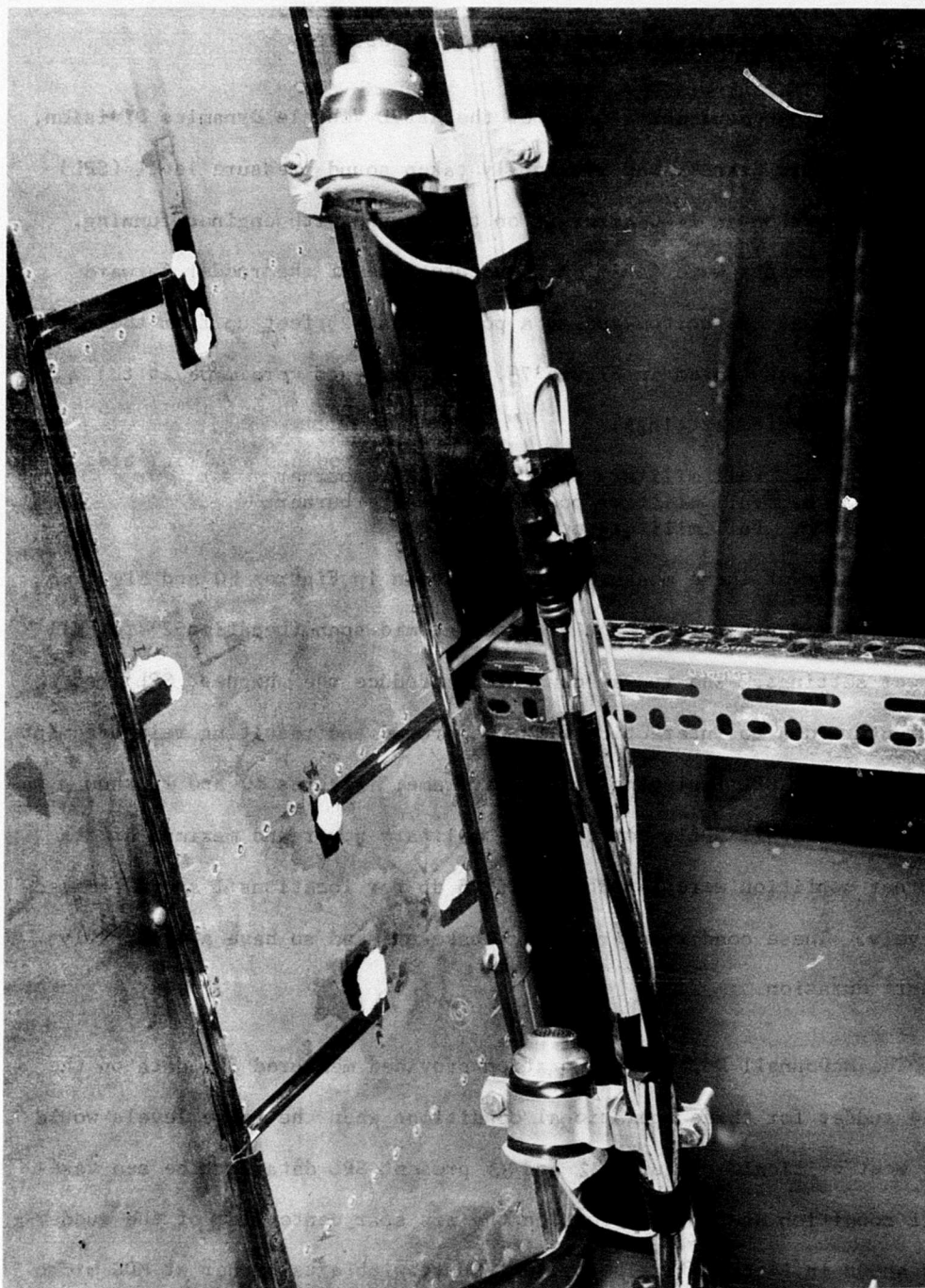


Figure 79 - Close-Up of the Strain Gage and Microphone
Instrumentation Used On the Bottom Panel of
the Rudder During the Acoustic Tests

beryllium rudder and analysis of the test results.

The Field Measurements Group of the AFFDL Vehicle Dynamics Division, Aero-Acoustic Branch, had previously taken sound pressure level (SPL) measurements on an F-4C aircraft on the ground with engines running. The measurements were taken on the centerline of the rudder forward torque box at the bottom and at a point about $2\frac{1}{2}$ feet up from the bottom as illustrated in Figure 78. Measurements were made at the following engine settings:

- a. Full military power + max. afterburner
- b. Full military power + min. afterburner
- c. Full military power

The results of these measurements are shown in Figures 80 and 81. Peak SPL measurements were slightly higher at mid-span (Location 2) for all power settings. The runway conditions produce the highest SPL's on the structure due to interaction with the ground and resulting reinforcement of the total SPL impinging on the airframe. Figures 80 and 81 show that the overall SPL's for the full military power and maximum afterburner condition were 146 db and 152.5 db for locations 1 and 2, respectively. These conditions represent take-off and so have a reasonably short duration.

The McDonnell Douglas Corporation provided measured SPL data on the F-4 rudder for three operational conditions when the noise levels would be most critical. Figures 82 and 83 present SPL data for the sea take-off condition at two locations on the aft spar centerline of the rudder as shown in Figure 78. The overall SPL's with afterburner at MDC microphone locations 1 and 2 are 149 db and 147.5 db, respectively. These measurements closely approximate those obtained by the AFFDL with vari-

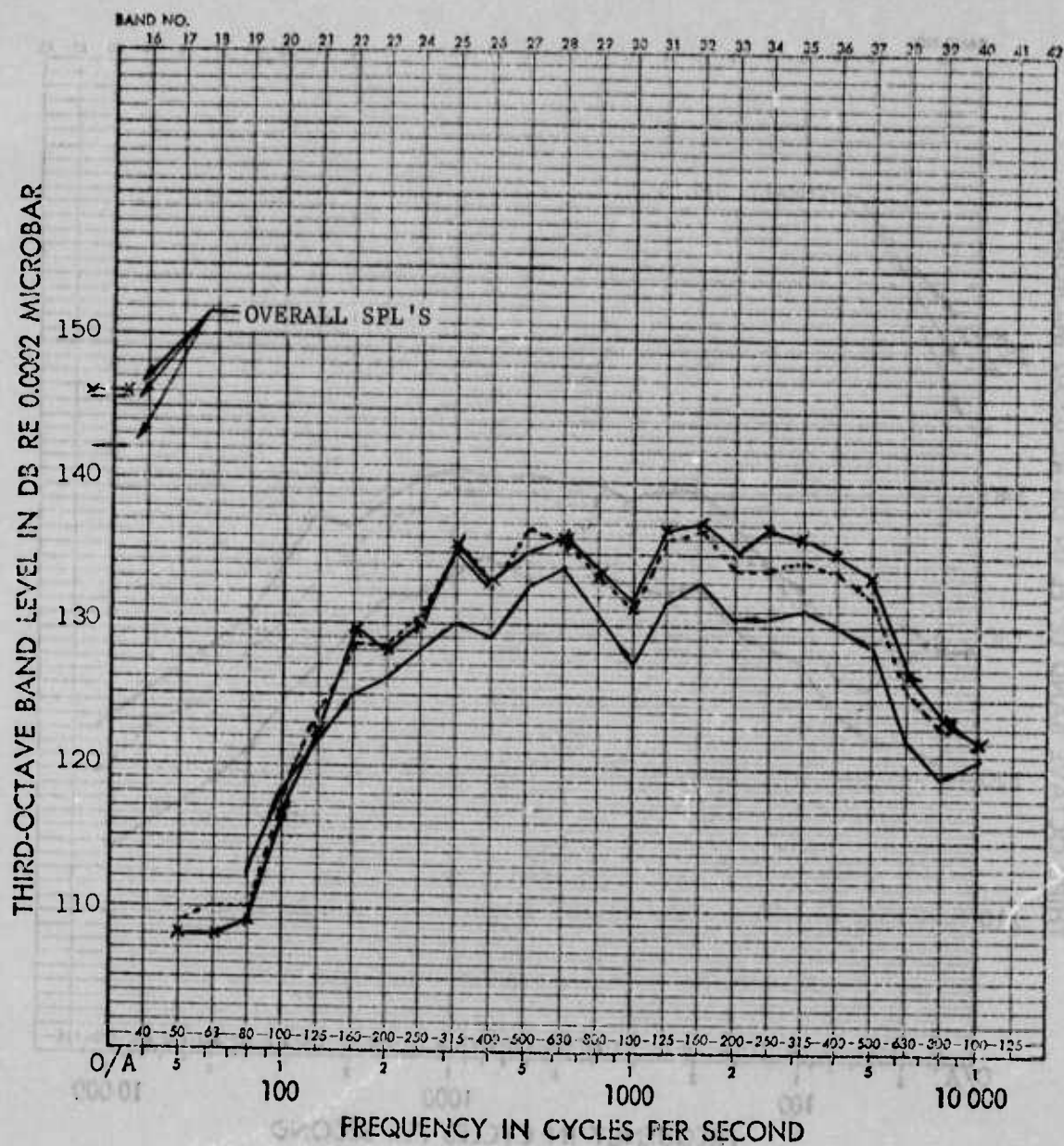


Figure 80 - SPL's Measured on Rudder of F-4 AFFDL Data Location 1

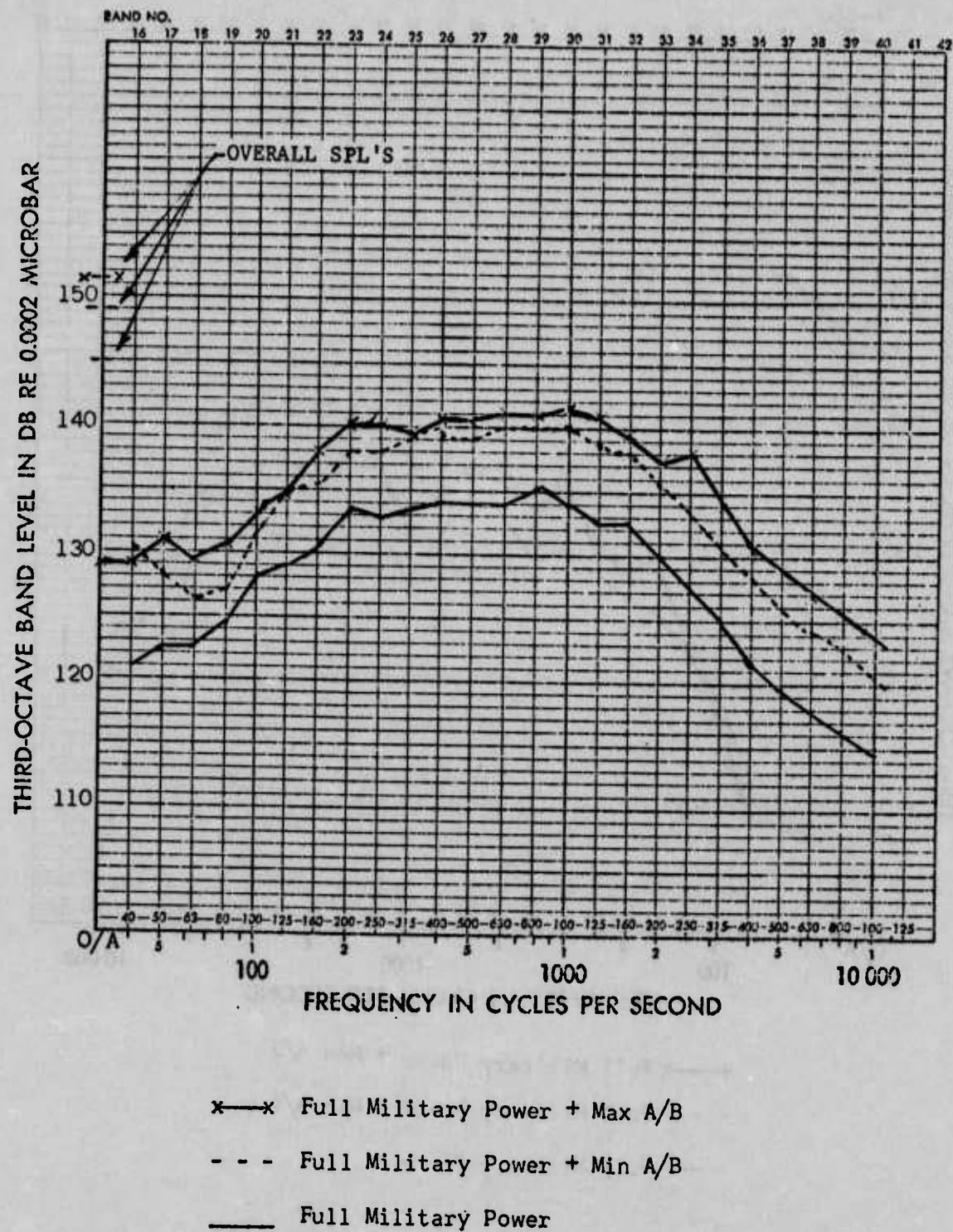
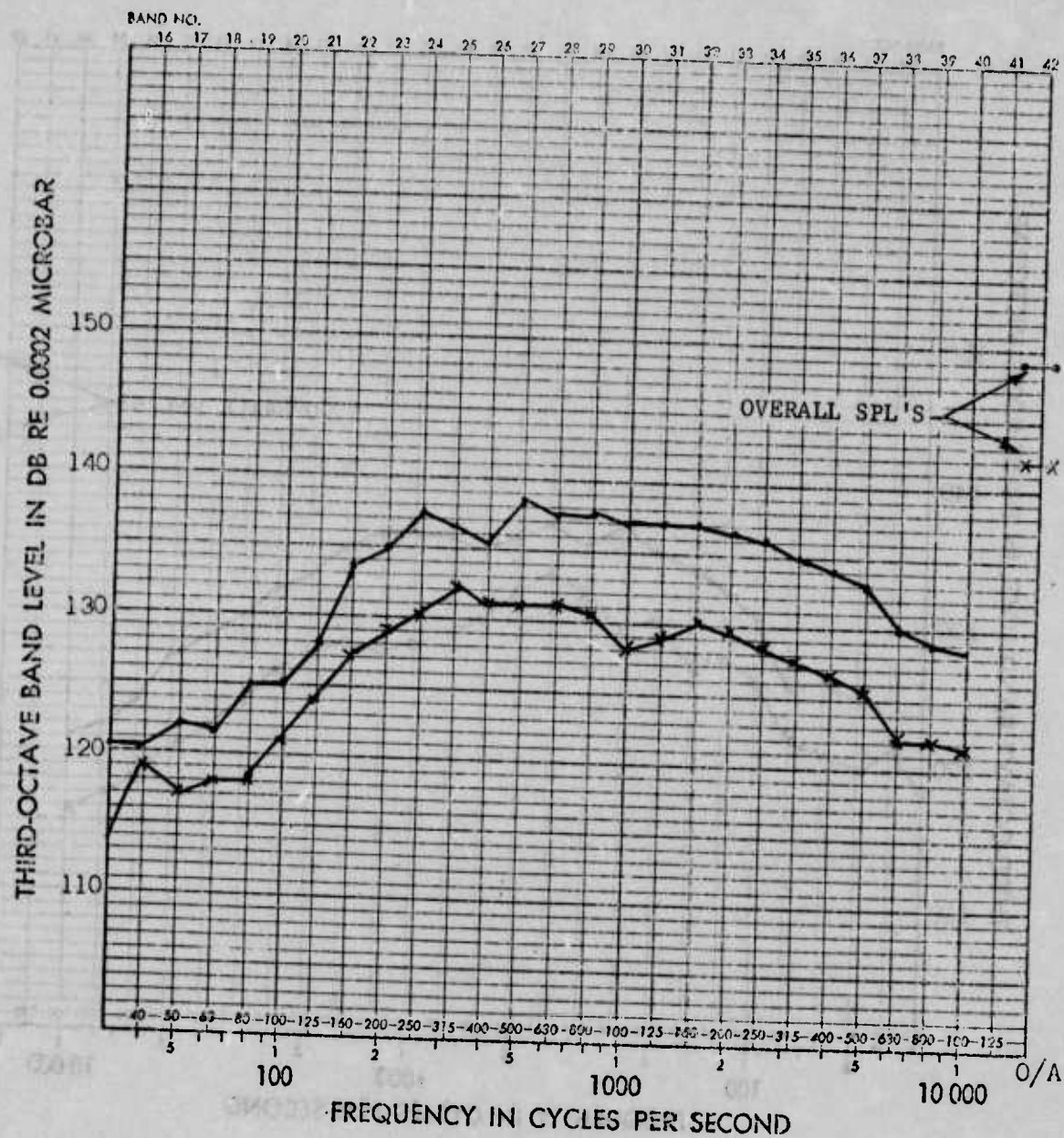


Figure 81 - SPL's Measured on Rudder of F-4 AFFDL Data Location 2



x—x Military Power (Take-off)
 —•— Afterburner (Take-off)

Figure 82 - SPL Data on the Rudder of the F-4 Aircraft
 McDonnell Douglas Corp., Location 1

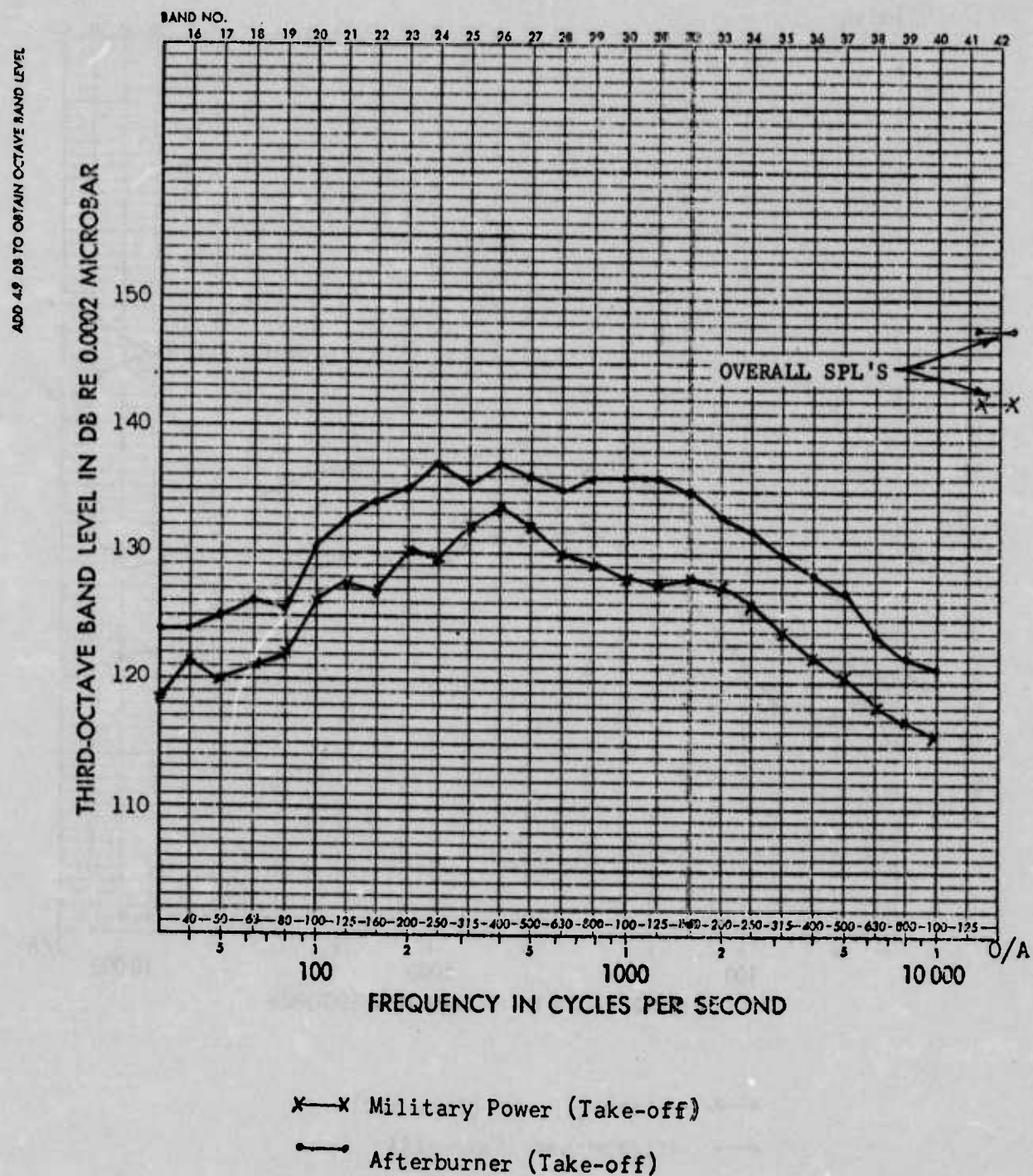


Figure 83 - SPL Data on the Rudder of the F-4 Aircraft
McDonnell Douglas Corp., Location 2

ations in engine settings, atmospheric conditions and placement of microphones contributing to the range of measurements recorded. Figure 84 is a presentation of maximum and minimum SPL measurements made by AFFDL and MDC for the military power and military power plus maximum afterburner settings during ground operations. This presentation illustrates the range of SPL to which the F-4 rudder will be exposed on take-off and is useful in planning acoustic fatigue tests and analyzing the results.

The other two critical operating conditions for which the McDonnell Douglas Corporation provided SPL data on the F-4 rudder are the low and high altitude dash conditions. These data are presented in Figure 85 with the operational conditions more fully described as:

- a. Military Power at Sea Level, Mach Nr. 0.9 (Low Altitude Dash)
- b. Military Power + Afterburner at 30,000 ft., Mach Nr 1.7 (High Altitude Dash).

Similarly these data were useful in planning the acoustic fatigue test and analyzing the results.

Another important element in acoustical fatigue is the time spent under various operational conditions. The McDonnell Douglas Corporation provided the following values which represent the average amount of time an F-4 aircraft with a life of 3000 flight hours spends in each of the above three operational conditions.

- a. Low altitude dash - 210 hours
- b. High altitude dash - 30 hours
- c. Take-off - 12 hours

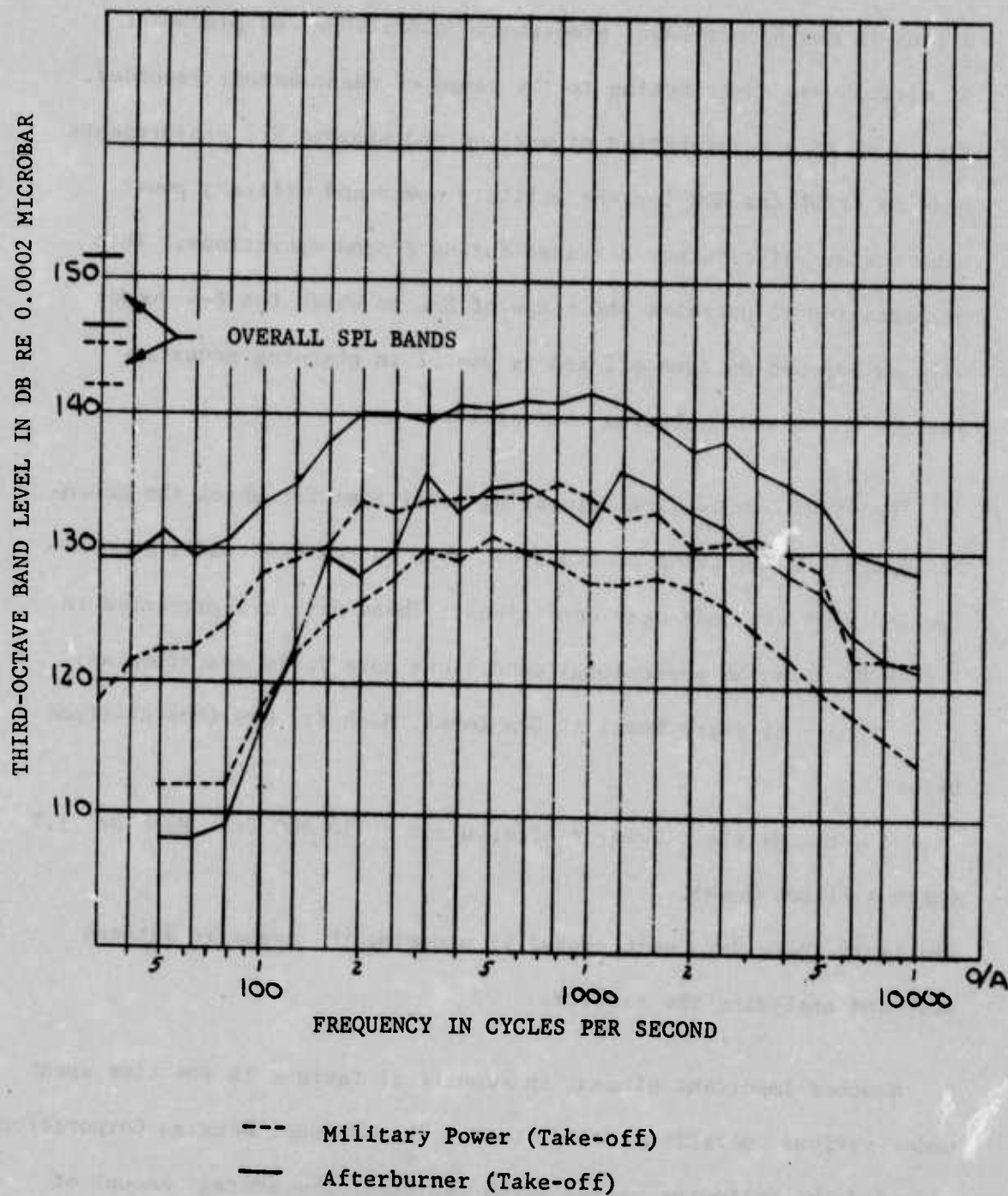


Figure 84 - Summary of SPL Data on the Rudder of the F-4 Aircraft for the Take-Off Condition

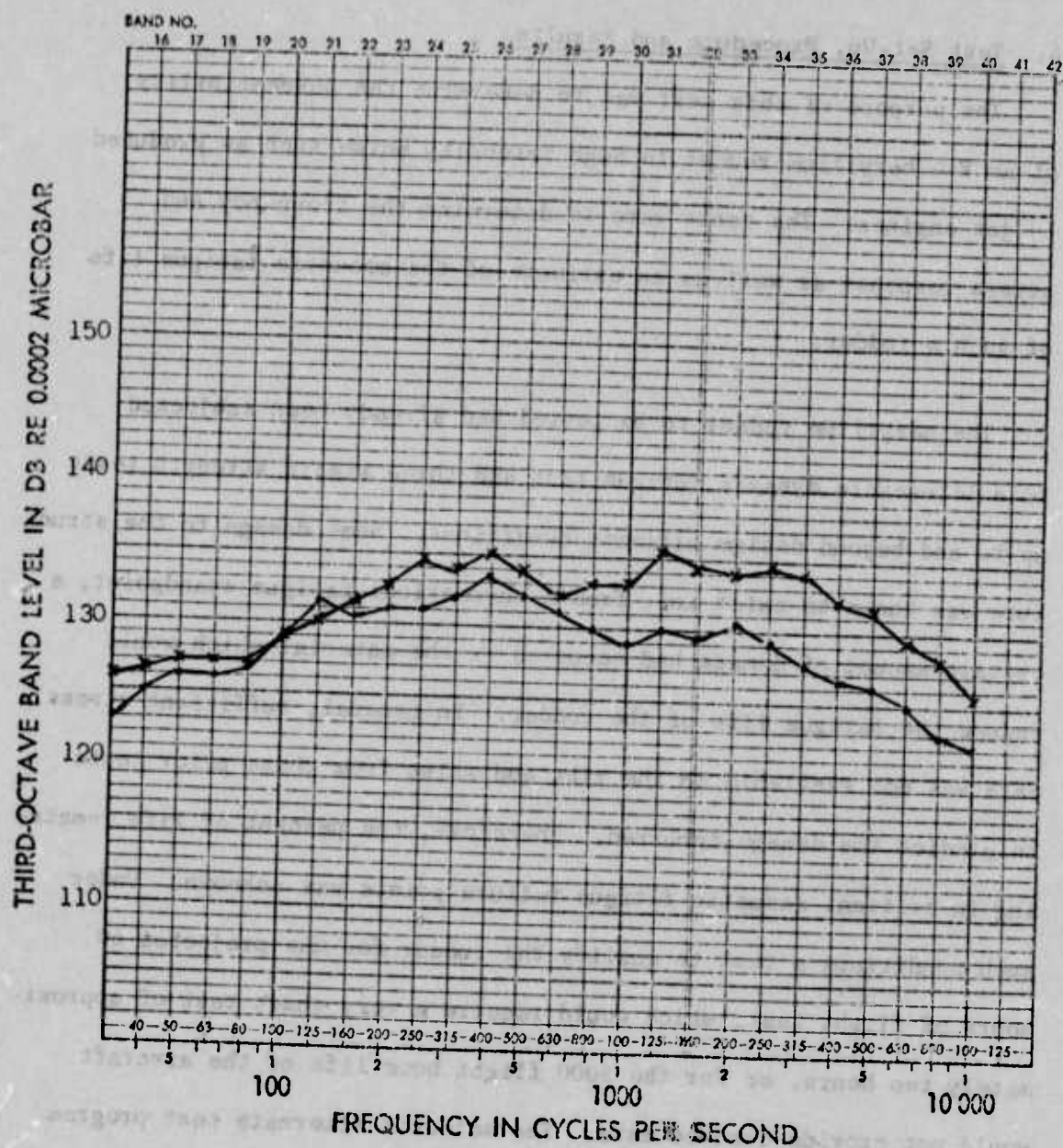


Figure 85 - SPL Data on the Rudder of the F-4 Aircraft
for Two Operational Conditions. McDonnell
Douglas Corp. Data

4. Test Set-Up, Procedure and Results

The purpose of this test was to determine the susceptibility of an F-4 beryllium rudder to high intensity noise such as produced by jet engines. The tests were to determine the frequency and stress response as well as an estimate of the acoustic fatigue life of such a rudder.

The beryllium rudder to be tested had already been subjected to a life-cycle dynamic fatigue test and three static strength tests up to and beyond design ultimate conditions. Some damage to the structure was known to exist and, from a theoretical fatigue standpoint, a certain amount of damage had occurred in the material which would reduce the fatigue life of the rudder. In general, sufficient stress data was not available on the ribs and skins from these prior tests to predict the damage incurred. Therefore, the percent of life remaining in critical acoustic fatigue failure points was unknown. Under such conditions a test to qualify the rudder for the projected 60 hours of flight test, which would require a very short test of approximately two hours, or for the 3000 flight hour life of the aircraft would not provide desired data. The selected alternate test program was a test until failure occurred. Failure was defined as a fastener failure or a break or crack in the beryllium material that could be detected by the unaided eye. This test would provide the greatest amount of information concerning the dynamic and fatigue properties of the rudder. Absolute values of time to failure would require interpretation since the rudder had incurred previous damage. However, since this was basically an R&D program, the most informative program

was selected.

The timing and nature of this test program provided a unique opportunity to correlate a non-destructive inspection technique which had recently been extended to include beryllium structures with the acoustic fatigue test of the rudder. As a part of the F-4 beryllium rudder flight test program the McDonnell Aircraft Co. had developed and demonstrated procedures for X-ray radiographic examination of the flight test rudder. Based on MCAIR's procedure, the Air Force Materials Laboratory's Processing and Nondestructive Testing Branch successfully applied radiographic inspection techniques to prepare a pictorial record of internal damage within the beryllium rudder prior to acoustic fatigue test, and growth of this damage at intervals during the test series. Details of this inspection will be covered in Section VI.

After a preliminary radiographic inspection, the instrumented rudder was installed in the AFFDL Wide Band Test Facility on a specially fabricated frame as shown in Figure 86. The orientation was similar to that of the rudder mounted on its hinge points with the noise source forward. Placement of the rudder within the chamber was such that the SPL was equally distributed on each side of the rudder. The horn mouth can be seen in the background of Figure 86. The rudder was then subjected to the high intensity noise field according to the schedule presented in Table 6. The test, with appropriate inspection periods, was continued until panel failure occurred.

The sound pressure level distribution over the rudder was measured



Figure 86 - Rudder Mounted in Test Stand Ready for Testing

by microphones at the locations shown in Figures 78 and 86. Measuring the distribution of sound pressure over the rudder was accomplished at the beginning and end of each test and at intermittent points during the test as determined by the test engineer. The monitoring microphones were continuously monitored. Strain gage data were continuously monitored and recorded during the duration of the test.

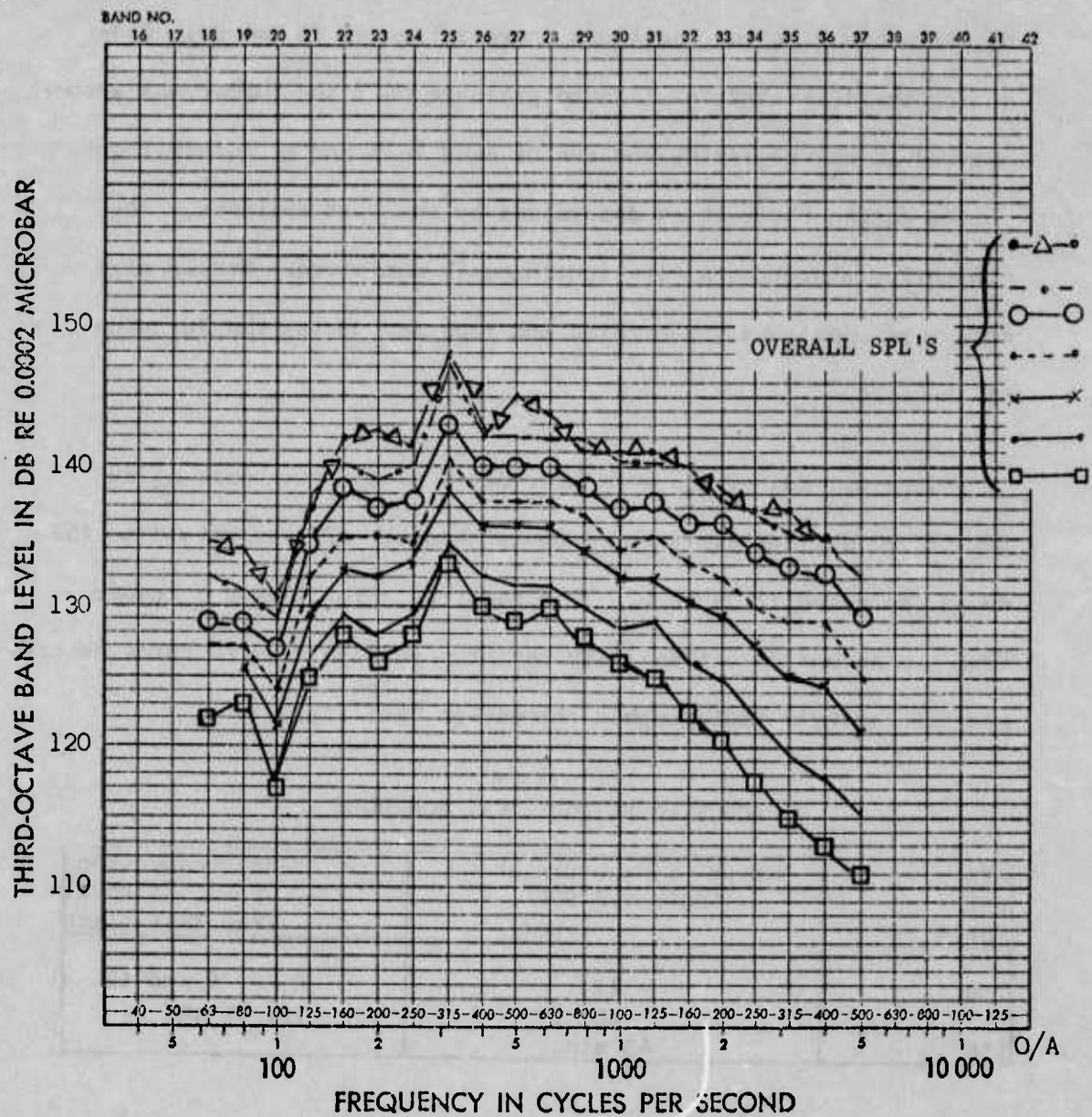
Follow-up radiographs were made after every four hours at an SPL of 150 db, and every three hours when the SPL was raised to 153 db as indicated in Table 6. This required removal of the rudder from the acoustic test facility for transport to the Air Force Materials Laboratory's Radiographic Inspection Facility.

TABLE 6
ACOUSTIC FATIGUE TEST SCHEDULE

O/A SPL (db)*	Length of Exposure at Indicated SPL (hrs)	X-Ray Inspection Previous (hrs) From Test Start
150	12	0, 4, 8 and 12
153	10	16, 19 and 22
156	45 min.	

The test spectra used in the facility are shown in Figure 87 for overall SPL's varying from 139.5 dB up to 156 dB as measured at microphone position 2 (Figure 78). Overall sound pressure levels measured at microphone positions 1, 2, 3, and 4 (Figure 78) were within ± 1 dB from the nominal values given in Table 6 throughout the duration of the test. The spectra used were the best approximation to the noise produced by the aircraft obtainable in the facility.

*All SPL's in this report are referenced to 0.0002 Dynes/cm².



- 139.5 dB O/A
- 142 dB O/A
- × 145 dB O/A
- 148 dB O/A
- 151 dB O/A
- · - 153 dB O/A
- △ 156 dB O/A

Figure 87 - Test Spectra, Microphone Position 2

The external parts of the rudder were visually inspected after each hour of test in addition to the radiographic examinations previously mentioned. Materials such as dyes were permitted in an effort to detect small unopened cracks. Visual inspections showed no failures during the 12 hours at 150 dB nor the 10 hours at 153 dB. However, after seven hours at 153 dB it was noticed that the skin panel between ribs R1 and R2 (Figure 78) was "oil canning". Radiographic inspections further showed a crack propagation in rib R2. The final test was made at 156 dB and an inspection after 45 minutes showed extensive failures in the lower skin panels on both sides of the rudder.

Pictorial evidence of this damage is shown in Figures 88 thru 93. As shown, both forward torque box cover skins and rib R2 were damaged extensively with the latter virtually ceasing to exist as a structural member (Figures 92 and 93). Acoustical fatigue failures in aircraft skin/stringer construction normally occur near the supporting stringers where bending stresses are highest. With previous experience having shown aircraft skin/stringer construction more susceptible to acoustic fatigue damage than honeycomb sandwich construction, preliminary estimates and placement of all instrumentation had been predicated upon failure of the forward torque box such as occurred.

5. Analysis of Rudder Frequency, Strain and Life Characteristics

During the acoustic tests, strains were measured at 9 different locations on the surface of the rudder (see Figure 78). Rosette gages were placed at two of these locations resulting in a total of 13 gages.

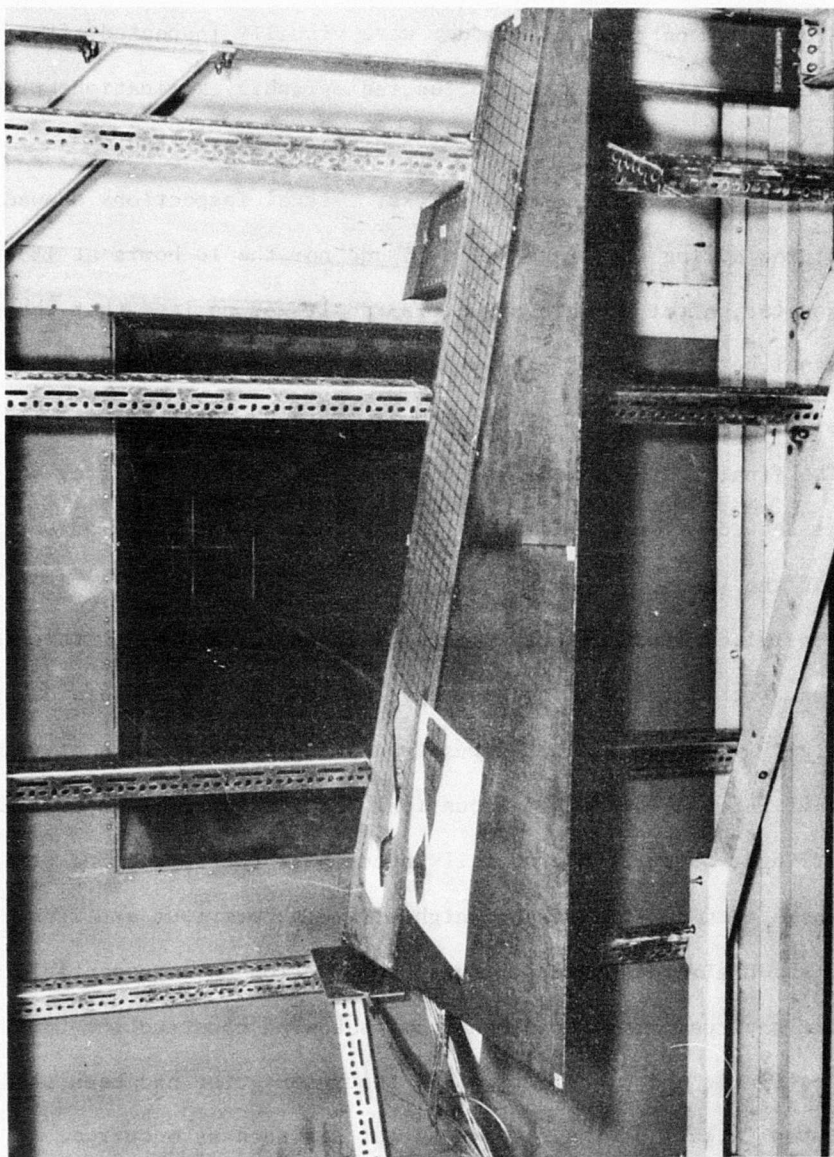


Figure 88 - Left Side of Rudder After Acoustic
Fatigue Tests Showing Failure

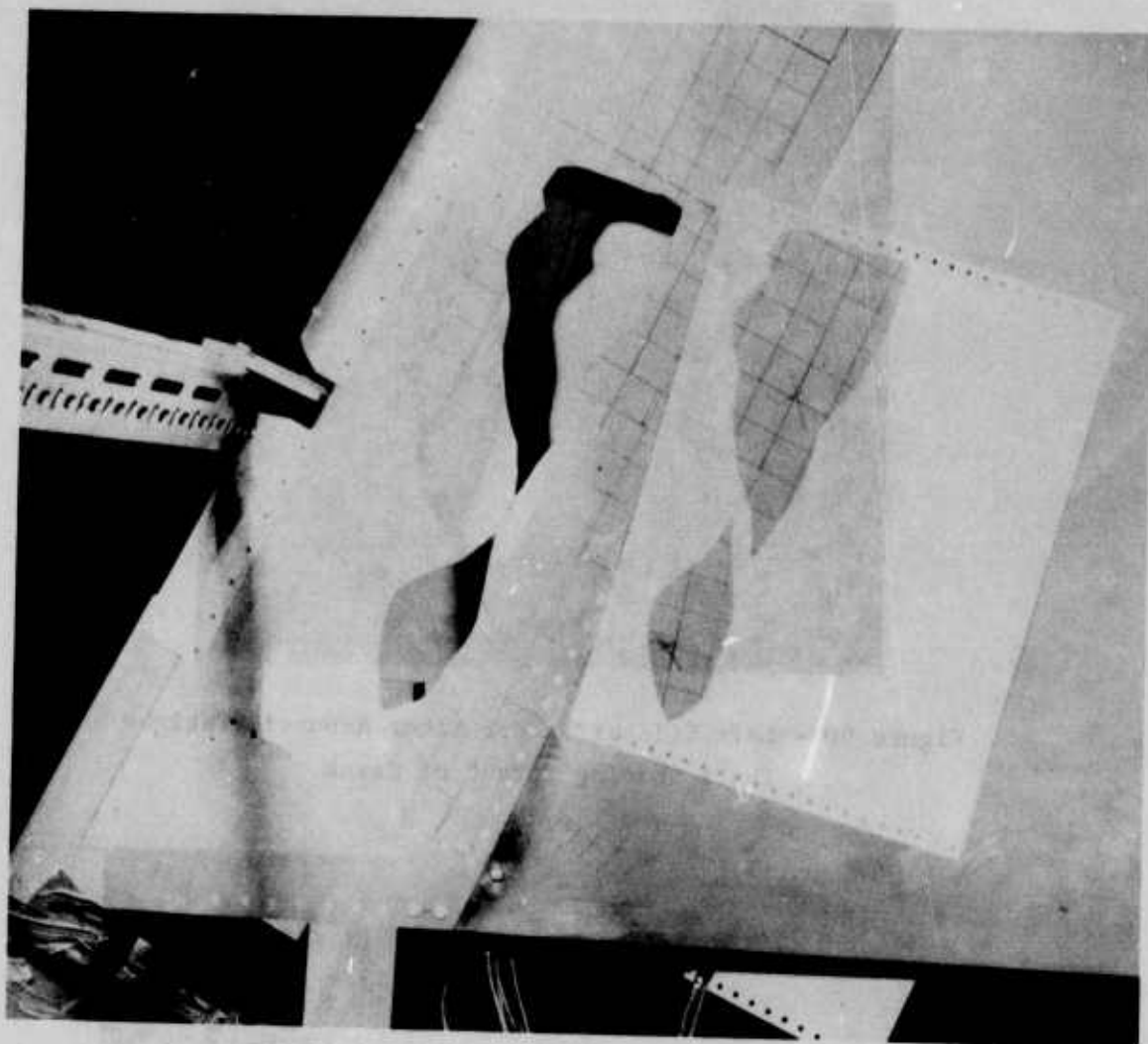


Figure 89 - Left Side of Rudder After Acoustic
Fatigue Tests (Close-Up)

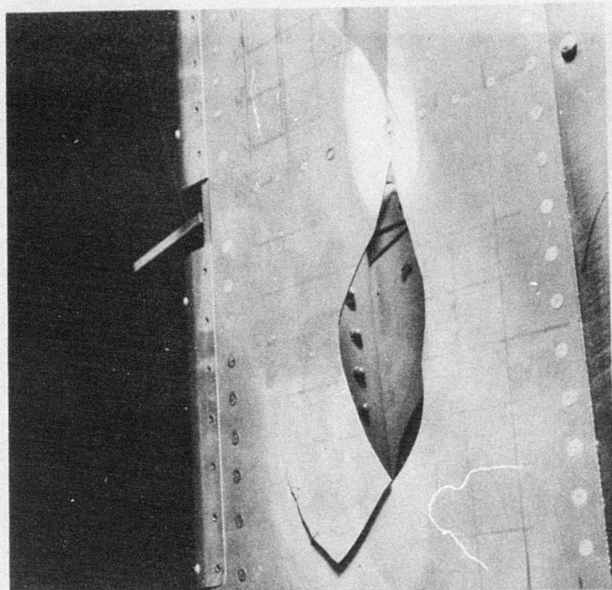


Figure 90 - Left Side of Rudder After Acoustic Fatigue Tests Showing Extent of Crack

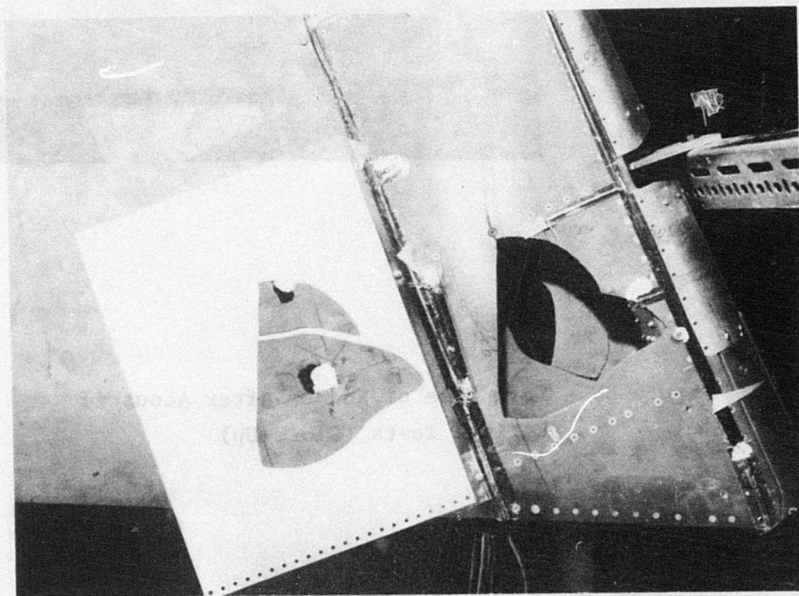


Figure 91 - Right Side of Rudder After Acoustic Fatigue Tests Showing Damage

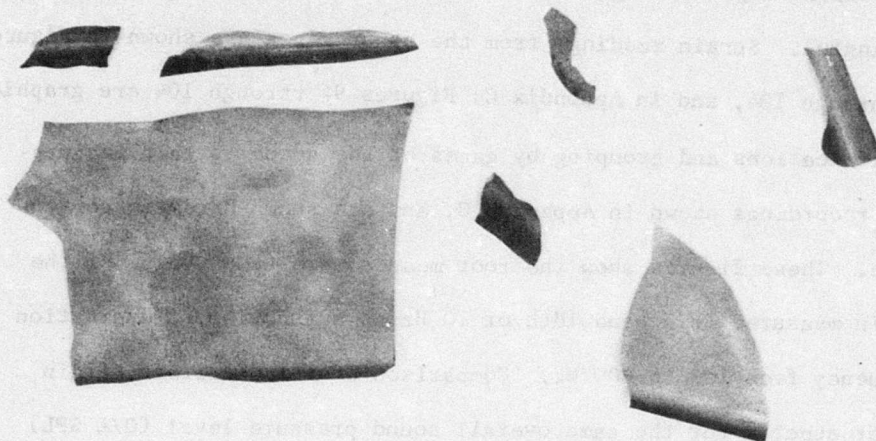


Figure 92 - Parts Broken Out of Rib R2

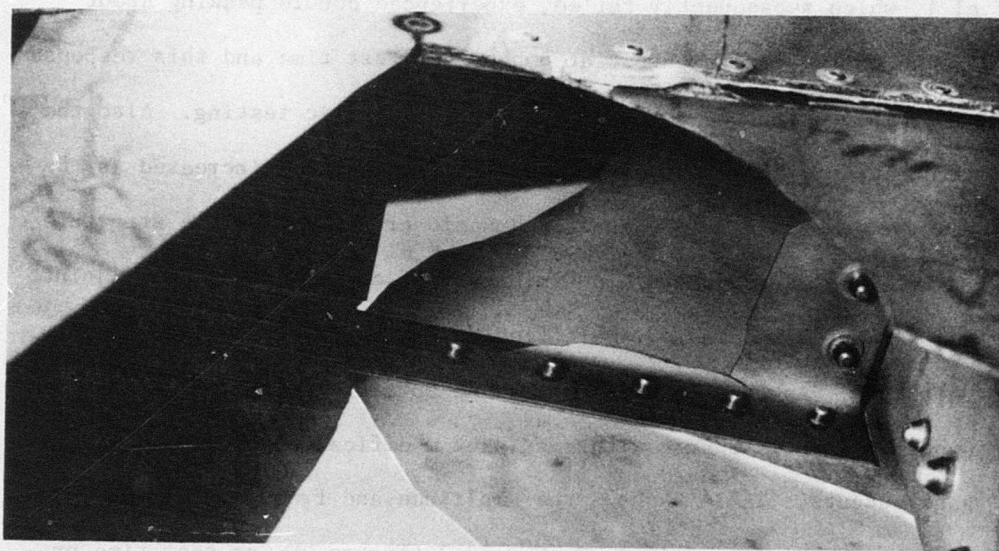


Figure 93 - Rib R2 After Acoustic Fatigue Tests

The strain output of Gages 3 and 4 was very low and not considered meaningful. Strain readings from the other gages are shown in Figures 94 through 104, and in Appendix C. Figures 94 through 104 are graphic simplifications and grouping by gages of the actual strain measurement recordings shown in Appendix C, and are shown here for convenience. These figures show the root mean square (RMS) value of the strain measured in a bandwidth of 10 Hz as a function of excitation frequency from 100 to 800 Hz. Comparison of the different strain output spectra for the same overall sound pressure level (O/A SPL) but for different test times show amplitude and frequency shifts and in some cases the shape of the output response curve has changes. Table 7 provides a numerical presentation of the maximum response frequency for each recording strain gage versus the cumulative test time. Panel 1, which subsequently failed, experienced double peaking about 470 Hz on the strain output at 8 hours of test time and this response phenomenon continued through 22 hours of acoustic testing. Also the frequency of the maximum response peak from panel 7 increased as the test progressed. This change in dynamic properties of the structure is interpreted as due to "loosening up" of some of the riveted joints and supported the radiographic finding that a crack was propagating in rib R2. As the structure "loosened up", its stiffness and damping properties would change with resultant modification of the strain gage outputs. Table 8 shows the amplitude and frequency of major resonant peaks in panels 1, 2, 3, and 7 (Figure 78) as test time progressed. Major resonant peaks on panels 1 and 7 were originally in the 470 Hz range with a second peak occurring about 580 Hz as loading

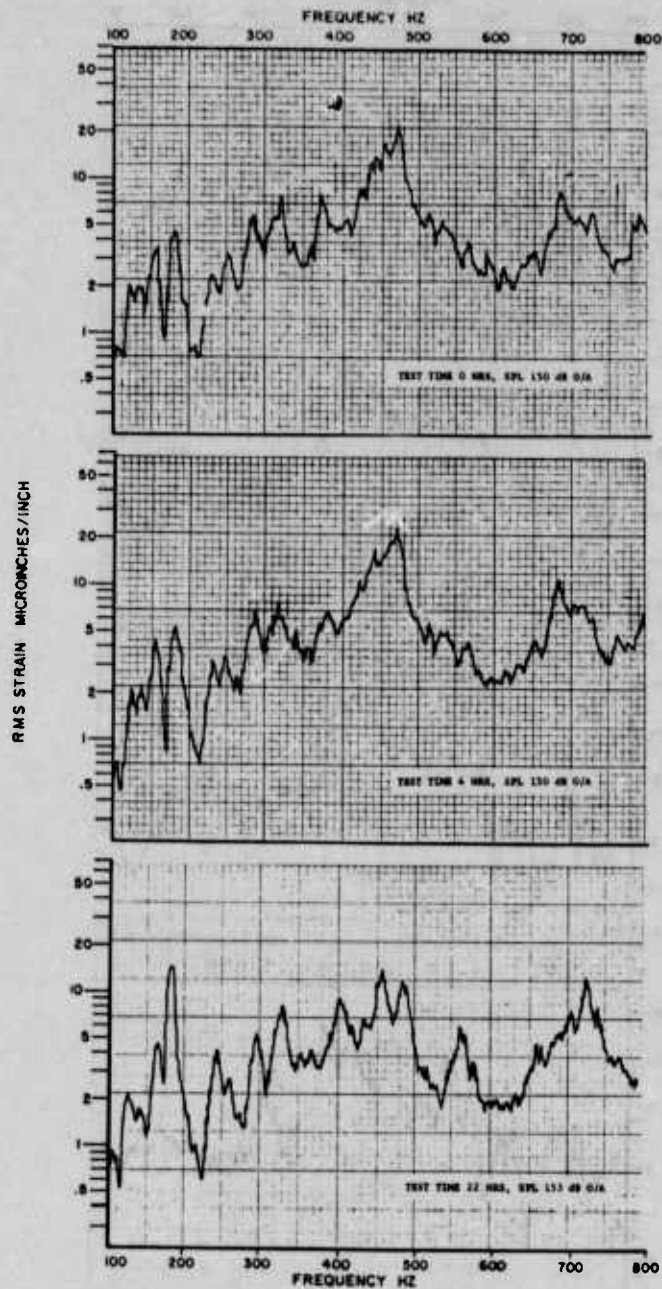


Figure 94 - Output of Gage Nr 1

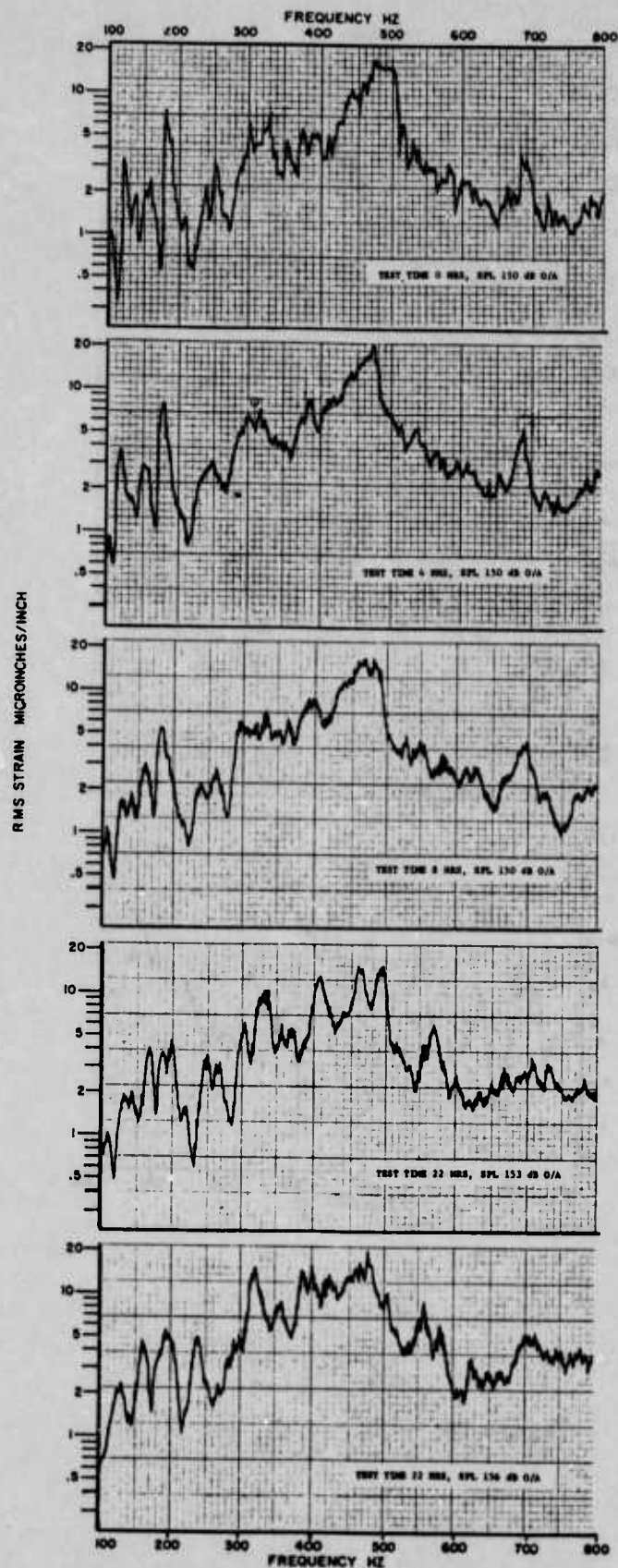


Figure 95 - Output of Gage Nr 2

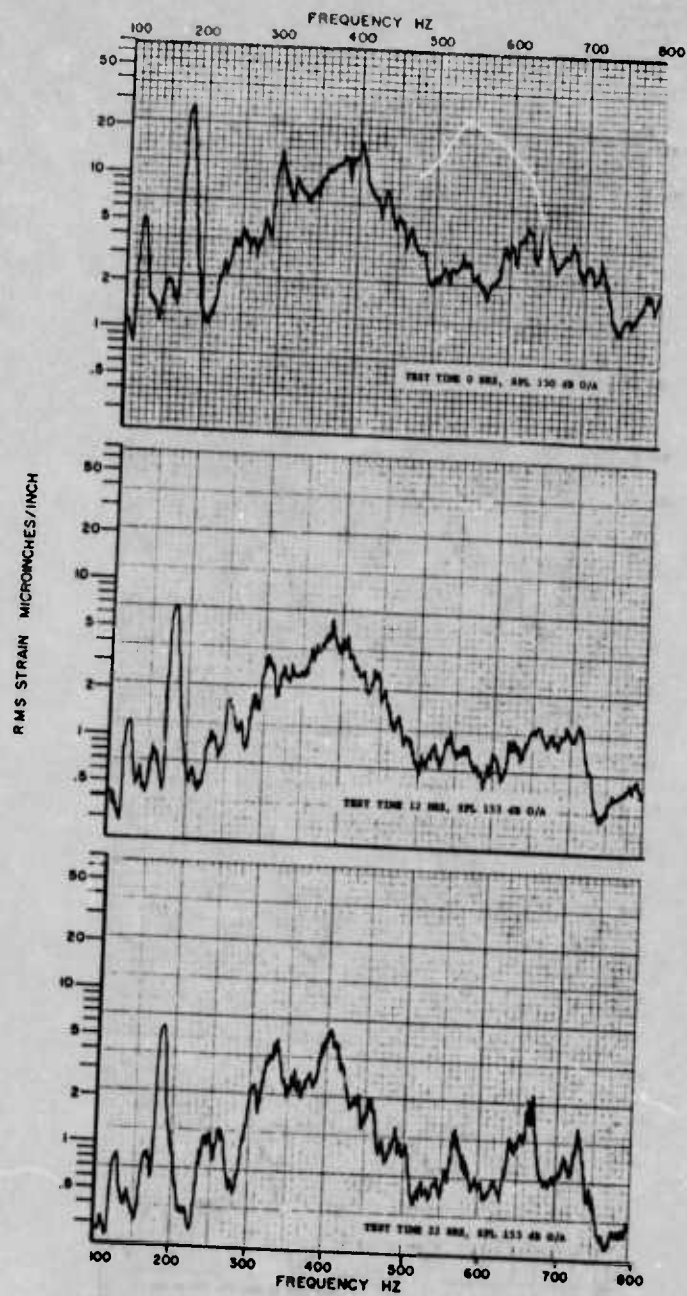


Figure 96 - Output of Gage Nr 5

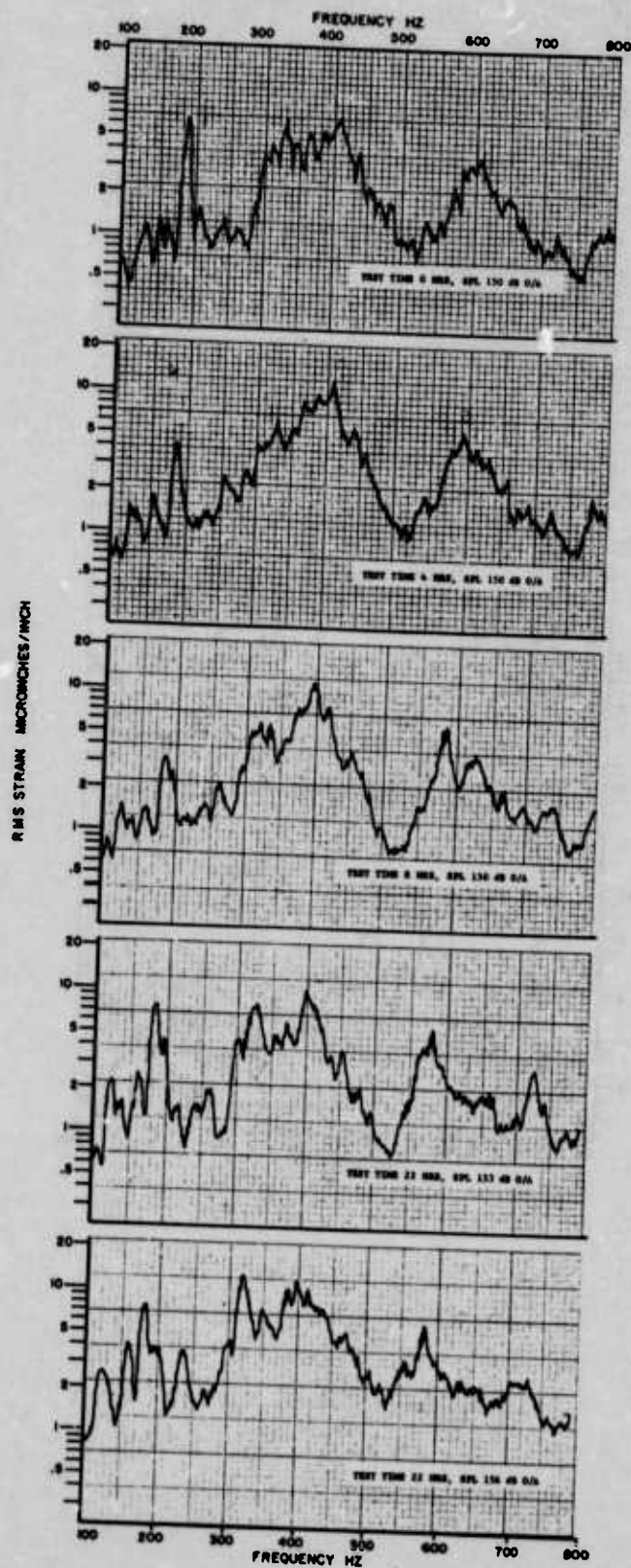


Figure 97 - Output of Gage Nr 6

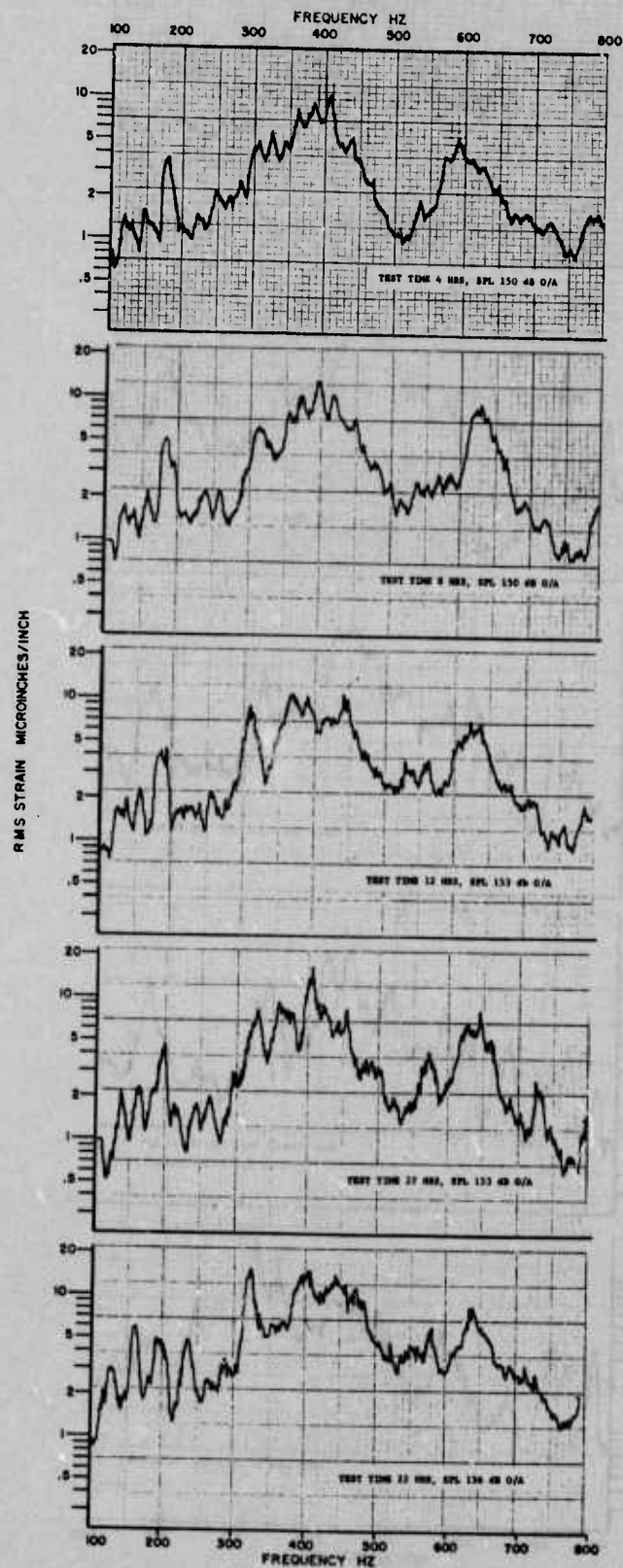


Figure 98 - Output of Gage Nr 7

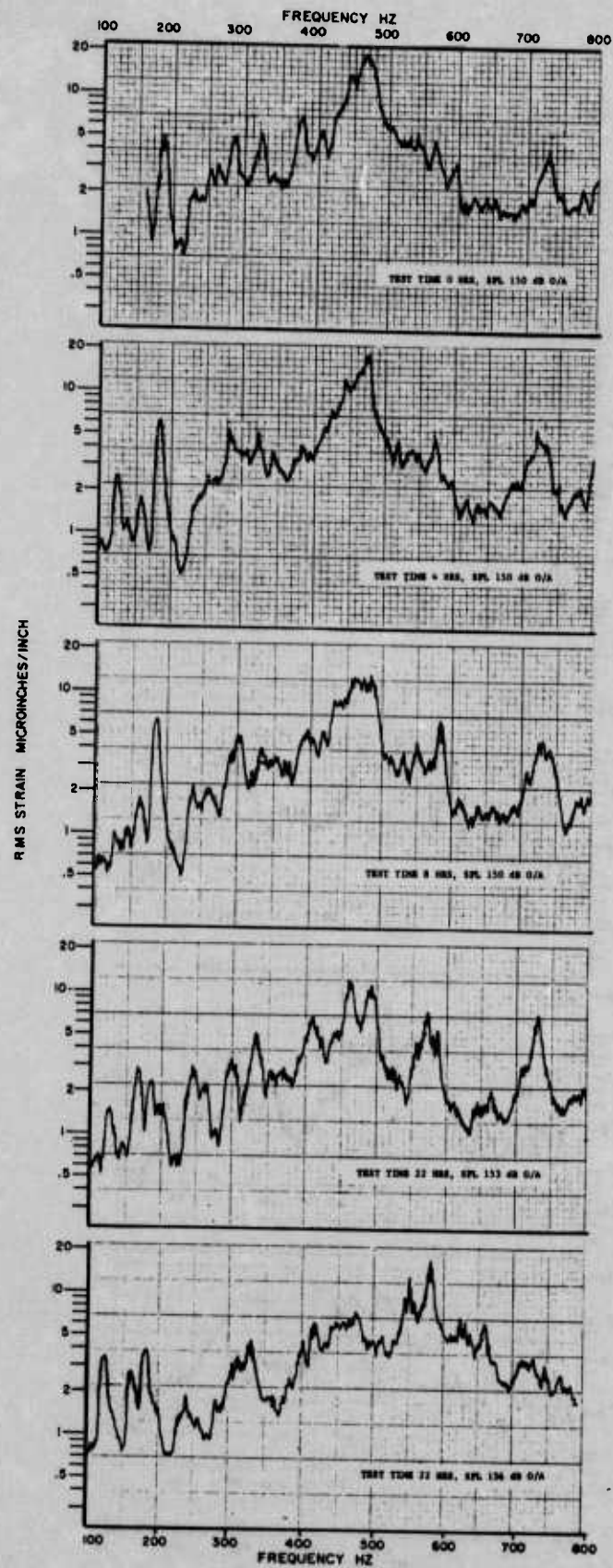


Figure 99 - Output of Gage Nr 8

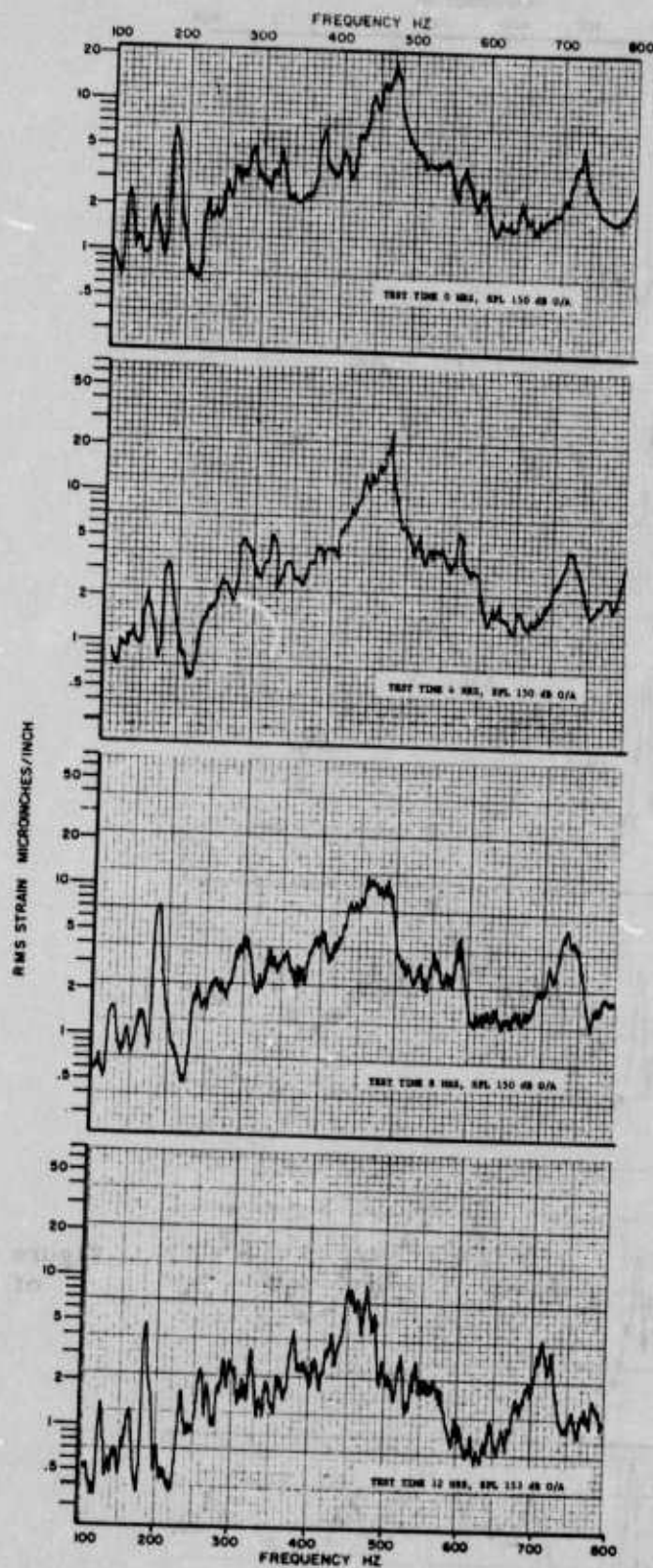


Figure 100 - Output of Gage Nr 9

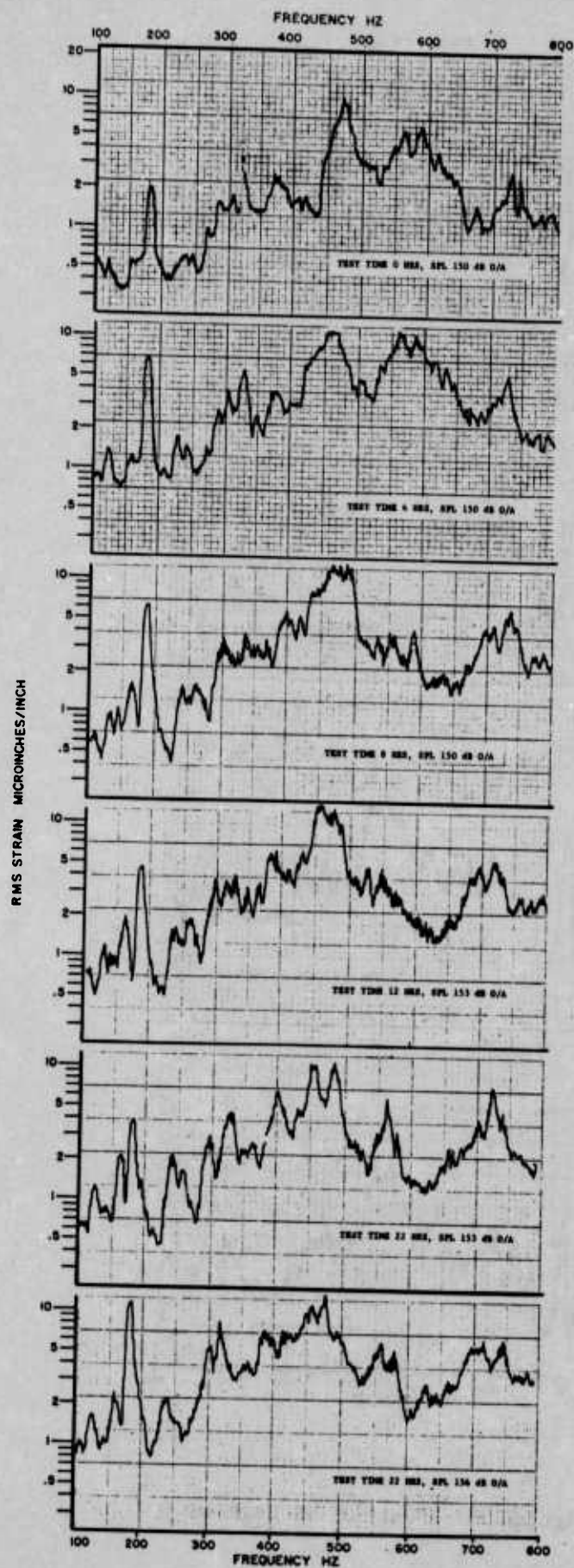


Figure 101 - Output
of Gage Nr 10

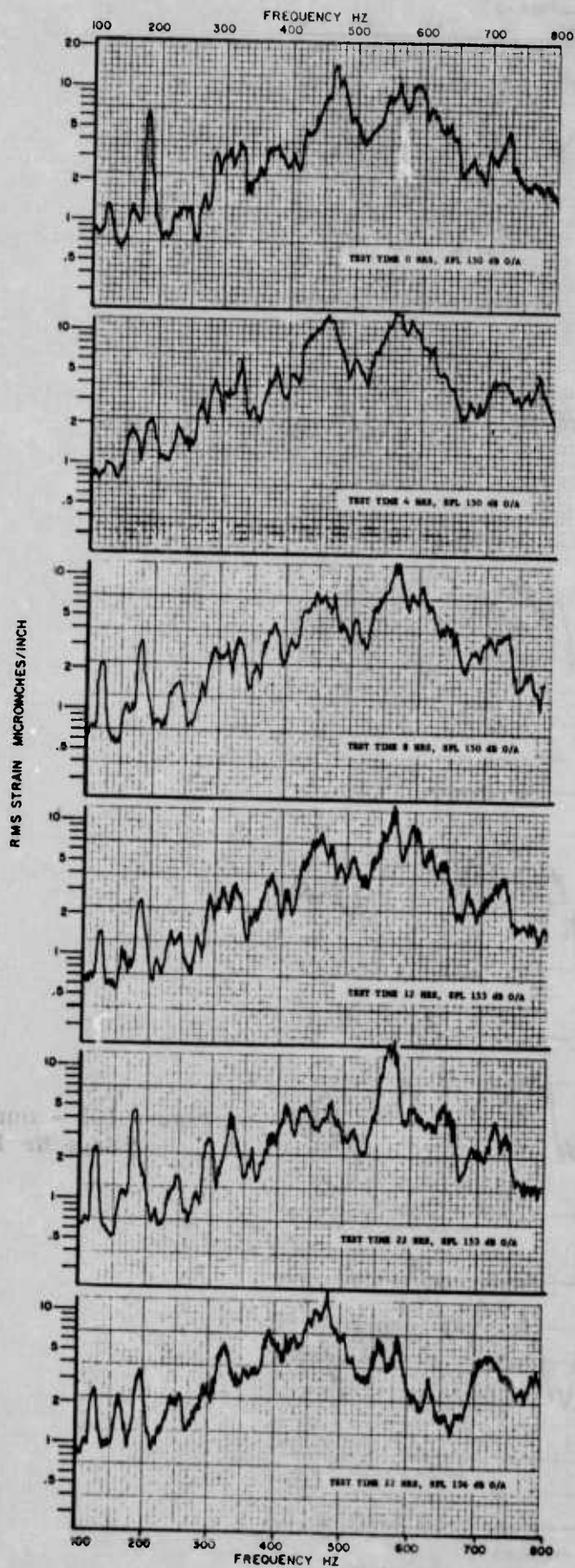


Figure 102 - Output
of Gage Nr 11

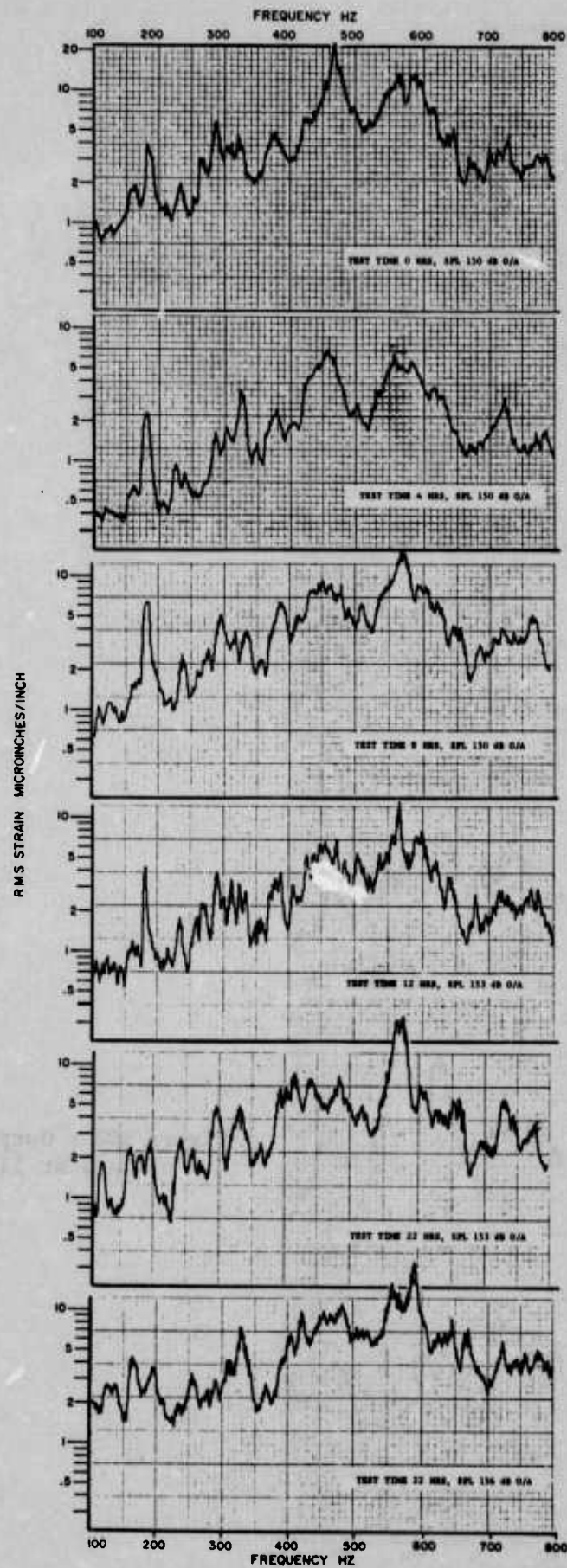


Figure 103 - Output
of Gage Nr 12

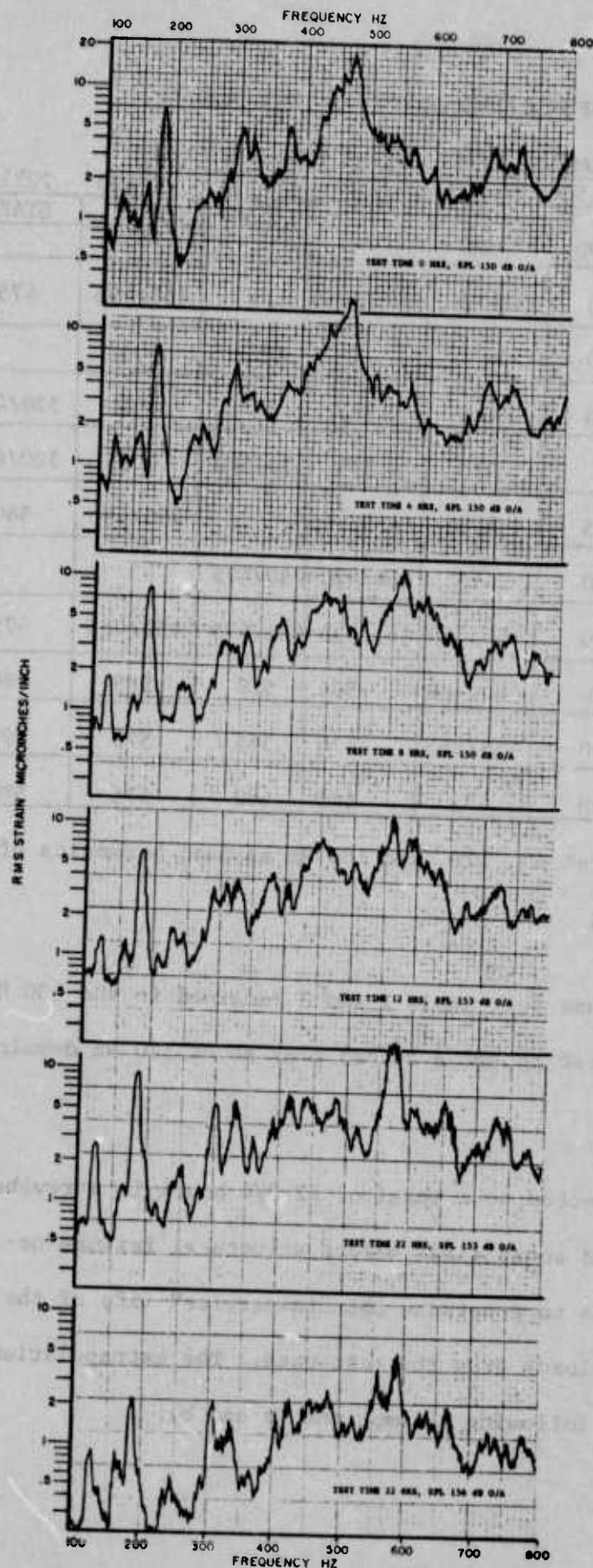


Figure 104 - Output
of Gage Nr 13

TABLE 7

MAXIMUM RESPONSE FREQUENCY* vs TEST TIME

GAGE NR./PANEL NR.	CUMULATIVE TEST TIME (HR.)/SPL (dB)					
	0 ⁺ /150	4/150	8/150	12 ⁺ /153	22 ⁺ /153	22 ⁺ /156
1/1	470Hz	470		START	END 455	START
2/1	475	472	460/480		460/495	475
5/2	400			385	405	
6/2	410	410	395		395	320/400
7/3		410	395	370/440	405	320/405
8/1	465	475	455/485		460/490	580
9/1	470	475	460/490	450/475		
10/1	470	460/560	465/495	455/475	450/485	475
11/7	470	460/560	565	570	575	480
12/7	470	455/555	570	565	575	590
13/7	470	475	565	560	575	590

*Note: Response peaks at 60, 120, and 180 Hz assumed harmonics of line frequency.

continued. Peak response for panels 2 and 3 remained in the 400 Hz range throughout the test though a second peak about 320 Hz developed at 156 dB.

Having been subjected to a total of 22 3/4 hours in a reverberant wide frequency band sound field before structural failure occurred, the problem was to determine the "in-service" life of the rudder under acoustic loads from the test data. The extrapolation was made based on the following assumptions (a and b):

TABLE 8

AMPLITUDE AND FREQUENCY RESPONSE OF MAJOR PEAKS

SPL (dB)	Test Time (HRS)	AMPLITUDE AND FREQUENCY RESPONSE OF MAJOR PEAKS*			
		Panel Nr. 1	Panel Nr. 2	Panel Nr. 3	Panel Nr. 7
150	0+	22 in/in	18		20
		470 Hz	410		470
150	4	23		10	
		470	410	410	470-555
150	8	16	12	12	15
		460-490	395	395	565-570
153	12+	13		10	12
		450-475	385	370-440	560-570
153	22-	16	10	15	20
		460-490	400	405	575
156	22+	18	12	16	20
		475-580	320-405	320-405	480-590

*NOTES: (1) Maximum strain values recorded without regard to strain gage location at stated frequency

(2) Values not shown under 10 in/in

(3) Analyzer bandwidth 10 Hz

(4) Response peaks at 60, 120 and 180 Hz assumed

- a. Damage incurred by the rudder prior to the acoustic test did not appreciably affect its life or dynamic properties,
- b. The rudder accepts energy from the acoustic field in the test chamber in approximately the same manner as it would "in-service". This may be true under near-field conditions such as take-off but not for far-field flight conditions. The test chamber is most efficient in exciting structural vibrations in comparison with the jet engine noise field or the vibration caused by the turbulent boundary layer. Therefore, the extrapolation is considered conservative.

TABLE 9
COMPARISON OF SPL AND EXPOSURE TIMES FOR
THE TEST CHAMBER AND "IN-SERVICE" ENVIRONMENT

Average Test Conditions	1/3 O/B SPL dB CF=500Hz	140	142	144
	Time T _a Hours	12	10	0.75
In-Service Conditions Requirements	1/3 O/B SPL dB CF=500 Hz	Low Alt. Dash	High Alt. Dash	Take-Off
	Time T _r Hours	132	134	136
		210	30	12
Average Increase in Strain in Gages on Panel 1 Due to Increase in Test SPL	R	2.1	2.2	2.3
$T_s = R^a T_a$ Equivalent "In-Service" Hours	T _s (HRS)	492	520	48
Time Factor	$\frac{T_s}{T_r}$	2.3	17	4

The frequency response curves show that panel 1, the failure point, had a maximum response at a frequency of about 470 Hz. Table 9 compares the SPL in a one-third octave band (CF=500 Hz), and the exposure times for the chamber and "in-service" environment. It can be noted in Table 9 that the SPL in the one-third octave band around 500 Hz for each test condition is 8 dB above each "in-service" environmental condition. Figures 105-107 plot the strain measured by gages 8, 9, and 10 respectively in a bandwidth of 10 Hz during the reverberant chamber test as a function of O/A SPL. The SPL in a 1/3 octave band is also recorded on the figure for each test condition. The average increase in strain for each test and "in-service" condition is also given in Table 9 and noted as R. Let

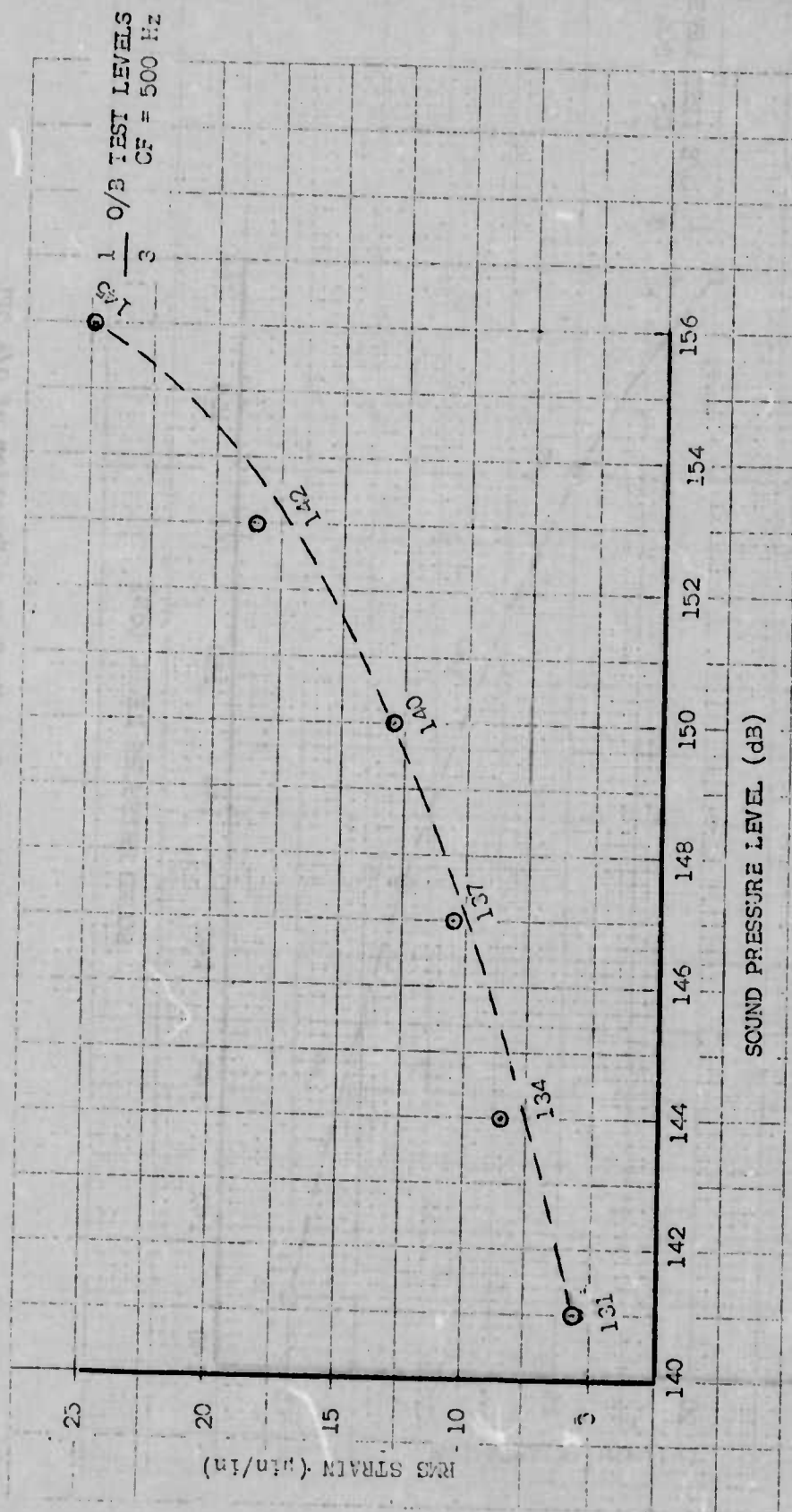


Figure 105 - Output of Strain Gage Nr 8 as a Function of O/A SPL
Frequency 470 Hz; Bandwidth 10 Hz

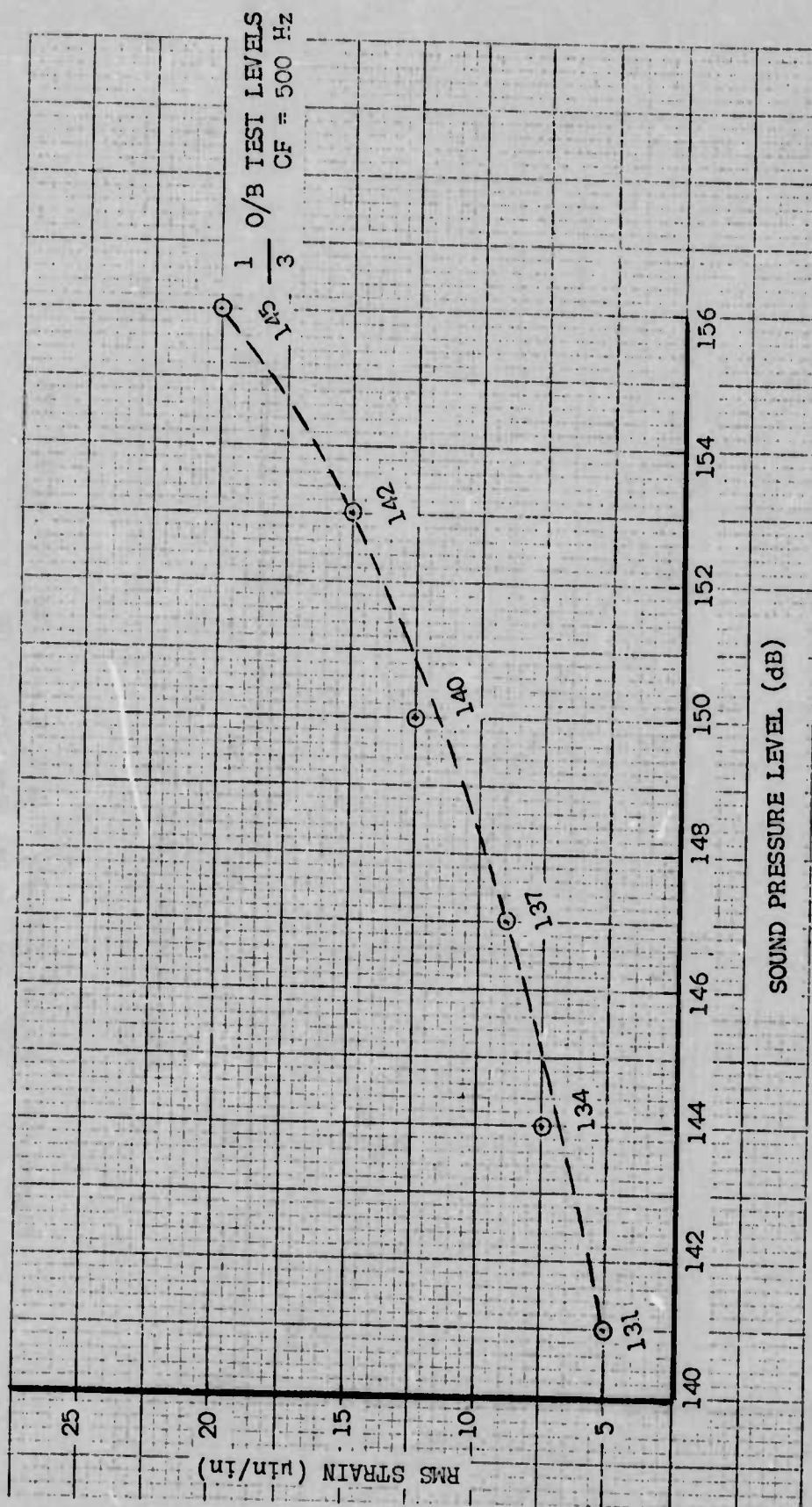


Figure 106 - Output of Strain Gage Nr 9 as a Function of O/A SPL
Frequency 470 Hz; Bandwidth 10 Hz

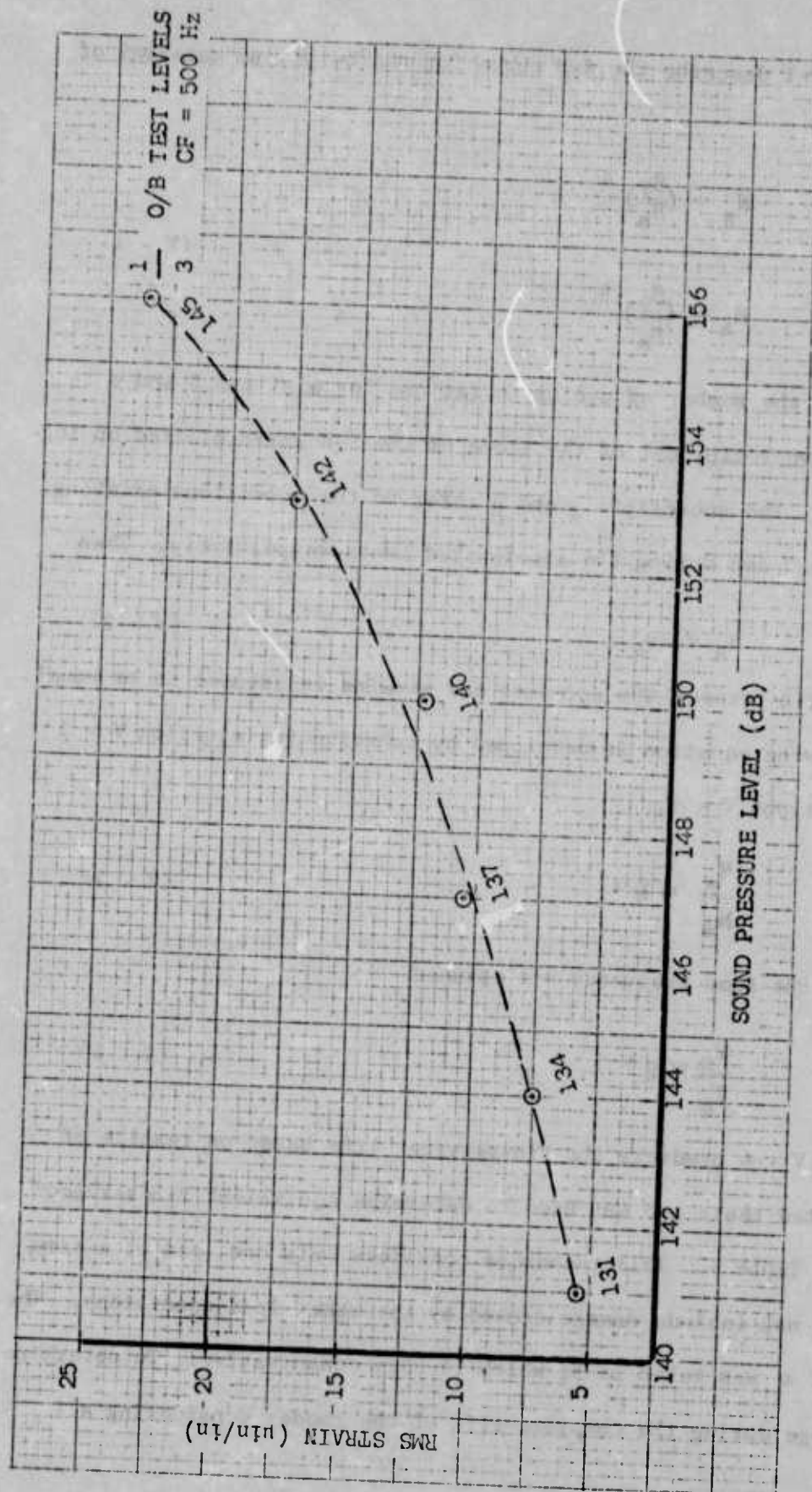


Figure 107 - Output of Strain Gage Nr 10 as a Function of O/A SPL
Frequency 470 Hz; Bandwidth 10 Hz

equations V-1 describe the S-N curve for the beryllium material of the rudder:

$$N_s = \left(\frac{S_1}{S_s} \right)^\alpha \quad (V - 1)$$

$$N_a = \left(\frac{S_1}{S_a} \right)^\alpha$$

where N is the number of cycles to failure for a stress S and α is the negative reciprocal of the slope of the S-N curve plotted on log-log paper. The subscripts s and a refer to the conditions existing "in-service" and during the accelerated tests respectively. Then

$$S_a = RS_s \quad (V - 2)$$

if the ratio between the stresses and strains is assumed to be equal. The following equation is developed by substituting equation V - 2 into equations V - 1.

$$\frac{N_s}{N_a} = R^\alpha \quad (V - 3)$$

Or, since the same frequency was assumed

$$\frac{T_s}{T_a} = R^\alpha \quad (V - 4)$$

Equation V - 4 predicts the "in-service" life based on results of accelerated tests and was used to determine equivalent "in-service" hours in Table 9. This technique considers only one load at a time and does not include damage caused by the other load conditions. The value of α was taken as 5, which is very conservative. To determine the damage during the complete life of the rudder considering all

loading conditions, the following technique may be used. The damage due to all loads may be summed as follows:

$$D_M = \sum_{i=1}^k \frac{n_i}{N_i} \quad (V - 5)$$

where i is a specified stress level and there are k levels, n is the number of stress reversals at the i^{th} level and N is the number of stress reversals to cause failure at that level. The damage caused by the facility test, D_{M_a} , since there were three test levels, is then

$$D_{M_a} = \frac{n_{140}}{N_{140}} + \frac{n_{142}}{N_{142}} + \frac{n_{144}}{N_{144}} \quad (V - 6)$$

where the subscripts on the n 's and N 's in equation V - 6 represent the one-third octave band test levels (CF=500 Hz) used during the test. Substituting eq V - 1 into eq V - 6 with proper subscript changes gives the following:

$$D_{M_a} = n_{140} \left(\frac{S_{140}}{S_1} \right)^a + n_{142} \left(\frac{S_{142}}{S_1} \right)^a + n_{144} \left(\frac{S_{144}}{S_1} \right)^a \quad (V - 7)$$

Then, assuming the damage occurs at primarily one frequency f and using the data from Table 9, eq V - 7 becomes

$$D_{M_a} = \frac{f}{(S_1)^a} [12 (S_{140})^a + 10 (S_{142})^a + 0.75 (S_{144})^a] \quad (V - 8)$$

The in-service damage D_{M_s} for one life can also be given in a similar equation as follows

$$D_{M_s} = \frac{f}{(S_1)^a} [210 (S_{132})^a + 30 (S_{134})^a + 12 (S_{136})^a] \quad (V - 9)$$

The number of lives for which the test specimen survived is then

$$\frac{D_{M_a}}{D_{M_s}} = \frac{12 \left(\frac{S_{140}}{S_{132}}\right)^a + 10 \left(\frac{S_{142}}{S_{132}}\right)^a + 0.75 \left(\frac{S_{144}}{S_{132}}\right)^a}{210 (1)^a + 30 \left(\frac{S_{134}}{S_{132}}\right)^a + 12 \left(\frac{S_{136}}{S_{132}}\right)^a} \quad (V - 10)$$

$$= \frac{12 (2.1)^5 + 10 (2.8)^5 + 0.75 (3.5)^5}{210 (1)^5 + 30 (1.2)^5 + 12 (1.5)^5}$$

$$\approx 7$$

where the stress ratios were average values taken from Figures 105-107, as explained previously in equation V - 2.

The overall RMS value of the strain was measured on the panels after eight hours of testing at an overall SPL of 150 dB. Measurements were taken at an overall SPL range of 141 to 156 dB. The maximum strain values were found at gage locations 1 and 8 on panel 1. See Figures 108 and 109. The maximum value of the strain measured at 156 dB was 90 μ in/in at gage location 1.

6. Conclusions

The beryllium rudder has been subjected to a reverberant acoustic field with overall sound pressure levels (O/A SPL's) ranging from 150 to 156 dB for a total time of 22 3/4 hours before failure occurred. If the total number of loading conditions are taken into consideration, it is conservatively shown in the previous section that this total test time is equivalent to about seven normal lives of the rudder. If each load condition is considered separately, the test indicates that the rudder was acoustically tested from 2.3 to 17 times the "in-service" requirement for the individual conditions. These conclusions are based

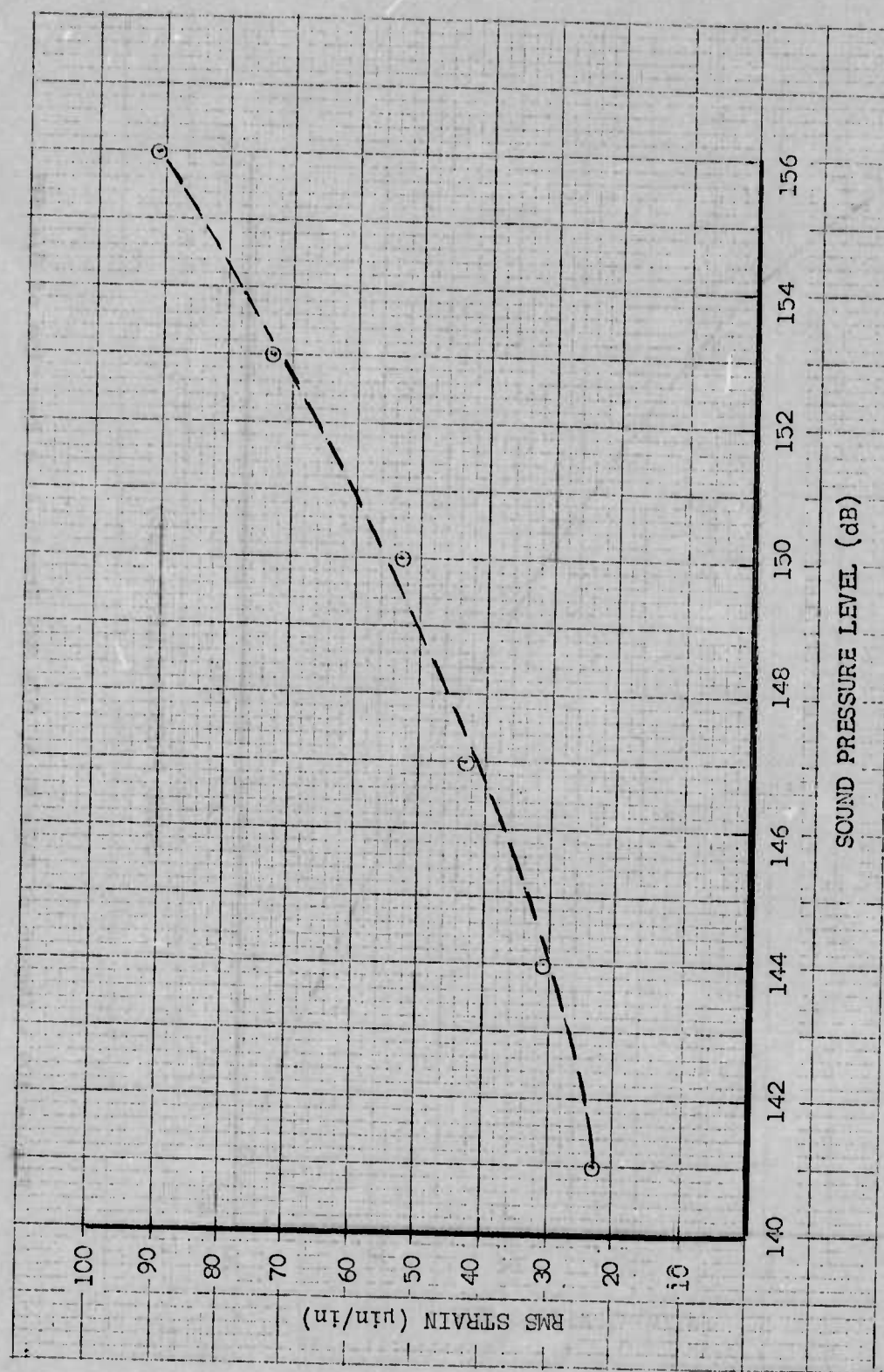


Figure 108 - Output of Gage Nr 1, O/A RMS Strain as a Function of O/A SPL

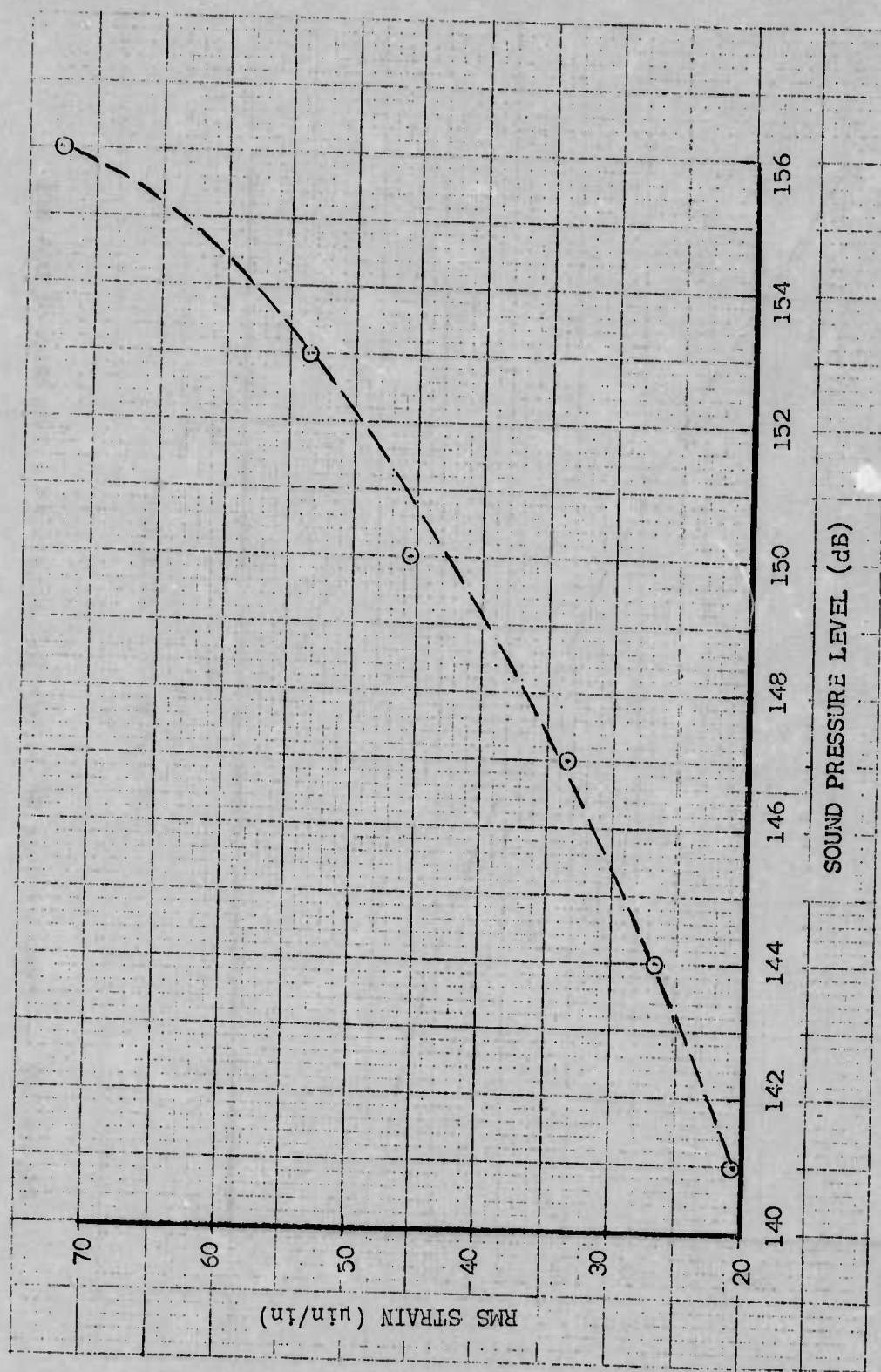


Figure 109 - Output of Gage Nr 8, O/A RMS Strain as a Function of O/A SPL

upon test data, operational data supplied by the McDonnell-Douglas Corporation, and material data. It should be noted that the time factors are very dependent upon the value of α taken from the material S-N curve, and become very large if less conservative values of α are chosen.

With the maximum overall RMS strain measured at 90 in/in at gage position 1 at an overall SPL of 156 dB and an E of 42×10^6 psi (290×10^3 MN/m²) for beryllium, the apparent stress under the gage would be about 3800 psi (26 MN/m²). Assuming a maximum stress concentration factor of 2, the maximum skin stress in the rudder during the test would be about 7400 psi (52 MN/m²). This figure appears to be below the fatigue strength of beryllium based on extrapolated data and supports the radiographic findings that the rib R2 was damaged prior to the acoustic fatigue test. This is also supported by the fact that panel 1 was the failure point when the SPL over the rudder for the duration of the test was uniform within ± 1 dB.

SECTION VI

RADIOGRAPHIC INSPECTION OF THE BERYLLIUM RUDDERS

1. Introduction

Concurrent with the acoustic fatigue endurance test discussed in the previous Section, a series of radiographic (X-Ray) inspections was conducted by the Processing and Nondestructive Testing Branch, Metals and Ceramics Division of the Air Force Materials Laboratory as reported in Reference 5. The purpose of this inspection series was to detect flaws or damage to the structure which were not detectable visually, to document the progressive growth of such damage relative to applied loads for correlation with test results, and to extend the non-destructive inspection (NDI) radiographic data base for confident and reliable surveillance of beryllium structures.

The techniques used in successful radiographic examination of the ground test beryllium rudder had been pioneered by MCAIR on the flight test rudder as discussed in Reference 2. Though subtle variations in techniques were required due to the differences in equipments used by AFML and MCAIR, the principal of low applied kilovoltage permitted both to achieve reasonable image contrast on the exposed film. The order of discussion of the techniques and results of radiographic inspection of the two rudders was chosen for editorial convenience rather than chronological order since the time span of the flight test rudder inspections bridge those of the ground test rudder.

2. Equipment and Procedure - Ground Test Rudder X-Rays

Radiographic inspections of the ground test rudder, conducted by the Air Force Materials Laboratory (Reference 5), were performed using a Sperry 275 KVP unit having a lower operating limit of 50 KVP. Radiographic contrast is a function of the density and thickness of the material. Because the density of beryllium is so low, its probability of absorbing radiation is low except when the longer wavelengths are employed. The beryllium rudder is also a structure with relatively thin sections (Figure 21). Exposures for this series of inspections were confined to the forward torque box area since experience indicated acoustic fatigue damage was more likely to occur in the area of skin-stringer construction than in the area of full depth honeycomb. The total thickness of both panels to be penetrated by the radiation varies between 0.046" outside of the spar and ribs areas to a maximum of 0.260" within a typical section of the forward spar. The two factors of low material density and thin sections require a low kilovoltage applied to the X-ray tube to achieve adequate image contrast. The optimum energy was estimated between 10 and 20 KVP for the thickness of the forward spar section. However, this low voltage was not possible using the standard Air Force stock item X-Ray equipment which was available. Operating at the lower limit of 50 KVP and using type M ready pack film, successful exposures were made with 225 milli-ampere-second at a target, to film a distance of 68 inches. A series of radiographic inspections were conducted in conjunction with the acoustic fatigue endurance test as discussed in Section V. Table 6 presents a summary of this inspection schedule with the zero time being after the static and dynamic flight qualification tests but prior to acoustic fatigue

tests. The results of this zero time inspection served as a base for locating prior damage or detecting new damage caused by acoustic loading, and tracing damage growth due to acoustic fatigue.

3. Results and Discussion - Ground Test Rudder X-Rays

Prior to radiographic examination of the ground test beryllium rudder, the only damage reported was a crack in the lower closure rib (Figure 68) generated during Test 4. The first radiographic examination of this rudder in November 1967, prior to acoustic fatigue testing, disclosed other anomalies which were tracked during the test. The most significant was a crack-like indication within rib R2 (Figure 110) strategically located aft of the lower hinge as shown in Figure 78. The arrow on Figure 110 points to the barely discernible discontinuity in the rib flange which indeed developed into a readily identified crack which grew during the acoustic fatigue test and was a part of the eventual failure. Extension of the crack to the rivet hole after 4 hours at a SPL of 150 dB is shown in Figure 111. After a total of 8 hours of sonic testing at 150 dB the crack had extended beyond the fastener hole and a piece of the rib had broken off as shown in Figure 112. See Figure 42 to compare irregular shadow in lower center of Figure 112 with actual broken pieces of the rib recovered after termination of the acoustic fatigue test.

The equipment utilized for these X-ray exposures was the Air Force facilities. The limitation on lowest usable kilovoltage (50 KVP) results in lower image contrast than would be available in the kilovoltage range from 10 to 50 KVP reported by McClung in Reference 8.

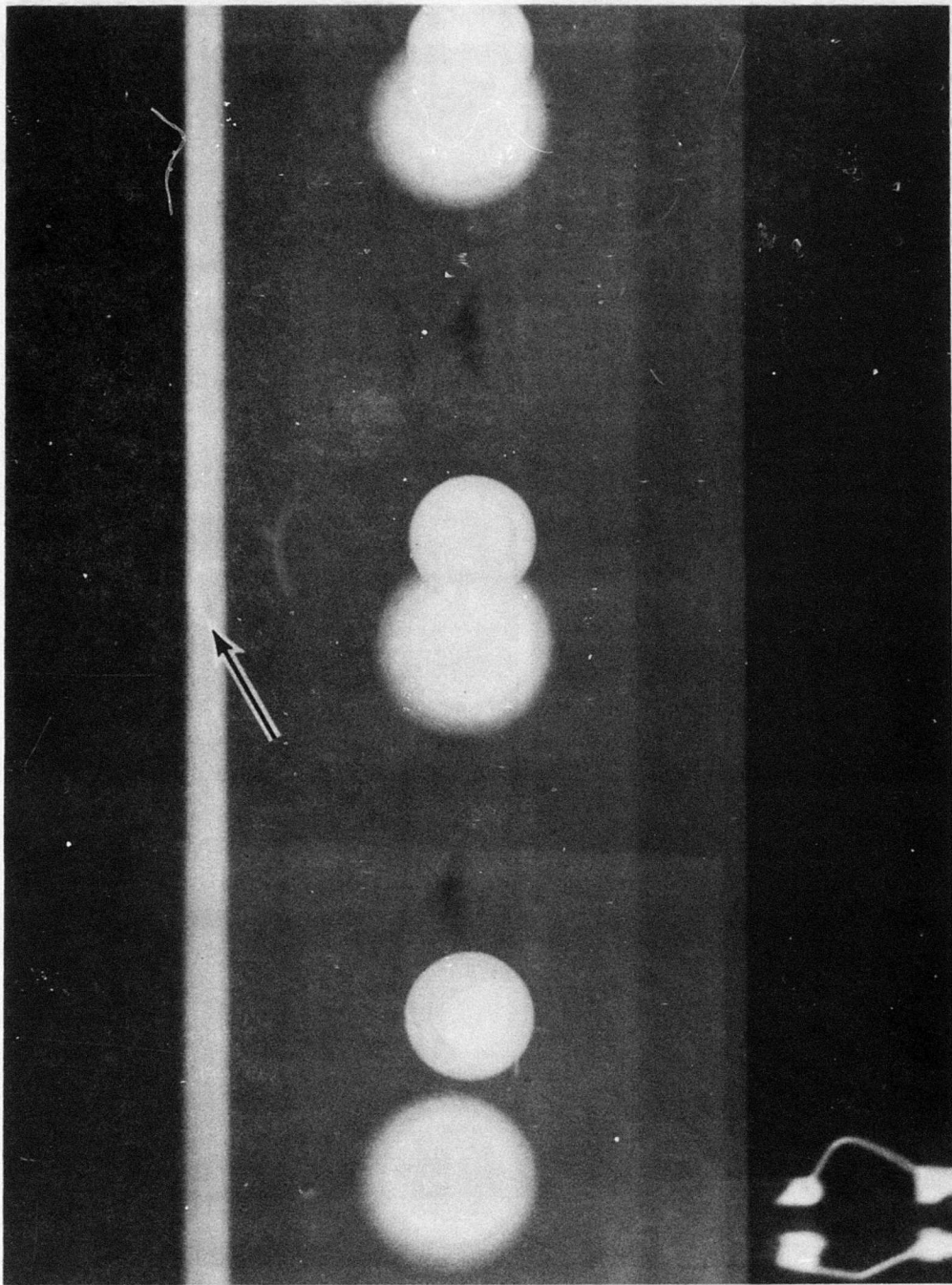


Figure 110 - Photograph of the Radiograph Showing Crack in Rib R2 Before Start of Acoustic Fatigue Test

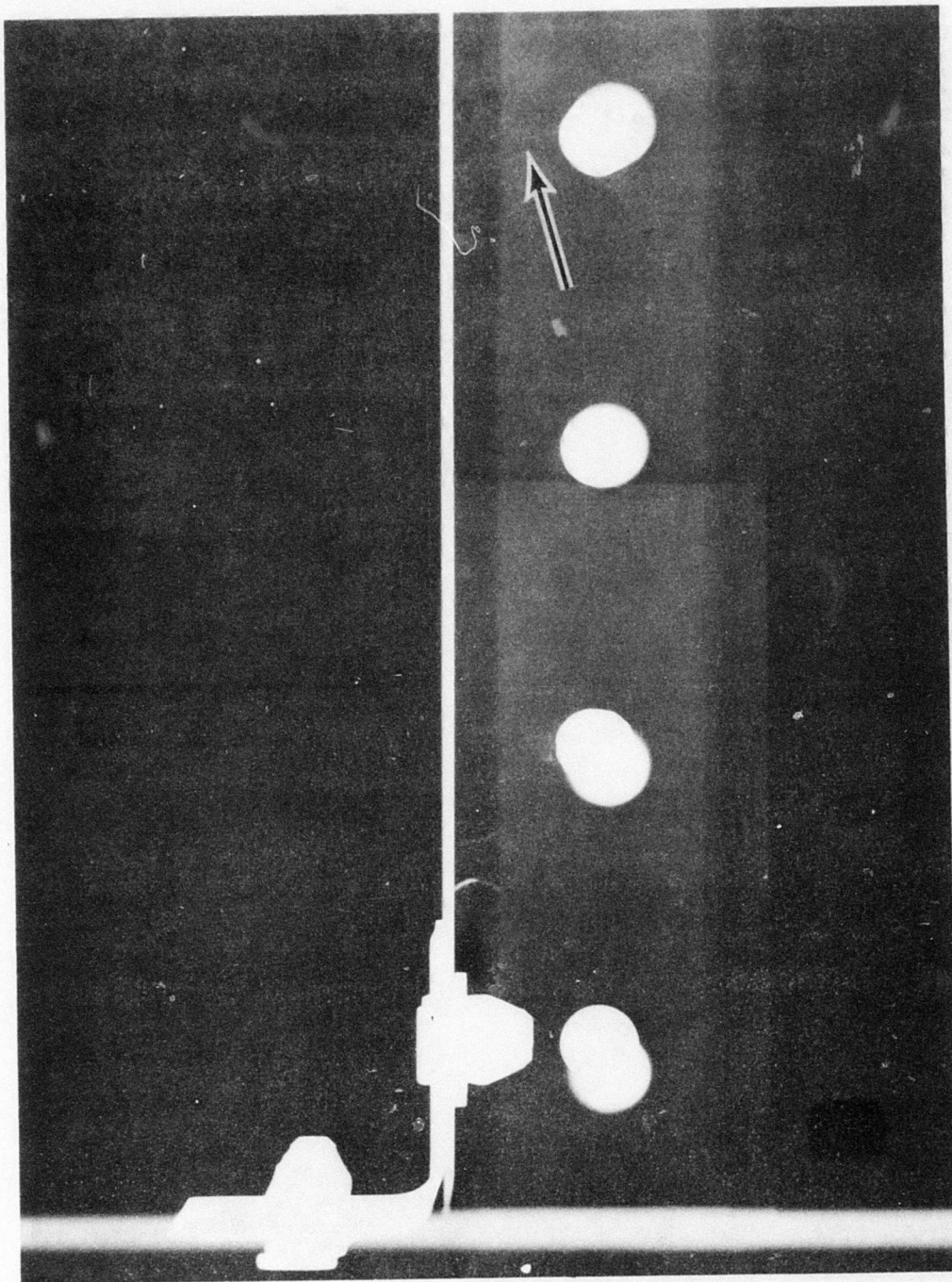


Figure 111 - Photograph of the Radiograph Showing Crack in Rib R2 After 4 Hours of Testing at 150 dB

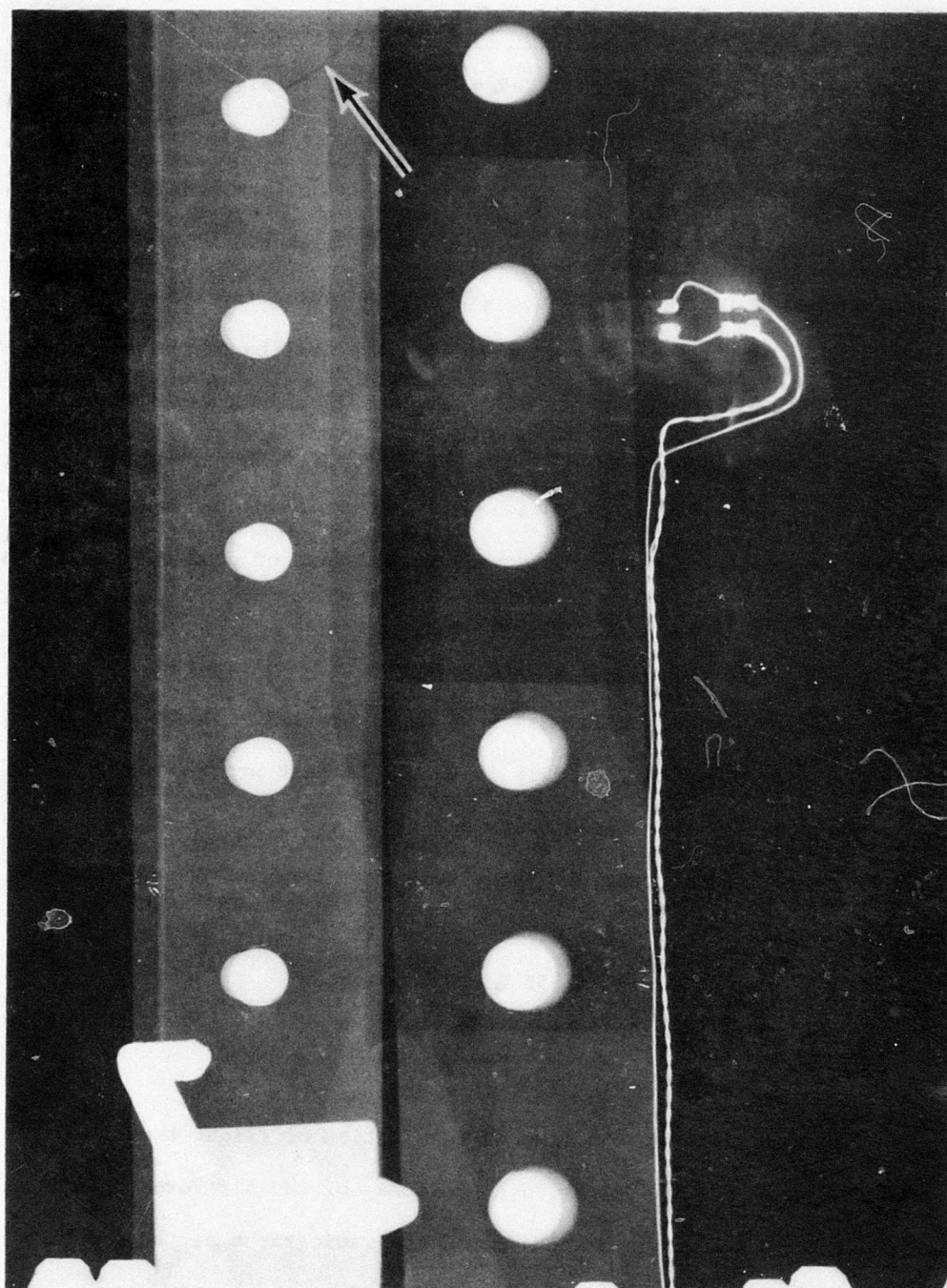


Figure 112 - Photograph of the Radiograph Showing Crack in Rib R2 After 8 Hours of Testing at 150 dB

4. Equipment and Procedure - Flight Test Rudder X-Rays

A Model T55-52, 50 KV Picker X-Ray Unit shown in Figure 113 was used by MCAIR to radiographically inspect the entire beryllium structure of the flight test rudder. The rudder was placed on foam pads resting on a table as shown in Figure 114. The X-ray tube, which had a beryllium window and a focal length of 40 inches, was located above the rudder. Penetrators were located on the rudder so that the quality of the radiographs could be determined later. Type "B" film, 14 x 17 inches was placed between the rudder and the foam pads. The film was exposed using 26 KV, 10 ma, and an exposure time of 30 seconds, and was developed by an X-Omat Automatic Processor. The developed radiographs were of good quality and were viewed on an illuminated viewer.

A series of thirteen overlapping radiographs were required to obtain complete coverage of the rudder as shown on Figure 115. Three sets of radiographs were taken at intervals in the flight test program and compared in an attempt to locate damaged areas and track crack growth if suspect indications were indeed cracks. These sets were taken at the following flight intervals.

1st SET - 47 flights, 53 hours 18 minutes

2nd SET - 90 " ,100 " 30 "

3rd SET -158 " ,184 " 24 "

The last set was taken at the time of termination of flight tests. In addition to review by MCAIR, Mr. J.A. Holloway of the Air Force Materials Laboratory NDT & Mechanics Branch viewed the radiographs as they became available. This was done to obtain an independent and knowledgeable

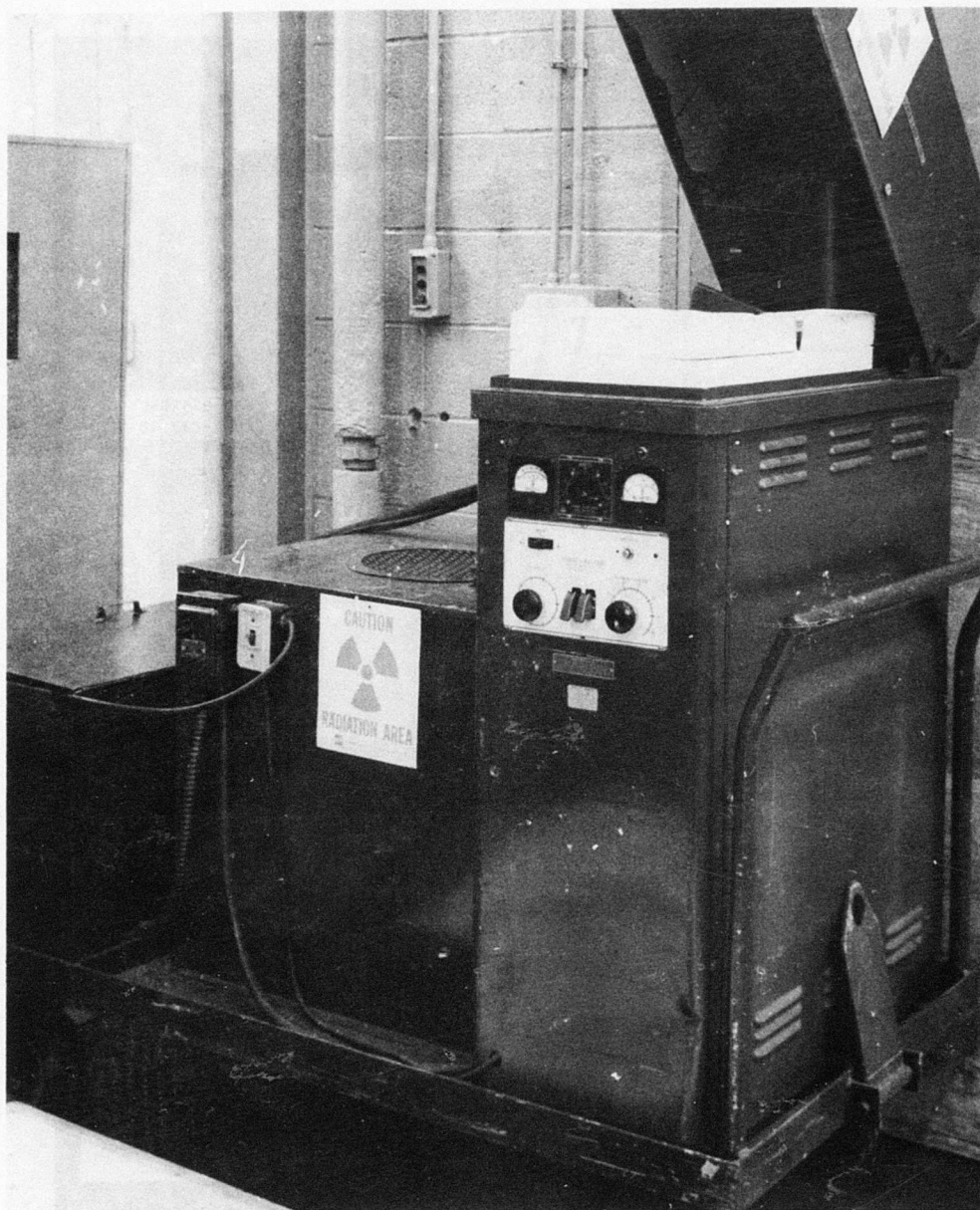


Figure 113 - Picker X-Ray Unit

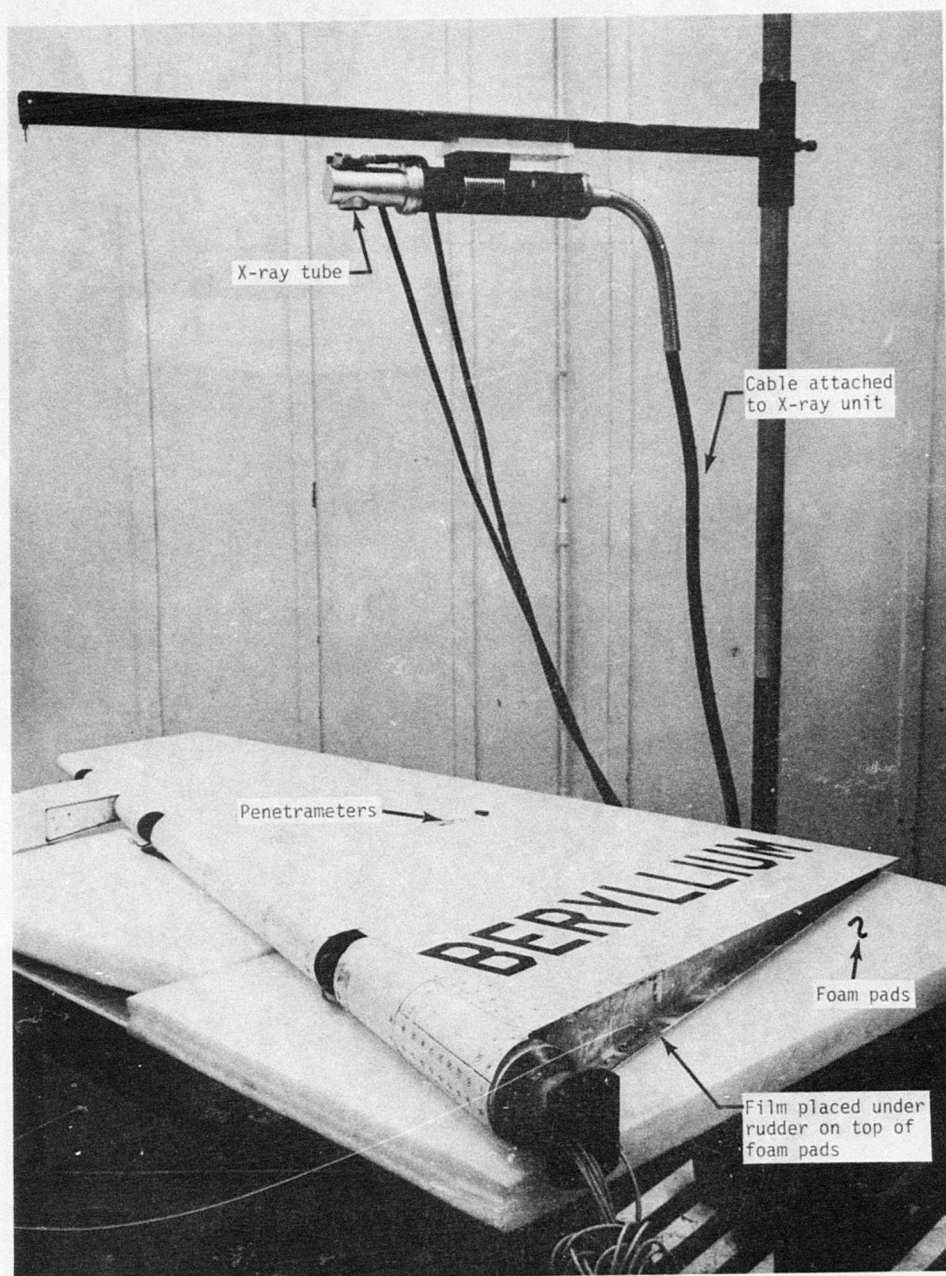


Figure 114 - Radiographic Inspection Set-Up

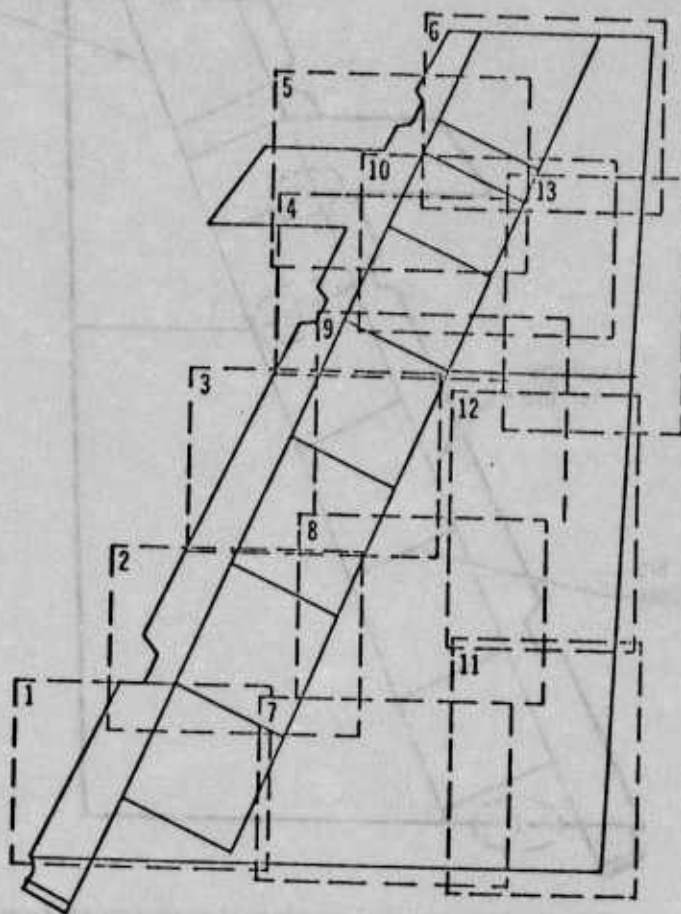
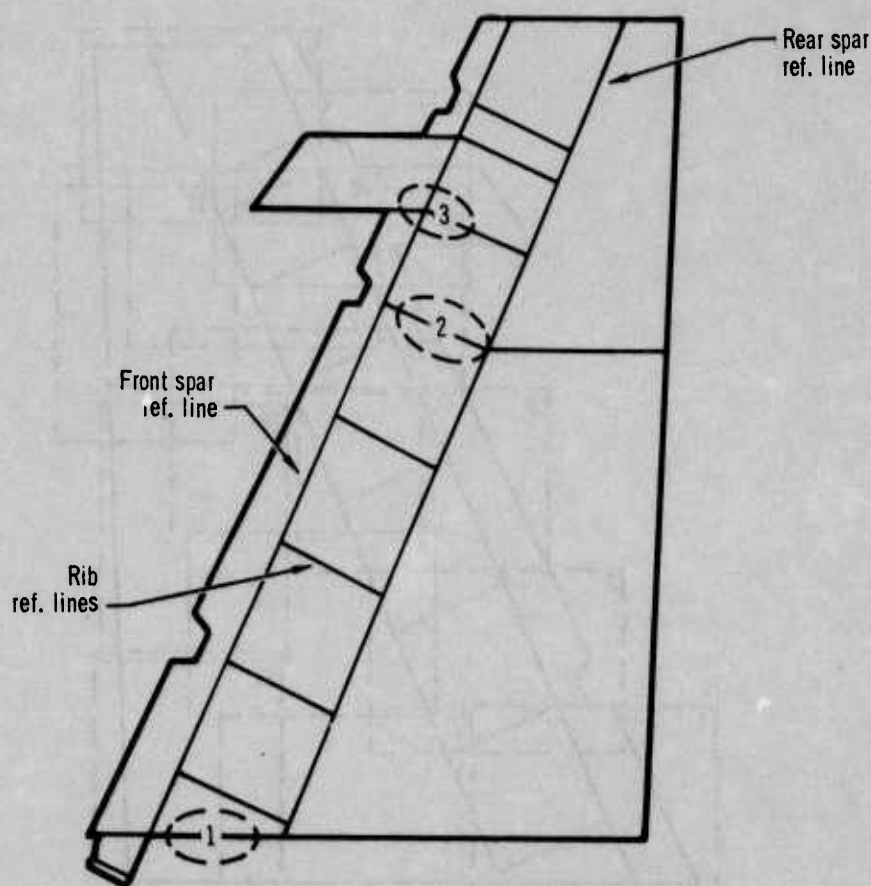


Figure 115-Layout for Radiographic Inspection
of Beryllium Flight Test Rudder

assessment of the radiographs since reading and analyzing the film is subject to interpretation. This also permitted direct comparison of ground and flight test rudder radiographs since the radiographic inspection series on the ground test rudder was performed by Mr. Holloway.

5. Results and Discussion - Flight Test Rudder X-Rays

Irregular dark lines in the three areas of the rudder as indicated in Figure 116 provide visual evidence of possible cracks in the beryllium. In general, such indications are difficult to locate on the radiographs because of the very fine width and low contrast. Sketches of these



Notes 1. Areas containing indications of possible damage shown by (---).

Figure 116 - Areas of Beryllium Rudder Where Indications of Possible Damage Were Discovered During Radiographic Inspection

indications are shown in Figures 117, 118, and 119 for areas 1, 2 and 3, respectively. All appear to be on the right side of the rudder. Since the indication in Area 1 was located in a part that was completely exposed except for the surface between the skin and the channel flange, the paint was stripped from the exposed surface of both and a dye penetrant inspection was made after the first set of radiographs were taken. No cracks were found, indicating that if a crack did exist in this area it is not through the thickness and it originates on the faying surface

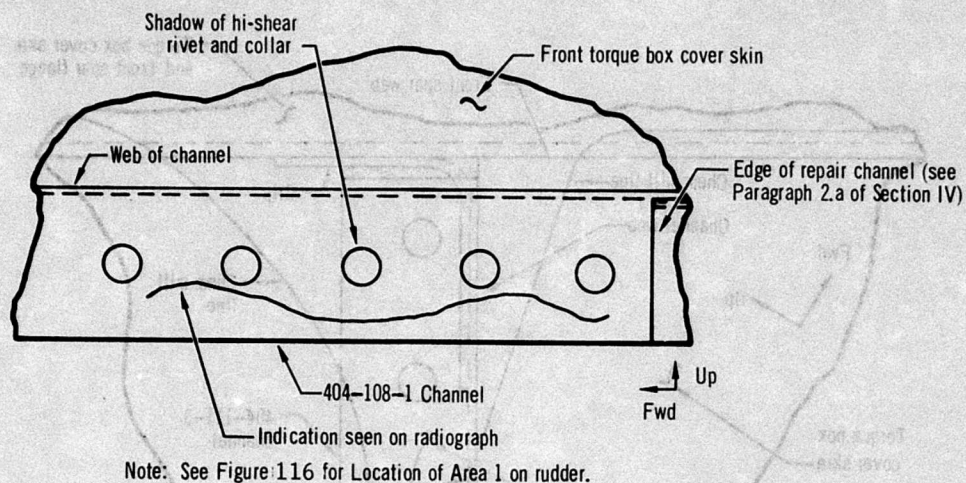


Figure 117 - Indication Located in Area 1

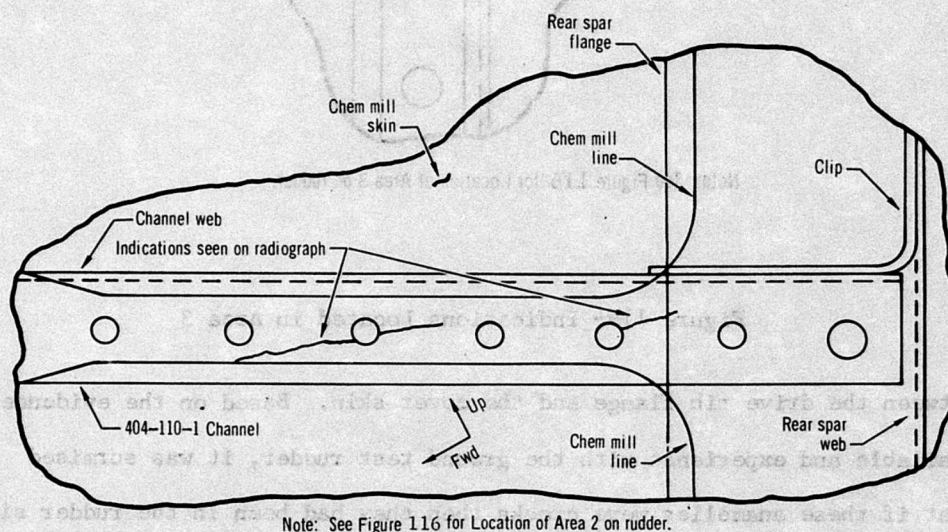
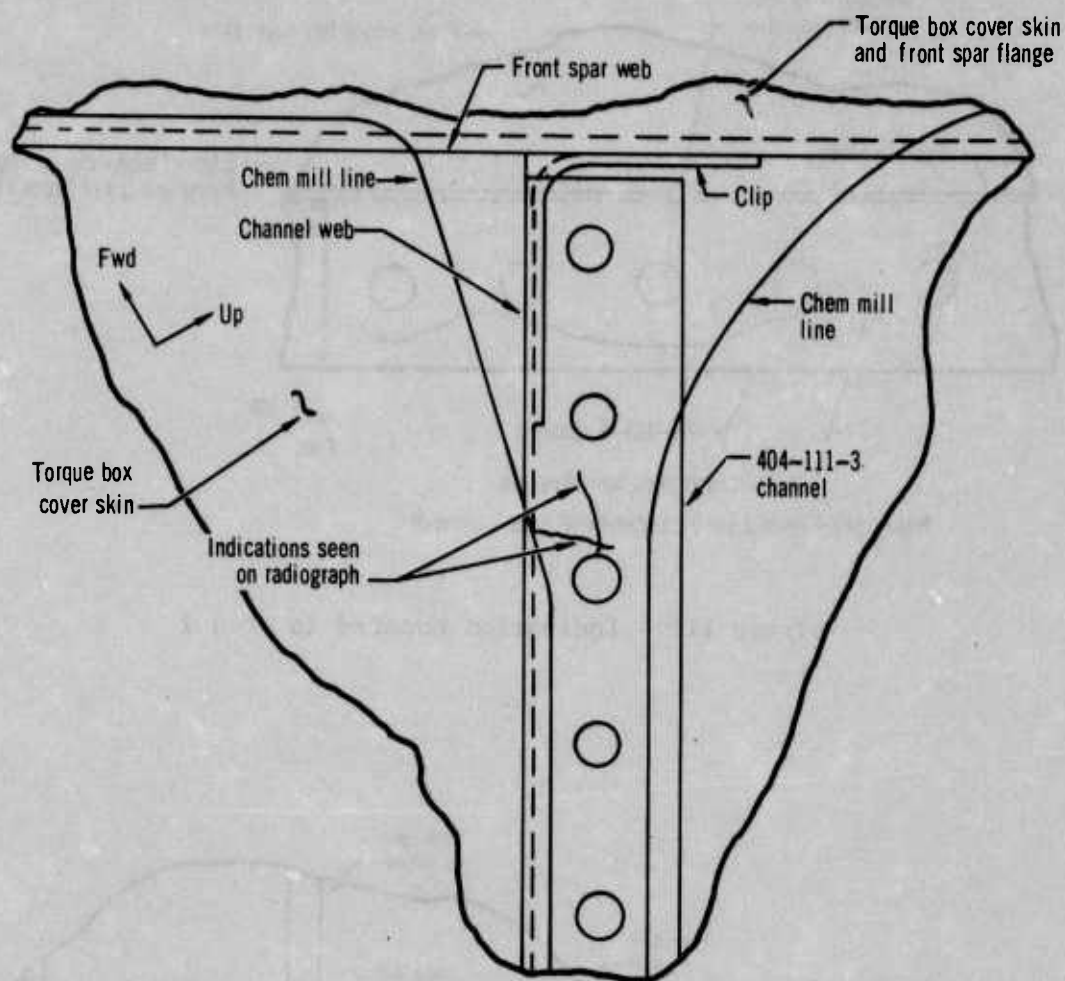


Figure 118 - Indications Located in Area 2



Note: See Figure 116 for Location of Area 3 on rudder.

Figure 119- Indications Located in Area 3

between the drive rib flange and the cover skin. Based on the evidence available and experience with the ground test rudder, it was surmised that if these anomalies were cracks then they had been in the rudder since fabrication, and could have resulted from installation of the fasteners attaching the cover skins to the ribs. Since the rudder is not a safety-of-flight item and had been flown successfully with these indicated

anomalies, it was decided that the rudder was structurally capable of further flight testing provided pre- and post-flight visual inspections were made and that these areas were monitored periodically by subsequent radiographic inspections.

Comparison of the second and third sets of radiographs with the original set revealed no indication of crack growth or other change in the structural condition of the rudder in the intervals between inspections. If the indicated anomalies were indeed cracks there was no growth during the last 130 hours of flight, lending credence to the belief that the cause of these indications existed from the time of fabrication.

6. Commentary

As a result of the work done by MCAIR and AFML, radiographic inspection techniques have been developed and demonstrated as a valid non-destructive inspection procedure for complex, thin-gage beryllium structures. However, the radiographic technique employed leaves some doubt regarding equipment capabilities due to low image contrast. Should re-usable aerospace structures fabricated of thin sections of beryllium become production items, an X-ray machine falling within the kilovoltage range from 5 to 50 KVP would be a necessary Air Force stock item for field maintenance inspection. Further technique development in this area would also be required. Penetrameters* employed as quality indicators are

* A penetrameter is a thin section of the material representing 2% of the total thickness radiographed and containing a series of drilled holes; the diameters being equal to 1, 2, and 4 times the thickness of the penetrameter.

difficult to machine in this section because of the brittle nature of the material. The detection of cracks using radiography also depends upon the beam orientation and the crack size. Both of these factors are interrelated. Unfortunately, information in this area is not available. However, other NDI techniques such as ultrasonics, penetrants, and eddy currents can be used to further characterize the structure for lack of bond and external cracks.

SECTION VII

TEST 6 - RESIDUAL STRENGTH STATIC TEST

1. Introduction

After the acoustic fatigue test of the ground test F-4 beryllium rudder was completed with considerable damage to vital members but with the component basically intact, the question of residual strength became significant. The damage sustained was similar to that which may occur from ballistic impact during combat operations. The rudder was further damaged by mishandling, such as one might expect as the result of improper care during field operations. This damage was in the form of several punctures in the skin aft of the torque box and the trailing edge closure rib (Figure 120).

No vertical fin-aft fuselage section was available at Wright-Patterson AFB on which to install the rudder for tests such as was done for flight qualification tests. With the damaged forward torque box cover skins and hinge back-up rib designed for Condition III loads which produce maximum vertical tail bending deflections, Section II.4, it was decided to conduct the residual strength static test under loading conditions similar to Test 3. However, installation of the rudder in the relatively rigid I-beam test set-up as compared with a normal airframe mounting system restricted the deflection of the forward spar and modified the strain on aft structural members. By monitoring and recording strain, deflection and load data it was possible to accurately determine the response of the damaged rudder to simulated critical flight load conditions. After a series of incremental

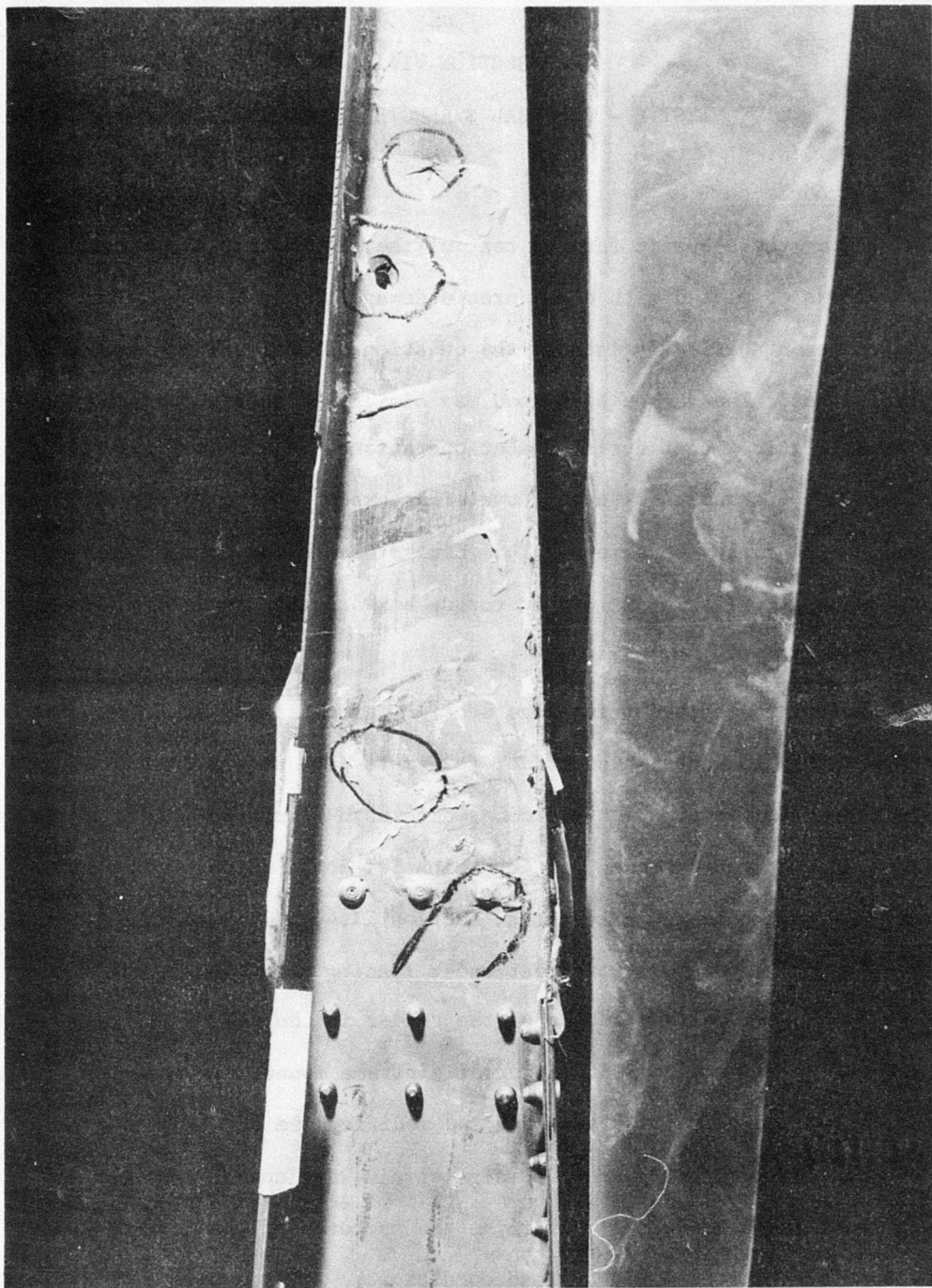


Figure 120 - Post Acoustic Fatigue Test Damage
to Lower Closure Rib

load increases, failure occurred after 15 seconds at 200% DLL.

2. Instrumentation

The location of instrumentation was of prime importance to record response to loads both as a measure of the rudder strength itself and for comparison with previous tests to determine changes in load distribution in the rudder due to structural damage and increased rigidity of mounting fixture. While instrumentation used during previous tests was partially duplicated to supply reference values for direct comparison other gages were strategically located to supply data concerning redistribution of loads and deflections.

A total of twenty (20) deflection locations were instrumented as shown in Figure 121 as compared with twenty-eight (28) for previous static tests (Figure 38). The identification number for each location remains the same to simplify data comparisons. It was felt that some of the data points could be eliminated from this test without loss of significant information; however, all data points in the vicinity of the structural damage were retained. Displacement transducers used were Research, Inc. Models 4040 and 4046.

Strains were measured at twenty locations, ten on each surface, as shown schematically in Figure 122. By comparison, only sixteen locations were instrumented for previous static tests (Figure 37). Because of the damage sustained it was necessary to relocate some strain gages in the area of damage and add additional ones to determine load distribution in this area. The numerical identity of similarly located strain gages are the same for comparative purposes with new or relocated gages

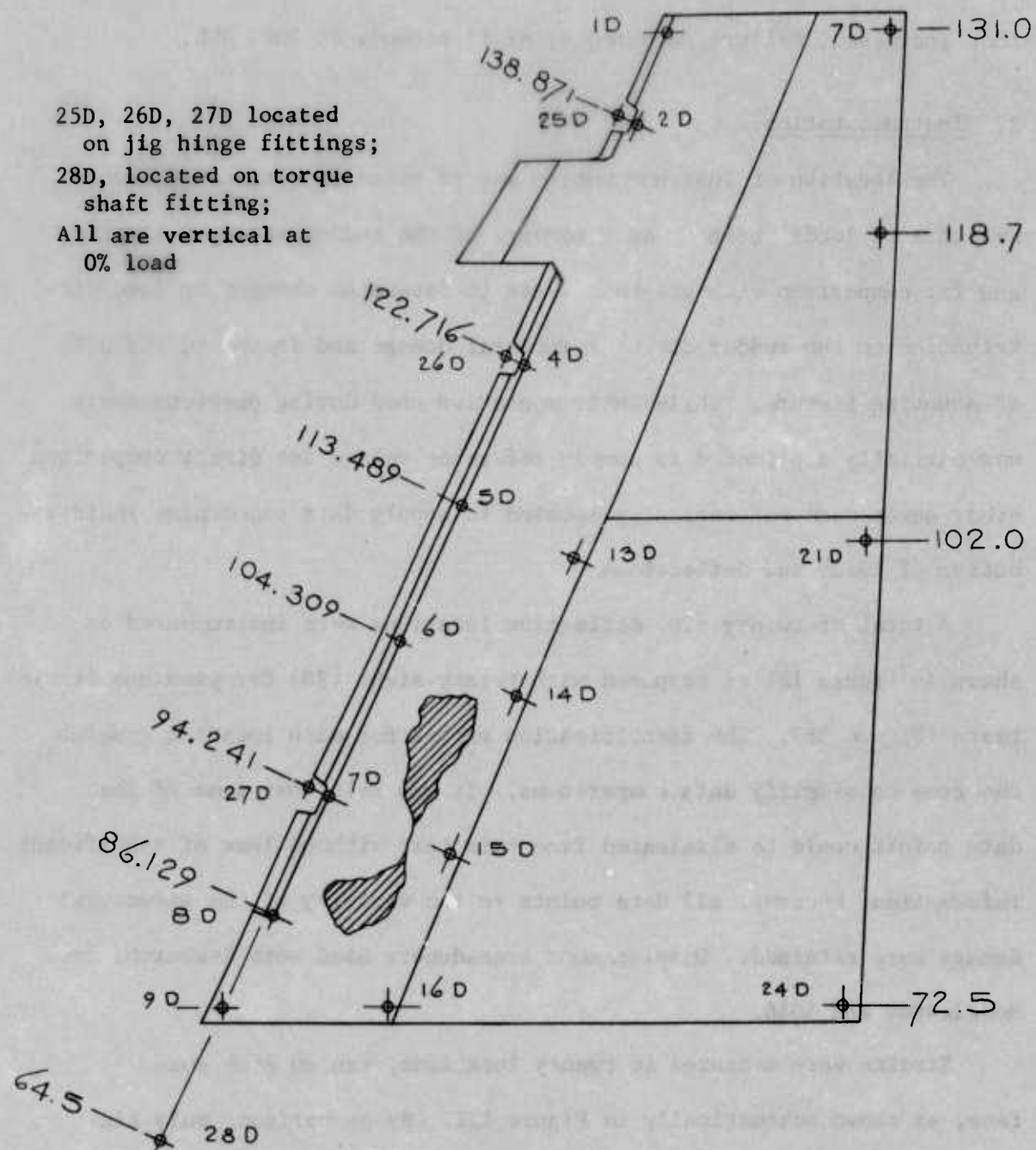


Figure 121 - F-4 Beryllium Rudder Deflection
Transducer Locations

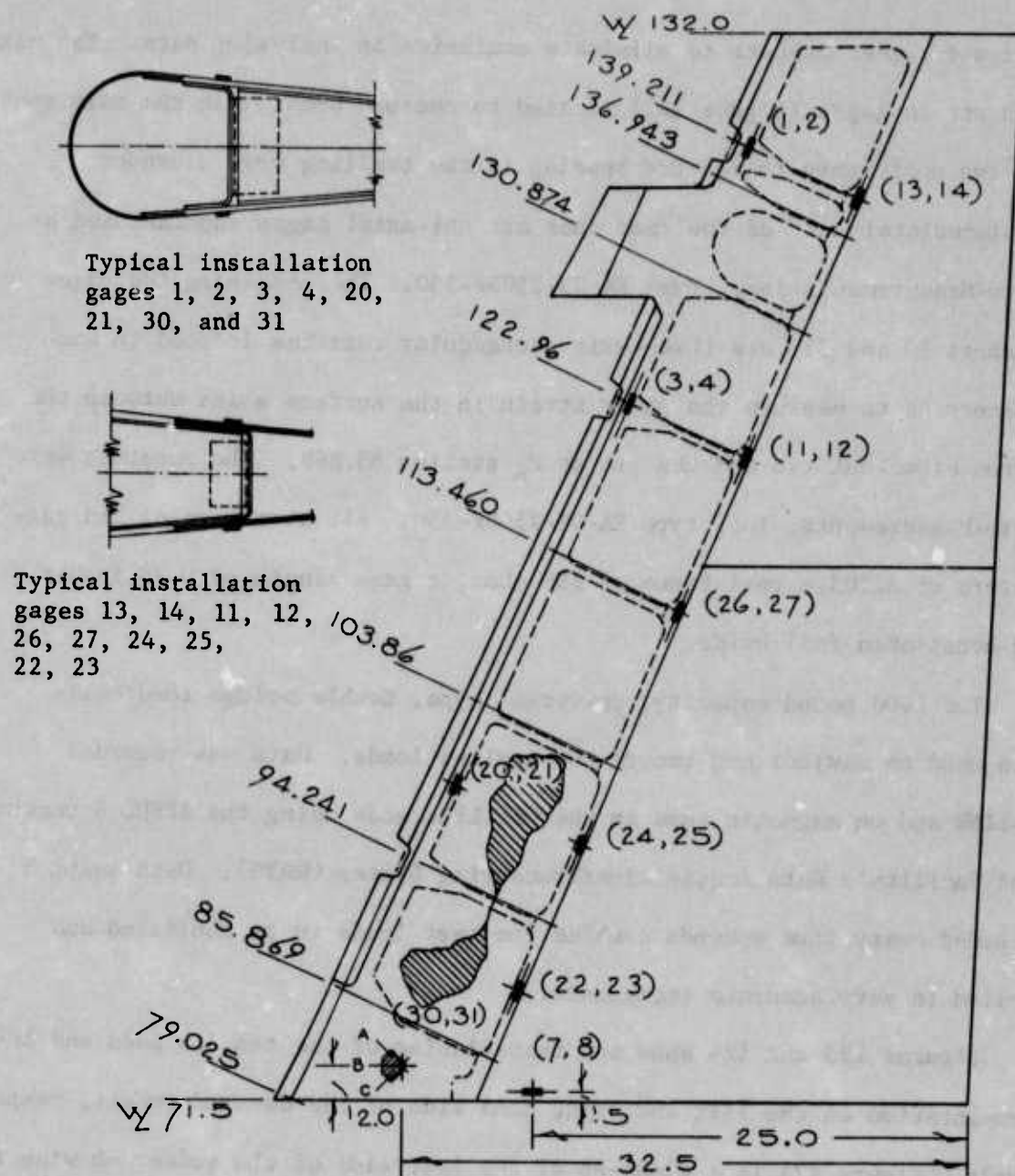
assigned higher numbers to eliminate confusion in analyzing data. The sixteen strain gages (Figure 122) located to measure bending in the main spars and two positioned to measure bending in the trailing edge closeout rib immediately aft of the rear spar are uni-axial gages manufactured by Micro-Measurements Inc., type EA-05-250BF-350. The remaining two gages (Numbers 30 and 31) are three-axis rectangular rosettes located in such a manner as to measure the shear strain in the surface skins between the bottom close-out rib and the rib at Z_R station 85.869. The rosettes were Micro-Measurements, Inc. type EA-05-250BF-350. All strain gages had gage factors of 2.105, a resistance of 350 ohms, a gage length of 0.25 inches, and constantan foil grids.

Two 1000 pound capacity, universal type, double bridge load cells were used to monitor and record the applied loads. Data was recorded ON-LINE and on magnetic tape in the OFF-LINE mode using the AFFDL Structures Test Facility's Data Acquisition/Processing System (DAPS). Data samples recorded every five seconds enabled the test loads to be monitored and applied in very accurate increments.

Figures 123 and 124 show the installation of the tension pads and instrumentation on the left and right hand side of the damaged rudder, respectively. Figure 125 is a close-up of the left side of the rudder showing the extensive damage to the lower hinge back-up rib. The damage shown in these photographs was generated during the acoustic fatigue test discussed in Section V.

3. Residual Strength Test Set-Up and Procedure

Test 6 was conducted in May 1969 by personnel of the AFFDL Structures



The second nr in () refers
to lower or R.H.S. strain
gage.

Figure 122 - F-4 Beryllium Rudder Strain
Gage Locations

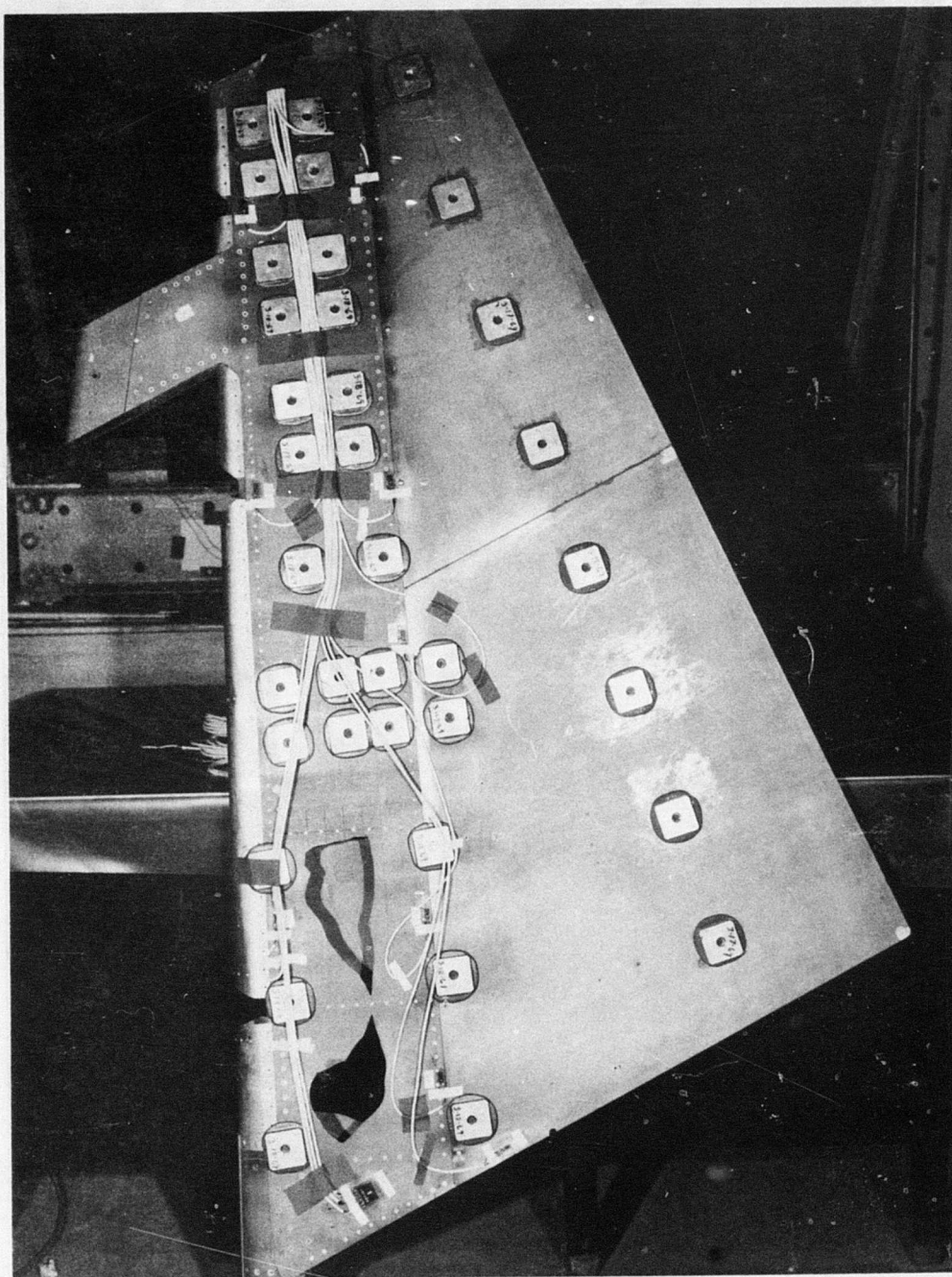


Figure 123 - F-4 Beryllium Rudder with Tension Pads
and Strain Gages Installed on Left Side

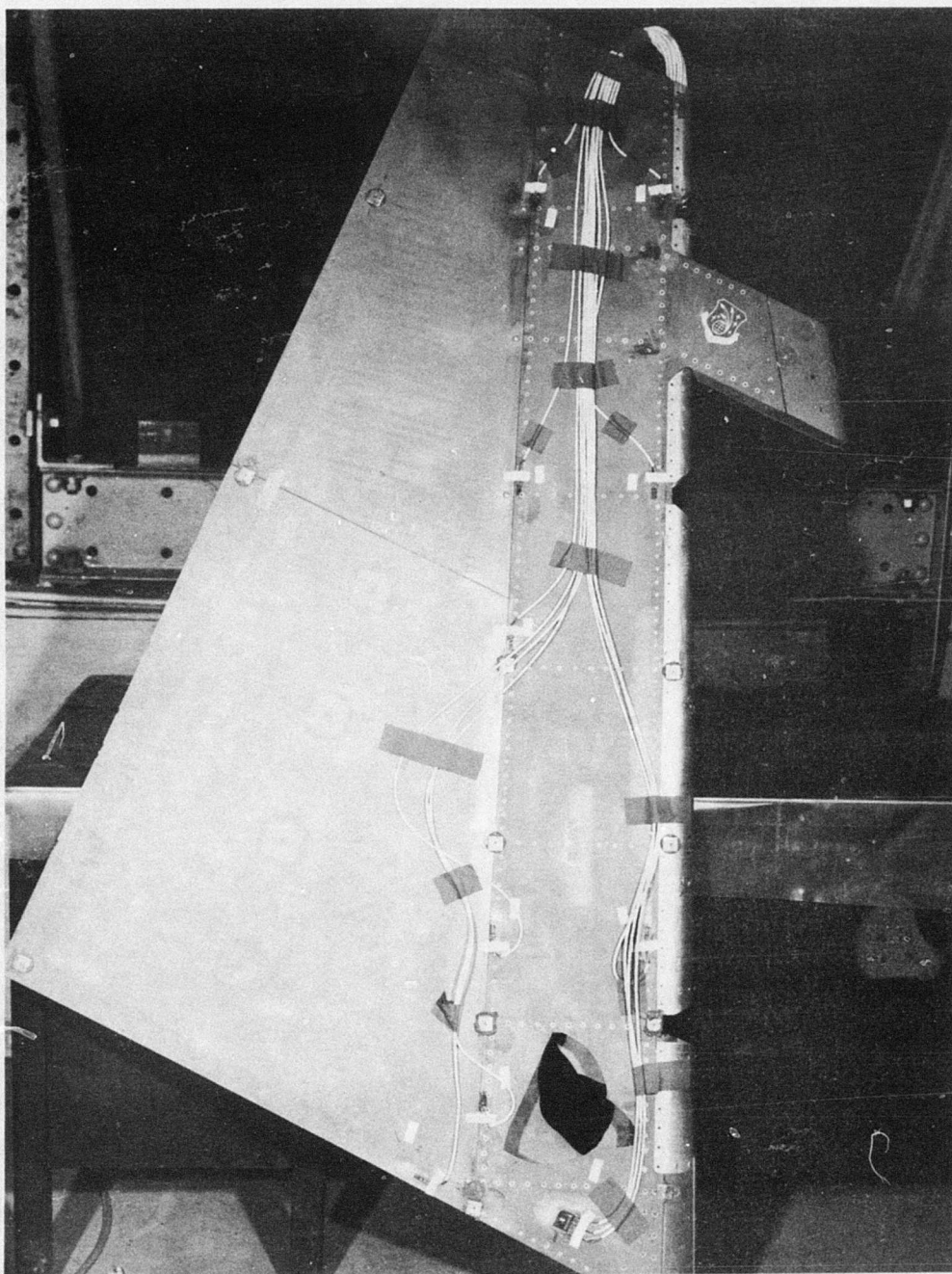


Figure 124 - F-4 Beryllium Rudder with Deflection
Transducer Pads and Strain Gages
Installed on Right Side

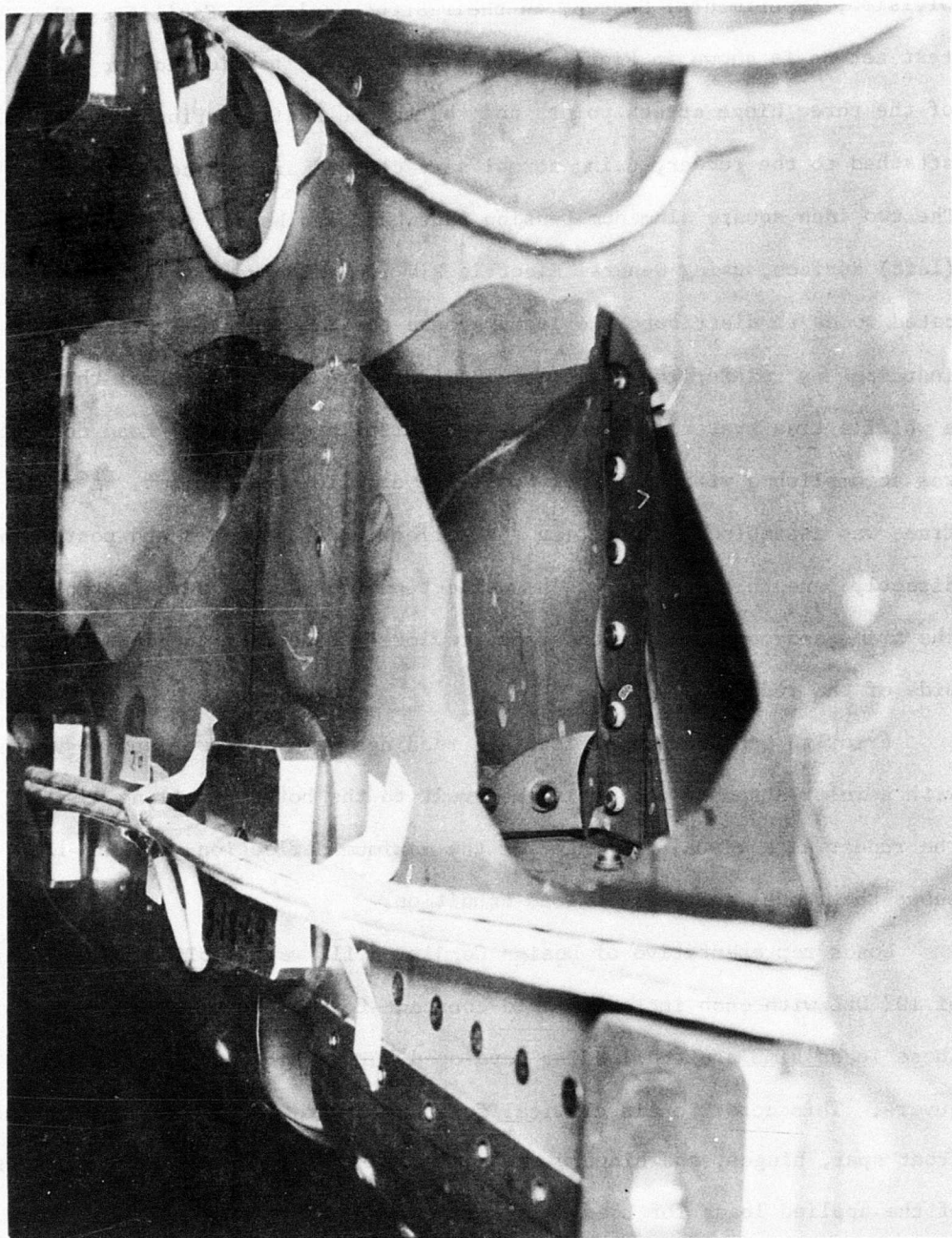


Figure 125 - Acoustic Damage to Lower Hinge
Back-Up Rib of F-4 Beryllium Rudder

Division, Experimental Branch, in their Structural Test Facility. The test set-up is shown in Figure 126. Fittings were fabricated for each of the three hinge attach points and the torque shaft fitting and attached to the rudder, using normal service hardware and torque values. The two inch square aluminum tension pads had been bonded to the upper (left) surface, using General Electric RTV 106 adhesive. These were located so as to distribute the loads around the damaged areas without inducing any reinforcing effects. The pads were linked together through a whiffle-tree system connected to two hydraulic cylinders. Load control was accomplished with an Edison Model D Hydraulic Load Cabinet. A rigid frame was assembled for mounting the deflection transducers and positioned directly beneath the rudder. The deflection transducers were fastened to the frame and connected to the pads previously bonded to the lower (right) side of the rudder.

Prior to application of load all readings were "zeroed" and an upright with a ruler attached was positioned next to the bottom trailing edge of the rudder as a visual indicator of the maximum deflection. Figure 127 shows the rudder in the zero load condition.

Loads representative of Design Condition III were applied in increments of 10% DLL with each increment held constant for approximately 30 seconds. These loads simulate the loading developed during rolling pull-out maneuvers. This condition is critical for the forward torque box cover skins, front spar, hinges, and hinge back-up ribs. Figures 128 and 129 are plots of the applied loads for Load Cell 1 and Load Cell 2, respectively. When applied load reached 80% DLL a loud noise was heard in the structure;

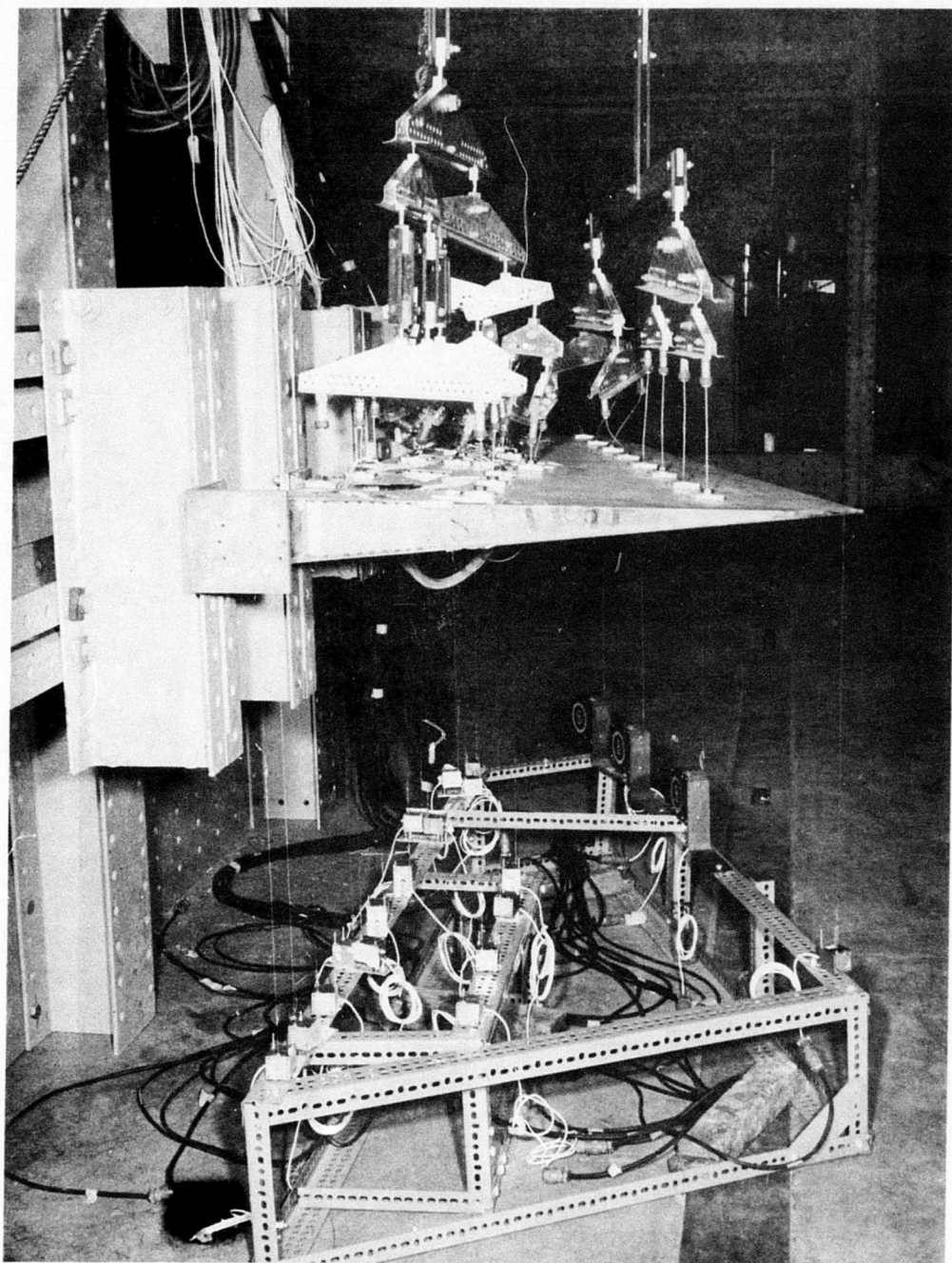


Figure 126 - F-4 Beryllium Rudder Residual Static
Strength Test Set-Up

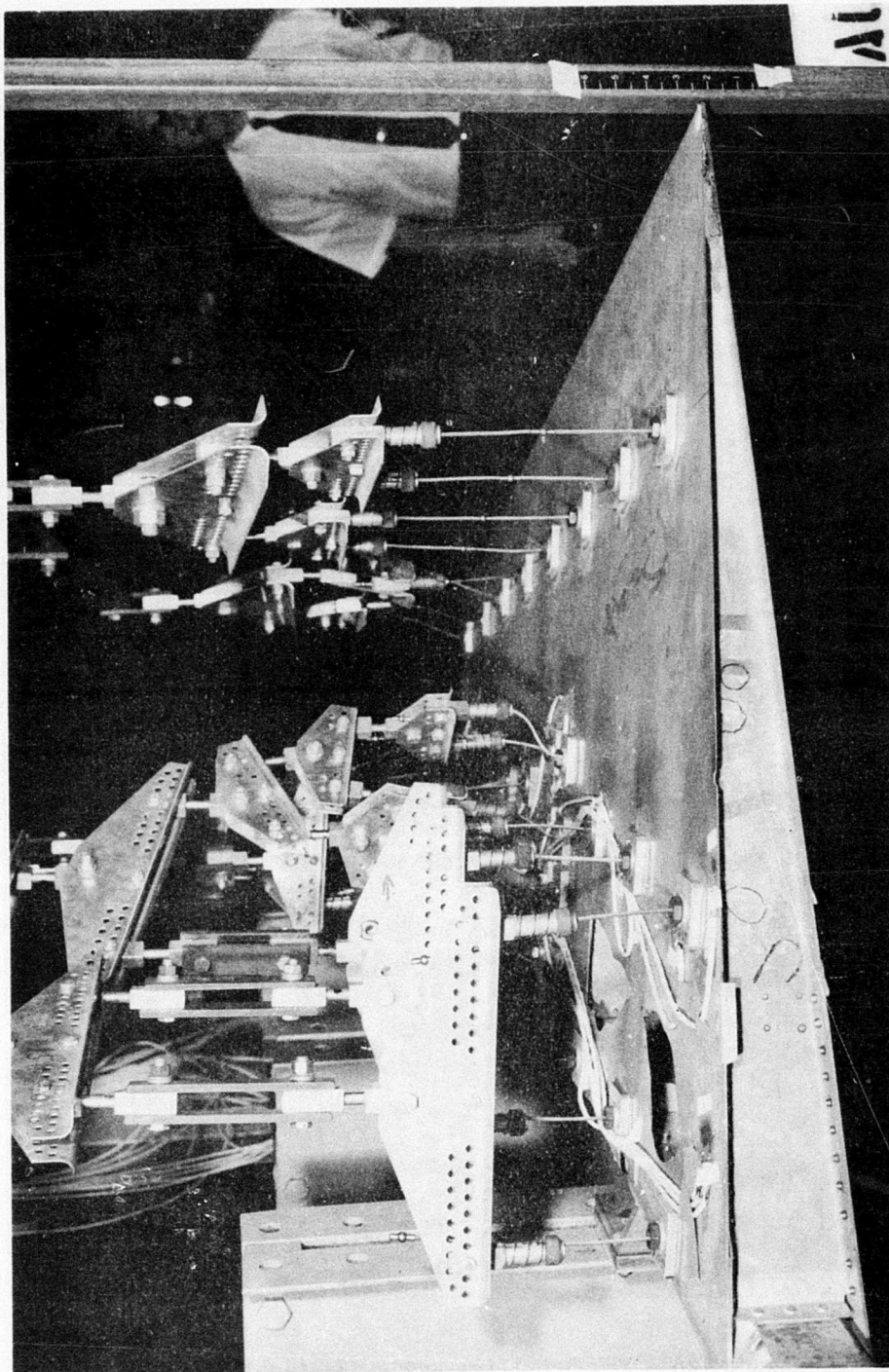


Figure 127 - F-4 Beryllium Rudder at Zero Load

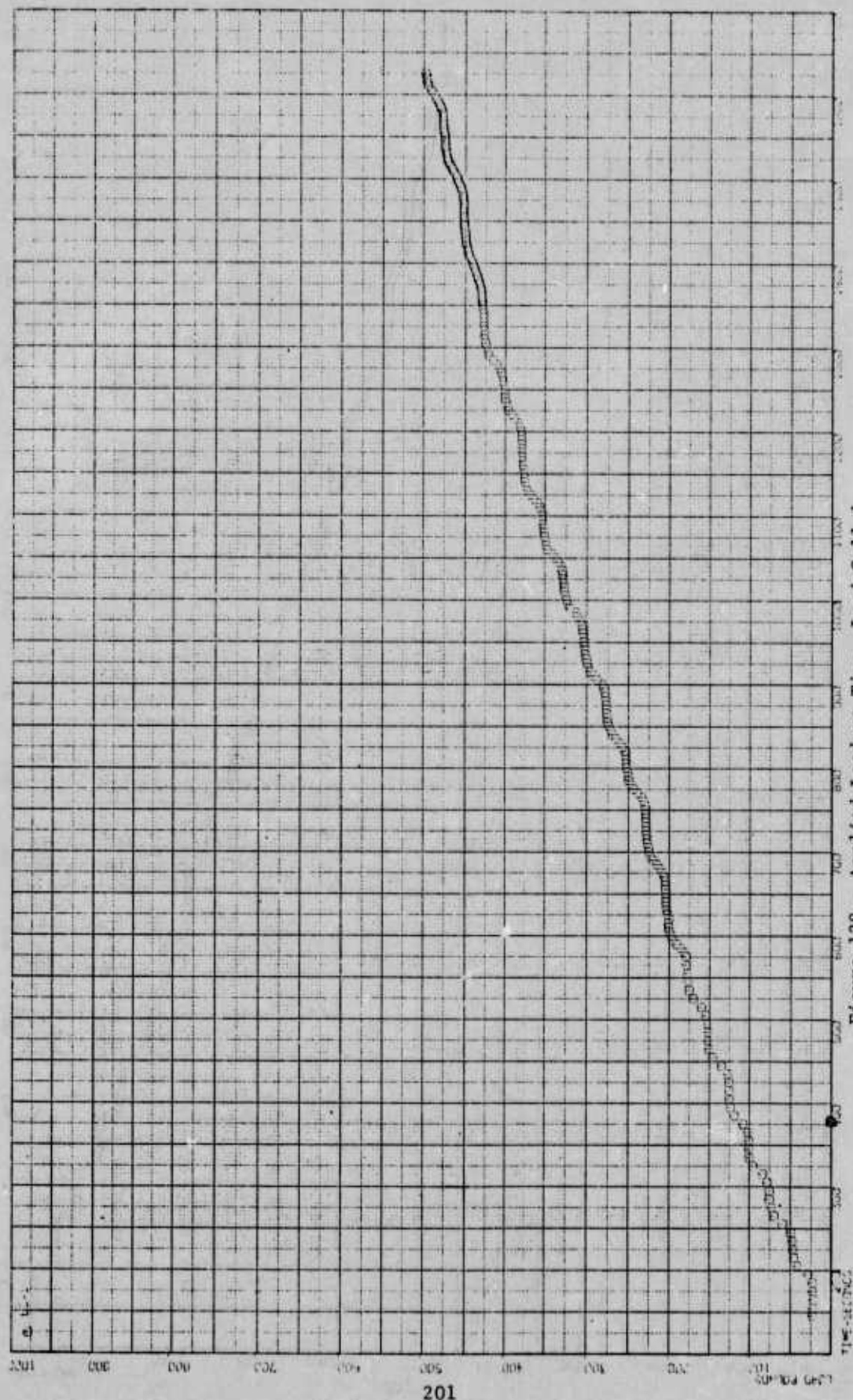


Figure 128 - Applied Load vs Time, Load Cell 1

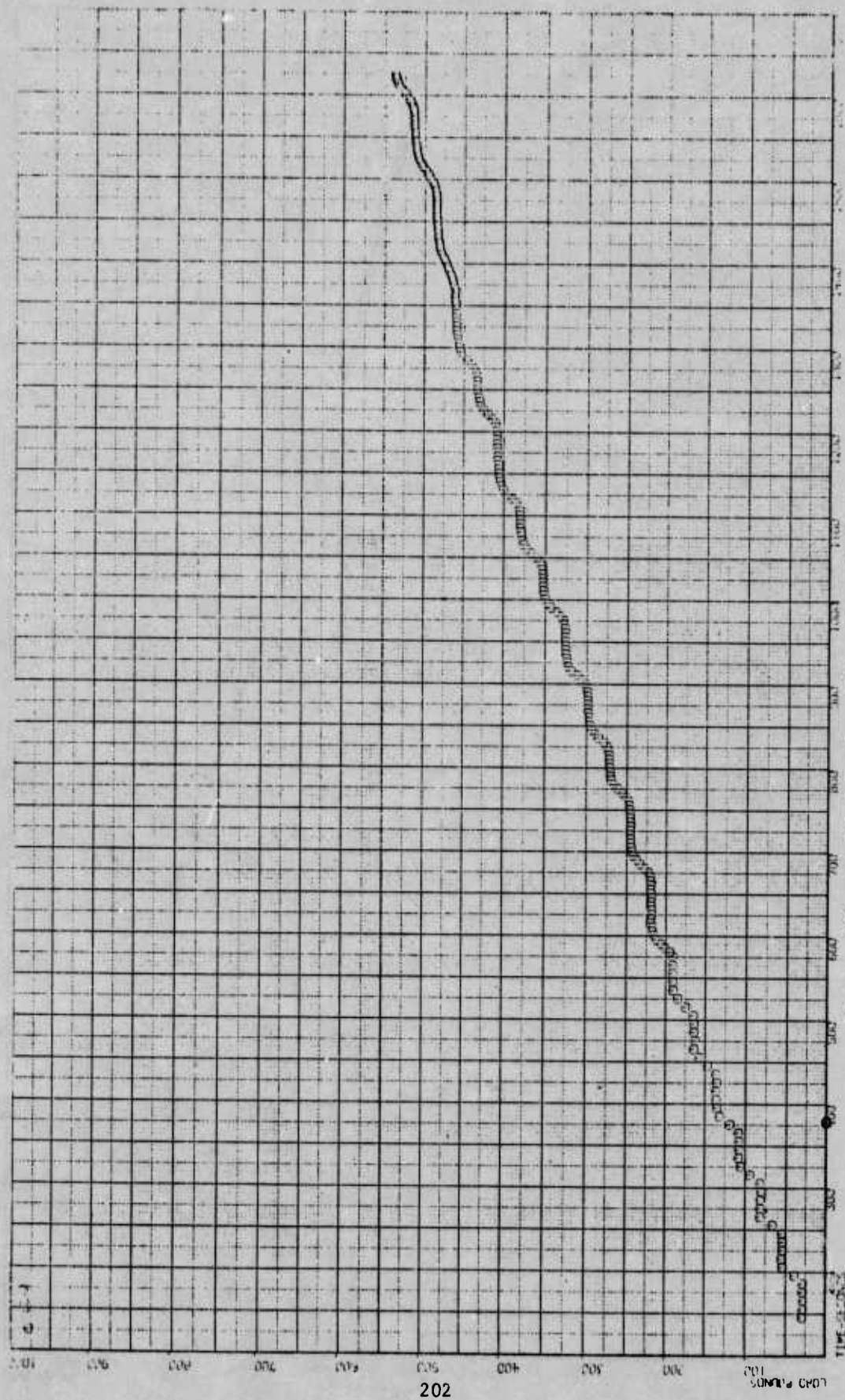


Figure 129 - Applied Load vs Time, Load Cell 2

however, loads did not drop off and there was no visual indication of increased damage. Loading was continued and at 150% DLL the combined load totaled 785 pounds producing a hinge moment of 9,650 inch-pounds. At a combined load of 1079 pounds (200% DLL) the bottom trailing edge deflection was approximately two inches, as can be seen by comparing Figure 130 with Figure 127. Approximately 15 seconds after this load was reached the rudder failed catastrophically as shown in Figures 131, 132, and 133.

4. Test Results and Discussion

The failure of the rudder was instantaneous, permitting no documentation of initiation point and progress through the structure. However, by considering the stresses in the several members along with the known damage in existence, the test engineer was able to develop a most likely sequence. The failure apparently began at the crack previously created in the trailing edge lower closure rib, continued through the heavily damaged lower section of the torque box and ended immediately above the lower hinge attachment fitting. Figures 131 - 133 show the irregular, brittle-like failure of the beryllium rudder.

A review of the data reveals relatively high stresses in the vicinity of the damaged area just prior to failure with a maximum stress of about 36,000 psi (248×10^6 N/M²). Figures 134 - 138 are plots of the stresses vs. time converted from strain gage data. The largest stresses were recorded in the immediate vicinity of the crack in the lower closure rib, with the next higher stresses measured at the front spar near the lower hinge. It was these areas through which the final break occurred.

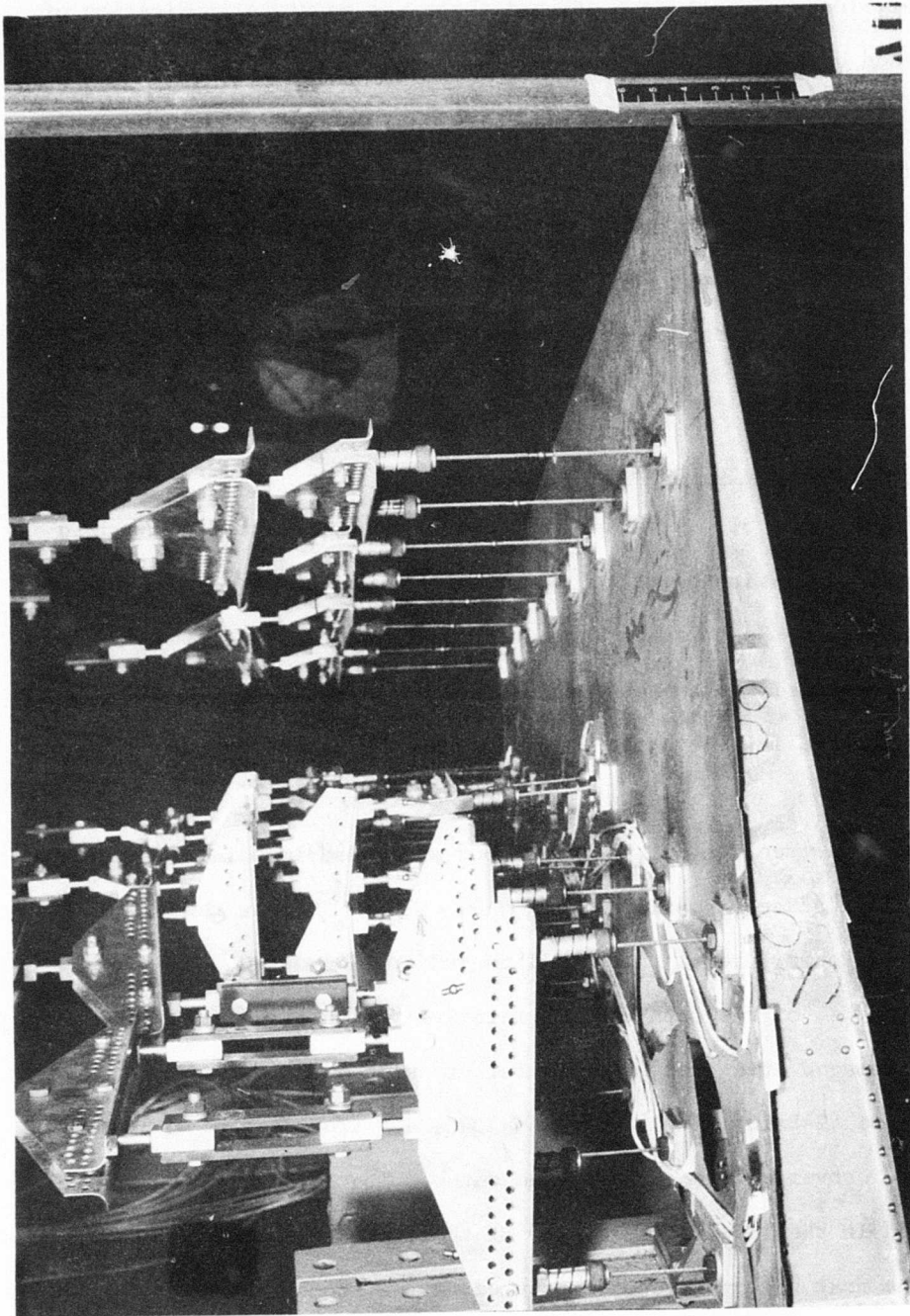


Figure 130 - F-4 Beryllium Rudder at 200% Design Limit Load

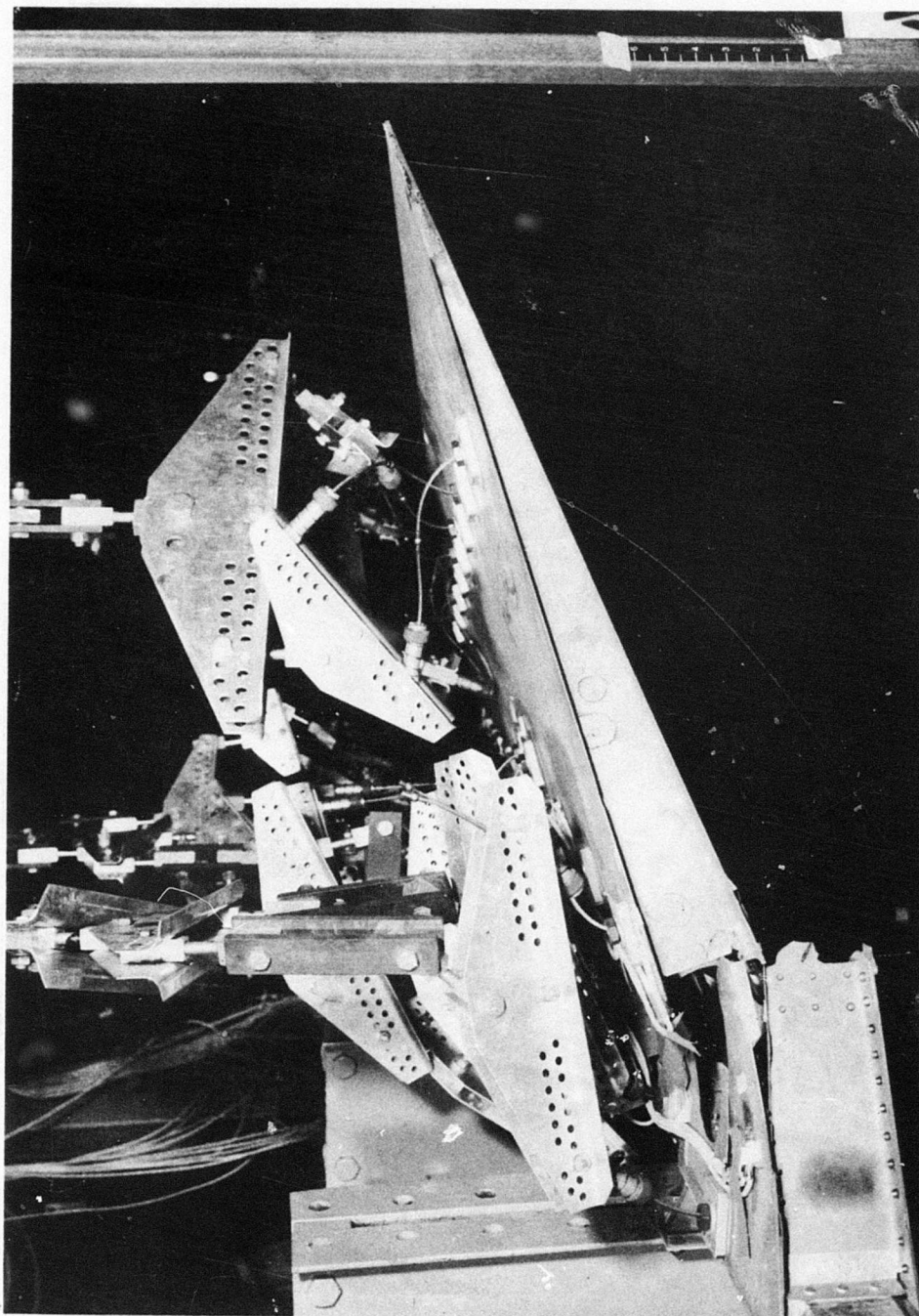


Figure 131 - Residual Static Strength Failure of F-4 Beryllium Rudder

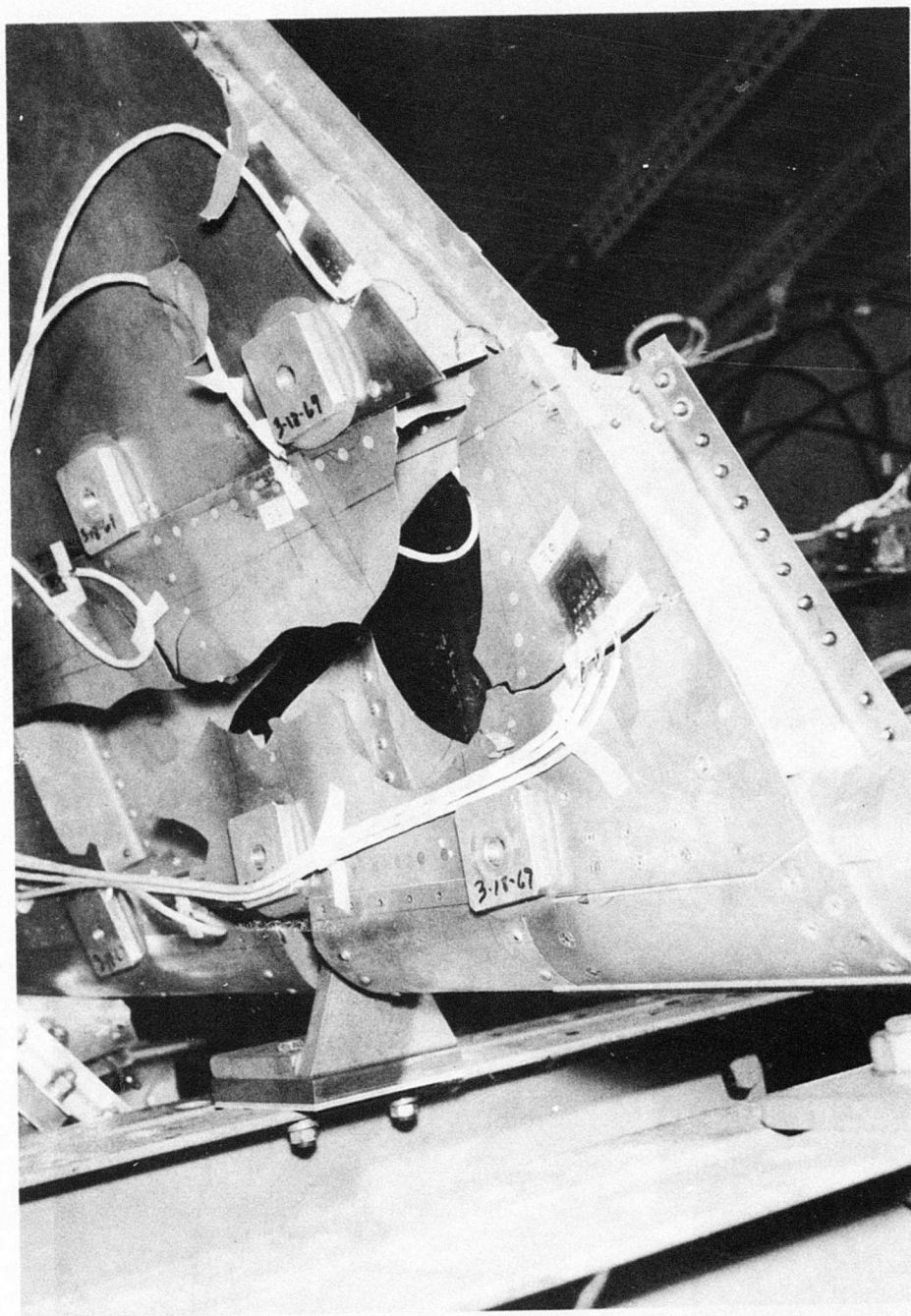


Figure 132 - F-4 Beryllium Rudder; Failure Area on Left Side

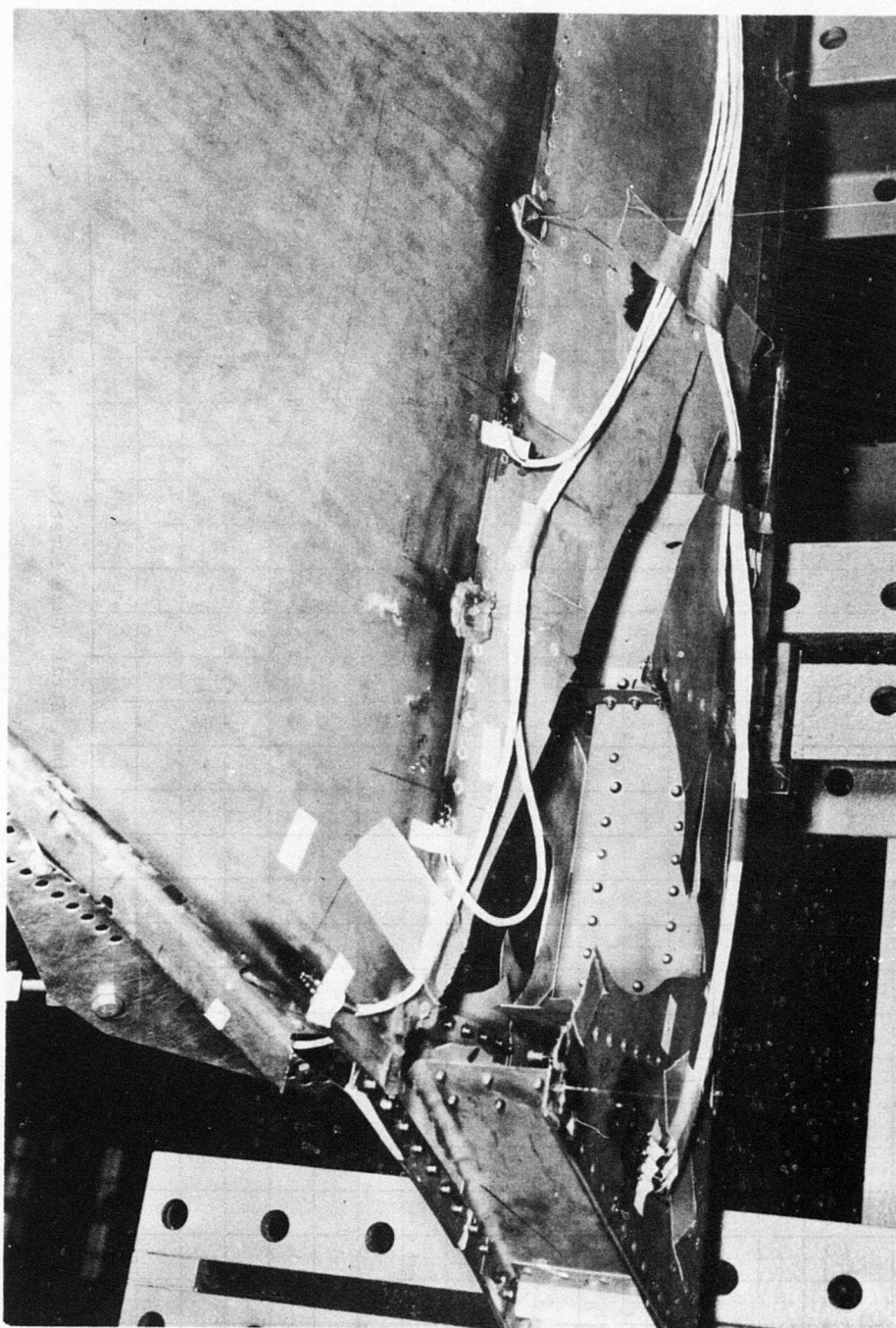


Figure 133 - F-4 Beryllium Rudder; Failure Area on Right Side

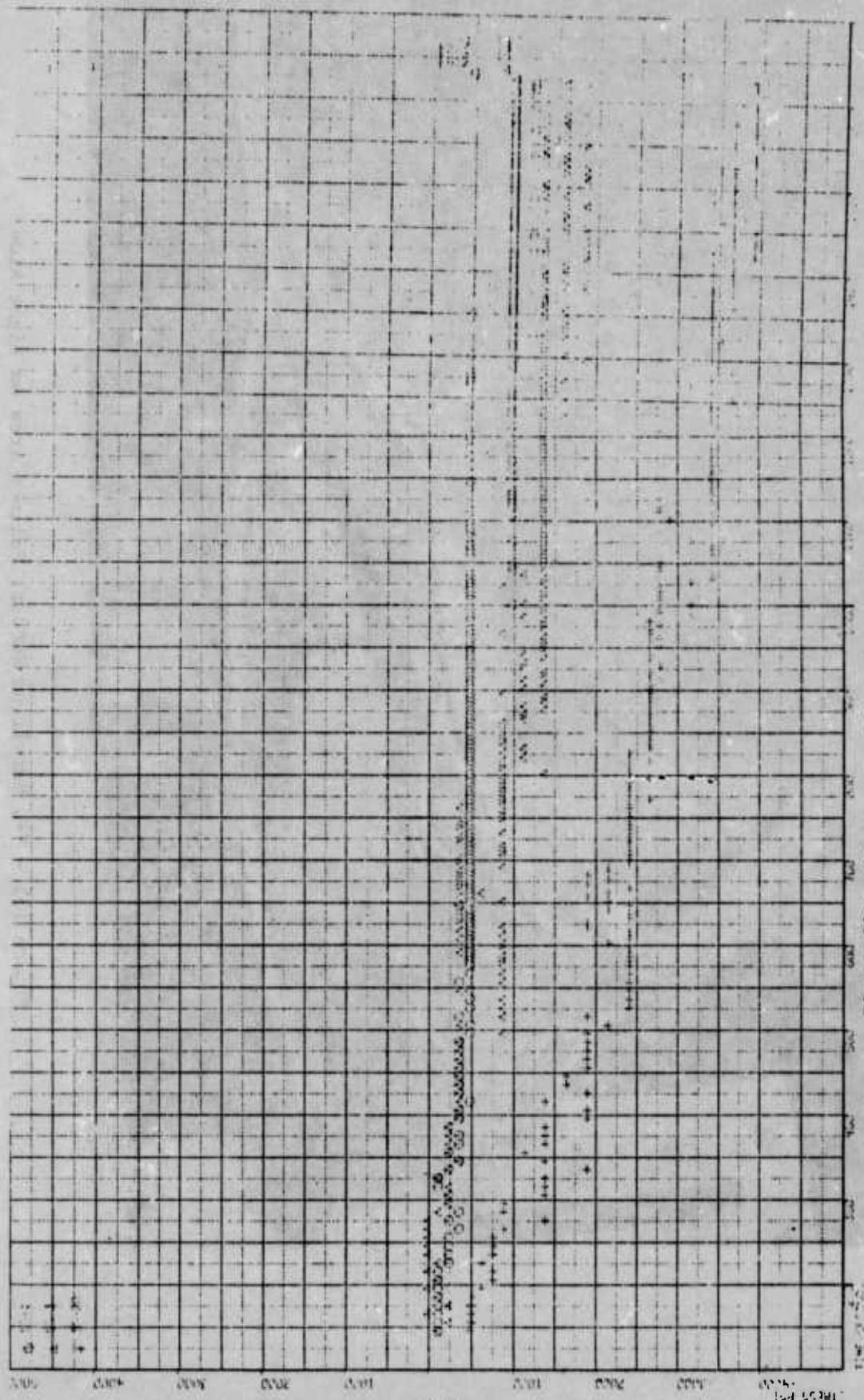


Figure 134 - Stresses vs Time, Strain Gage Locations 1, 3, & 20

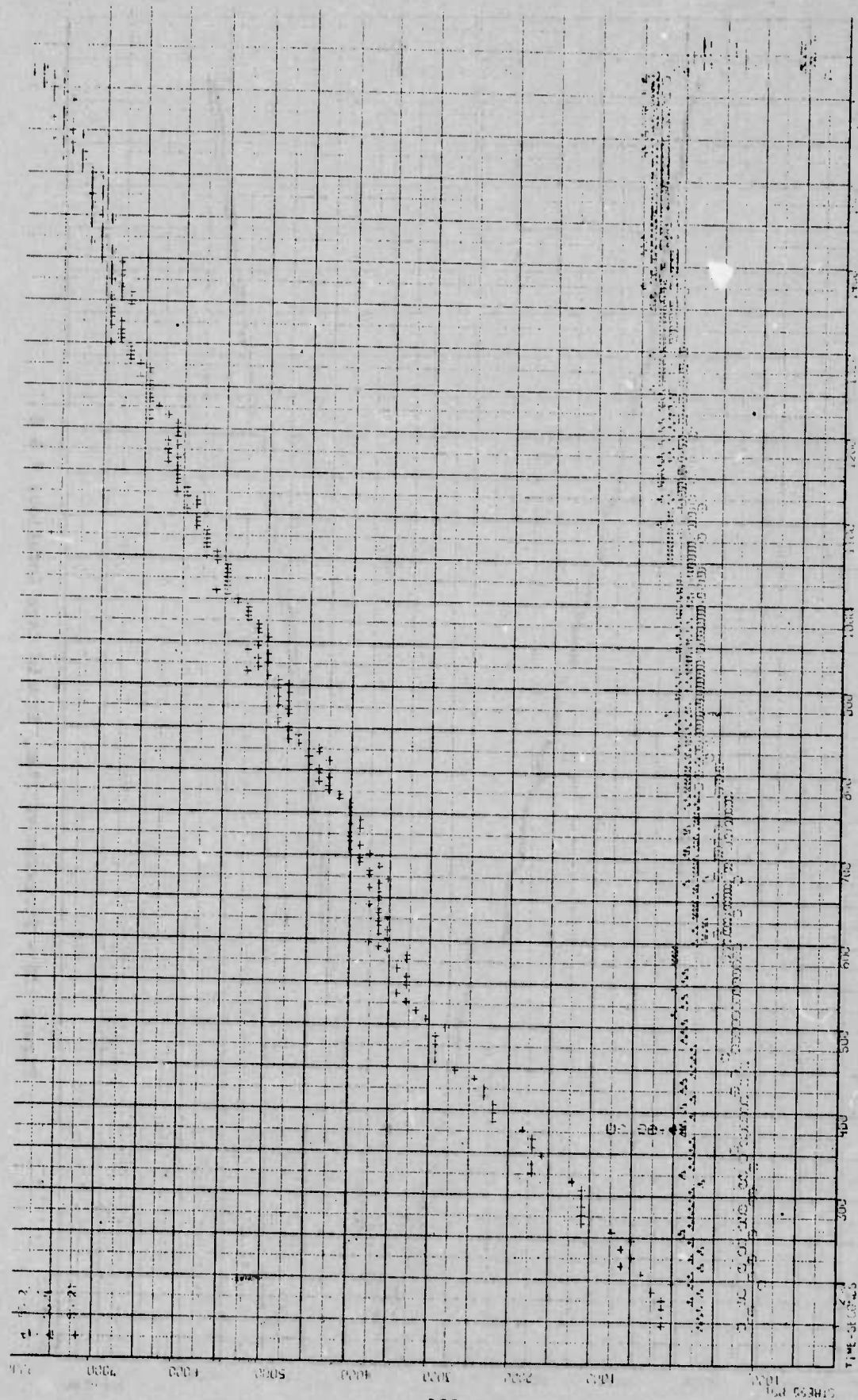


Figure 135 - Stresses vs Time, Strain Gage Locations 2, 4, & 21

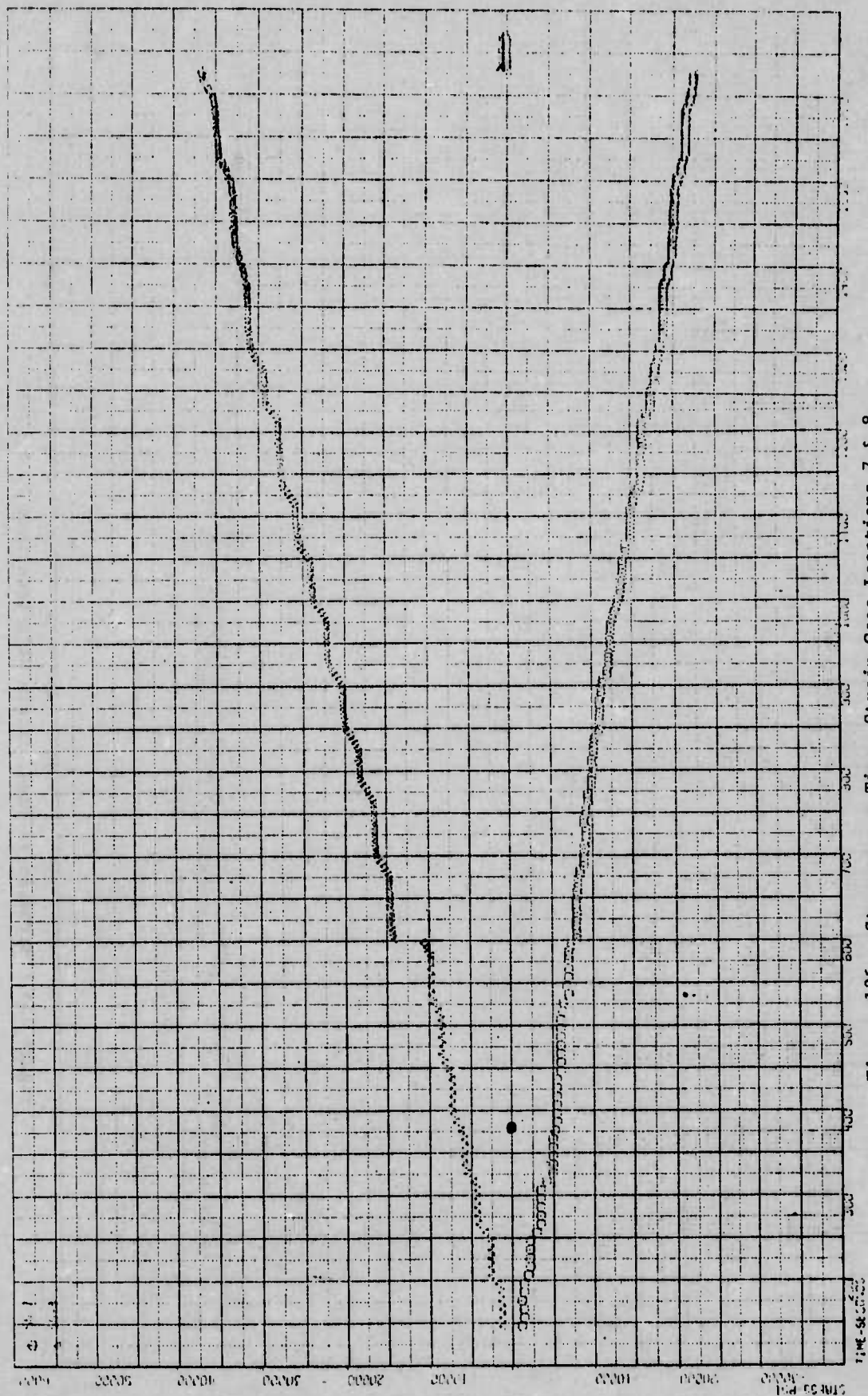


Figure 136 - Stresses vs Time, Strain Gage Locations 7 & 8

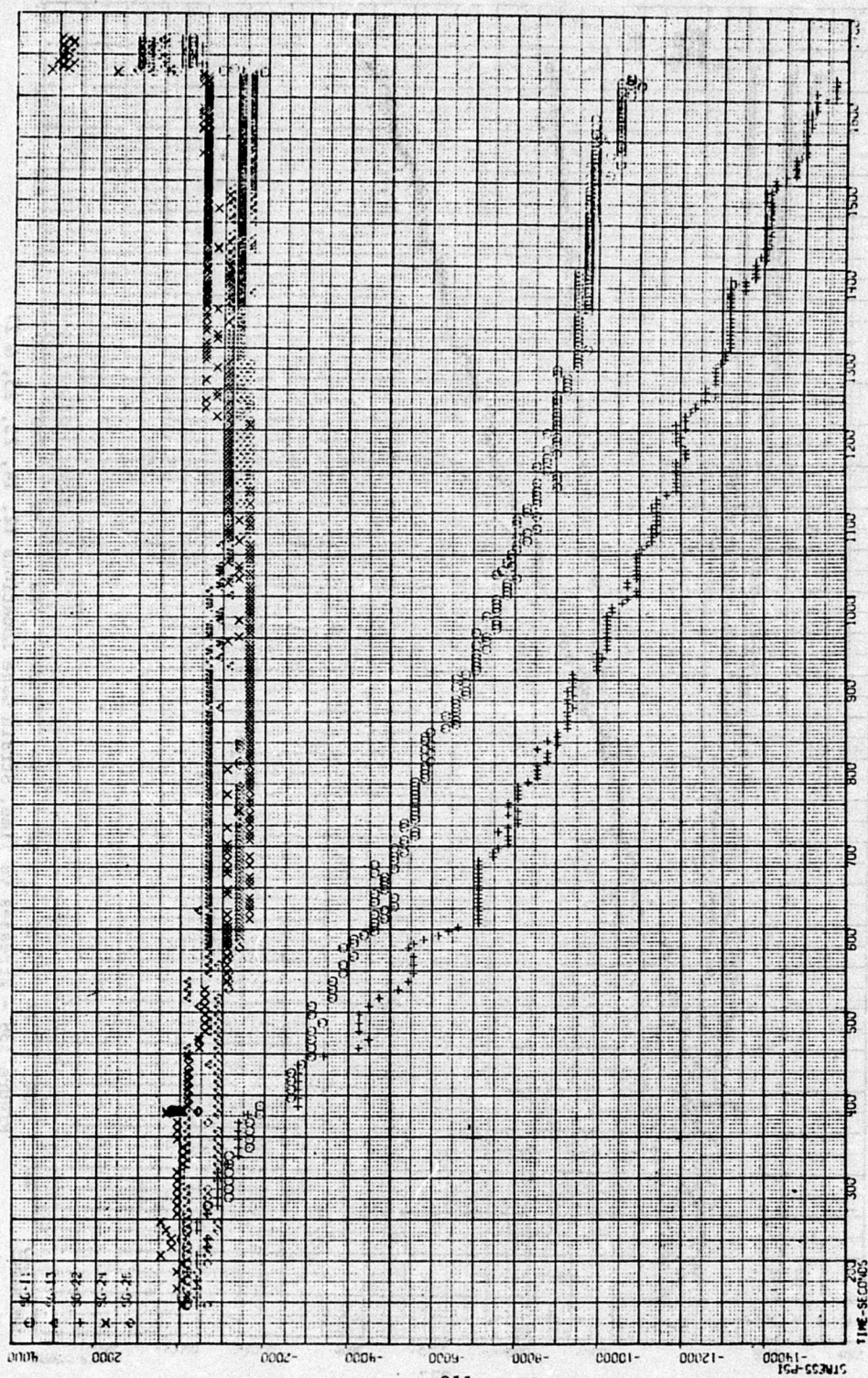


Figure 137 - Stresses vs Time, Strain Gage Locations 11, 13, 22, 24, & 26

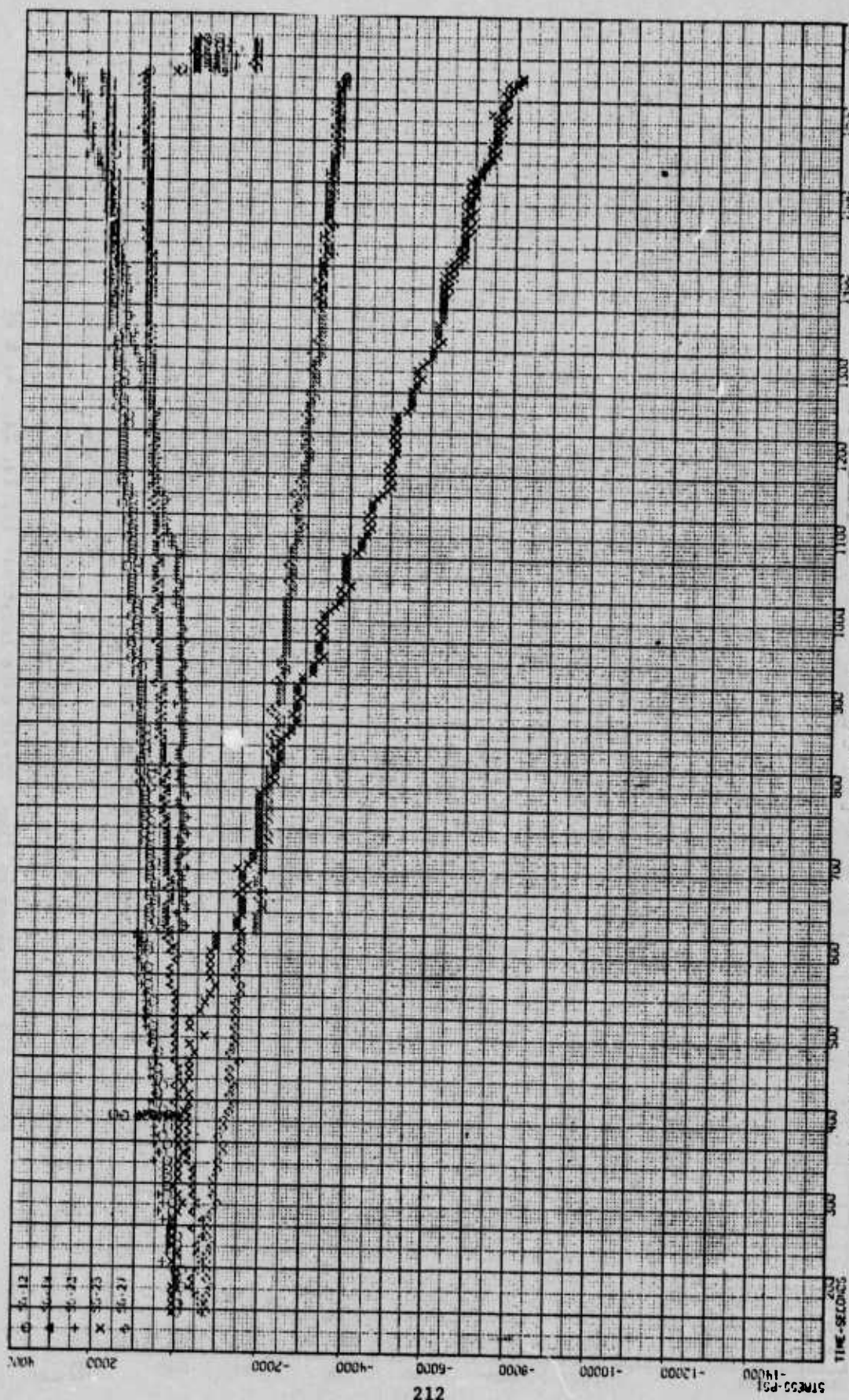


Figure 138 - Stresses vs Time, Strain Gage Locations 12, 14, 23, 25, & 27

Figures 139 through 142 plot the deflections measured throughout the beryllium rudder residual strength test. At 200% DLL the maximum recorded deflection was 1.99 inches (5.06 cm) as measured by deflection transducer 24D. Table 10 shows the maximum deflections measured for each of the four static tests to design ultimate load (150% DLL) conditions or beyond.

Table 10 - Beryllium Rudder Maximum Deflections in Inches

Deflection Point	<u>Test 2</u>	<u>Test 3</u>	<u>Test 4</u>	<u>Test 6</u>
1D	0.61	5.38	1.15	0.12
2D	0.54	5.00	1.03	0.05
3D	0.50	4.50	0.98	
4D	0.44	3.95	0.80	0.05
5D	0.36	3.40	0.75	0.02
6D	0.31	2.88	0.62	0.03
7D	0.25	2.25	0.48	0.06
8D	0.20	1.95	0.45	0.09
9D	0.18	1.72	0.37	0.11
10D	1.10	5.80	1.98	
11D	1.10	5.45	2.00	
12D	0.98	4.32	1.80	
13D	0.86	3.70	1.58	0.58
14D	0.83	3.32	1.55	0.57
15D	0.80	2.80	1.44	0.56
16D	0.67	2.22	1.20	0.55
17D	1.43	6.30	2.50	0.83
18D	1.50	5.95	2.63	
19D	1.64	5.70	2.75	1.15
20D	1.65	5.30	2.92	
21D	1.75	5.00	3.05	1.48
22D	1.83	4.50	3.22	
23D	1.98	4.10	3.43	
24D	2.04	3.78	3.60	1.99

While the loads for Test 6 were the same as those applied to the rudder in Test 3, the use of a rigid mounting system for Test 6 resulted in a deflection pattern more closely resembling Test 2 and 4. This is shown graphically in Figure 143 where maximum recorded deflections are plotted against a zero load position for comparison. The deflections are scaled

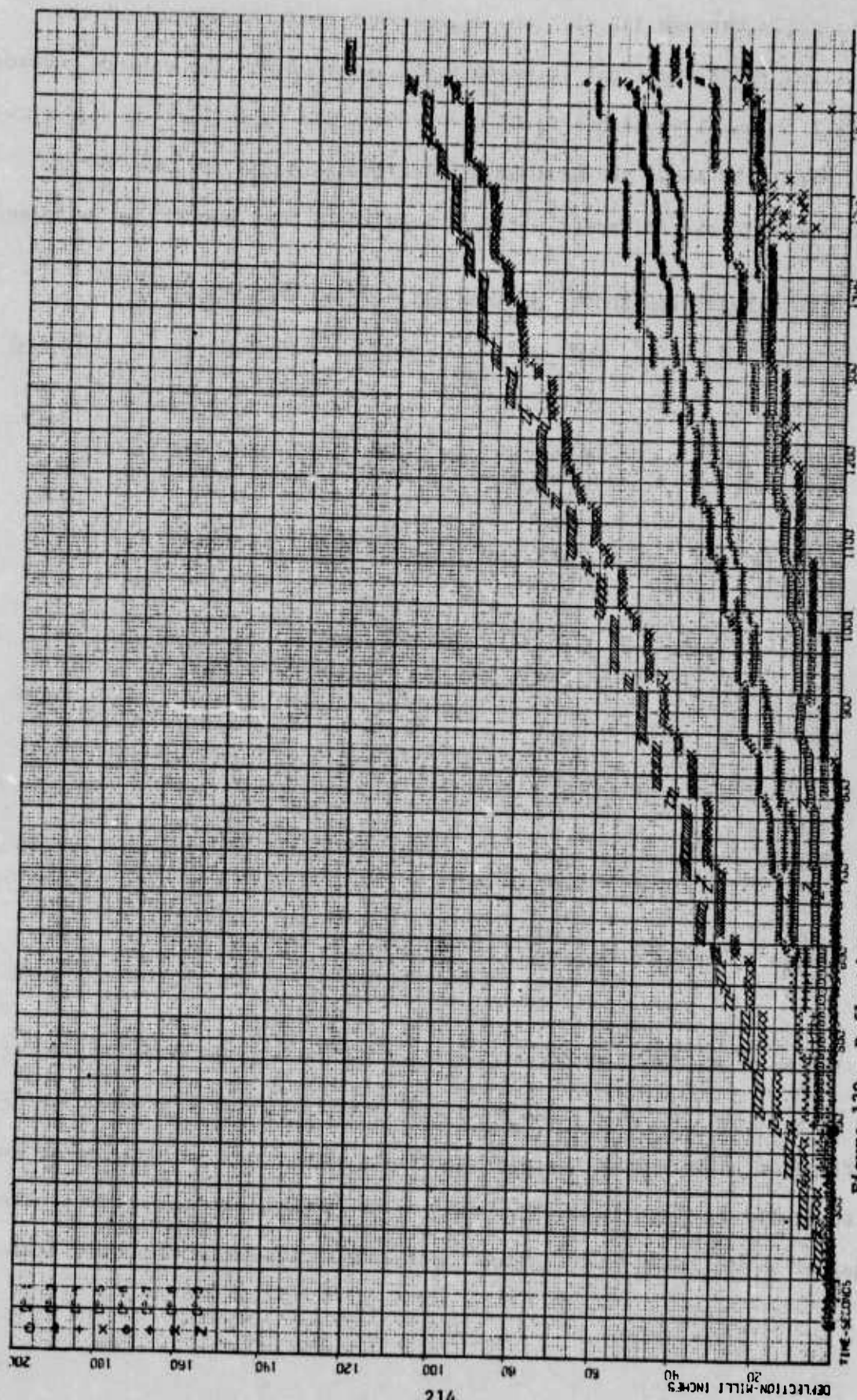


Figure 139 - Deflections vs Time, Potentiometer Positions 1, 2, 4, 5, 6, 7, 8, & 9

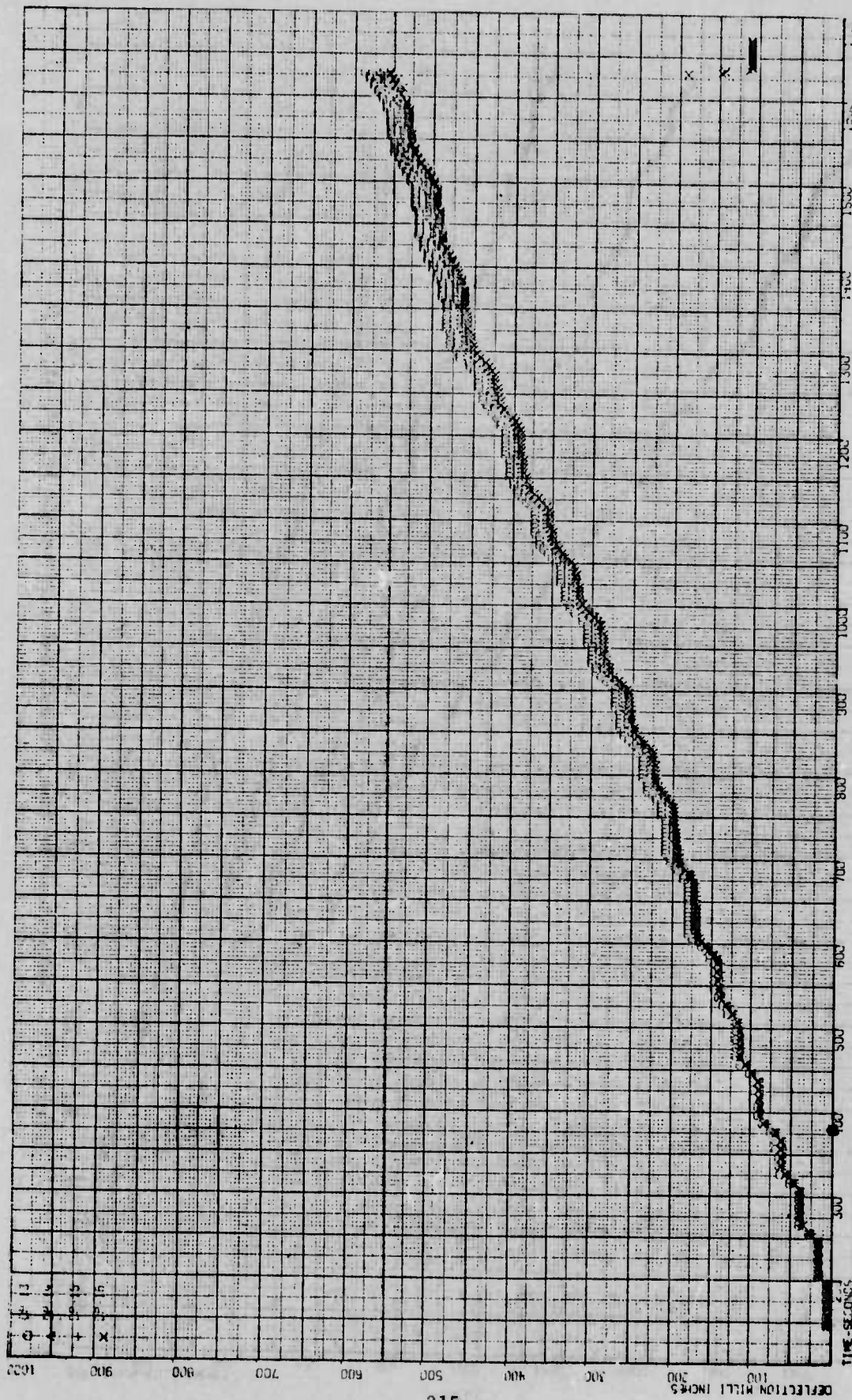


Figure 140 - Deflections vs Time, Potentiometer Positions 13, 14, 15, & 16

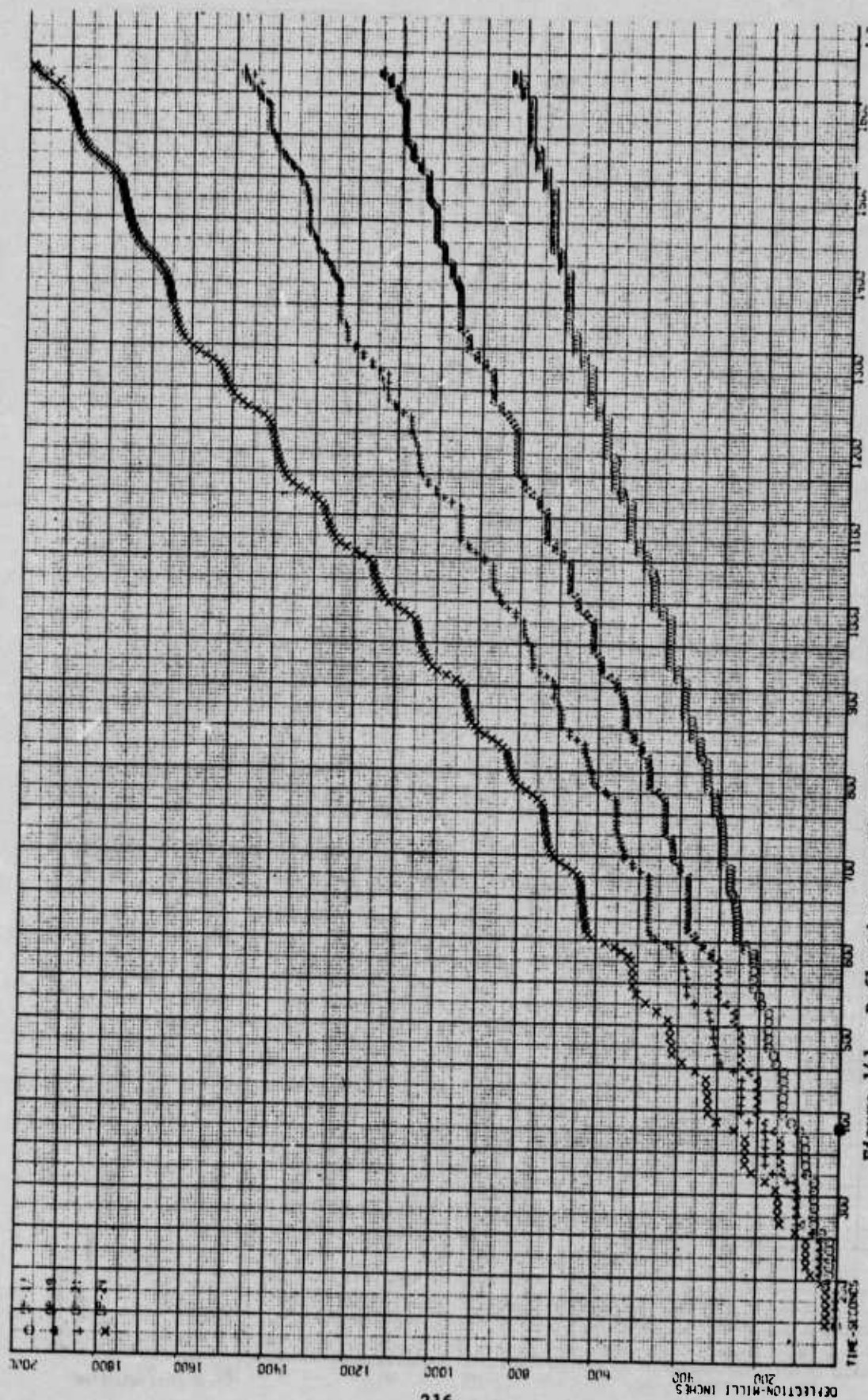


Figure 141 - Deflections vs Time, Potentiometer Positions 17, 19, 21, & 24

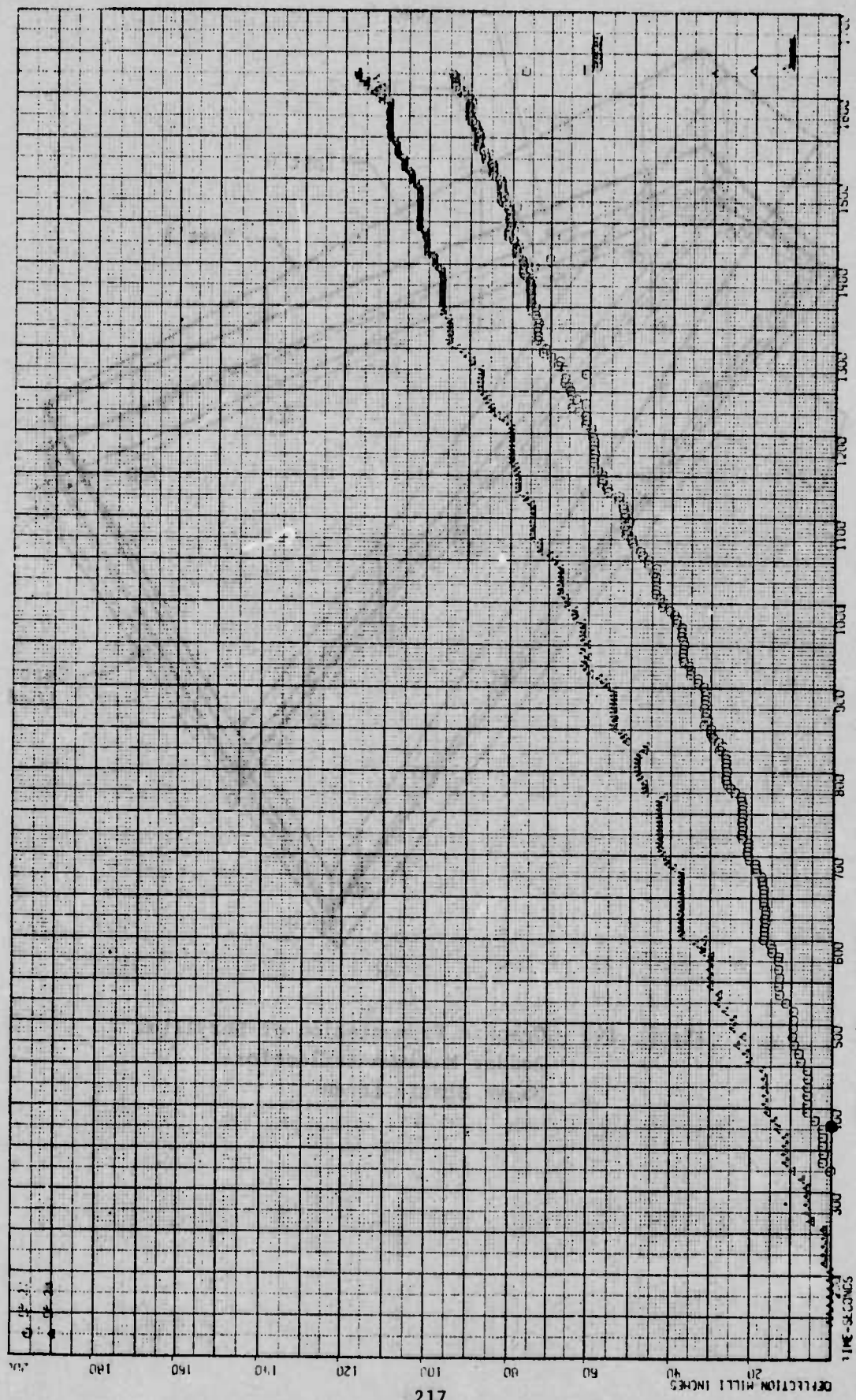


Figure 142 - Deflections vs Time, Potentiometer Positions 27 & 28

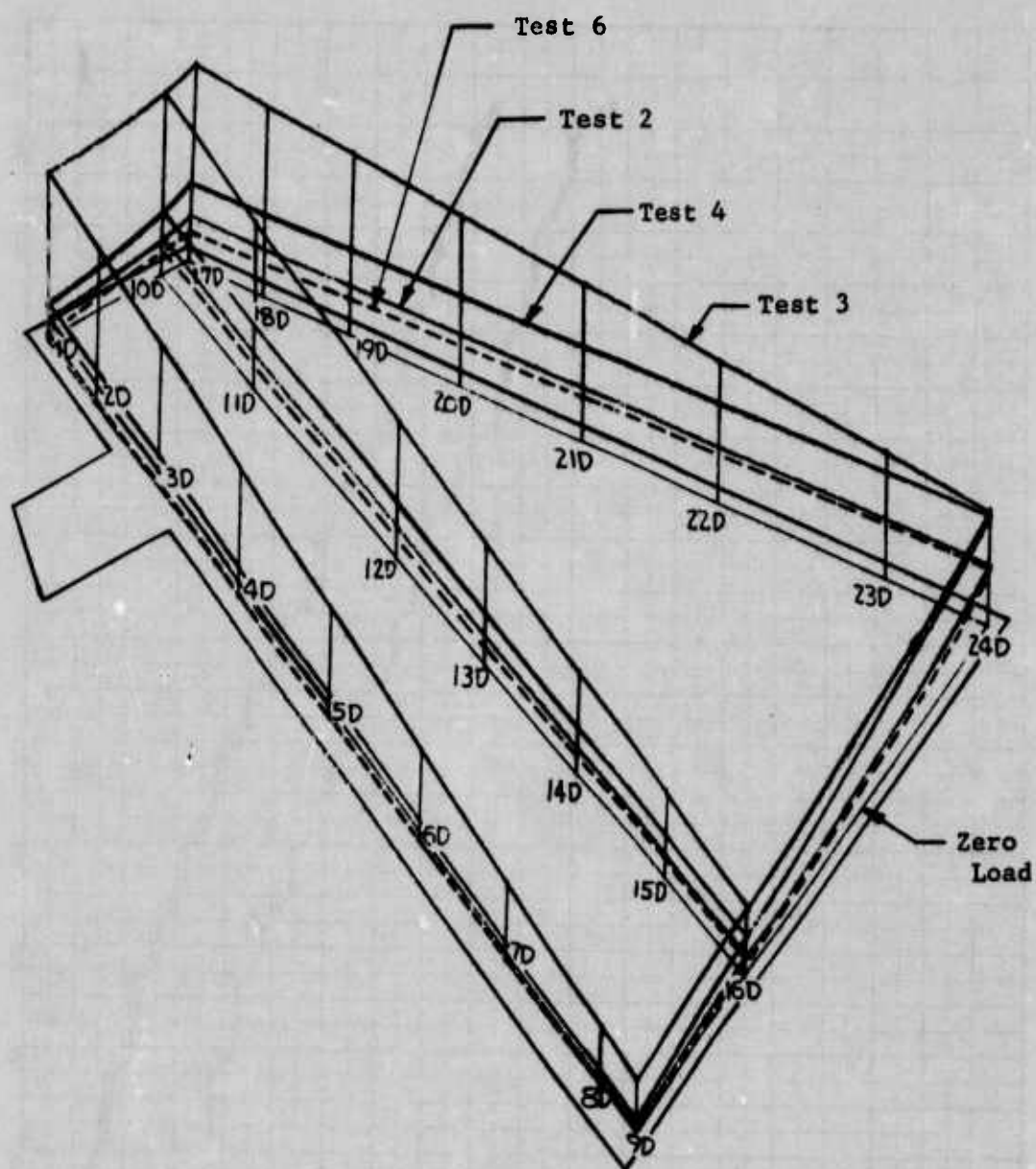


Figure 143 - Graphic Presentation of Beryllium
Rudder Maximum Deflections
Under Static Loads

relative to each other though exaggerated relative to dimensions of the rudder to better show the deflection patterns. Though severely damaged with much load-bearing material destroyed, the forward torque box retained exceptional rigidity up until total failure of the rudder.

Based upon the results of the extremely rugged series of tests to which this beryllium ground test rudder was subjected, and its response to loads, it can be safely said that the beryllium rudder exceeds the strength requirements for this application. This test series also shows that thin-gage beryllium structures, though the material is extremely limited in short transverse ductility, can survive loads which cause bending even in a damaged condition.

SECTION VIII

BERYLLIUM RUDDER FLIGHT TEST PROGRAM

1. Introduction

The flight test demonstration program was an extension of the flight qualification program discussed previously in this report and in more detail in Reference 1. Reference 2 provides a detailed description of the flight demonstration program through 90 flights totaling 100 hours and 30 minutes of flight time over a 15-month time period. At this point the contract was closed out, all goals having been met; however, the rudder remained aboard the bailed aircraft by mutual agreement between MCAIR and AFFDL. The beryllium rudder remained on flight status for an additional two years until in August 1971 it was removed during modification for the "Fly-by-Wire" flight test program. At this time the rudder had accumulated a total of 158 flights, logging 184 hours 24 minutes of flight time in a variety of environments including visits to Ramey AFB, Puerto Rico, and McDill AFB, Florida in addition to the primary operational site of Lambert St. Louis Municipal Airport.

The flight test beryllium rudder is structurally identical to the ground test beryllium rudder except for minor design improvements (Figure 22) and an added corrosion protection system. The beryllium flight test rudder weighed 40.11 pounds (18.19 kgs) as compared to 37.59 pounds (17.05 kgs) for the ground test rudder. The weight increase was basically caused by the addition of the corrosion protection system and an accompanying increase in balance weight. Fully instrumented and balanced for flight

testing, the fly weight of the rudder was 42.06 pounds (19.08 kgs), which represents a 34.6% weight savings over the production aluminum rudder.

Prior to installing the rudder on an aircraft, it was proof tested as a safeguard against the possibility of existence of undetected damage. The beryllium rudder was then installed and flown on a flight test YF-4E aircraft as shown in Figure 144. Flight tests were conducted on a ride-along basis and no flight restrictions whatsoever were imposed on the aircraft because of the beryllium rudder. In fact, during the early flights when recording capacity was available and the instrumentation hooked up, the aircraft was subjected to steady yaw and rolling pullout maneuvers which impose maximum design limit loads on the rudder, and data was recorded to measure structural response. During one rolling pullout maneuver two consecutive 360° rolls were inadvertently performed, exceeding the aircraft flight envelope and imposing loads on the rudder estimated at 205% of design limit loads. This occurred in flight #10, with approximately 10 accumulated flight hours on the rudder. As a result of these loads a permanent buckle was formed in the skin of the forward torque box. A subsequent inspection of the area around the buckle, of the remainder of the rudder, and of the complete aircraft did not reveal any other damage; therefore, flight testing was continued. After 53 hours 18 minutes of accumulated flight time, the rudder was removed from the aircraft and underwent a thorough visual, dye penetrant, and radiographic inspection in the laboratory. No evidence of any further rudder damage was found with the exception of some paint flaking and some minor indications.



Figure 144 - F-4 Aircraft in Flight
with Beryllium Rudder

During manufacturing certain areas were selected for continuous monitoring during test as indicators of the effects of production operations on the integrity of the finished component. Throughout the flight test demonstration, surveillance of these areas was maintained and no damage

detrimental to the structural integrity of the rudder was found. At no time was there any indication that the beryllium rudder might not be flight worthy, and testing was terminated because of the unique requirements of Phase II of the Survivable Flight Control Program for which the aircraft was modified including replacement of the beryllium rudder with a standard aluminum rudder.

2. Differences Between the Ground Test and Flight Test Rudders

Two minor changes were incorporated in the design of the flight test beryllium rudder as a result of the Reference (1) program. Furthermore, the flight test rudder was protected against corrosion and its trailing edge assembly sealed against moisture. These differences between the ground test and flight test rudders are discussed below.

a. Leading Edge Skin Splice

The leading edge splice at the lower end of the flight test rudder was modified as shown in Figure 22, to eliminate the interference between the splice and the seal on the fin closure spar. As indicated, the beryllium skin was chem-milled down to a thickness of 0.060 inch where it attaches to the splice, and the splice thickness was reduced from 0.100 inch to 0.090 inch. To eliminate the possibility of a knife edge due to countersinks, the depth of the countersinks was at least 0.015 inch less than the plate thickness of $0.090 \begin{smallmatrix} +.003 \\ -.000 \end{smallmatrix}$. The modified splice was attached with the same fasteners (3/16 inch diameter steel Jo-Bolts) as previously used. Strength analysis of the modified joint indicated a large margin of safety.

b. Hinge Fitting Fasteners

Steel Hi-Lok Fasteners were used exclusively for attaching the hinge fittings to the front spar flanges of the flight test beryllium rudder. In fabricating the ground test rudder, Hi-Shear aluminum rivets were installed for this purpose at hinge position $Z_R = 122.72$. However, one of these aluminum Hi-Shear rivets failed during the balance weight fatigue test conducted on the ground test rudder and subsequently they were replaced, before proceeding with the ground test program, with steel Hi-Lok fasteners. The change to Hi-Loks improved static and fatigue strength and facilitated fastener installation.

c. Sealing the Rudder Trailing Edge Assembly

The trailing edge assembly was sealed against moisture in accordance with the requirements established for the production rudder. This procedure is followed to prevent deterioration of the honeycomb core caused by repeated freezing and thawing of moisture which might otherwise enter the bonded assembly during its service life. All clips attached to the aft spar, their fasteners, and all other areas where the possibility of moisture entry exists, were sealed with EC-2216-B/A Sealant (Minnesota Mining and Manufacturing). Figure 145 shows a rib clip fastened to the aft spar and sealed as required.

d. Rudder Corrosion Protection

During the Reference 1 program, corrosion tests were performed in a 5% salt solution spray to establish the effectiveness of the candidate surface finishes for corrosion protection of beryllium structures. A chromic acid electrolyte was used to anodize (chemically oxidize) the

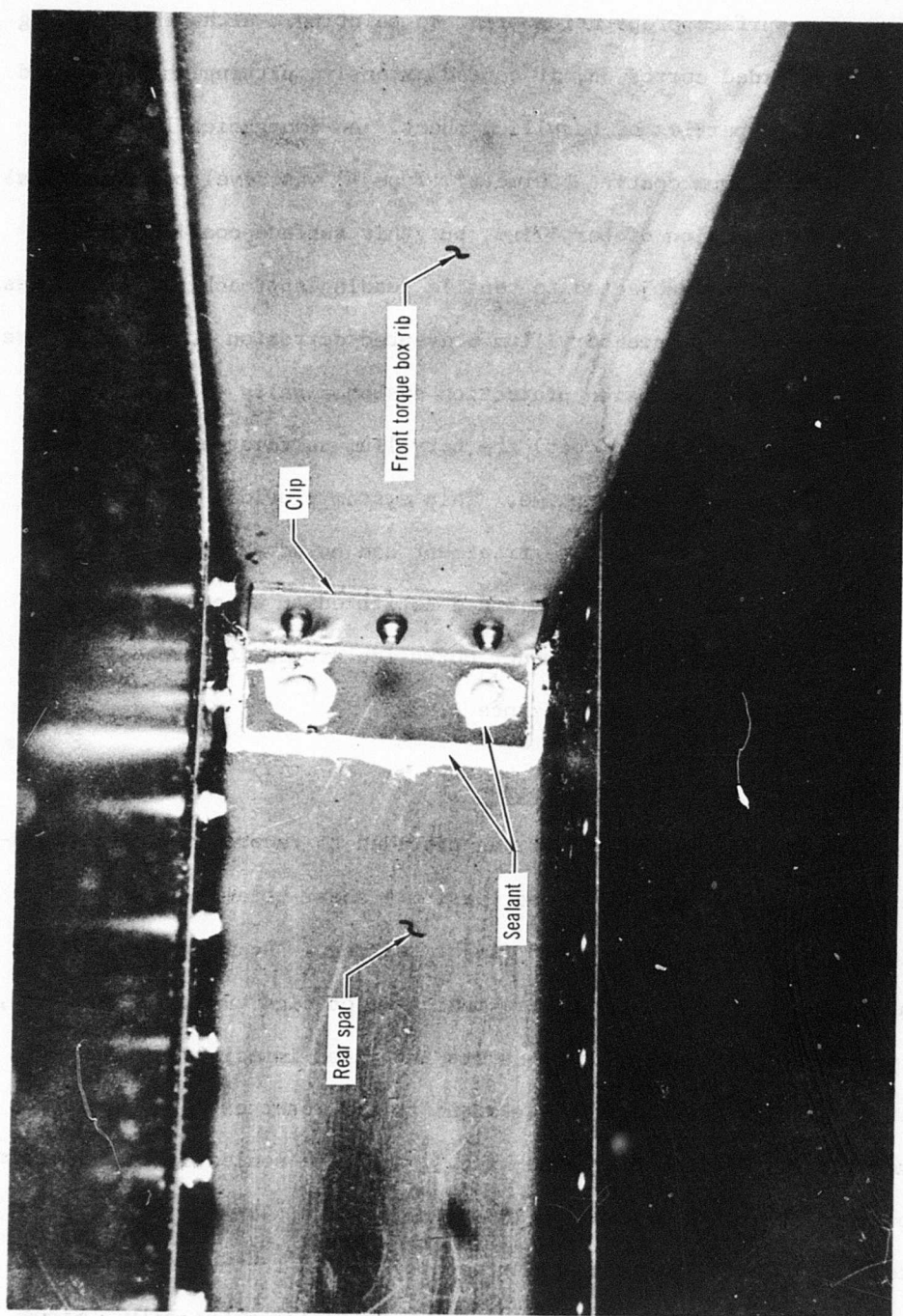


Figure 145 - Sealing of Rudder Honeycomb Assembly

beryllium as a surface preparation prior to painting. Although anodizing effectively retarded corrosion, it caused extensive pitting which reduced the mechanical properties of beryllium sheet. An inorganically (ceramically) bonded aluminum coating (Sermetal, Type W) was developed specifically for corrosion protection of beryllium, but this surface coating spalled when the specimen was subjected to tensile loading approaching yield stress. Epoxy paint applied to bare beryllium prevented corrosion but did not pass adhesion tests. The corrosion protection system finally selected was to alodine (chromate conversion coat) the beryllium surfaces and then epoxy enamel paint or zinc chromate prime. This system provided satisfactory corrosion protection; the alodine treatment had no adverse effect on the mechanical properties of beryllium and constituted an excellent surface preparation for painting. The rudder corrosion protection process is described more completely in Reference 1.

3. Flight Test Rudder Instrumentation

Instrumentation on the rudder was provided to record front spar bending strains at three locations, and torsional shear strains in the torque tube during both proof testing and flight testing. The locations of the strain gages and strain rosettes are indicated on Figure 146. In addition, a 100 percent backup system of gages was installed immediately adjacent to the gages shown. All strain gages and strain rosettes were bonded to the rudder using GA-2 cement (Budd, Inc.), and were sealed against moisture and contamination with Gagekate 5 (Micro Measurements). The 90° strain rosettes (EA-13-12TD-350 Micro Measurements) bonded to the torque tube were wired into a single bridge to record torsional strains only. Since

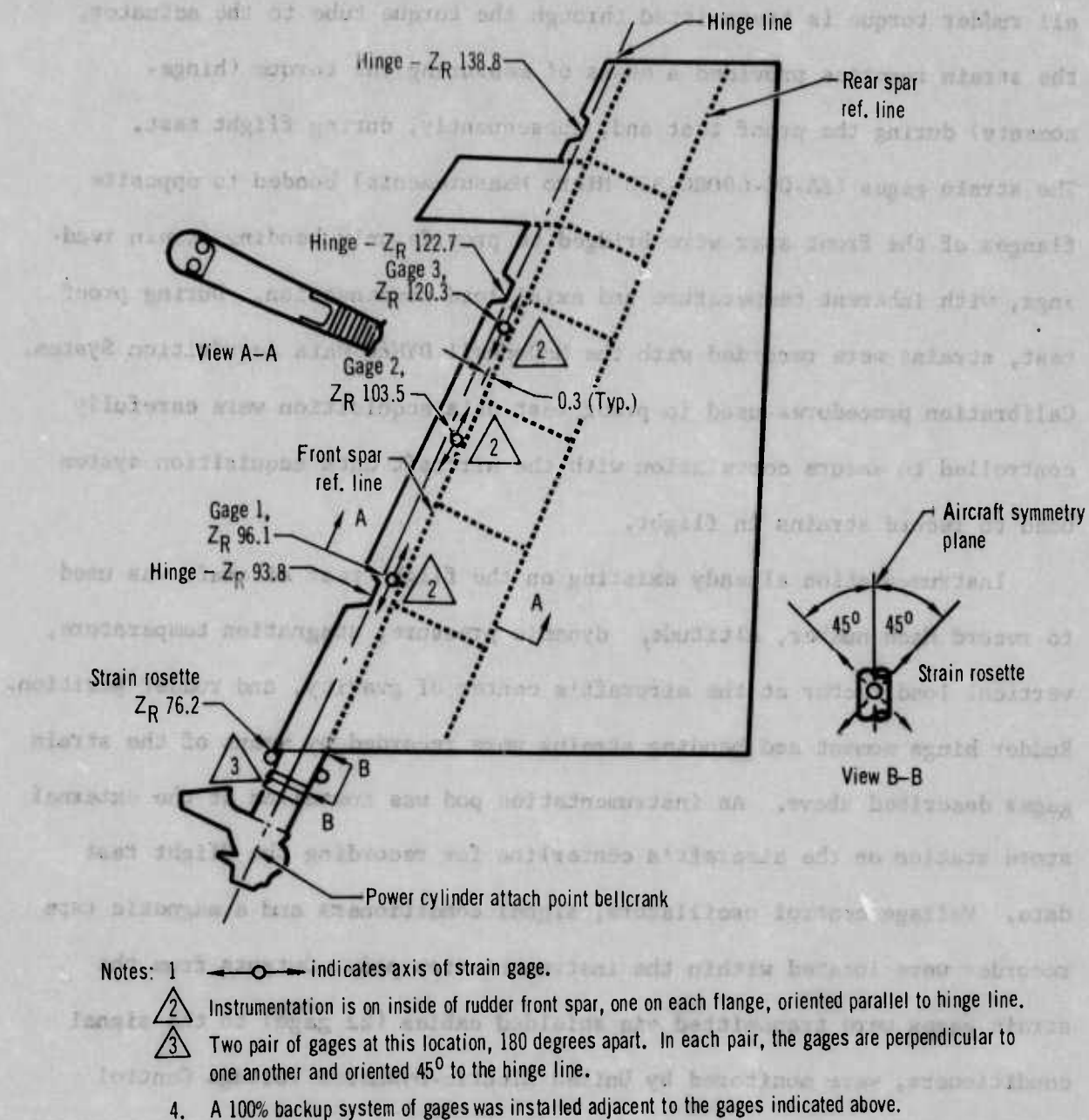


Figure 146 - Strain Gage Locations for Flight Test Rudder

all rudder torque is transmitted through the torque tube to the actuator, the strain rosettes provided a means of measuring the torque (hinge-moments) during the proof test and, subsequently, during flight test.

The strain gages (EA-06-090EG-350 Micro Measurements) bonded to opposite flanges of the front spar were bridged to provide only bending strain readings, with inherent temperature and axial load compensation. During proof test, strains were recorded with the McDonnell DYMEC Data Acquisition System. Calibration procedures used in proof test data acquisition were carefully controlled to ensure correlation with the aircraft data acquisition system used to record strains in flight.

Instrumentation already existing on the flight test aircraft was used to record Mach number, altitude, dynamic pressure, stagnation temperature, vertical load factor at the aircraft's center of gravity, and rudder position. Rudder hinge moment and bending strains were recorded by means of the strain gages described above. An instrumentation pod was installed at the external store station on the aircraft's centerline for recording the flight test data. Voltage control oscillators, signal conditioners and a magnetic tape recorder were located within the instrumentation pod. Outputs from the strain gages were transmitted via shielded cables (22 gage) to the signal conditioners, were monitored by United Electro-Dynamics Voltage Control Oscillators, and were recorded on a 14 track Parsons Model AIR 2400 magnetic tape recorder.

4. Rudder Mass Balancing

Mass balancing of the rudder is required to decouple dynamically the rudder motion from that of the fin. The procedures for the flight test

rudder reflect adjustments to give good agreement with measured inertia properties, though they are basically the same as for the ground test rudder. The equipment used to mass balance the beryllium rudders is essentially the same as used for production aluminum rudders. A description of the balancing procedure is as follows:

- (1) The lower and upper balance weights were removed from the rudder assembly, the attaching bolts were reinstalled, and the rudder was weighed.
- (2) The rudder was supported in the balance fixture as shown in Figure 147.
- (3) With the rudder hinge line in a horizontal position and the upper surface of the rudder at an angle of depression of 2.6° measured perpendicular to the rudder hinge line at W.L. 84.886, the magnitude of the rudder underbalance (tail heavy), S_B , about the rudder hinge line was measured.
- (4) With the rudder in the position specified in (3), the upperbalance weight was installed and adjusted to give an underbalance condition about the rudder hinge line of from $0.372 S_B$ to $(0.372 S_B - 2.0)$ inch-pounds.
- (5) With the rudder balanced as specified in (4), the lower balance weight was installed and adjusted to give an overbalance (nose heavy) condition about the rudder hinge line of 17.0 to 21.0 inch-pounds, (192 to 2.37 m-N).

The final balance condition was established as 17.1 in-lbs (1.34 m-N) overbalance about the hinge line. The final weights of the upper and lower

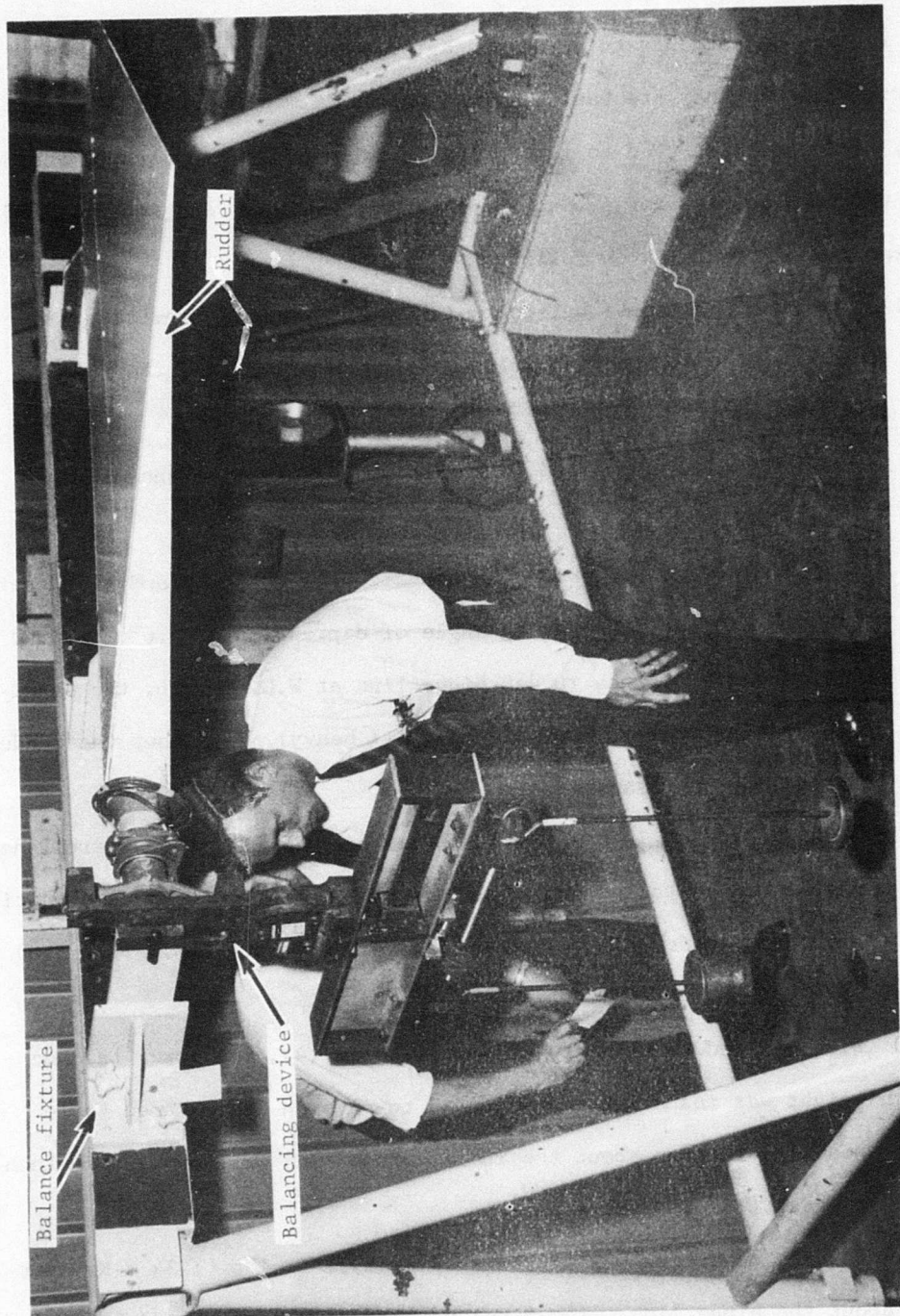


Figure 147 - Balancing the Flight Test Beryllium Rudder

balance weights are 9.96 and 7.30 lbs. (4.52 and 3.31 kgs), respectively.

5. Proof Testing the Flight Test Beryllium Rudder

The objective of this test was to verify the structural integrity of the beryllium rudder fabricated for the flight test program and to provide an in situ calibration of the strain gages to be used for recording rudder strains in flight. The structural integrity of the beryllium rudder design had been demonstrated by the static and dynamic test conducted on the ground test rudder. Though the design had proved adequate and the concept was fully qualified for flight testing within the flight test profile of the F-4 aircraft, a proof test was conducted on the flight test rudder as a safeguard against the possibility of existence of undetected damage. The proof test loads simulated the loads of Design Condition I, described in Section II, and were carried to design limit load.

The test set-up is shown on Figure 148. The rudder was installed in an F-4 vertical fin-aft fuselage assembly with the fin in a horizontal position. Rudder hinges were connected as in a normal service installation. A fixed link simulated the rudder actuator. Neoprene rudder tension pads were bonded to the rudder surface using EC1300 adhesive (Minnesota Mining and Manufacturing) for applying the test loads. The tension pads were linked through a whiffletree loading system to a hydraulic actuator. Loads were controlled manually and were measured with a calibrated strain link.

Proof test loads were applied to the rudder at a rate of 40% of design limit load per minute, in increments of 20% of design limit load, up to design limit load. Figure 149 shows a schematic of the tension pad layout and indicates maximum loads applied to the rudder during the proof test.

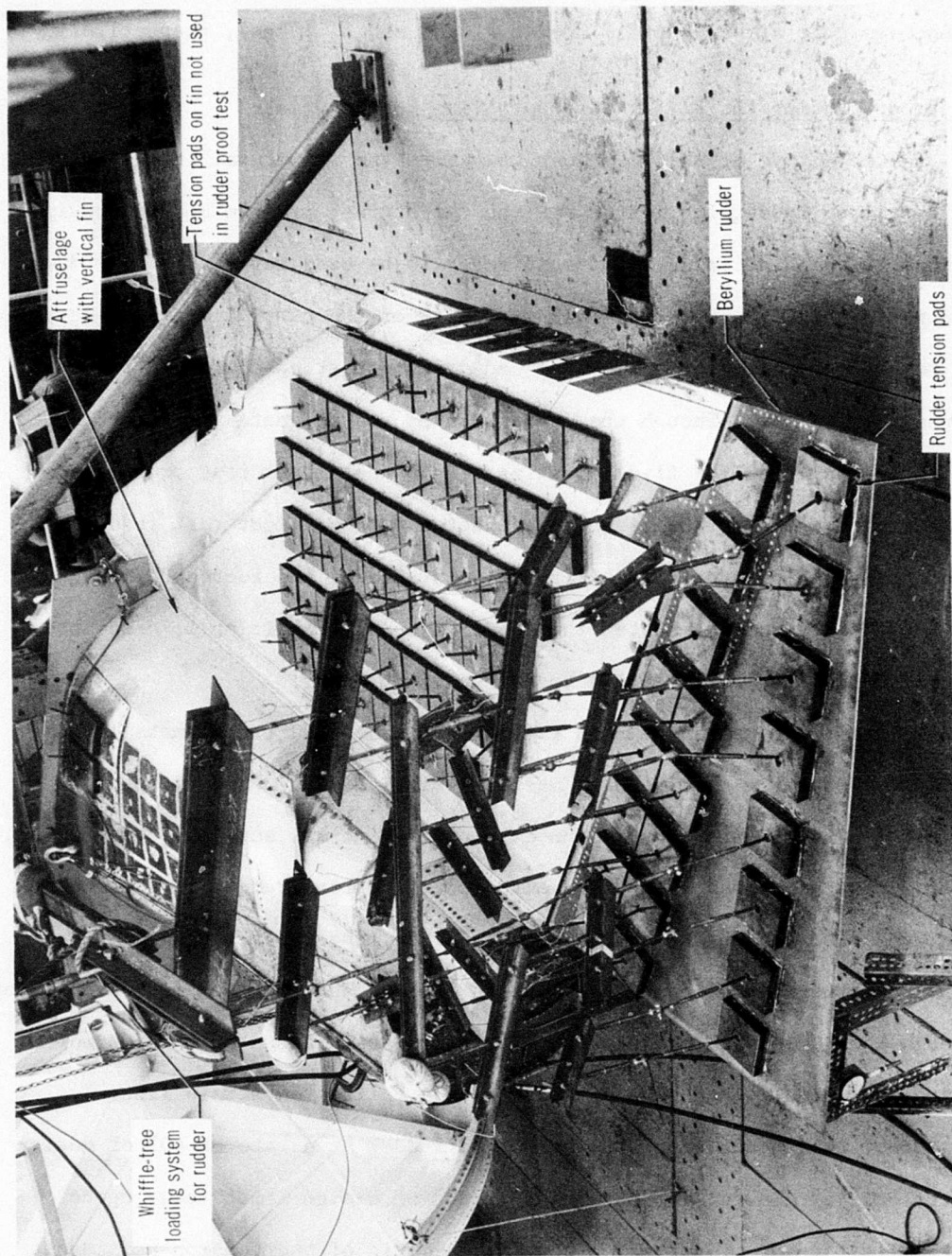
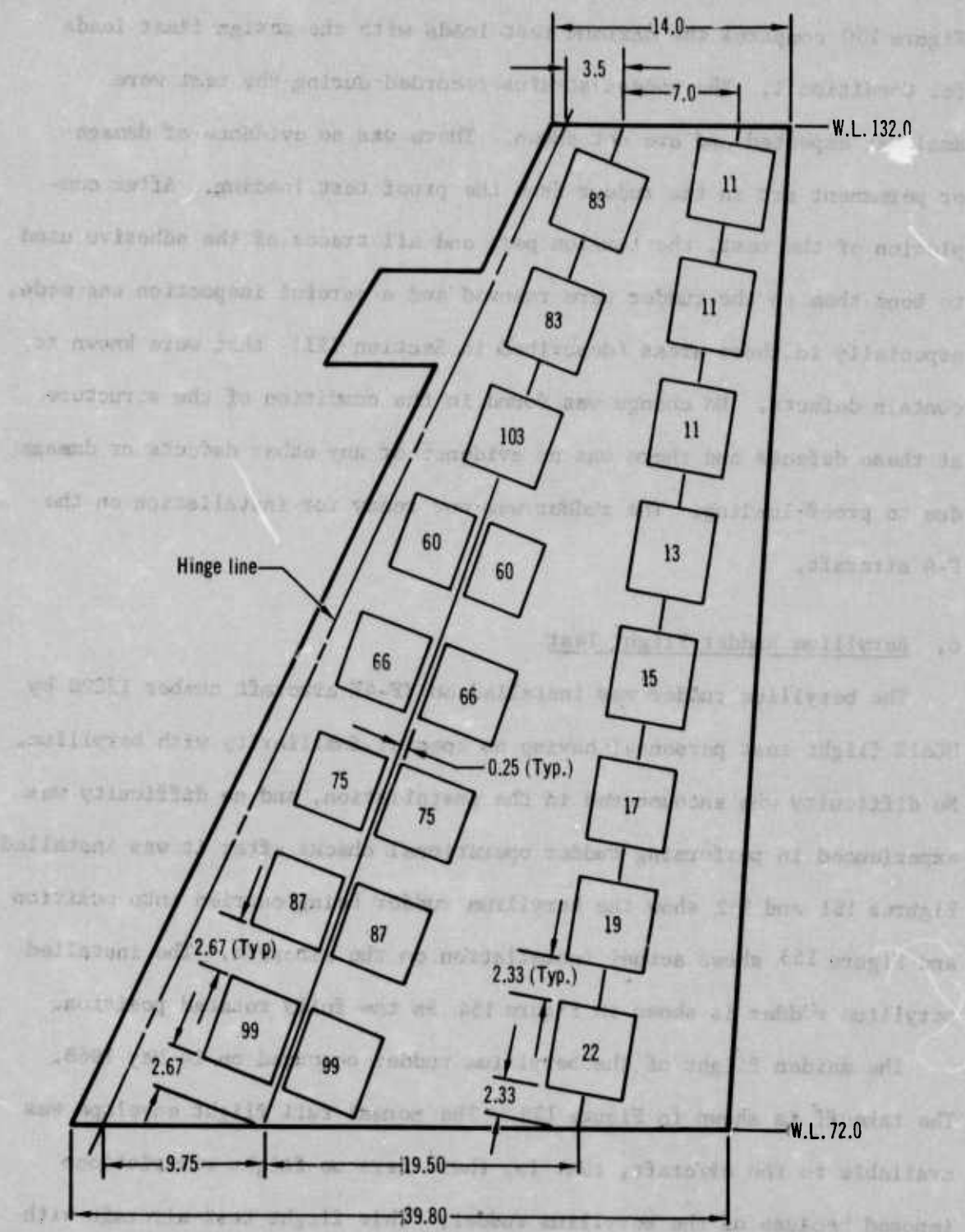


Figure 148 - Proof Test Set-Up



- Notes: 1. indicates tension pad location; numbers represent load in pounds.
 2. All tension pads were 5 inch x 5 inch except two pads with 60 lb. loads, these pads were 4 inch x 5 inch.
 3. Limit load = 1162 lb. Limit hinge moment = 9000 in.-lb. Center of pressure at 30% chord.

Figure 149 - Rudder Tension Pad Layout and Proof Test Loads

Figure 150 compares the maximum test loads with the design limit loads for Condition I. The rudder strains recorded during the test were small as expected and are not shown. There was no evidence of damage or permanent set in the rudder from the proof test loading. After completion of the test, the tension pads and all traces of the adhesive used to bond them to the rudder were removed and a careful inspection was made, especially in those areas (described in Section III) that were known to contain defects. No change was found in the condition of the structure at these defects and there was no evidence of any other defects or damage due to proof loading. The rudder was now ready for installation on the F-4 aircraft.

6. Beryllium Rudder Flight Test

The beryllium rudder was installed on YF-4E aircraft number 12200 by MCAIR flight test personnel having no special familiarity with beryllium. No difficulty was encountered in the installation, and no difficulty was experienced in performing rudder operational checks after it was installed. Figures 151 and 152 show the beryllium rudder being carried into position and Figure 153 shows actual installation on the aircraft. The installed beryllium rudder is shown in Figure 154 in the fully rotated position.

The maiden flight of the beryllium rudder occurred on 14 May 1968. The takeoff is shown in Figure 155. The normal full flight envelope was available to the aircraft, that is, there were no flight restrictions imposed because of the beryllium rudder. This flight test aircraft with the beryllium rudder installed was flown by several MCAIR test pilots as well as by Navy and Air Force pilots. All were asked to comment on

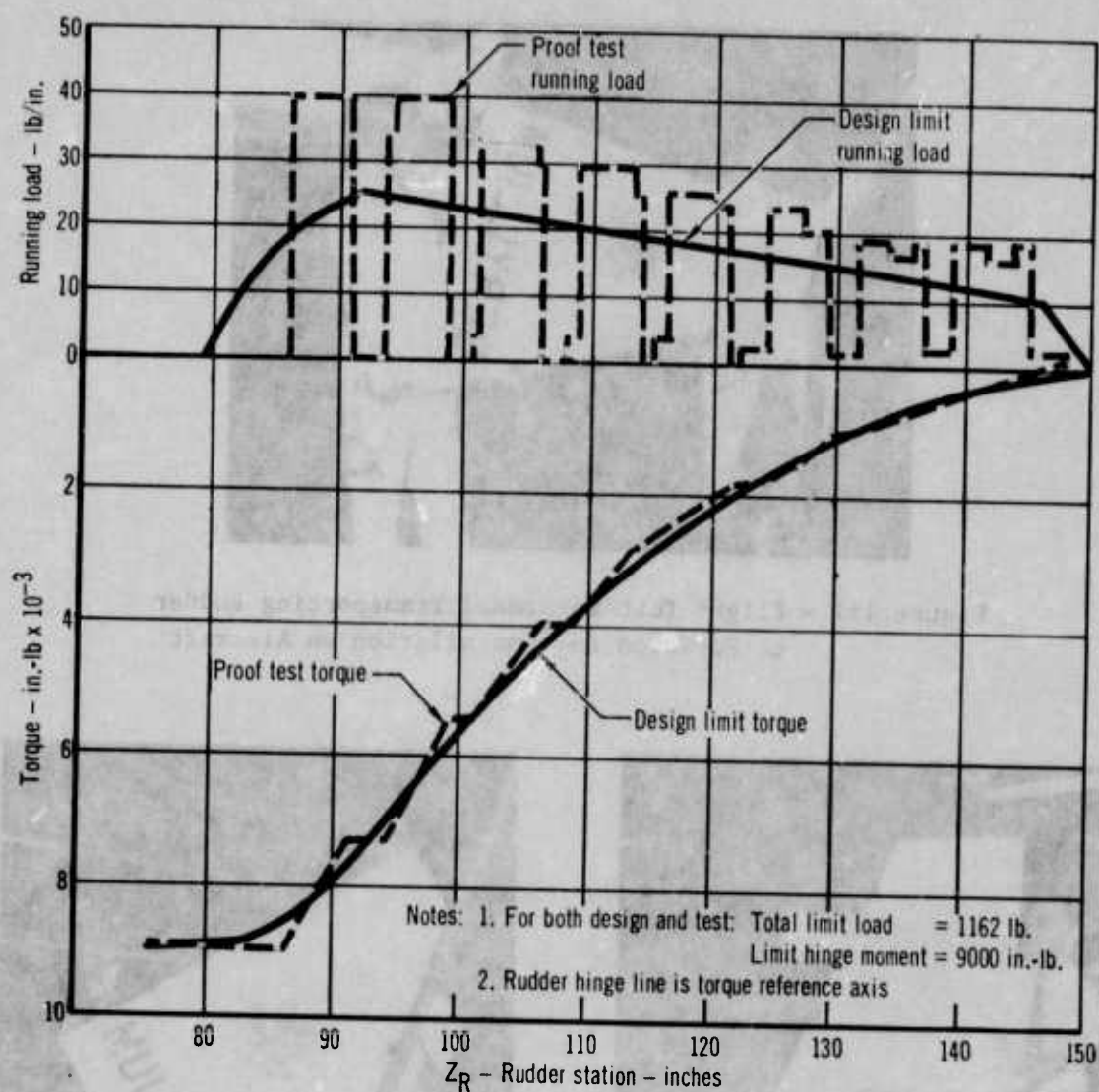


Figure 150 - Comparison of Rudder Proof Test and Design Limit Loads

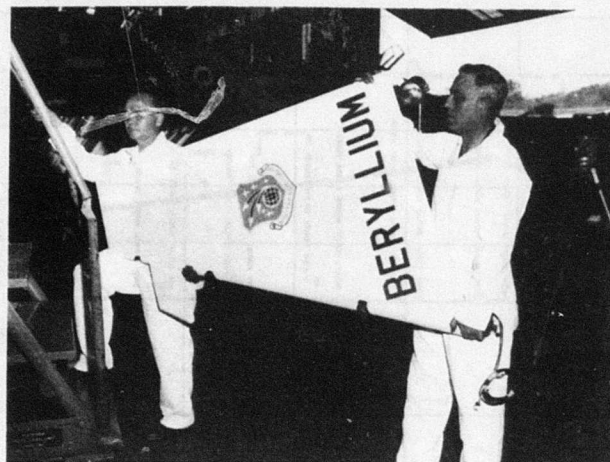


Figure 151 - Flight Test Personnel Transporting Rudder to Position for Installation on Aircraft



Figure 152 - Beryllium Rudder Enroute to Aircraft Installation



Figure 153 - Installation of Flight Test Beryllium Rudder



Figure 154 - Beryllium Rudder in Fully Rotated Position

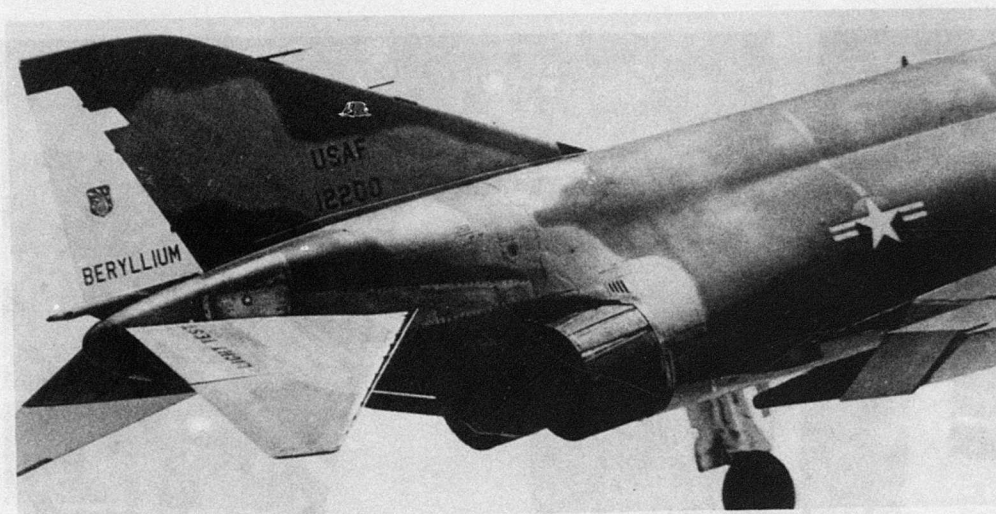
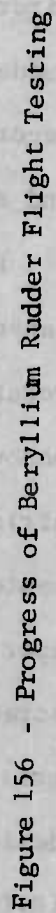


Figure 155 - Maiden Flight Take-Off of F-4 Aircraft
with Beryllium Rudder

handling performance of the aircraft. None of the pilots reported a difference in the aircraft's response with the beryllium rudder from that normally obtained with production aluminum rudder. Figure 156 is a progress chart of flight testing accomplished vs. time.

During the first several flights the aircraft was subjected to maneuvers which impose maximum loads on the rudder and flight test data was recorded to measure the structural response of the rudder. Time histories of rudder strains were recorded during the maneuvers which impose maximum rudder torsion and maximum rudder bending. These maneuvers included:

- (1) Steady yaw flight at 10,000 feet (3.05 km) at $M = .5$ and $.8$, with maximum rudder rotation, to produce full available rudder hinge moment.
- (2) Rolling pullouts at 35,000 feet (10.68 km) with $M = 1.65$ and load factors up to 5.2 g's, to produce maximum vertical fin and rudder bending loads



The steady yaw and rolling pullout maneuvers impose rudder loads corresponding to Design Conditions I and II, and Design Condition III, respectively, for which the rudder was designed and ground tested in the Reference 1 program.

Data recorded during flight testing included Mach number, altitude, dynamic pressure, stagnation temperature, vertical load factor at the aircraft's center of gravity, rudder position, rudder hinge moment, and rudder bending strains. Rudder hinge moment and bending strains were recorded by means of the strain gages described previously in this section and shown on Figure 146.

Figures 157 through 160 show the data recorded during the steady yaw maneuvers at 10,000 feet (3.05km), at $M = .5$ and $.8$ with maximum rudder rotation to produce full available rudder hinge moment. These flight maneuvers develop design limit loads of Design Conditions I and II. The airload center of pressure in flight was not determined, so the actual center of pressure could be anywhere from 30% to 45% chord. The front spar bending strains are quite small indicating that the front spar bending stresses are small. The bending strains recorded in the flight test program appear to be in agreement with the front spar strains recorded at design limit load during static test of the ground test beryllium rudder (Reference 1).

Figures 161 and 162 show the data recorded during the rolling pullout maneuvers at 35,000 feet (10.68 km), with $M = 1.65$ and load factors up to 5.2 g's, to produce maximum vertical fin and rudder bending loads. These

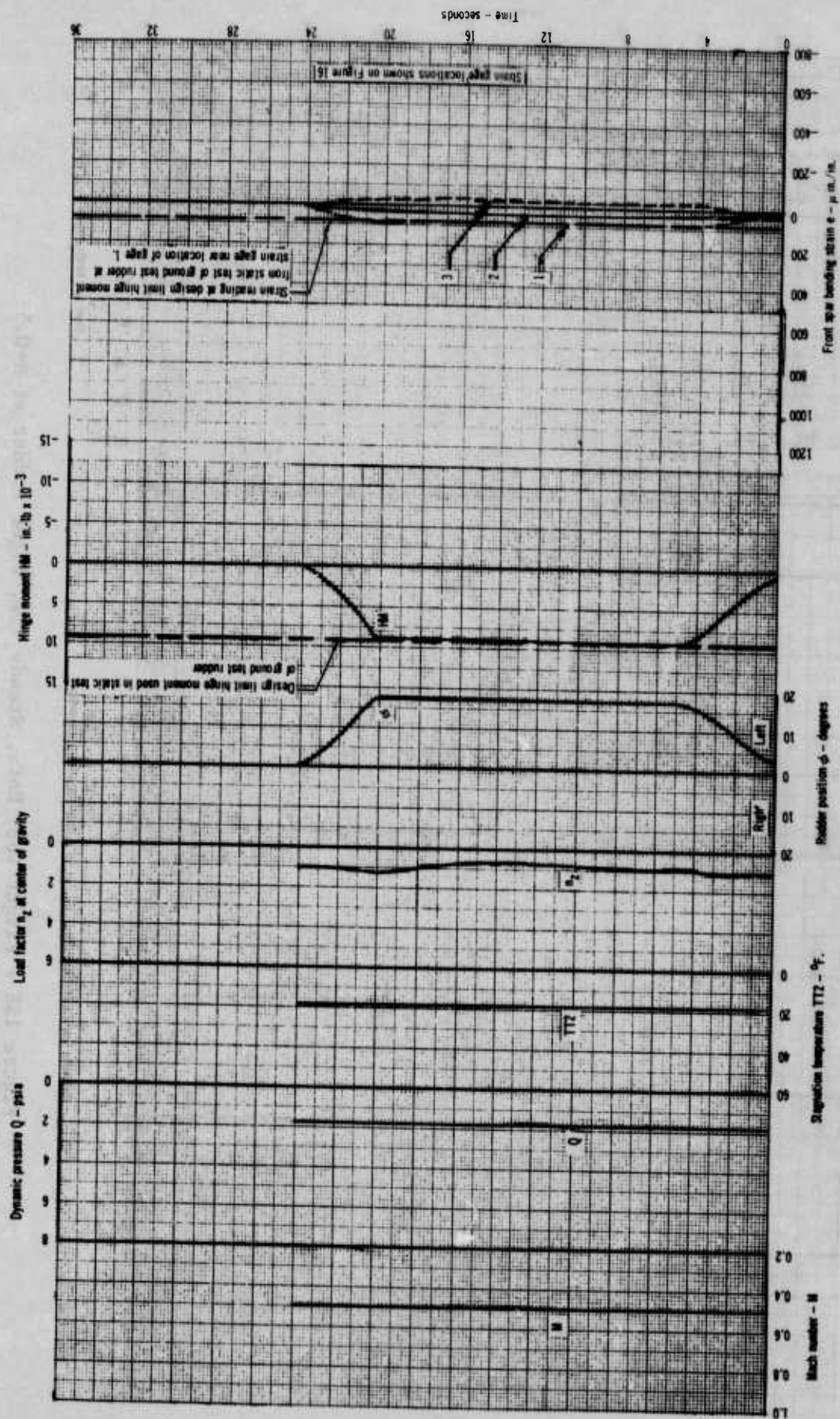


Figure 157 - Flight Test Data, Steady Yaw, Left Rudder at $M=0.5$

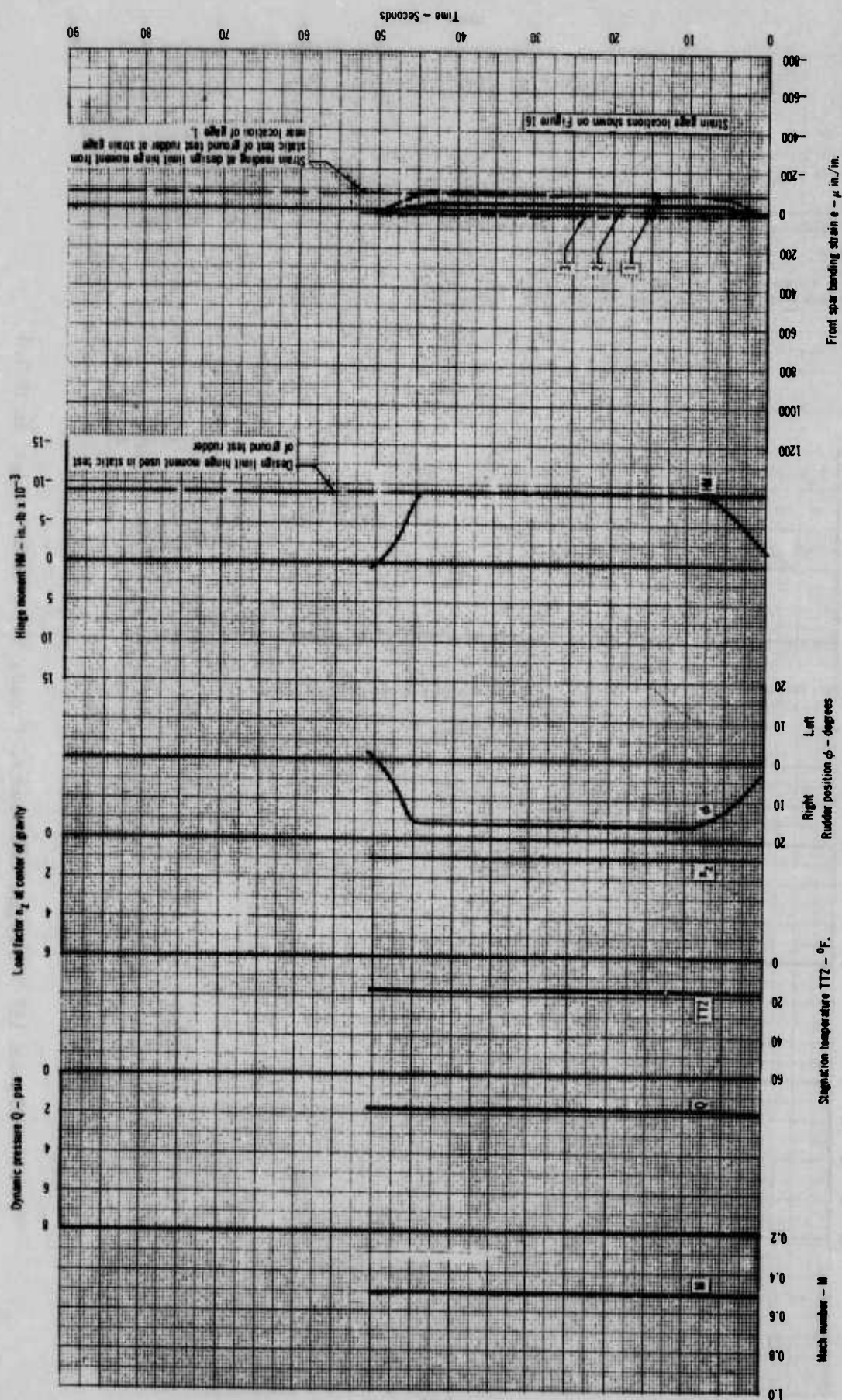


Figure 158 - Flight Test Data, Steady Yaw, Right Rudder at $M=0.5$

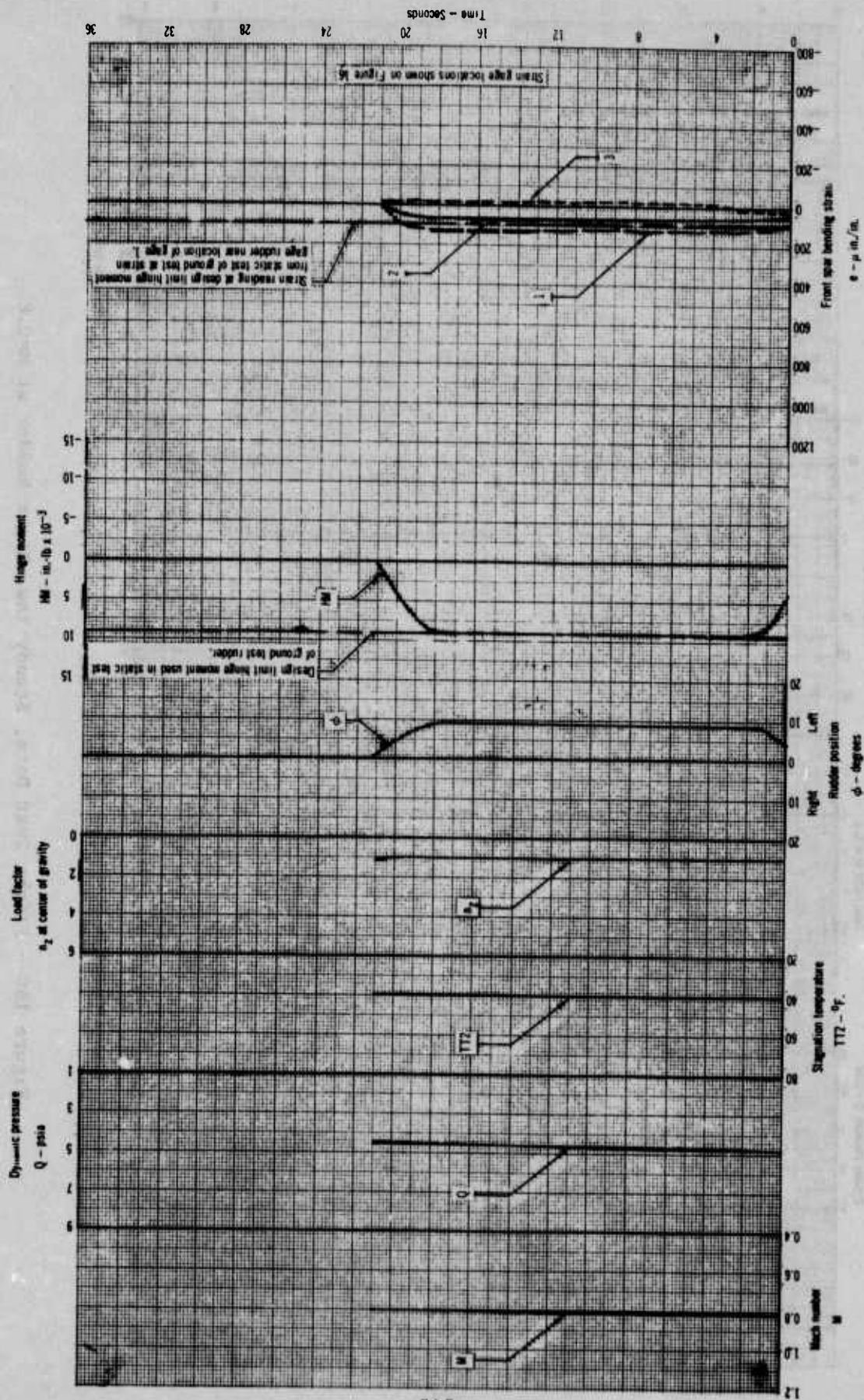


Figure 159 - Flight Test Data, Steady Yaw, Left Rudder at M=0.8

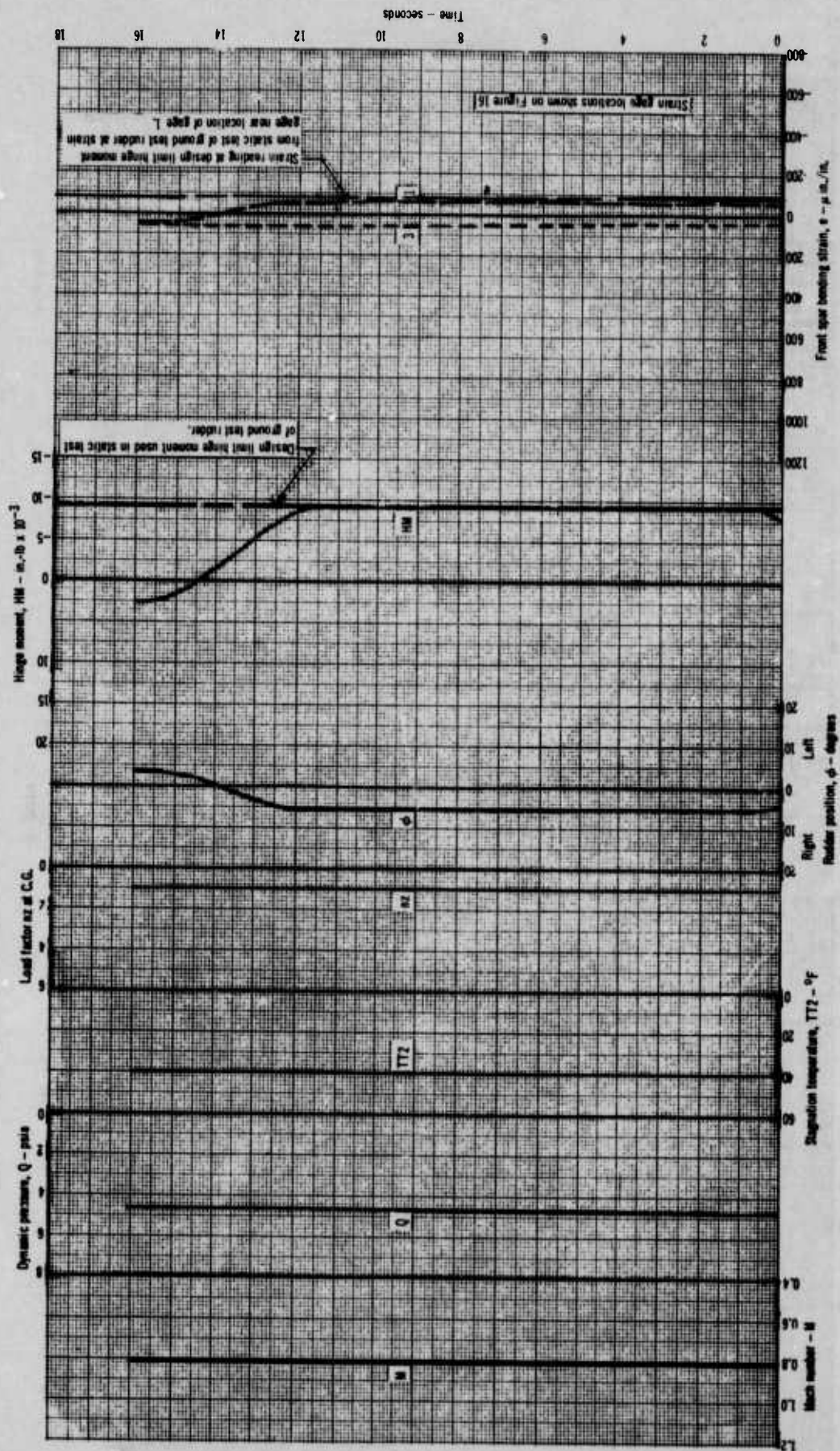


Figure 160 - Flight Test Data, Steady Yaw, Right Rudder at $M=0.8$

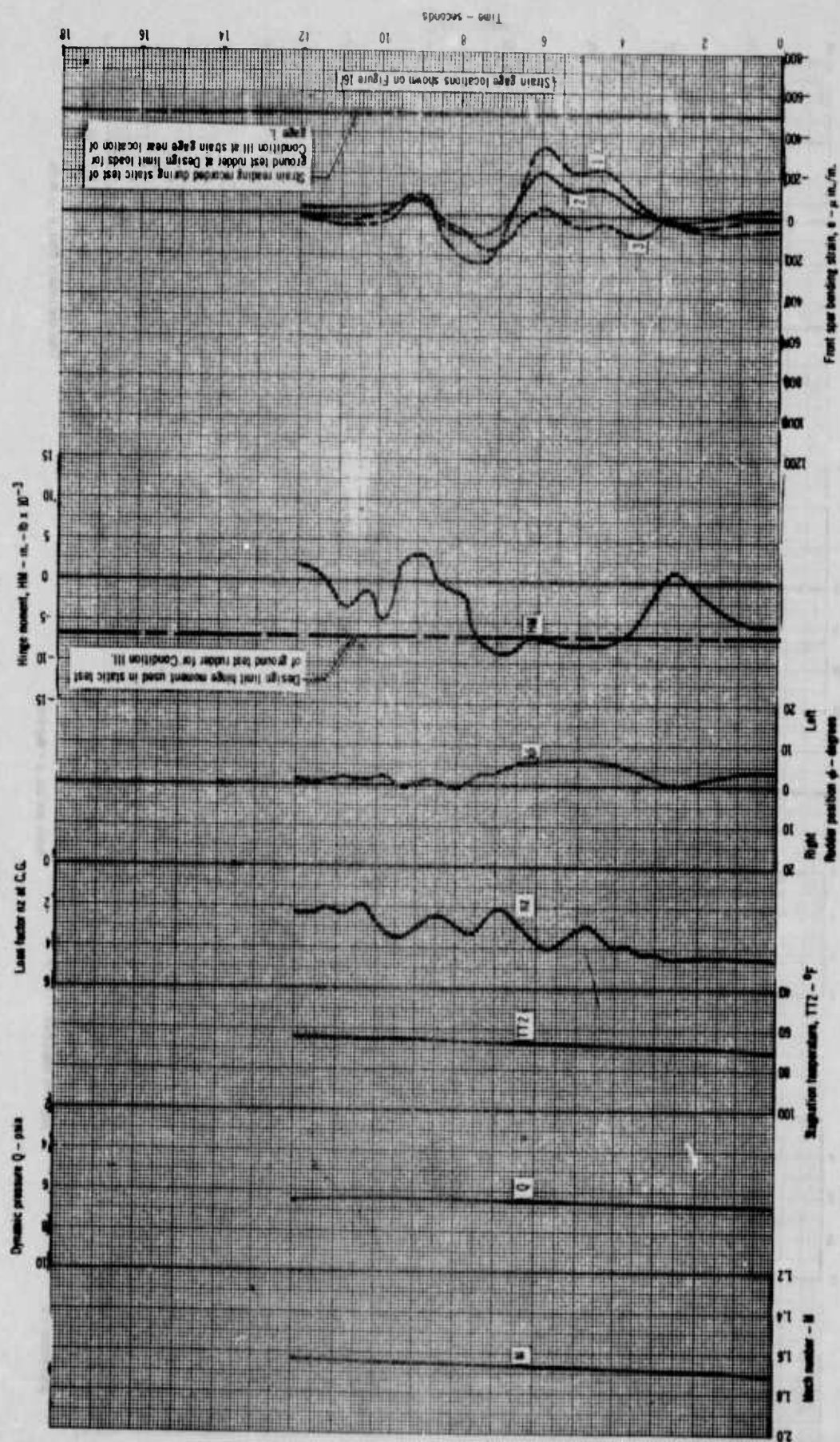


Figure 161 - Flight Test Data for Rolling Pullout

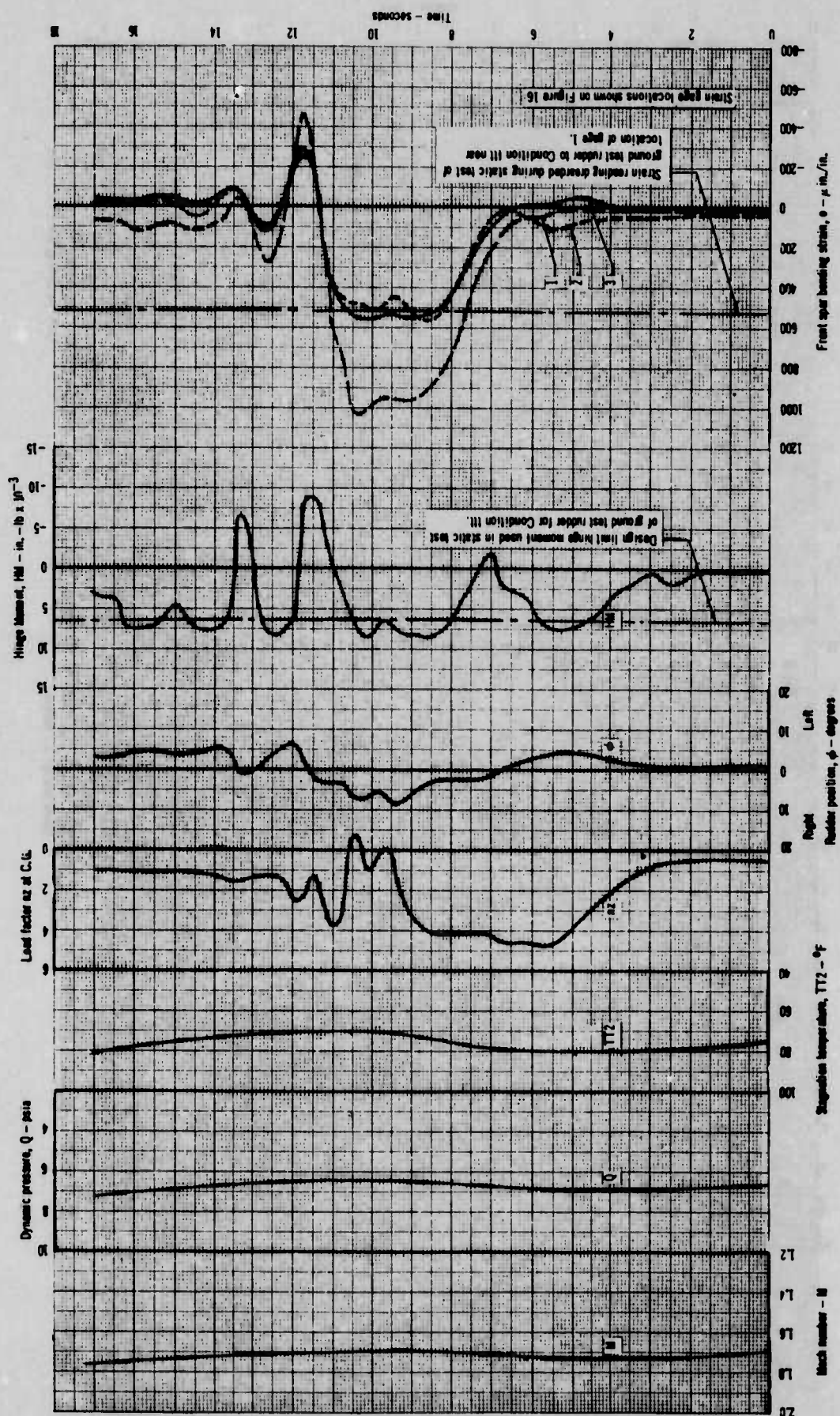


Figure 162 - Flight Test Data, 720° Roll Condition

flight maneuvers produce loads of Design Condition III. Figure 161 indicates a hinge moment or rudder torque of 7,000 to 9,000 in-lb (791 to 1002 m-N) which is slightly higher than the 6,840 in-lb (773 m-N) limit torque developed in the static test of the ground test rudder to Design Condition III. The recorded front spar bending strains on the flight test rudder are less than those recorded during static test of the ground test rudder.

The normal flight envelope of the F-4 aircraft requires a change in bank angle of less than 120° during rolling maneuvers performed with an initial vertical load factor greater than 1.0g. During the 10th flight, after approximately 10 hours of flight time had been accumulated, the aircraft became roll-yaw coupled during a rolling pullout maneuver completing a double roll before control was regained. This inadvertent 720° bank angle change occurred with an initial vertical load factor of 5.2g, exceeding the flight envelope boundaries and resulting in an overload on the fin and rudder. Figure 162 shows the data collected during this maneuver. The peak rudder hinge moment of 9000 in-lbs (1002 m-N) while greater than Design Condition III, was slightly less than the 10,260 in-lbs (1160 m-N) ultimate static test torque for the ground test rudder. The maximum front spar bending strains were significantly higher than the front spar strains recorded in the static test of the ground test rudder for Design Condition III, making it apparent that the design loads for the rudder were exceeded. This overload caused a permanent buckle to be developed in the rudder's beryllium cover skin as shown in Figure 163.

The highest strain recorded during static test for Design Condition III



Figure 163 - Permanent Buckle in Rudder Torque Box Skin

Pages - 249 250 + 251 + 252 missing

occurred on one side of the rudder more than on the other side and was more than experienced on other areas of the aircraft. It appears that on that side of the rudder there was an adhesion problem resulting in blisters forming and eventually flaking off. Figure 165 shows an area of the trailing edge honeycomb assembly having paint blisters and one of the largest areas where the paint has flaked off.

The loss of paint from the external surface of the rudder results in a significant, but not complete, loss of corrosion protection in the affected area. When the paint flakes off, the alodined beryllium surface is exposed. The alodine finish, which is applied to the beryllium prior to painting, does provide a degree of corrosion protection as indicated by the corrosion tests described in Reference 1. In those tests, the specimens were subjected to a 5% salt (NaCl) spray solution for 500 hours. The bare beryllium specimens were pitted after 12 hours and after 500 hours deep pits, blisters and exfoliation existed over the entire surface. The alodined beryllium surface was pitted after 22 hours and after 500 hours pitting had increased to about 30 active corrosion sites but no blistering or exfoliation was observed. No corrosion was observed on the specimens that were first alodined and then received the epoxy paint system. Based on these tests, it appeared that, even though the paint flaked off locally, the alodine finish would provide adequate corrosion protection for the duration of the flight test program in the environment encountered in the vicinity of St. Louis, Missouri, where the majority of flight testing was conducted. Therefore, no attempt was made to repaint areas where paint flaking occurred. No evidence of corrosion was found anywhere on the rudder

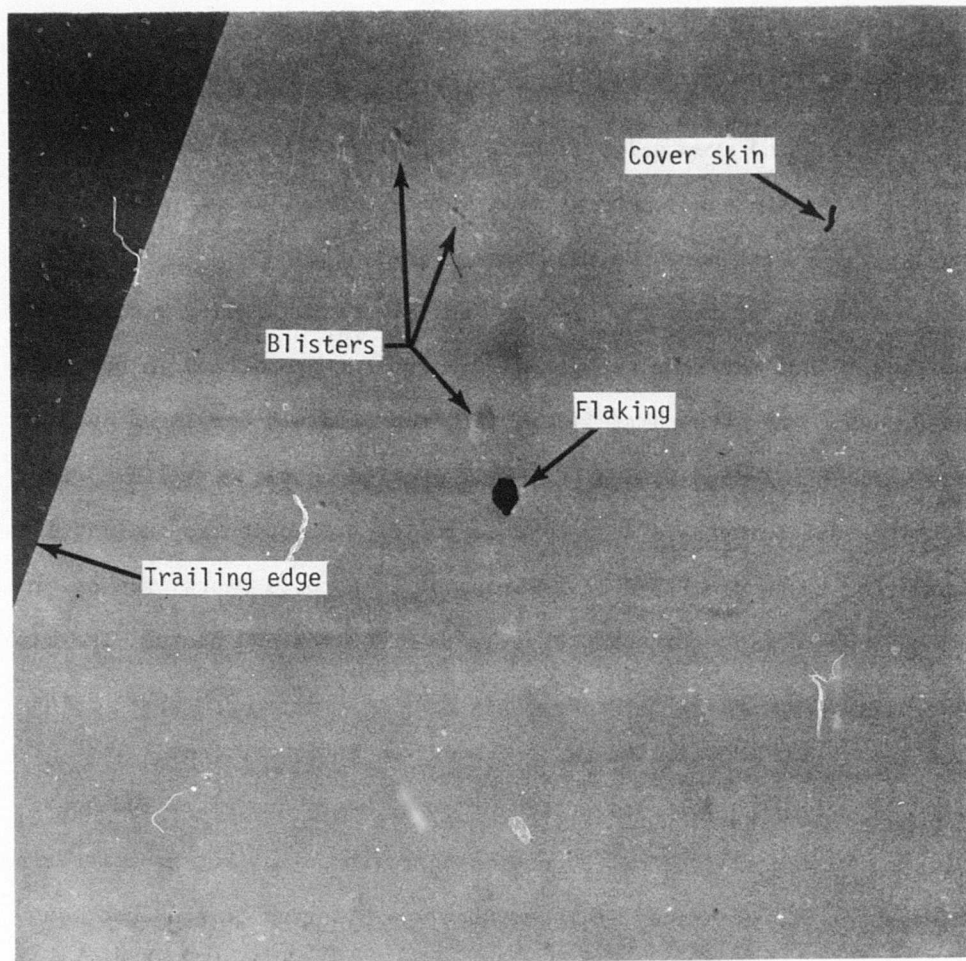


Figure 165 - Area of Trailing Edge Cover Skin Having Paint Blisters and Flaking

during the flight demonstration program. For aircraft service in a more corrosive environment, the areas where paint flaking occurs should be "touched up" periodically to ensure a corrosion free structure.

Pages 255 + 256 missing

in Section VI. A comparison of the radiographs failed to reveal indications of crack growth or other damage detrimental to the structural integrity of the beryllium rudder.

8. Summary

The flight test effort achieved its objective to demonstrate that a primary load carrying component can be fabricated of beryllium and used in a service environment. The rudder verified its structural integrity by withstanding loads in excess of ultimate, and showed its durability by its continuing maintenance-free operation.

While 184 hours and 24 minutes of flight do not constitute proof of the life expectancy of beryllium airframe components, it does show thin gage structures capable of multi-flight operations such as required by aircraft can be produced of this lightweight, high stiffness metal. Coupled with the results of the extensive ground test effort, this constitutes the single demonstration of berylliumized aircraft primary structure integrity to date which has been carried through to flight evaluation.

REFERENCES

1. Finn, J. M., Koch, L. C. and Muehlberger, D. E., AFFDL-TR-67-68, "Design, Fabrication and Ground Testing of the F-4 Beryllium Rudder", April 1967, AD 816 139.
2. Finn, J. M., Koch, L. C. and Rich, D. L., AFFDL-TR-69-74, "Fabrication, Instrumentation, Flight Test and Evaluation of an F-4 Beryllium Rudder", August 1969, AD 859 013.
3. Wolf, N. D., and van der Heyde, R. C. W., AFFDL Report Nr: FDD-A-5-68, "Test Report on Acoustic Fatigue Endurance Tests of the McDonnell-Douglas F-4 Beryllium Rudder", 14 June 1968.
4. Kolb, A. W., and Magrath, H. A., "RTD Sonic Fatigue Facility, Design and Performance Characteristics", The Shock and Vibration Bulletin, Number 37 - Supplement, January 1968, Page 17.
5. Holloway, J. A., AF Materials Laboratory Technical Memorandum TM-MAM-68-16, "Radiographic Inspection of the F-4 Beryllium Rudder", December 1968.
6. Richardson, M. D., AFFDL Report Nr: FDTT-69-3, "Test Report on Structural Test - F-4 Beryllium Rudder", 1 October 1969.
7. Barnett, F. E., "F-4 Beryllium Rudders", Technical Paper W70-12.4, ASM/SME 1970 Western Metal and Tool Conference and Exposition, 9-12 March 1970.
8. McClung, R.W., "Techniques for Low Voltage Radiography", ORNL 3252, Oak Ridge National Laboratory, Oak Ridge, Tennessee, March 1962.

Pages 259 + 260 missing

APPENDIX A

MCDONNELL MATERIAL SPECIFICATION 191 REVISION B

FOR BERYLLIUM SHEET AND PLATE

1.0 SCOPE

- 1.1 This specification covers the chemical and mechanical properties of one type of beryllium metal for use in aerospace parts where a high strength-to-weight ratio and high modulus of elasticity are required.

2.0 APPLICABLE DOCUMENTS

- 2.1 The following documents of the issue in effect on the date of invitation for bids, form a part of this specification to the extent specified herein.

Federal Test Method Std. 151 - Metals; Test Method
MIL-STD-10 - Surface Roughness, Waviness and Lay
MAC P.S. 21202 - Penetrant Inspection

3.0 REQUIREMENTS

- 3.1 MATERIAL AND WORKMANSHIP - Material shall be uniform in quality and condition, clean, sound and free from foreign materials and from internal and external defects detrimental to fabrication or performance of parts.
- 3.1.1 The extent of surface defects shall be determined by the use of penetrant inspection per MAC P.S. 21202.
- 3.2 CONDITION - Unless otherwise specified, the material shall be supplied in the cross rolled, stress relieved, ground and pickled condition. Surface finish shall be 56 roughness height rating or finer.
- 3.2.1 The density of the product shall be not less than 0.066 pounds per cubic inch.
- 3.3 COMPOSITION - The chemical composition of the material in percent by weight shall be as follows:

Beryllium Oxide	2.0 Max.
Iron	0.20 Max.
Aluminum	0.20 Max.
Carbon	0.15 Max.
Silicon	0.12 Max.
Magnesium	0.08 Max.
Other Impurities, each	0.04 Max.
Beryllium	98.00 Min.

- 3.4 ULTRASONIC INSPECTION All plate (0.250" and over) supplied to this specification shall be ultrasonically inspected, using the immersion method. A UW Reflectoscope transducer containing a beam reducer on the probe shall be utilized. Unless otherwise specified, a frequency of 10 megacycles shall be used. The criteria for acceptance or rejection shall be agreed upon between the producer and purchaser.

3.5 MECHANICAL PROPERTIES

- 3.5.1 Room Temperature Properties - The room temperature tensile properties of the material tested in any direction, using a strain rate of 0.003 - 0.007 inch per inch per minute to failure shall conform to the following requirements.

THICKNESS RANGE (INCHES)	MINIMUM TENSILE STRENGTH (PSI)	MINIMUM YIELD STRENGTH @.2% OFFSET (PSI)	MINIMUM ELONGATION (% IN 1")
Under 0.250	70,000	50,000	5.0
Over 0.250 to 0.375	65,000	45,000	4.0
Over 0.375 to 0.500	60,000	40,000	3.0

3.5.2 Elevated Temperature Tensile Properties

- 3.5.2.1 Mechanical properties at elevated temperature shall be negotiated and as agreed upon between the producer and purchaser.

- 3.6 TOLERANCES - Unless otherwise specified, tolerances shall conform to the following:

3.6.1 Sheet

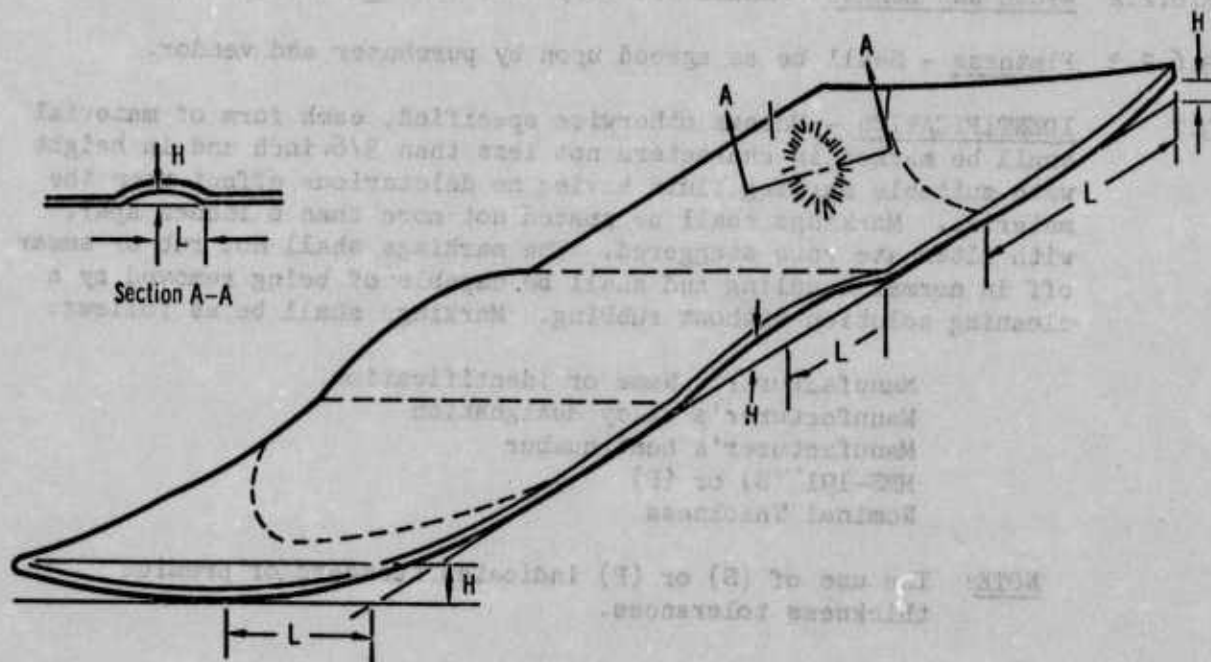
3.6.1.1 Sheet Thickness

NOMINAL THICKNESS (INCHES)	TOLERANCES (INCHES)			
	STANDARD		PREMIUM	
	PLUS	MINUS	PLUS	MINUS
0.020 to 0.025, incl.	0.003	0.003	0.002	0.002
Over 0.025 to 0.034, incl.	0.004	0.004	0.002	0.002
Over 0.034 to 0.056, incl.	0.005	0.005	0.003	0.003
Over 0.056 to 0.070, incl.	0.006	0.006	0.003	0.003
Over 0.070 to 0.078, incl.	0.007	0.007	0.004	0.004
Over 0.078 to 0.093, incl.	0.008	0.008	0.004	0.004
Over 0.093 to 0.109, incl.	0.009	0.009	0.005	0.005
Over 0.109 to 0.125, incl.	0.010	0.010	0.005	0.005
Over 0.125 to 0.140, incl.	0.012	0.010	0.006	0.005
Over 0.140 to 0.171, incl.	0.014	0.010	0.007	0.005
Over 0.171 to 0.249, incl.	0.015	0.010	0.007	0.005

- 3.6.1.2 Width - Shall not vary more than plus 0.125, minus 0.000 inch.

- 3.6.1.3 Length - Shall not vary not more than plus 0.250, minus 0.000 inch.
- 3.6.1.4 Straightness - Maximum edgewise curvature (depth of arc) shall not exceed 1/16 inch in any foot of length.
- 3.6.1.5 Flatness - Shall not vary more than the following when measured and calculated as shown in the figure which follows:

<u>THICKNESS (INCHES)</u>	<u>FLATNESS</u>	
	<u>STANDARD</u>	<u>PREMIUM</u>
Under 0.035	3.0%	2.0%
Over 0.035	2.0%	1.0%



H = Maximum distance between flat surface and lower surface of sheet

L = Minimum distance between highest point on sheet and point of contact with flat surface

Line of tangency between sheet and flat surface

$H/L \times 100 = \% \text{ flatness deviation}$

Method of Determining Percent Flatness Deviation

3.6.2 Plate

3.6.2.1 Plate Thickness

<u>NOMINAL THICKNESS (T)</u> (INCHES)	<u>TOLERANCES</u>	
	PLUS	MINUS
0.250 to 0.3125, incl.	0.113T	0.010
Over 0.3125 to 0.375, incl.	0.094T	0.010
Over 0.375 to 0.4375, incl.	0.080T	0.010
Over 0.4375 to 0.500, incl.	0.075T	0.010
Over 0.500 to 0.625, incl.	0.063T	0.010
Over 0.625 to 0.750, incl.	0.057T	0.010
Over 0.750	0.050T	0.010

3.6.2.2 Width and Length - Shall not vary more than \pm 0.125 inch.

3.6.2.3 Flatness - Shall be as agreed upon by purchaser and vendor.

3.7 IDENTIFICATION - Unless otherwise specified, each form of material shall be marked in characters not less than 3/8 inch and in height with suitable marking fluid having no deleterious effect upon the material. Markings shall be spaced not more than 6 inches apart with alternate rows staggered. The markings shall not rub or smear off in normal handling and shall be capable of being removed by a cleaning solution without rubbing. Markings shall be as follows:

Manufacturer's Name or identification
Manufacturer's alloy designation
Manufacturer's heat number
MMS-191 (S) or (P)
Nominal Thickness

NOTE: The use of (S) or (P) indicates standard or premium thickness tolerances.

4.0 QUALITY ASSURANCE PROVISIONS

4.1 Test coupons shall not be removed from the final product for material qualification tests unless specified on the purchase order for the material.

4.1.1 Inspection Performance - When authorized on the purchase order, compliance with this specification shall be checked by the MAC Quality Assurance Department and only those tests specified on the purchase order shall be accomplished. No other destructive tests shall be initiated without specified approval of the Project Strength Engineer.

4.2 SAMPLING, INSPECTION, AND TESTS - Sampling, inspection, and tests shall be in accordance with Federal Test Method Standard 151.

4.3 VENDOR REPORTS - Unless otherwise specified, the Vendor of the product shall furnish with each shipment three (3) copies of a report of the results of tests on each thickness or size from each powder batch. The report shall include results of a chemical analysis, room temperature, and elevated temperature tensile tests (if required), as well as purchase order number, heat number, material specification number, thickness, size, and quantity from each powder batch.

4.3.1 Unless otherwise specified, the Vendor of finished or semi-finished parts shall furnish with each shipment three copies of a report showing the purchase order number, material specification number, contractor or other direct supplier of the material, part number, and quantity.

4.4 REJECTION - Material not conforming to this specification or to authorized modification will be subject to rejection.

5.0 PREPARATION FOR DELIVERY

5.1 PACKAGING AND PACKING - Unless otherwise specified on the procurement document, all material shall be separated by condition, size, and thickness and packed in crates or boxes or size and construction commonly used for shipment. The crating or boxing shall be such as to insure acceptance by common or other carriers for safe transportation, at the lowest rate, to the point of delivery.

6.0 NOTES

6.1 INTENDED USE - The material covered by this specification is intended for use in the fabrication of aerospace parts where a high strength-to-weight ratio and high modulus of elasticity are required.

6.2 ORDERING DATA - Procurement documents should specify the following:

- (a) Number, title, and date of specification.
- (b) Condition of material (see 3.2).
- (c) Tolerances, standard or premium as specified in 3.6.1.1 and 3.6.1.5.
- (d) Elevated temperature tensile tests by the Vendor, if required (see 3.5.2).
- (e) Identification, if other than as specified in 3.7.
- (f) Packaging and packing, if other than as specified in 5.1
- (g) Inspection, if any, to be accomplished by the MAC Quality Assurance Department upon receipt of the shipment. (Reference Paragraphs 3.5.1 and 3.5.2.) Inspection operations to be required at MAC shall be indicated on the APL and on the purchase order for the material.

- 6.3 Vendors or subcontractors needing this specification should direct their request for copies to the attention of MAC Purchasing or Subcontracting, as applicable. Information pertaining to the technical aspects of this specification can be obtained from MAC Material and Process Development (Dept. 272).

7.0 APPROVED PRODUCTS

Not applicable

TABLE A-1
CHEMICAL ANALYSIS OF BERYLLIUM SHEET
FOR GROUND TEST RUDDER (Reference 1)

Lot No.	Be (%)	BeO (%)	Fe (%)	Si (%)	Al (%)	Mg (%)	C (%)	Other (%)
2452	98.50	1.70	0.120	0.030	0.090	0.020	0.130	< 0.04
2938	98.60	1.69	0.140	0.040	0.090	0.010	0.100	< 0.04
3516	98.21	1.70	0.140	0.040	0.110	0.008	0.130	< 0.04
3379	98.68	1.77	0.120	0.040	0.110	0.020	0.130	< 0.04
3422	98.59	1.90	0.150	0.050	0.130	0.020	0.130	< 0.04
3318	98.57	1.57	0.160	0.040	0.100	0.010	0.110	< 0.04
3890	98.30	1.93	0.130	0.020	0.090	0.020	0.100	< 0.04
3900	98.30	2.00	0.130	0.030	0.100	0.020	0.130	< 0.04
3939	98.30	1.68	0.120	0.030	0.090	0.020	0.120	< 0.04
3957	98.30	1.94	0.130	0.030	0.100	0.020	0.100	< 0.04
013J	98.30	2.00	0.073	0.076	0.066	0.031	0.063	< 0.04
109H	98.38	1.73	0.168	0.052	0.050	0.008	0.106	< 0.04
804H	98.46	1.49	0.092	0.056	0.070	0.008	0.100	< 0.04
H349	98.17	1.99	0.095	0.069	0.068	0.062	0.131	< 0.04
MMS-191 (2)	98.00 (min.)	2.00 (max.)	0.200 (max.)	0.120 (max.)	0.200 (max.)	0.080 (max.)	0.150 (max.)	0.04 (max.)

Notes:

1. Hot rolled, stress relieved, ground and etched beryllium sheet.
- (2) Required per McDonnell Material Specification MMS-191.

Table A-2 - Chemical Analysis of Beryllium Sheet
FOR FLIGHT TEST RUDDER (Reference 2)

Lot No.	Be (%)	BeO (%)	Fe (%)	Si (%)	Al (%)	Mg (%)	C (%)	Other (%)
993J	98.40	1.75	0.080	0.050	0.042	0.025	0.092	< 0.04
629J	98.35	1.85	0.120	0.080	0.090	0.006	0.114	< 0.04
4477	98.10	1.80	0.130	0.030	0.060	0.007	0.120	< 0.04
4367	98.60	1.70	0.130	0.030	0.090	0.009	0.110	< 0.04
088K	98.50	1.51	0.122	0.080	0.065	0.079	0.074	< 0.04
4785	98.40	1.60	0.110	0.030	0.070	0.030	0.090	< 0.04
804H	98.46	1.49	0.092	0.056	0.070	0.008	0.100	< 0.04
670H	98.17	1.99	0.095	0.069	0.068	0.062	0.131	< 0.04
MMS-191 (2)	98.00 (min.)	2.00 (max.)	0.200 (max.)	0.120 (max.)	0.200 (max.)	0.080 (max.)	0.150 (max.)	< 0.04 (max.)

Notes:

1. Hot rolled, stress relieved, ground and etched beryllium sheet.
- (2) Required per McDonnell Material Specification MMS-191.

TABLE A-3
PROPERTIES OF BERYLLIUM SHEET USED FOR
ELEMENT TEST SPECIMENS AND GROUND TEST RUDDER
(Reference 1)

Sheet No.	Lot or Heat	Longitudinal			Transverse		
		F _{tu} (ksi)	F _{ty} (ksi)	e (%)	F _{tu} (ksi)	F _{ty} (ksi)	e (%)
996B	2452	77.2	51.2	27.0	75.3	51.8	20.0
1026A	2938	79.2	54.6	14.0	70.8	55.4	5.0
1026B	2938	79.2	54.6	14.0	70.8	55.4	5.0
1072B	3516	84.2	60.2	15.0	82.2	60.1	18.0
1040A	3379	83.2	58.9	27.5	81.9	56.5	21.0
1048B1	3379	81.6	57.0	22.5	77.7	55.6	29.0
1062B	3422	79.4	59.7	15.0	75.2	58.1	11.0
1053A	3422	79.2	55.1	28.0	78.6	56.5	21.0
1034B	3318	78.5	52.5	19.0	79.4	56.5	27.0
1187C	3890	83.0	60.5	20.0	80.8	61.2	17.0
1197A	3900	74.2	52.3	11.0	76.9	60.7	17.0
1210A2	3939	87.1	64.4	17.0	85.1	60.6	15.0
1211A2	3939	84.0	60.1	17.0	77.1	55.6	6.0
1219A	3957	84.0	58.2	24.0	80.2	58.4	19.0
HR385	013J	74.5	51.0	24.0	72.4	52.1	19.0
HR228-1	109H	74.4	57.3	25.0	73.5	58.5	27.0
HR380	804H	81.5	55.1	22.0	75.4	55.4	14.0
HR382	804H	83.8	58.7	24.0	84.9	60.1	19.0
H-349	-	76.0	53.2	24.0	-	-	-

TABLE A-4
PRODUCERS CERTIFIED MECHANICAL PROPERTIES OF
BERYLLIUM SHEET USED FOR FLIGHT TEST RUDDER
(Reference 2)

Sheet No.	Lot or Heat	Longitudinal			Transverse		
		F _{tu} (ksi)	F _{ty} (ksi)	e (%)	F _{tu} (ksi)	F _{ty} (ksi)	e (%)
HR-521	993J	77.3	57.1	23.0	78.5	58.4	32.0
HR-427	629J	80.7	56.1	17.0	77.6	55.9	10.0
1440A	4477	85.1	67.0	19.0	81.6	67.5	27.0
1363	4367	84.2	57.6	18.5	77.5	55.6	14.5
HR-538	088K	80.3	57.3	26.0	75.5	51.1	15.0
1504A	4785	86.1	64.7	18.0	82.8	63.7	16.0
HR382	804H	83.8	58.7	24.0	84.9	60.1	19.0
HR348	670H	85.9	59.9	29.0	78.5	59.0	17.0

Note:

1. Hot rolled, stress relieved, ground and etched beryllium sheet.

APPENDIX B

DETAIL DRAWINGS

Composite Section Drawing

No. 404-005, "Rudder Composite Section" (3 sheets)

Beryllium Rudder Drawings

No. 404-100, "Rudder Installation Beryllium Rudder"

No. 404-101, "Rudder Assembly"

No. 404-102, "Structure Assembly Beryllium Rudder"

No. 404-103, "Trailing Section Assembly - Rudder Honeycomb (2 sheets)"

No. 404-104, "Forward Spar Assembly"

No. 404-105, "Fitting - Rudder Torque Tube Upper"

No. 404-106, "Hinge - Rudder"

No. 404-107, "Rib Assembly Rudder Upper Balance Weight"

No. 404-108, "Rib Assembly"

No. 404-109, "Rib Assembly"

No. 404-110, "Ribs - Rudder Assembly"

No. 404-111, "Ribs - Rudder Assembly"

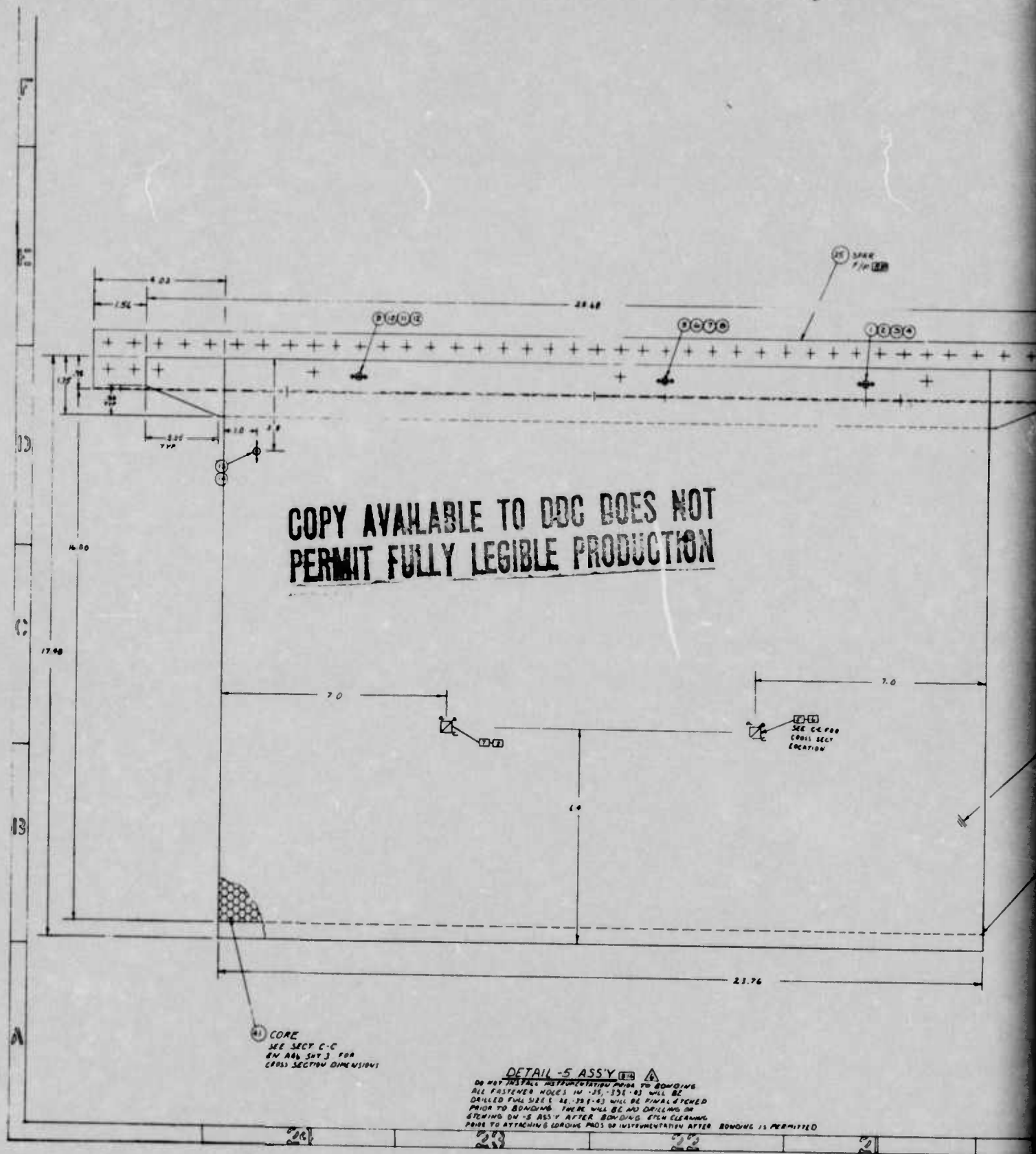
No. 404-112, "Ribs - Rudder Assembly"

No. 404-113, "Skins - Torque Box Upper & Lower"

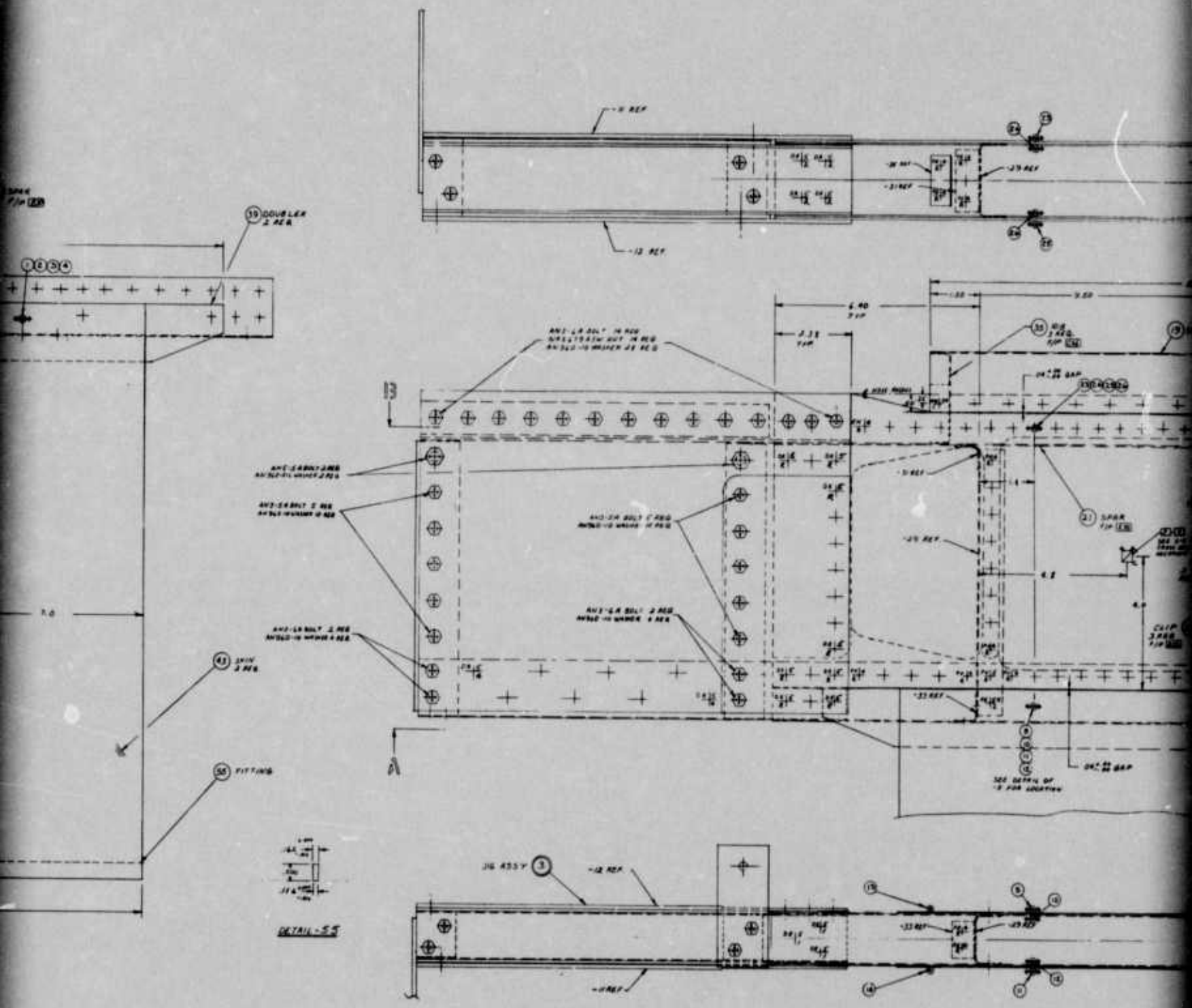
No. 404-114, "Fitting - Rudder Leading Edge Rib"

No. 404-115, "Leading Edge Rib - Rudder"

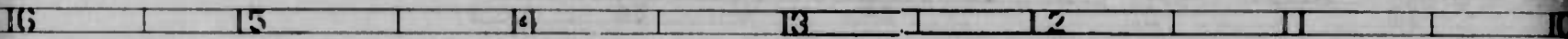
No. 32-24004, "Support Assembly - Balance Weight & Horn"



2



1



NO

5

2674 ± .005 DIA 2 HOLES
80 DEEP
1/4-24 UNF-38 THD (MIL-S-7742)
1/4-24 UNF-38 THD (MIL-S-7742)
1/4-24 UNF-38 THD (MIL-S-7742)
1/4-24 UNF-38 THD (MIL-S-7742)

1562 ± .0079 DIA 21 HOLES
45 DEEP
1/4-24 UNF-38 THD (MIL-S-7742)
1/4-24 UNF-38 THD (MIL-S-7742)
1/4-24 UNF-38 THD (MIL-S-7742)
1/4-24 UNF-38 THD (MIL-S-7742)

2 ALL BERYLLIUM GAGES ARE PRIOR TO FINAL ETCH EXCEPT AS NOTED.

STOCK FOR .45 TO BE MADE AT MAC MAKE WHATEVER SIZE THAT IS NECESSARY FOR MACHINING.

17 OOD DASH NO'S SHN - EVEN DASH NO'S, OPP.

18 CORE SHALL BE IN ACCORDANCE WITH MMS 701.

EXCEPT THAT THE FOIL SHALL BE NON-PERFORATED.

19 ALL STEEL PARTS MAY BE MARKED WITH STEEL STAMPS.

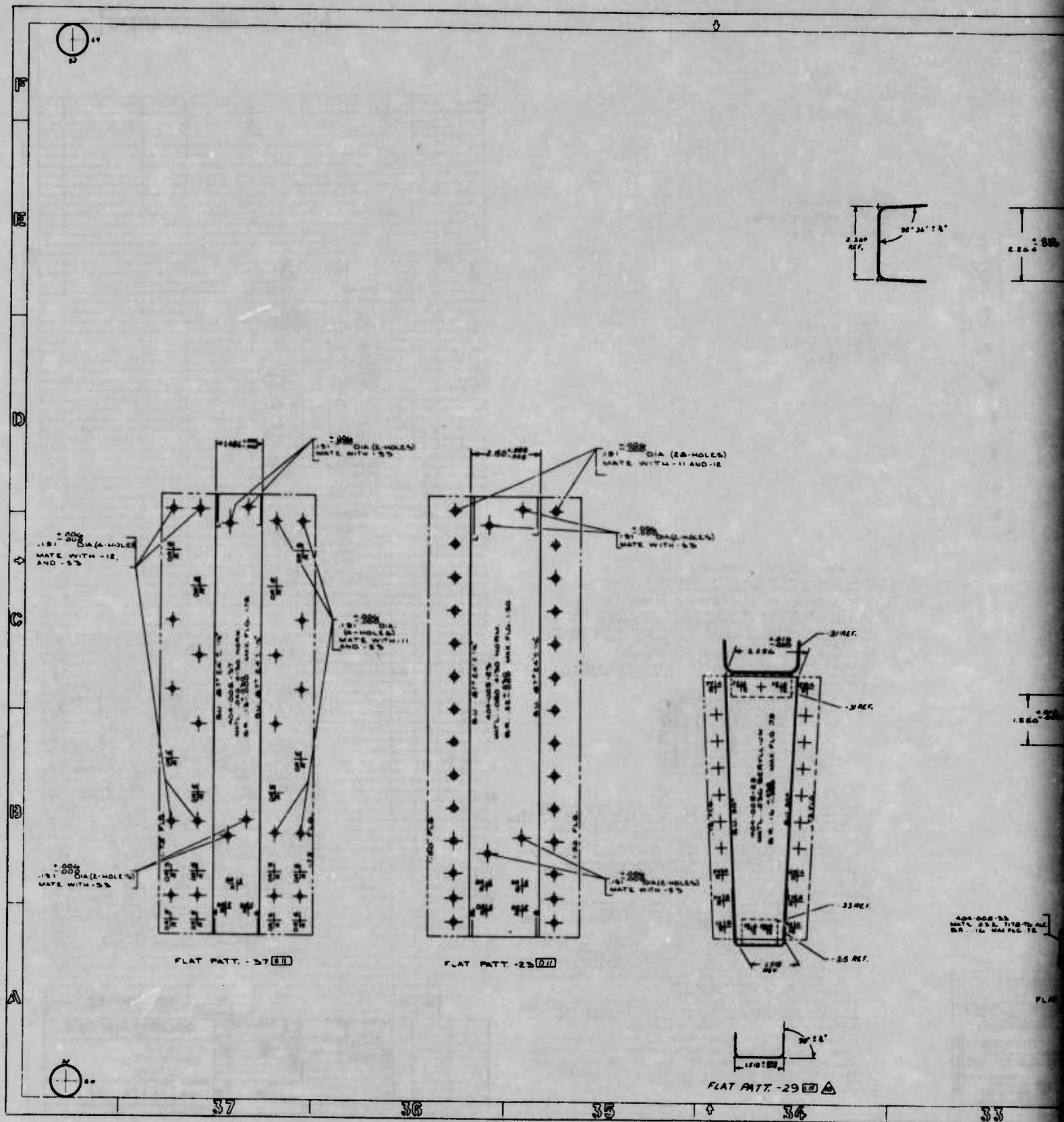
DO NOT MARK ANY BERYLLIUM PARTS. USE TAGS TO IDENTIFY BERYLLIUM.

20 BREAK ALL SHARP EDGES. (STEEL PARTS ONLY)

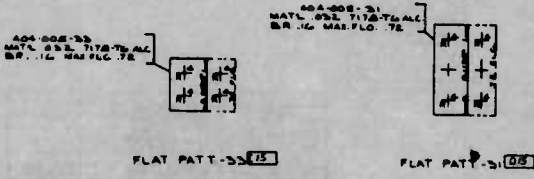
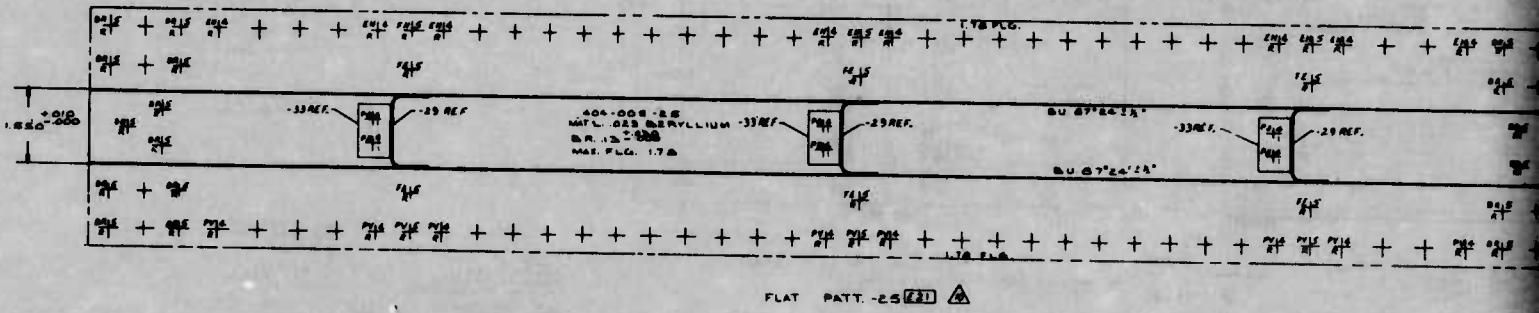
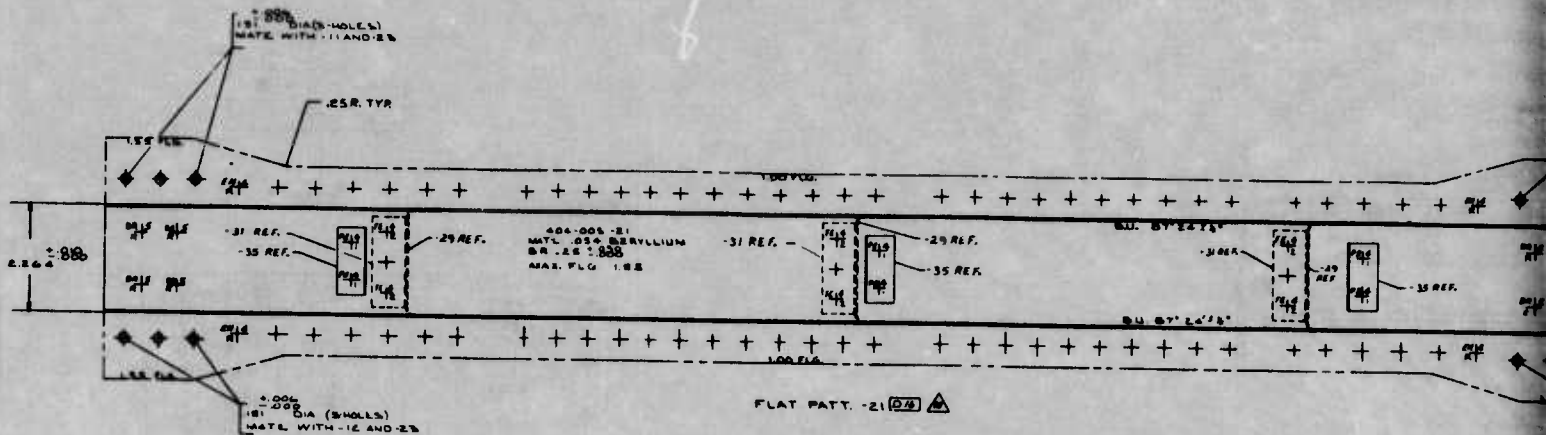
21 MACHINE FINISH 1/32" OR BETTER - ALL MACHINED PARTS.

22 HOLE SIZES FOR FASTENERS IN BERYLLIUM PARTS ARE AS FOLLOWS:

FOLLOW:				
FASTENER	DIA	ST	DIA	ST
ORF	1/16	1/16	1/16	1/16
ORF	1/8	1/8	1/8	1/8
ORF	1/4	1/4	1/4	1/4
ORF	3/8	3/8	3/8	3/8
ORF	1/2	1/2	1/2	1/2
ORF	3/4	3/4	3/4	3/4
ORF	1	1	1	1
ORF	1 1/4	1 1/4	1 1/4	1 1/4
ORF	1 1/2	1 1/2	1 1/2	1 1/2
ORF	1 3/4	1 3/4	1 3/4	1 3/4
ORF	2	2	2	2
ORF	2 1/4	2 1/4	2 1/4	2 1/4
ORF	2 1/2	2 1/2	2 1/2	2 1/2
ORF	2 3/4	2 3/4	2 3/4	2 3/4
ORF	3	3	3	3
ORF	3 1/4	3 1/4	3 1/4	3 1/4
ORF	3 1/2	3 1/2	3 1/2	3 1/2
ORF	3 3/4	3 3/4	3 3/4	3 3/4
ORF	4	4	4	4
ORF	4 1/4	4 1/4	4 1/4	4 1/4
ORF	4 1/2	4 1/2	4 1/2	4 1/2
ORF	4 3/4	4 3/4	4 3/4	4 3/4
ORF	5	5	5	5
ORF	5 1/4	5 1/4	5 1/4	5 1/4
ORF	5 1/2	5 1/2	5 1/2	5 1/2
ORF	5 3/4	5 3/4	5 3/4	5 3/4
ORF	6	6	6	6
ORF	6 1/4	6 1/4	6 1/4	6 1/4
ORF	6 1/2	6 1/2	6 1/2	6 1/2
ORF	6 3/4	6 3/4	6 3/4	6 3/4
ORF	7	7	7	7
ORF	7 1/4	7 1/4	7 1/4	7 1/4
ORF	7 1/2	7 1/2	7 1/2	7 1/2
ORF	7 3/4	7 3/4	7 3/4	7 3/4
ORF	8	8	8	8
ORF	8 1/4	8 1/4	8 1/4	8 1/4
ORF	8 1/2	8 1/2	8 1/2	8 1/2
ORF	8 3/4	8 3/4	8 3/4	8 3/4
ORF	9	9	9	9
ORF	9 1/4	9 1/4	9 1/4	9 1/4
ORF	9 1/2	9 1/2	9 1/2	9 1/2
ORF	9 3/4	9 3/4	9 3/4	9 3/4
ORF	10	10	10	10
ORF	10 1/4	10 1/4	10 1/4	10 1/4
ORF	10 1/2	10 1/2	10 1/2	10 1/2
ORF	10 3/4	10 3/4	10 3/4	10 3/4
ORF	11	11	11	11
ORF	11 1/4	11 1/4	11 1/4	11 1/4
ORF	11 1/2	11 1/2	11 1/2	11 1/2
ORF	11 3/4	11 3/4	11 3/4	11 3/4
ORF	12	12	12	12
ORF	12 1/4	12 1/4	12 1/4	12 1/4
ORF	12 1/2	12 1/2	12 1/2	12 1/2
ORF	12 3/4	12 3/4	12 3/4	12 3/4
ORF	13	13	13	13
ORF	13 1/4	13 1/4	13 1/4	13 1/4
ORF	13 1/2	13 1/2	13 1/2	13 1/2
ORF	13 3/4	13 3/4	13 3/4	13 3/4
ORF	14	14	14	14
ORF	14 1/4	14 1/4	14 1/4	14 1/4
ORF	14 1/2	14 1/2	14 1/2	14 1/2
ORF	14 3/4	14 3/4	14 3/4	14 3/4
ORF	15	15	15	15
ORF	15 1/4	15 1/4	15 1/4	15 1/4
ORF	15 1/2	15 1/2	15 1/2	15 1/2
ORF	15 3/4	15 3/4	15 3/4	15 3/4
ORF	16	16	16	16
ORF	16 1/4	16 1/4	16 1/4	16 1/4
ORF	16 1/2	16 1/2	16 1/2	16 1/2
ORF	16 3/4	16 3/4	16 3/4	16 3/4
ORF	17	17	17	17
ORF	17 1/4	17 1/4	17 1/4	17 1/4
ORF	17 1/2	17 1/2	17 1/2	17 1/2
ORF	17 3/4	17 3/4	17 3/4	17 3/4
ORF	18	18	18	18
ORF	18 1/4	18 1/4	18 1/4	18 1/4
ORF	18 1/2	18 1/2	18 1/2	18 1/2
ORF	18 3/4	18 3/4	18 3/4	18 3/4
ORF	19	19	19	19
ORF	19 1/4	19 1/4	19 1/4	19 1/4
ORF	19 1/2	19 1/2	19 1/2	19 1/2
ORF	19 3/4	19 3/4	19 3/4	19 3/4
ORF	20	20	20	20
ORF	20 1/4	20 1/4	20 1/4	20 1/4
ORF	20 1/2	20 1/2	20 1/2	20 1/2
ORF	20 3/4	20 3/4	20 3/4	20 3/4
ORF	21	21	21	21
ORF	21 1/4	21 1/4	21 1/4	21 1/4
ORF	21 1/2	21 1/2	21 1/2	21 1/2
ORF	21 3/4	21 3/4	21 3/4	21 3/4
ORF	22	22	22	22
ORF	22 1/4	22 1/4	22 1/4	22 1/4
ORF	22 1/2	22 1/2	22 1/2	22 1/2
ORF	22 3/4	22 3/4	22 3/4	22 3/4
ORF	23	23	23	23
ORF	23 1/4	23 1/4	23 1/4	23 1/4
ORF	23 1/2	23 1/2	23 1/2	23 1/2
ORF	23 3/4	23 3/4	23 3/4	23 3/4
ORF	24	24	24	24
ORF	24 1/4	24 1/4	24 1/4	24 1/4
ORF	24 1/2	24 1/2	24 1/2	24 1/2
ORF	24 3/4	24 3/4	24 3/4	24 3/4
ORF	25	25	25	25
ORF	25 1/4	25 1/4	25 1/4	25 1/4
ORF	25 1/2	25 1/2	25 1/2	25 1/2
ORF	25 3/4	25 3/4	25 3/4	25 3/4
ORF	26	26	26	26
ORF	26 1/4	26 1/4	26 1/4	26 1/4
ORF	26 1/2	26 1/2	26 1/2	26 1/2
ORF	26 3/4	26 3/4	26 3/4	26 3/4
ORF	27	27	27	27
ORF	27 1/4	27 1/4	27 1/4	27 1/4
ORF	27 1/2	27 1/2	27 1/2	27 1/2
ORF	27 3/4	27 3/4	27 3/4	27 3/4
ORF	28	28	28	28
ORF	28 1/4	28 1/4	28 1/4	28 1/4
ORF	28 1/2	28 1/2	28 1/2	28 1/2
ORF	28 3/4	28 3/4	28 3/4	28 3/4
ORF	29	29	29	29
ORF	29 1/4	29 1/4	29 1/4	29 1/4
ORF	29 1/2	29 1/2	29 1/2	29 1/2
ORF	29 3/4	29 3/4	29 3/4	29 3/4
ORF	30	30	30	30
ORF	30 1/4	30 1/4	30 1/4	30 1/4
ORF	30 1/2	30 1/2	30 1/2	30 1/2
ORF	30 3/4	30 3/4	30 3/4	30 3/4
ORF	31	31	31	31
ORF	31 1/4	31 1/4	31 1/4	31 1/4
ORF	31 1/2	31 1/2	31 1/2	31 1/2
ORF	31 3/4	31 3/4	31 3/4	31 3/4
ORF	32	32	32	32
ORF	32 1/4	32 1/4	32 1/4	32 1/4
ORF	32 1/2	32 1/2	32 1/2	32 1/2
ORF	32 3/4	32 3/4	32 3/4	32 3/4
ORF	33	33	33	33
ORF	33 1/4	33 1/4	33 1/4	33 1/4
ORF	33 1/2	33 1/2	33 1/2	33 1/2
ORF	33 3/4	33 3/4	33 3/4	33 3/4
ORF	34	34	34	34
ORF	34 1/4	34 1/4	34 1/4	34 1/4
ORF	34 1/2	34 1/2	34 1/2	34 1/2
ORF	34 3/4	34 3/4	34 3/4	34 3/4
ORF	35	35	35	35
ORF	35 1/4	35 1/4	35 1/4	35 1/4
ORF	35 1/2	35 1/2	35 1/2	35 1/2
ORF	35 3/4	35 3/4	35 3/4	35 3/4
ORF	36	36	36	36
ORF	36 1/4	36 1/4	36 1/4	36 1/4
ORF	36 1/2	36 1/2	36 1/2	36 1/2
ORF	36 3/4	36 3/4	36 3/4	36 3/4
ORF	37	37	37	37
ORF	37 1/4	37 1/4	37 1/4	37 1/4
ORF	37 1/2	37 1/2	37 1/2	37 1/2
ORF	37 3/4	37 3/4	37 3/4	37 3/4
ORF	38	38	38	38
ORF	38 1/4	38 1/4	38 1/4	38 1/4
ORF	38 1/2	38 1/2	38 1/2	38 1/2
ORF	38 3/4	38 3/4	38 3/4	38 3/4
ORF	39	39	39	39
ORF	39 1/4	39 1/4	39 1/4	39 1/4
ORF	39 1/2	39 1/2	39 1/2	39 1/2
ORF	39 3/4	39 3/4	39 3/4	39 3/4
ORF	40	40	40	40
ORF	40 1/4	40 1/4	40 1/4	40 1/4
ORF	40 1/2	40 1/2	40 1/2	40 1/2
ORF	40 3/4	40 3/4	40 3/4	40 3/4
ORF	41	41	41	41
ORF	41 1/4	41 1/4	41 1/4	41 1/4
ORF	41 1/2	41 1/2	41 1/2	41 1/2
ORF	41 3/4	41 3/4	41 3/4	41 3/4
ORF	42	42	42	42
ORF	42 1/4	42 1/4	42 1/4	42 1/4
ORF	42 1/2	42 1/2	42 1/2	42 1/2
ORF	42 3/4	42 3/4	42 3/4	42 3/4
ORF	43	43	43	43
ORF	43 1/4	43 1/4	43 1/4	43 1/4
ORF	43 1/2	43 1/2	43 1/2	43 1/2
ORF	43 3/4	43 3/4	43 3/4	43 3/4
ORF	44	44	44	44
ORF	44 1/4	44 1/4	44 1/4	44 1/4
ORF	44 1/2	44 1/2	44 1/2	44 1/2
ORF	44 3/4	44 3/4	44 3/4	44 3/4
ORF	45	45	45	45
ORF	45 1/4	45 1/4	45 1/4	45 1/4
ORF	45 1/2	45 1/2	45 1/2	45 1/2
ORF	45 3/4	45 3/4	45 3/4	45 3/4
ORF	46	46	46	46
ORF	46 1/4	46 1/4	46 1/4	46 1/4
ORF	46 1/2	46 1/2	46 1/2	46 1/2
ORF	46 3/4	46 3/4	46 3/4	46 3/4
ORF	47	47	47	47
ORF	47 1/4	47 1/4	47 1/4	47 1/4
ORF	47 1/2	47 1/2	47 1/2	47 1/2
ORF	47 3/4	47 3/4	47 3/4	47 3/4
ORF	48	48	48	48
ORF	48 1/4	48 1/4	48 1/4	48 1/4
ORF	48 1/2	48 1/2	48 1/2	48 1/2
ORF	48 3/4	48 3/4	48 3/4	48 3/4
ORF	49	49	49	49
ORF	49 1/4	49 1/4	49 1/4	49 1/4
ORF	49 1/2	49 1/2	49 1/2	49 1/2
ORF	49 3/4	49 3/4	49 3/4	49 3/4
ORF	50	50	50	50
ORF	50 1/4	50 1/4	50 1/4	50 1/4
ORF	50 1/2	50 1/2	50 1/2	50 1/2
ORF	50 3/4	50 3/4	50 3/4	50 3/4
ORF	51	51	51	51
ORF	51 1/4	51 1/4	51 1/4	51 1/4
ORF	51 1/2	51 1/2	51 1/2	51 1/2
ORF	51 3/4	51 3/4	51 3/4	51 3/4
ORF	52	52	52	52
ORF	52 1/4	52 1/4	52 1/4	52 1/4
ORF	52 1/2	52 1/2	52 1/2	52 1/2
ORF	52 3/4	52 3/4	52 3/4	52 3/4
ORF	53	53	53	53
ORF	53 1/4	53 1/4	53 1/4	53 1/4
ORF	53 1/2	53 1/2	53 1/2	53 1/2
ORF	53 3/4	53 3/4	53 3/4	53 3/4
ORF	54	54	54	54
ORF	54 1/4	54 1/4	54 1/4	54 1/4
ORF	54 1/2	54 1/2	54 1/2	54 1/2
ORF	54 3/4	54 3/4	54 3/4	54 3/4
ORF	55	55	55	55
ORF	55 1/4	55 1/4	55 1/4	55 1/4
ORF	55 1/2	55 1/2	55 1/2	55 1/2
ORF	55 3/4	55 3/4	55 3/4	55 3/4
ORF	56	56	56	56
ORF	56 1/4	56 1/4	56 1/4	56 1/4
ORF	56 1/2	56 1/2	56 1/2	56 1/2
ORF	56 3/4	56 3/4	56 3/4	56 3/4
ORF	57	57	57	57
ORF	57 1/4	57 1/4	57 1/4	57 1/4
ORF	57 1/2	57 1/2	57 1/2	57 1/2
ORF	57 3/4	57 3/4	57 3/4	57 3/4
ORF	58	58	58	58
ORF	58 1/4	58 1/4	58 1/4	58 1/4
ORF	58 1/2	58 1/2	58 1/2	58 1/2
ORF	58 3/4	58 3/4	58 3/4	58 3/4
ORF	59	59	59	59
ORF	59 1/4	59 1/4	59 1/4	59 1/4
ORF	59 1/2	59 1/2	59 1/2	59 1/2
ORF	59 3/4	59 3/4	59 3/4	59 3/4
ORF	60	60	60	60
ORF	60 1/4	60 1/4	60 1/4	60 1/4
ORF	60 1/2	60 1/2	60 1/2	60 1/2
ORF	60 3/4	60 3/4		



2



12	REVISION				
11	REVISION				
10	REVISION				
9	REVISION				
8	REVISION				
7	REVISION				
6	REVISION				
5	REVISION				
4	REVISION				
3	REVISION				
2	REVISION				
1	REVISION				

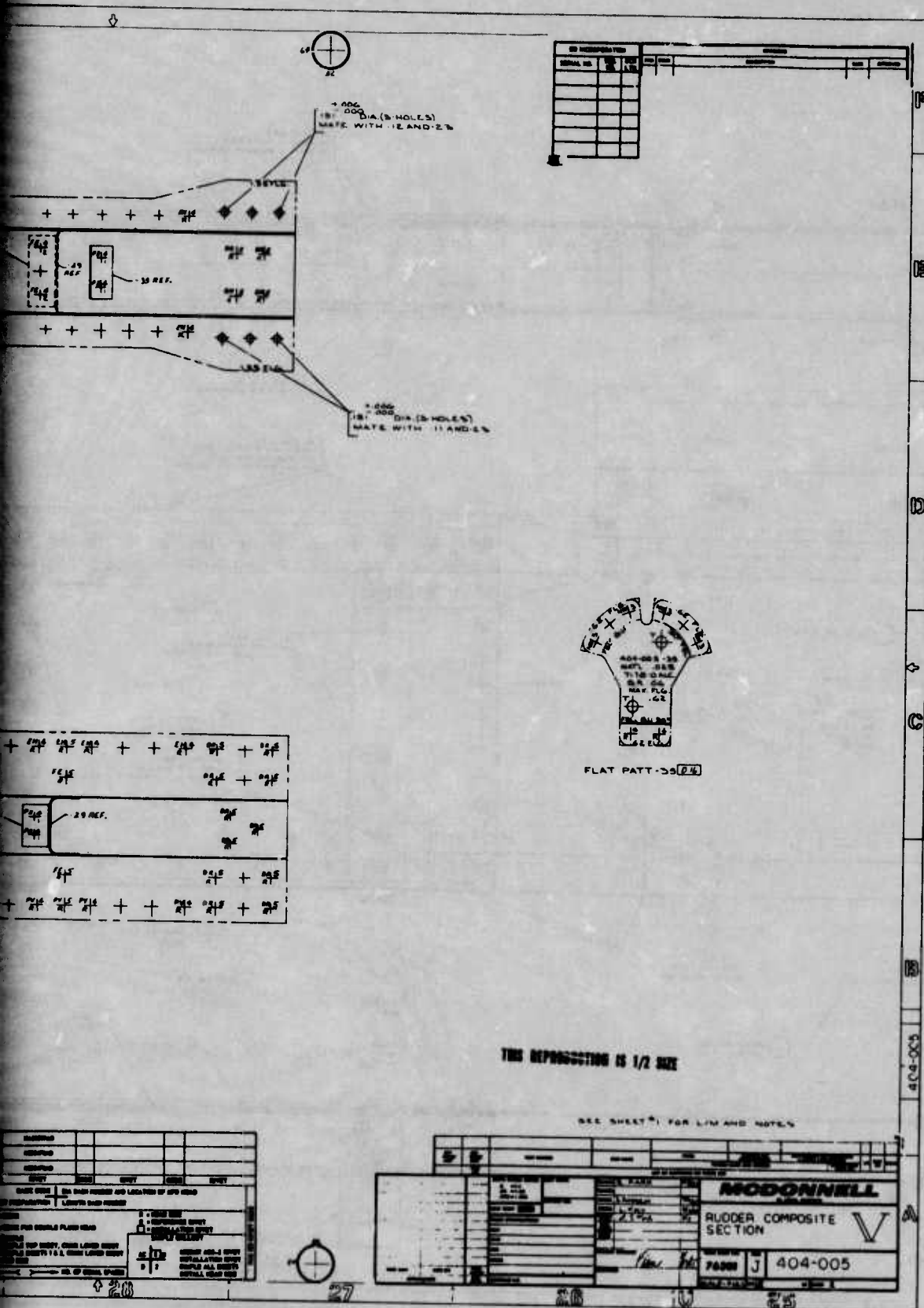
DATE: 10/10/10 BY: [Signature] CHECKED: [Signature] APPROVED: [Signature]

REVISIONS: 1. [Description] 2. [Description] 3. [Description] 4. [Description] 5. [Description] 6. [Description] 7. [Description] 8. [Description] 9. [Description] 10. [Description] 11. [Description] 12. [Description]

REVISIONS: 1. [Description] 2. [Description] 3. [Description] 4. [Description] 5. [Description] 6. [Description] 7. [Description] 8. [Description] 9. [Description] 10. [Description] 11. [Description] 12. [Description]

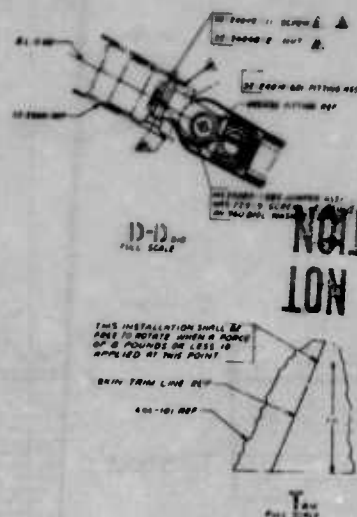


1



5

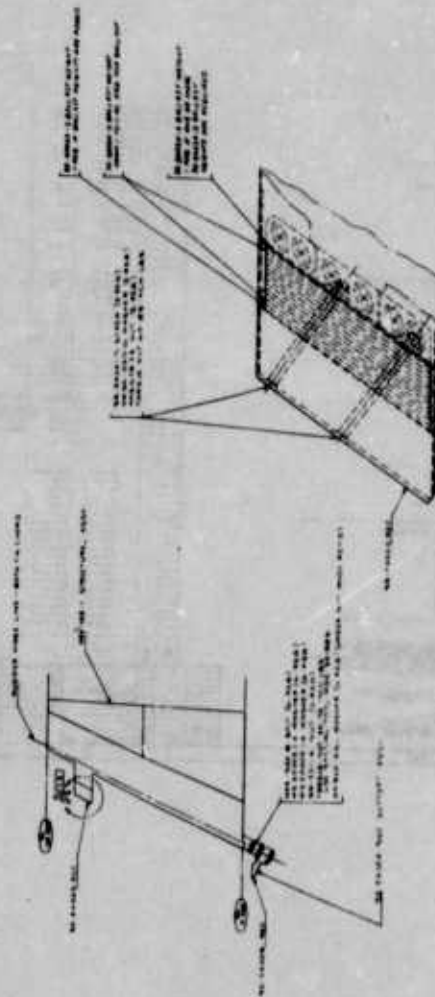
DOG BOES NOT
E PRODUCTION



- [illegible]

MODONNELL
BERYLLIUM RUDDER
PART 404-100
404-100

COPY AVAILABLE TO DDC DOES NOT
PERMIT FULLY LEGIBLE PRODUCTION



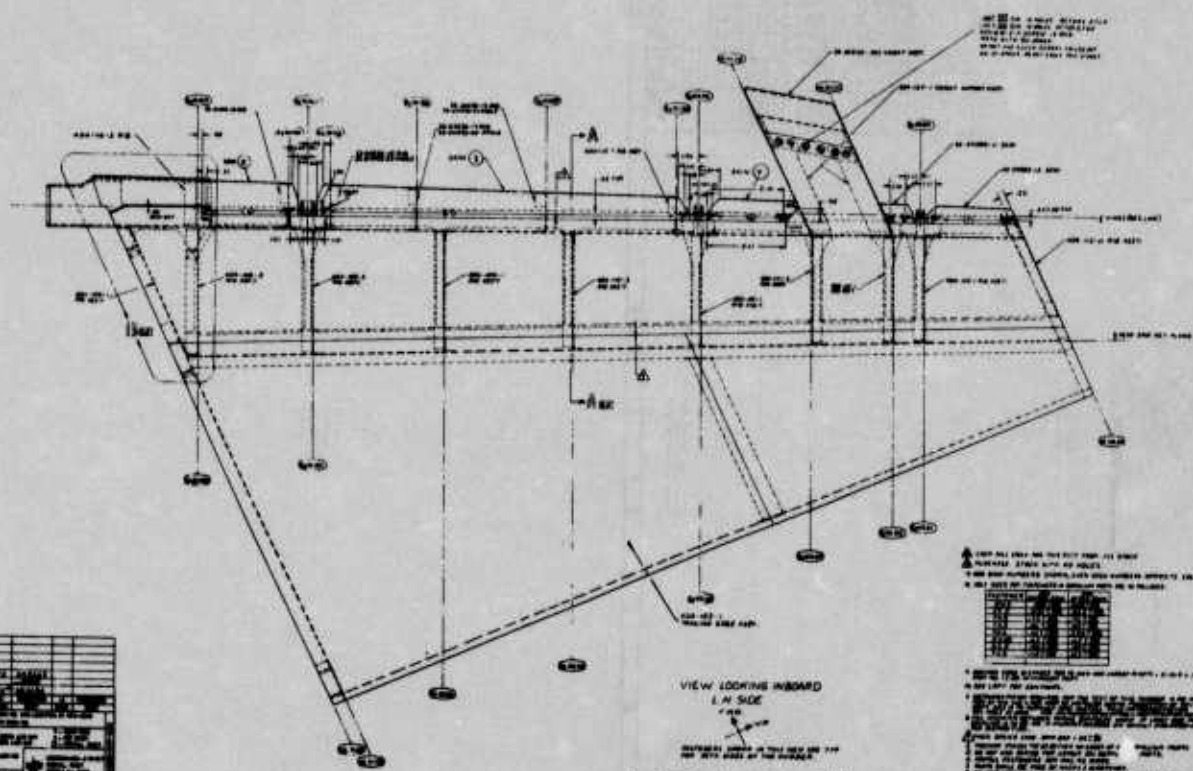
MATERIALS		QUANTITIES		UNIT PRICES		TOTALS	
STEEL	100	100	100	100	100	100	100
WOOD	200	200	200	200	200	200	200
CONCRETE	300	300	300	300	300	300	300
BRICK	400	400	400	400	400	400	400
ROOFING	500	500	500	500	500	500	500
PAINT	600	600	600	600	600	600	600
GLASS	700	700	700	700	700	700	700
DOORS	800	800	800	800	800	800	800
WINDOWS	900	900	900	900	900	900	900
PLUMBING	1000	1000	1000	1000	1000	1000	1000
ELECTRICAL	1100	1100	1100	1100	1100	1100	1100
MECHANICAL	1200	1200	1200	1200	1200	1200	1200
LABOR	1300	1300	1300	1300	1300	1300	1300
OVERHEAD	1400	1400	1400	1400	1400	1400	1400
TOTAL	1500	1500	1500	1500	1500	1500	1500

REVISIONS



2

1	2	3	4	5	6	7	8	9	10	11	12	13	14	15	16	17	18	19	20	21	22	23	24	25	26	27	28	29	30	31	32	33	34	35	36	37	38	39	40	41	42	43	44	45	46	47	48	49	50	51	52	53	54	55	56	57	58	59	60	61	62	63	64	65	66	67	68	69	70	71	72	73	74	75	76	77	78	79	80	81	82	83	84	85	86	87	88	89	90	91	92	93	94	95	96	97	98	99	100
---	---	---	---	---	---	---	---	---	----	----	----	----	----	----	----	----	----	----	----	----	----	----	----	----	----	----	----	----	----	----	----	----	----	----	----	----	----	----	----	----	----	----	----	----	----	----	----	----	----	----	----	----	----	----	----	----	----	----	----	----	----	----	----	----	----	----	----	----	----	----	----	----	----	----	----	----	----	----	----	----	----	----	----	----	----	----	----	----	----	----	----	----	----	----	----	----	----	----	-----



VIEW LOOKING INBOARD
L.H. SIDE

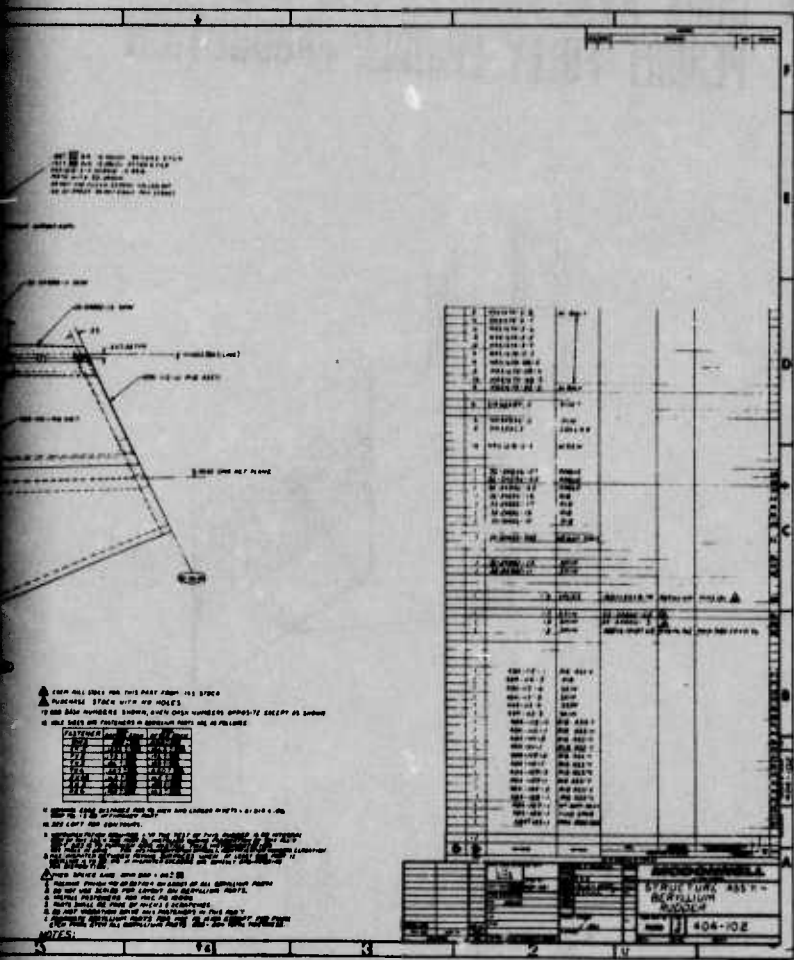
SECTIONAL SHEET IN THIS SET AND 719
AND 720 SHOW THE HULL

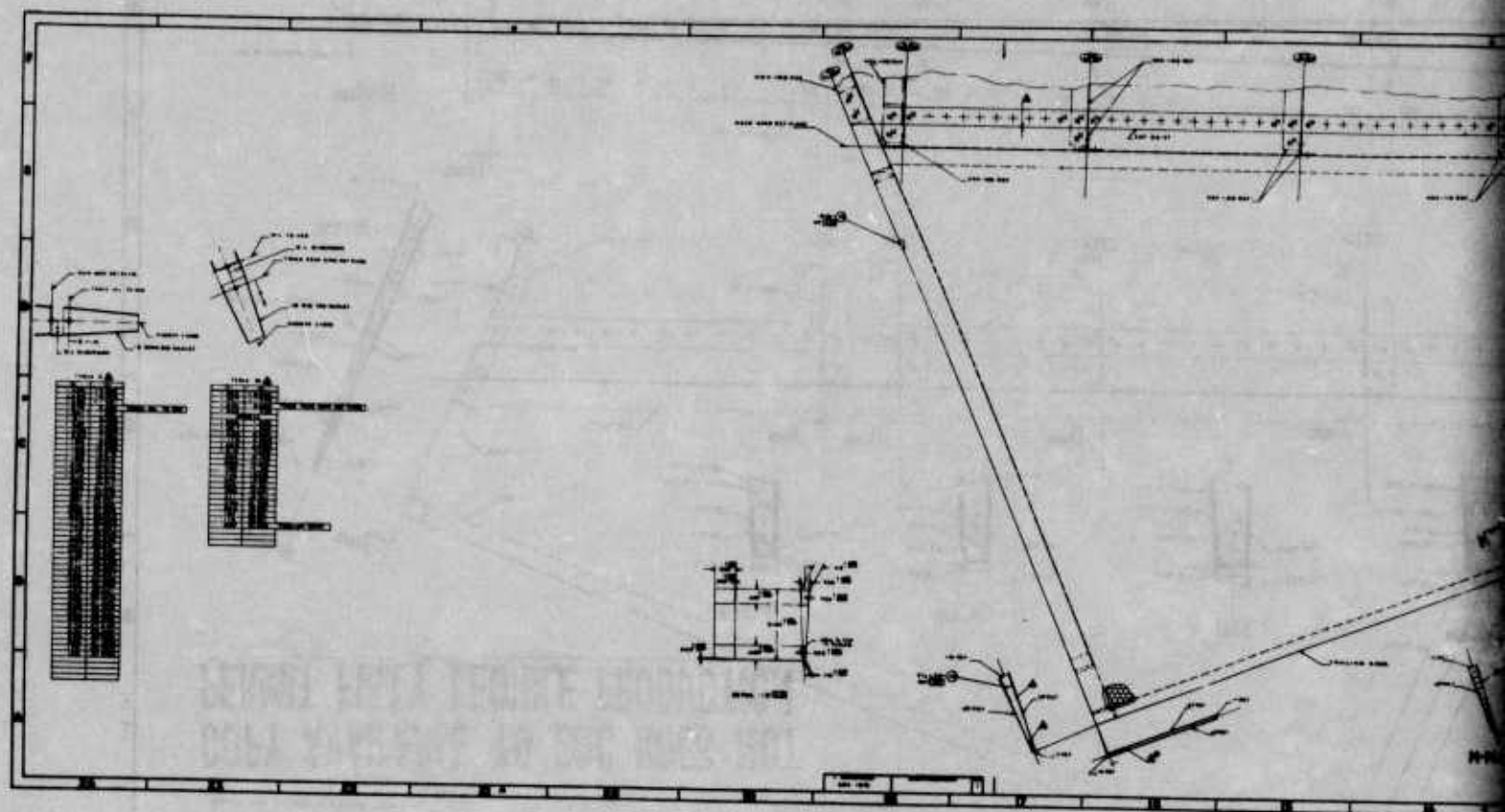
1. ALL DIMENSIONS ARE IN FEET AND INCHES
2. DIMENSIONS ARE TO CENTERLINE UNLESS OTHERWISE SPECIFIED
3. DIMENSIONS ARE TO CENTERLINE UNLESS OTHERWISE SPECIFIED

1	2	3	4	5	6	7	8	9	10	11	12	13	14	15	16	17	18	19	20	21	22	23	24	25	26	27	28	29	30	31	32	33	34	35	36	37	38	39	40	41	42	43	44	45	46	47	48	49	50	51	52	53	54	55	56	57	58	59	60	61	62	63	64	65	66	67	68	69	70	71	72	73	74	75	76	77	78	79	80	81	82	83	84	85	86	87	88	89	90	91	92	93	94	95	96	97	98	99	100
---	---	---	---	---	---	---	---	---	----	----	----	----	----	----	----	----	----	----	----	----	----	----	----	----	----	----	----	----	----	----	----	----	----	----	----	----	----	----	----	----	----	----	----	----	----	----	----	----	----	----	----	----	----	----	----	----	----	----	----	----	----	----	----	----	----	----	----	----	----	----	----	----	----	----	----	----	----	----	----	----	----	----	----	----	----	----	----	----	----	----	----	----	----	----	----	----	----	----	-----

1. ALL DIMENSIONS ARE IN FEET AND INCHES
2. DIMENSIONS ARE TO CENTERLINE UNLESS OTHERWISE SPECIFIED
3. DIMENSIONS ARE TO CENTERLINE UNLESS OTHERWISE SPECIFIED

3





H-Beam

I-Beam

GIRDER

PLATE

RIB

STIFFENER

WELD

BOLT

NUT

WASHER

FLANGE

HEAD

TAIL

END

START

STOP

HOLD DOWN

BRACE

SUPPORT

ANCHOR

FASTENING

CLAMP

SCREW

DRILL

PUNCH

DIE

CUTTER

GRINDER

MILLER

WELDER

PAINTER

CARPENTER

BLACKSMITH

FITTER

TURNER

ELECTRICIAN

MECHANIC

STEWARD

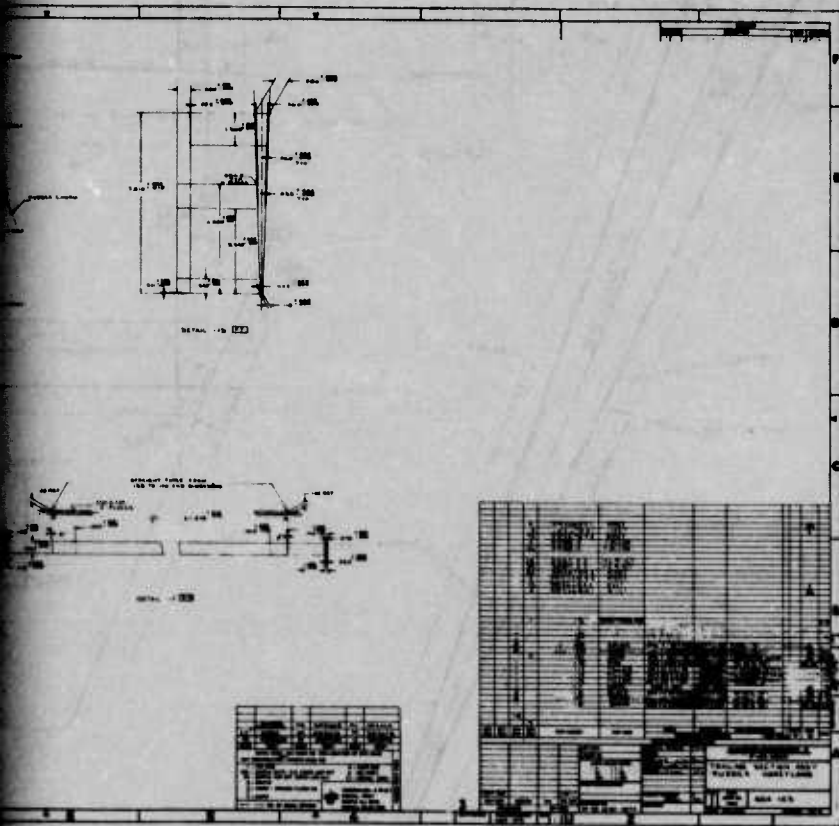
COOK

BOILERMAKER

SHIPYARD

Part Name	Quantity	Notes
H-Beam	10	
I-Beam	5	
Girder	3	
Plate	20	
Rib	15	
Stiffener	8	
Weld	12	
Bolt	50	
Nut	50	
Washer	50	
Flange	10	
Head	5	
Tail	5	
End	1	
Start	1	
Stop	1	
Hold Down	5	
Brace	3	
Support	2	
Anchor	1	
Fastening	10	
Clamp	5	
Screw	20	
Drill	1	
Punch	1	
Die	1	
Cutter	1	
Grinder	1	
Miller	1	
Welder	1	
Painter	1	
Carpenter	1	
Blacksmith	1	
Fitter	1	
Turner	1	
Electrician	1	
Mechanic	1	
Steward	1	
Cook	1	
Boilermaker	1	
Shipyard	1	

3



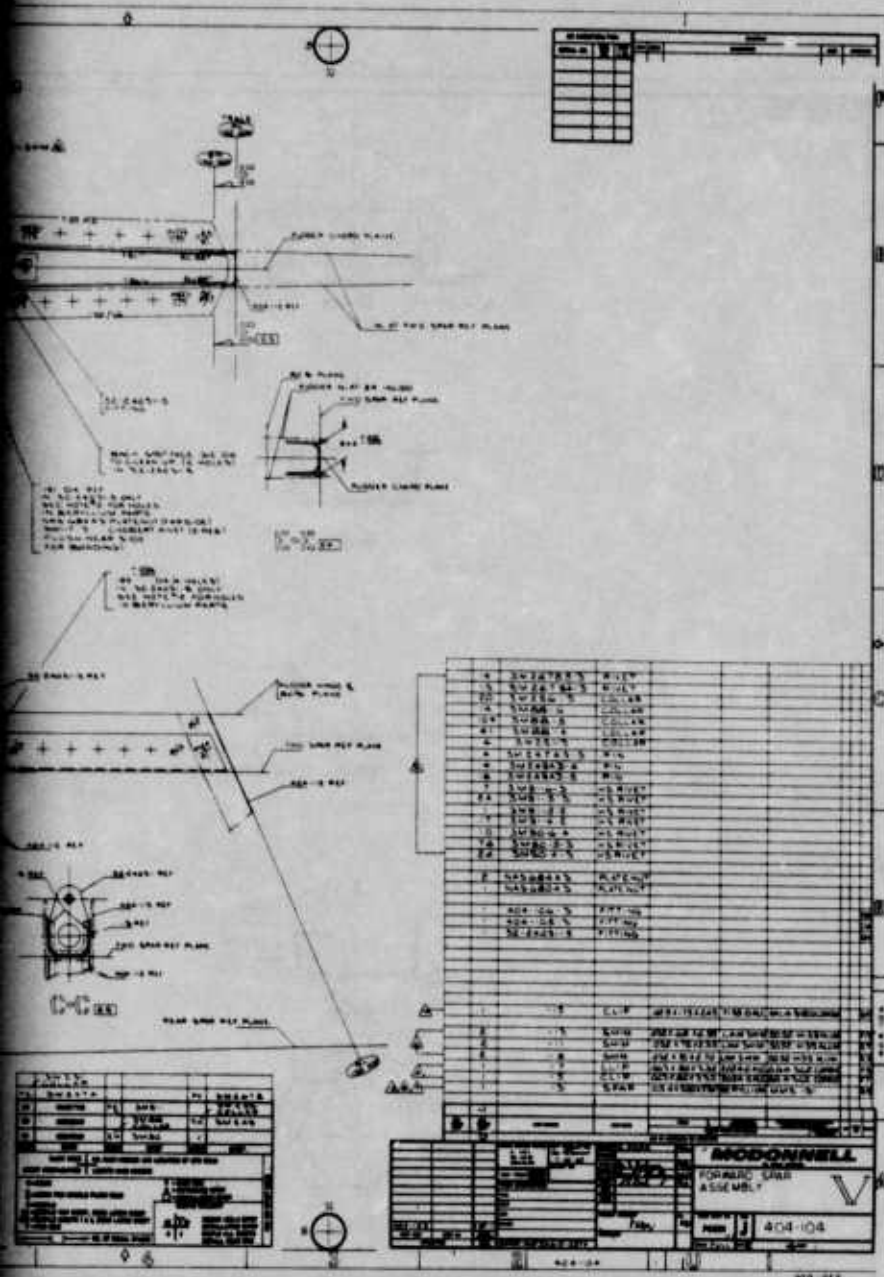
AVAILABLE TO DDC DOES NOT FULLY LEGIBLE PRODUCTION

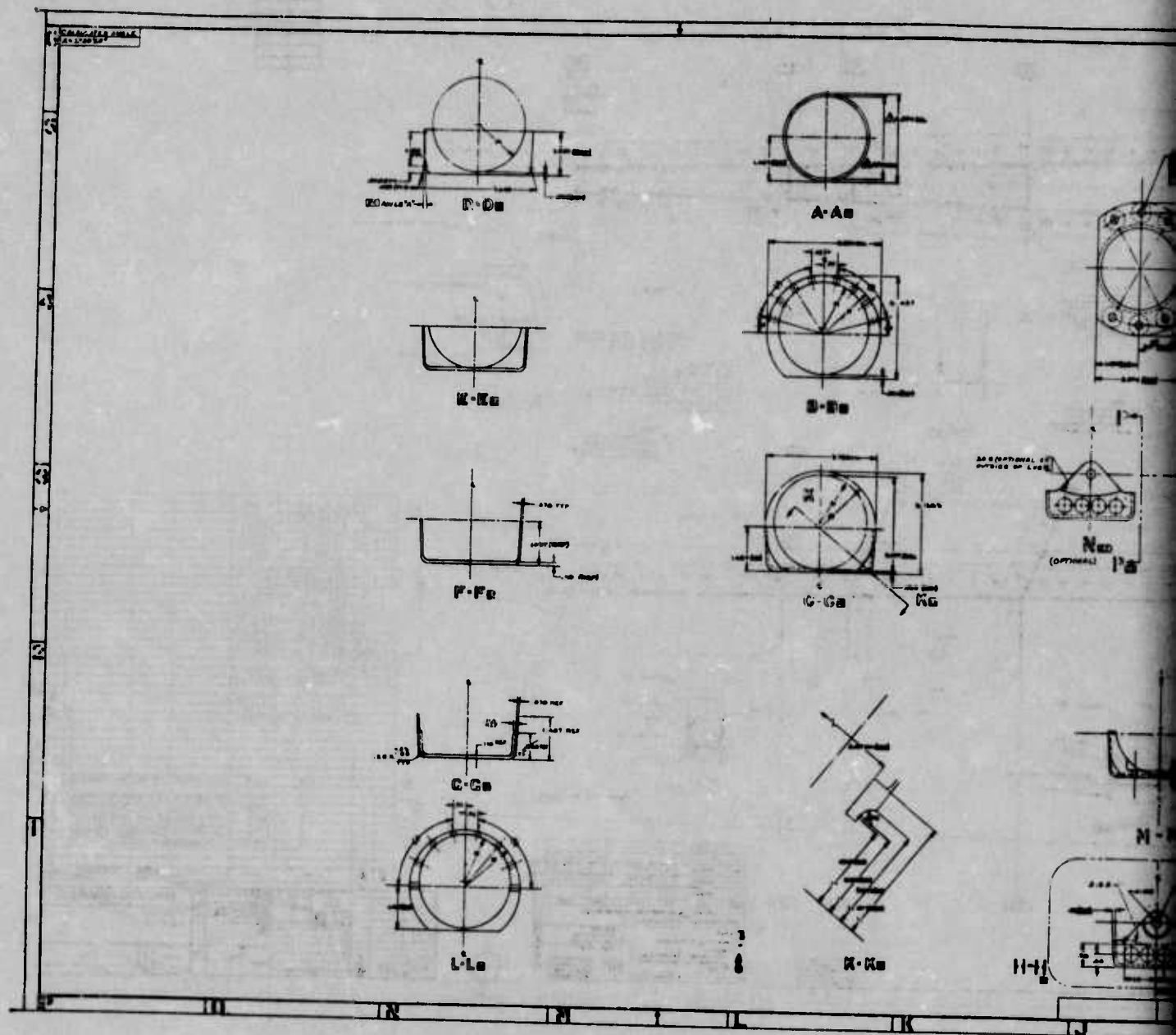


Technical drawing of a ship's hull, showing the L.H. side view and various structural details. The drawing includes numerous callouts, dimensions, and a table of specifications.

Table of Specifications:

ITEM	DESCRIPTION	QUANTITY	REMARKS
1	KEEL	1	
2	BOTTOM	1	
3	UPPER HULL	1	
4	LOWER HULL	1	
5	DECK	1	
6	WATER TIGHT	1	
7	WATER TIGHT	1	
8	WATER TIGHT	1	
9	WATER TIGHT	1	
10	WATER TIGHT	1	
11	WATER TIGHT	1	
12	WATER TIGHT	1	
13	WATER TIGHT	1	
14	WATER TIGHT	1	
15	WATER TIGHT	1	
16	WATER TIGHT	1	
17	WATER TIGHT	1	
18	WATER TIGHT	1	
19	WATER TIGHT	1	
20	WATER TIGHT	1	
21	WATER TIGHT	1	
22	WATER TIGHT	1	
23	WATER TIGHT	1	
24	WATER TIGHT	1	
25	WATER TIGHT	1	
26	WATER TIGHT	1	
27	WATER TIGHT	1	
28	WATER TIGHT	1	
29	WATER TIGHT	1	
30	WATER TIGHT	1	
31	WATER TIGHT	1	
32	WATER TIGHT	1	
33	WATER TIGHT	1	
34	WATER TIGHT	1	
35	WATER TIGHT	1	
36	WATER TIGHT	1	
37	WATER TIGHT	1	
38	WATER TIGHT	1	
39	WATER TIGHT	1	
40	WATER TIGHT	1	
41	WATER TIGHT	1	
42	WATER TIGHT	1	
43	WATER TIGHT	1	
44	WATER TIGHT	1	
45	WATER TIGHT	1	
46	WATER TIGHT	1	
47	WATER TIGHT	1	
48	WATER TIGHT	1	
49	WATER TIGHT	1	
50	WATER TIGHT	1	
51	WATER TIGHT	1	
52	WATER TIGHT	1	
53	WATER TIGHT	1	
54	WATER TIGHT	1	
55	WATER TIGHT	1	
56	WATER TIGHT	1	
57	WATER TIGHT	1	
58	WATER TIGHT	1	
59	WATER TIGHT	1	
60	WATER TIGHT	1	
61	WATER TIGHT	1	
62	WATER TIGHT	1	
63	WATER TIGHT	1	
64	WATER TIGHT	1	
65	WATER TIGHT	1	
66	WATER TIGHT	1	
67	WATER TIGHT	1	
68	WATER TIGHT	1	
69	WATER TIGHT	1	
70	WATER TIGHT	1	
71	WATER TIGHT	1	
72	WATER TIGHT	1	
73	WATER TIGHT	1	
74	WATER TIGHT	1	
75	WATER TIGHT	1	
76	WATER TIGHT	1	
77	WATER TIGHT	1	
78	WATER TIGHT	1	
79	WATER TIGHT	1	
80	WATER TIGHT	1	
81	WATER TIGHT	1	
82	WATER TIGHT	1	
83	WATER TIGHT	1	
84	WATER TIGHT	1	
85	WATER TIGHT	1	
86	WATER TIGHT	1	
87	WATER TIGHT	1	
88	WATER TIGHT	1	
89	WATER TIGHT	1	
90	WATER TIGHT	1	
91	WATER TIGHT	1	
92	WATER TIGHT	1	
93	WATER TIGHT	1	
94	WATER TIGHT	1	
95	WATER TIGHT	1	
96	WATER TIGHT	1	
97	WATER TIGHT	1	
98	WATER TIGHT	1	
99	WATER TIGHT	1	
100	WATER TIGHT	1	





Technical drawing of a machine, likely a pump or engine component, showing multiple views and dimensions. The drawing includes a top view, a side view, and a cross-section view. Dimensions are provided in inches and feet. The drawing is labeled with various parts and components, including a list of parts on the right side.

Top View Dimensions:

- Overall width: 10.00
- Overall height: 10.00
- Internal width: 8.00
- Internal height: 8.00
- Radius: R.10

Side View Dimensions:

- Overall length: 10.00
- Overall height: 10.00
- Internal length: 8.00
- Internal height: 8.00
- Radius: R.10

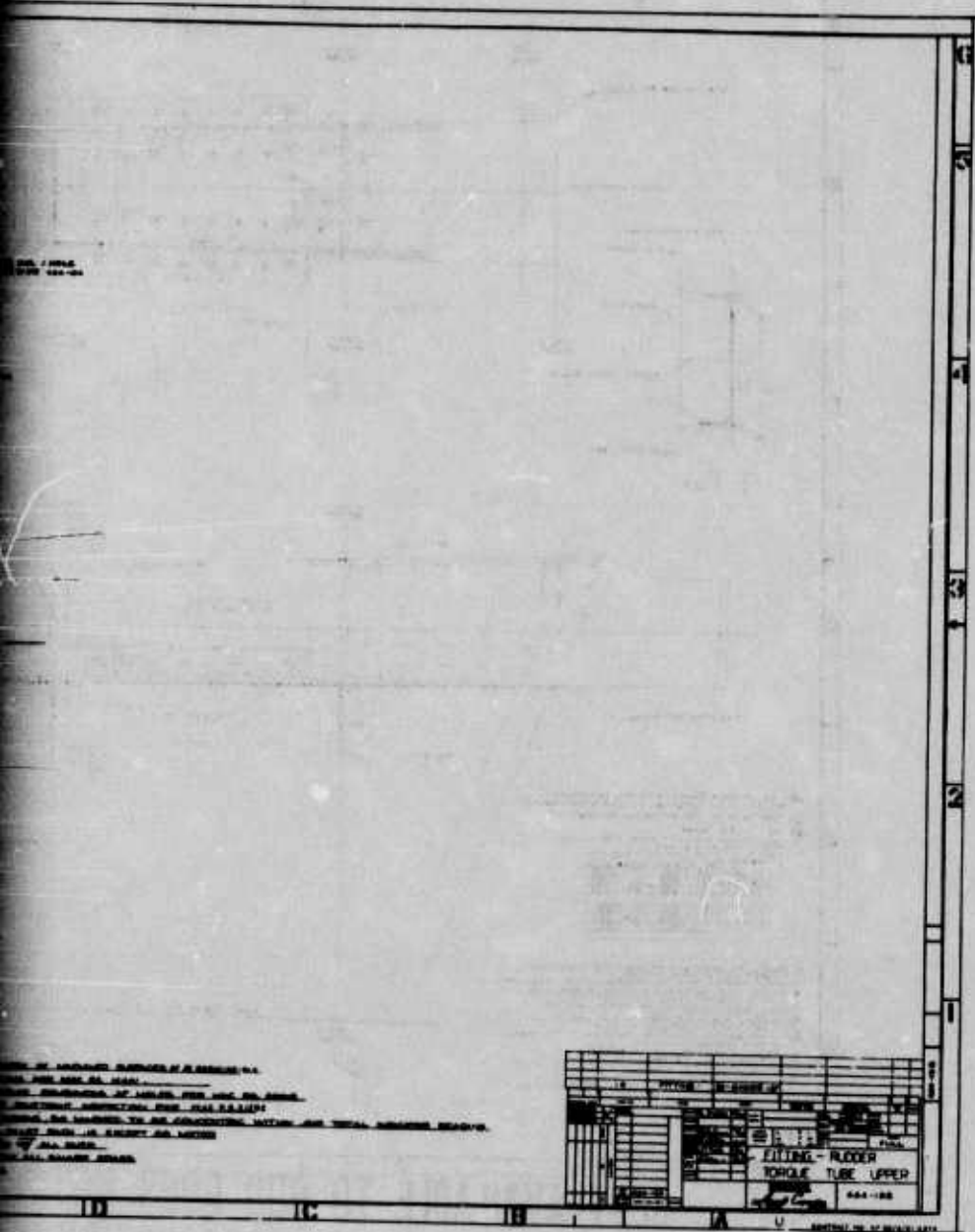
Cross-section View Dimensions:

- Overall width: 10.00
- Overall height: 10.00
- Internal width: 8.00
- Internal height: 8.00
- Radius: R.10

Parts List:

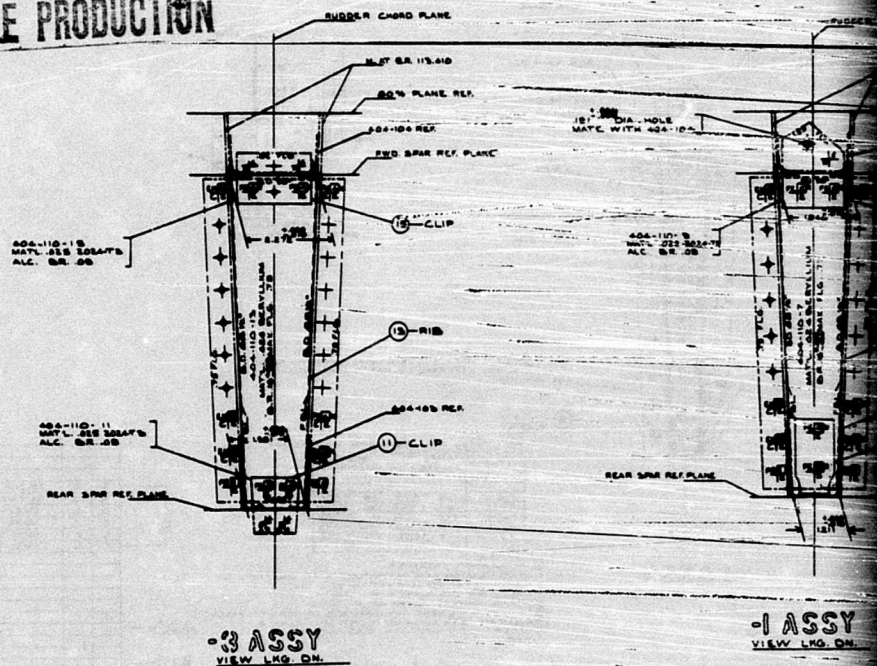
1. COVER PLATE
2. GASKET
3. BOLT
4. NUT
5. WASHER
6. O-RING
7. PUMP HOUSING
8. IMPELLER
9. IMPELLER NUT
10. IMPELLER KEY
11. IMPELLER KEYWAY
12. IMPELLER KEY
13. IMPELLER KEYWAY
14. IMPELLER KEY
15. IMPELLER KEYWAY
16. IMPELLER KEY
17. IMPELLER KEYWAY
18. IMPELLER KEY
19. IMPELLER KEYWAY
20. IMPELLER KEY
21. IMPELLER KEYWAY
22. IMPELLER KEY
23. IMPELLER KEYWAY
24. IMPELLER KEY
25. IMPELLER KEYWAY
26. IMPELLER KEY
27. IMPELLER KEYWAY
28. IMPELLER KEY
29. IMPELLER KEYWAY
30. IMPELLER KEY
31. IMPELLER KEYWAY
32. IMPELLER KEY
33. IMPELLER KEYWAY
34. IMPELLER KEY
35. IMPELLER KEYWAY
36. IMPELLER KEY
37. IMPELLER KEYWAY
38. IMPELLER KEY
39. IMPELLER KEYWAY
40. IMPELLER KEY
41. IMPELLER KEYWAY
42. IMPELLER KEY
43. IMPELLER KEYWAY
44. IMPELLER KEY
45. IMPELLER KEYWAY
46. IMPELLER KEY
47. IMPELLER KEYWAY
48. IMPELLER KEY
49. IMPELLER KEYWAY
50. IMPELLER KEY
51. IMPELLER KEYWAY
52. IMPELLER KEY
53. IMPELLER KEYWAY
54. IMPELLER KEY
55. IMPELLER KEYWAY
56. IMPELLER KEY
57. IMPELLER KEYWAY
58. IMPELLER KEY
59. IMPELLER KEYWAY
60. IMPELLER KEY
61. IMPELLER KEYWAY
62. IMPELLER KEY
63. IMPELLER KEYWAY
64. IMPELLER KEY
65. IMPELLER KEYWAY
66. IMPELLER KEY
67. IMPELLER KEYWAY
68. IMPELLER KEY
69. IMPELLER KEYWAY
70. IMPELLER KEY
71. IMPELLER KEYWAY
72. IMPELLER KEY
73. IMPELLER KEYWAY
74. IMPELLER KEY
75. IMPELLER KEYWAY
76. IMPELLER KEY
77. IMPELLER KEYWAY
78. IMPELLER KEY
79. IMPELLER KEYWAY
80. IMPELLER KEY
81. IMPELLER KEYWAY
82. IMPELLER KEY
83. IMPELLER KEYWAY
84. IMPELLER KEY
85. IMPELLER KEYWAY
86. IMPELLER KEY
87. IMPELLER KEYWAY
88. IMPELLER KEY
89. IMPELLER KEYWAY
90. IMPELLER KEY
91. IMPELLER KEYWAY
92. IMPELLER KEY
93. IMPELLER KEYWAY
94. IMPELLER KEY
95. IMPELLER KEYWAY
96. IMPELLER KEY
97. IMPELLER KEYWAY
98. IMPELLER KEY
99. IMPELLER KEYWAY
100. IMPELLER KEY
101. IMPELLER KEYWAY
102. IMPELLER KEY
103. IMPELLER KEYWAY
104. IMPELLER KEY
105. IMPELLER KEYWAY
106. IMPELLER KEY
107. IMPELLER KEYWAY
108. IMPELLER KEY
109. IMPELLER KEYWAY
110. IMPELLER KEY
111. IMPELLER KEYWAY
112. IMPELLER KEY
113. IMPELLER KEYWAY
114. IMPELLER KEY
115. IMPELLER KEYWAY
116. IMPELLER KEY
117. IMPELLER KEYWAY
118. IMPELLER KEY
119. IMPELLER KEYWAY
120. IMPELLER KEY
121. IMPELLER KEYWAY
122. IMPELLER KEY
123. IMPELLER KEYWAY
124. IMPELLER KEY
125. IMPELLER KEYWAY
126. IMPELLER KEY
127. IMPELLER KEYWAY
128. IMPELLER KEY
129. IMPELLER KEYWAY
130. IMPELLER KEY
131. IMPELLER KEYWAY
132. IMPELLER KEY
133. IMPELLER KEYWAY
134. IMPELLER KEY
135. IMPELLER KEYWAY
136. IMPELLER KEY
137. IMPELLER KEYWAY
138. IMPELLER KEY
139. IMPELLER KEYWAY
140. IMPELLER KEY
141. IMPELLER KEYWAY
142. IMPELLER KEY
143. IMPELLER KEYWAY
144. IMPELLER KEY
145. IMPELLER KEYWAY
146. IMPELLER KEY
147. IMPELLER KEYWAY
148. IMPELLER KEY
149. IMPELLER KEYWAY
150. IMPELLER KEY
151. IMPELLER KEYWAY
152. IMPELLER KEY
153. IMPELLER KEYWAY
154. IMPELLER KEY
155. IMPELLER KEYWAY
156. IMPELLER KEY
157. IMPELLER KEYWAY
158. IMPELLER KEY
159. IMPELLER KEYWAY
160. IMPELLER KEY
161. IMPELLER KEYWAY
162. IMPELLER KEY
163. IMPELLER KEYWAY
164. IMPELLER KEY
165. IMPELLER KEYWAY
166. IMPELLER KEY
167. IMPELLER KEYWAY
168. IMPELLER KEY
169. IMPELLER KEYWAY
170. IMPELLER KEY
171. IMPELLER KEYWAY
172. IMPELLER KEY
173. IMPELLER KEYWAY
174. IMPELLER KEY
175. IMPELLER KEYWAY
176. IMPELLER KEY
177. IMPELLER KEYWAY
178. IMPELLER KEY
179. IMPELLER KEYWAY
180. IMPELLER KEY
181. IMPELLER KEYWAY
182. IMPELLER KEY
183. IMPELLER KEYWAY
184. IMPELLER KEY
185. IMPELLER KEYWAY
186. IMPELLER KEY
187. IMPELLER KEYWAY
188. IMPELLER KEY
189. IMPELLER KEYWAY
190. IMPELLER KEY
191. IMPELLER KEYWAY
192. IMPELLER KEY
193. IMPELLER KEYWAY
194. IMPELLER KEY
195. IMPELLER KEYWAY
196. IMPELLER KEY
197. IMPELLER KEYWAY
198. IMPELLER KEY
199. IMPELLER KEYWAY
200. IMPELLER KEY
201. IMPELLER KEYWAY
202. IMPELLER KEY
203. IMPELLER KEYWAY
204. IMPELLER KEY
205. IMPELLER KEYWAY
206. IMPELLER KEY
207. IMPELLER KEYWAY
208. IMPELLER KEY
209. IMPELLER KEYWAY
210. IMPELLER KEY
211. IMPELLER KEYWAY
212. IMPELLER KEY
213. IMPELLER KEYWAY
214. IMPELLER KEY
215. IMPELLER KEYWAY
216. IMPELLER KEY
217. IMPELLER KEYWAY
218. IMPELLER KEY
219. IMPELLER KEYWAY
220. IMPELLER KEY
221. IMPELLER KEYWAY
222. IMPELLER KEY
223. IMPELLER KEYWAY
224. IMPELLER KEY
225. IMPELLER KEYWAY
226. IMPELLER KEY
227. IMPELLER KEYWAY
228. IMPELLER KEY
229. IMPELLER KEYWAY
230. IMPELLER KEY
231. IMPELLER KEYWAY
232. IMPELLER KEY
233. IMPELLER KEYWAY
234. IMPELLER KEY
235. IMPELLER KEYWAY
236. IMPELLER KEY
237. IMPELLER KEYWAY
238. IMPELLER KEY
239. IMPELLER KEYWAY
240. IMPELLER KEY
241. IMPELLER KEYWAY
242. IMPELLER KEY
243. IMPELLER KEYWAY
244. IMPELLER KEY
245. IMPELLER KEYWAY
246. IMPELLER KEY
247. IMPELLER KEYWAY
248. IMPELLER KEY
249. IMPELLER KEYWAY
250. IMPELLER KEY
251. IMPELLER KEYWAY
252. IMPELLER KEY
253. IMPELLER KEYWAY
254. IMPELLER KEY
255. IMPELLER KEYWAY
256. IMPELLER KEY
257. IMPELLER KEYWAY
258. IMPELLER KEY
259. IMPELLER KEYWAY
260. IMPELLER KEY
261. IMPELLER KEYWAY
262. IMPELLER KEY
263. IMPELLER KEYWAY
264. IMPELLER KEY
265. IMPELLER KEYWAY
266. IMPELLER KEY
- 26

3



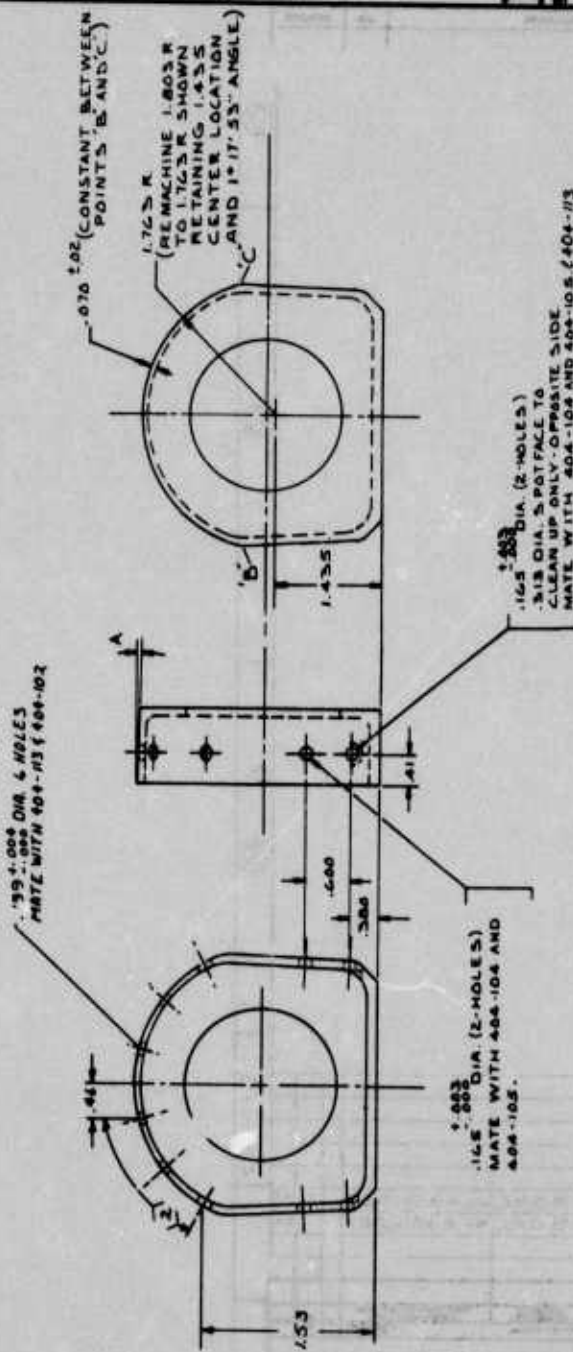
Pages 281, 282 283+284 missing

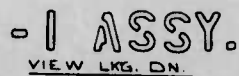
COPY AVAILABLE TO DDC DOES NOT
PERMIT FULLY LEGIBLE PRODUCTION



CALCULATED ANGLES
A: 1017.53"

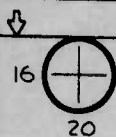
A USE 32-24037-5 FINISH MACHINED PART WITHOUT HOLES AND REWORK AS SHOWN. ALL MACHINING DIMENSIONS NOT SHOWN ARE SAME AS 32-24037-5.
 6. PART TO BE STRAIGHT WITHIN .016.
 7. 100% PENETRANT INSPECTION PER MAC P-5. 2/12/82.
 8. ALL MACHINED SURFACES USE
 9. MARKING PER MAC P-5 10/001.
 10. SURFACE INSPECTION IN ACCORDANCE WITH MAC P-5 23030.
 11. BREAK ALL SHARP EDGES.
 NOTES:

[illegible]



- | | | | | | |
|------|----------|------|--------|------|------|
| LE | RASTERED | PL | 3M26B | | |
| DB | REDFRAME | | 34B2 | | |
| | | | COLLAR | | |
| AI | REDFRAME | FL | 3M31 | | |
| CONE | SVET | CONE | SVET | CONE | SVET |
-
- | | | | |
|------------------|--------------------|--|--|
| TABC CODE | | ON PAGE NUMBER AND LOCATION OF INFO READ | |
| SVET PREPARATION | LENGTH DATA NUMBER | | |
-
- | | |
|--|---|
| C=CHINE
F=CHINE FOR DOUBLE FLAME READ
S=SMOKE
DC=DOUBLE TOP SVET, CHINE LOWER SVET
MC=DOUBLE SVETS T & A, CHINE LOWER SVET
P=PAR SVET | 1 = READ LINE
2 = REFERENCE SVET
3 = INSTALLATION SVET
4 = CAPLE CHART |
|--|---|
-
- | | |
|----------------|---|
| $\frac{AC}{D}$ | NUMBER ADD-2 SVET
INSTALLATION SVET
DOUBLE ALL SVETS
INSTALL READ SVET |
|----------------|---|
-
- | | |
|--|----------------------|
| | NO. OF SIGNAL SPACES |
|--|----------------------|

2

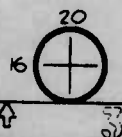


B3 INCORPORATION			APPROVAL			
SERIAL NO.	REV.	DATE	BY	CHKD.	DATE	APPROVED

4	3M266B-4-1	RIVET							
2	3M88-4	COLLAR							
2	3M91-4-2	H.S. RIVET							
1	-5	ANGLE	.025X1.30X1.30	7178-0 ALC	MIL-A-9183 COND-0				85
1	-3	RIB	.025X3.05X3.10	7178-0 ALC	MIL-A-9183 COND-0				84

10
C
B
404-115

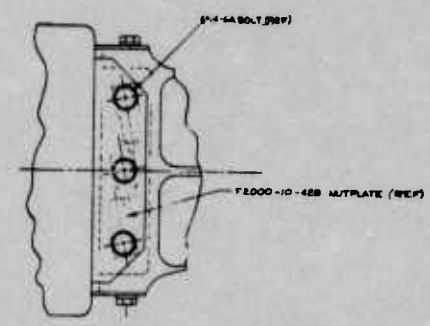
		LEADING EDGE RIB - RUDDER	
404-115		70001	
404-115		404-115	



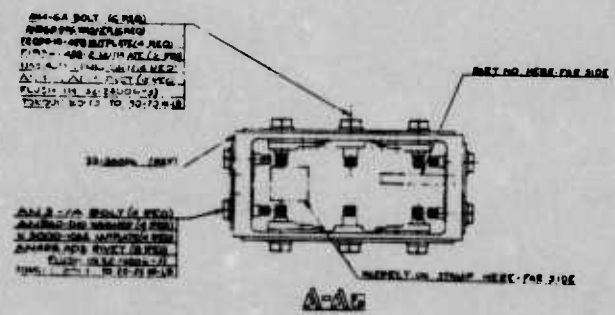
ION S
COPY AVAILABLE TO DGC DOES NOT
PERMIT FULLY LEGIBLE PRODUCTION



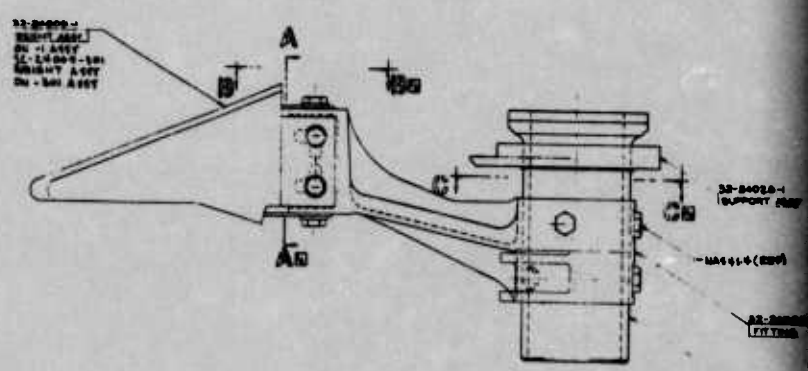
6-1, 6



B-3a



A-4a



DETAIL OF -1
DETAIL OF -301 SAME AS -1 EXCEPT AS SHOWN
-301 SUPERCEDES -1

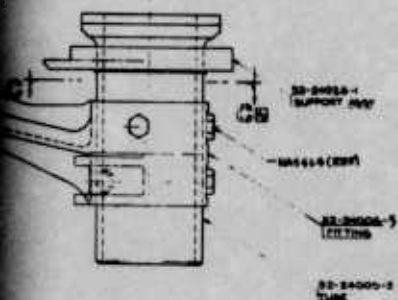
COPY AVAILABLE TO DGC DOES NOT
PERMIT FULLY LEGIBLE PRODUCTION



W1617-7 2-1 3/4" (3/4")
 W1617-7 2-1 3/4" (3/4")
 W1617-7 2-1 3/4" (3/4")
 W1617-7 2-1 3/4" (3/4")
 TOBOWE NUTS TO 70-5011-1A

6115 E

32-2400-10-428 NUTPLATE (WEP)



SAME AS -1 EXCEPT AS SHOWN

ITEM	QTY	DESCRIPTION	UNIT
1	1	32-2400-1 SUPPORT NUT	EA
2	1	W1617-7 (3/4")	EA
3	1	32-2400-5 LITING	EA
4	1	32-2400-2 TUBE	EA

4. INSTALL FASTENERS PER MAC PS. 19000.
 5. LAST SECTION LETTER USED C-4.
 6. NOMINAL SIZE LISTED IN L. 2. 4.
 7. NUTS-20: SHOW TOL. IN L. 2. 2.
 8. WASHERS PER MAC PS. 16000.
 9. NUTS

32-24004

ITEM	QTY	DESCRIPTION	UNIT
1	1	32-2400-1 SUPPORT NUT	EA
2	1	W1617-7 (3/4")	EA
3	1	32-2400-5 LITING	EA
4	1	32-2400-2 TUBE	EA
5	1	32-2400-10-428 NUTPLATE (WEP)	EA
6	1	32-2400-11-428 NUTPLATE (WEP)	EA
7	1	32-2400-12-428 NUTPLATE (WEP)	EA
8	1	32-2400-13-428 NUTPLATE (WEP)	EA
9	1	32-2400-14-428 NUTPLATE (WEP)	EA
10	1	32-2400-15-428 NUTPLATE (WEP)	EA
11	1	32-2400-16-428 NUTPLATE (WEP)	EA
12	1	32-2400-17-428 NUTPLATE (WEP)	EA
13	1	32-2400-18-428 NUTPLATE (WEP)	EA
14	1	32-2400-19-428 NUTPLATE (WEP)	EA
15	1	32-2400-20-428 NUTPLATE (WEP)	EA
16	1	32-2400-21-428 NUTPLATE (WEP)	EA
17	1	32-2400-22-428 NUTPLATE (WEP)	EA
18	1	32-2400-23-428 NUTPLATE (WEP)	EA
19	1	32-2400-24-428 NUTPLATE (WEP)	EA
20	1	32-2400-25-428 NUTPLATE (WEP)	EA
21	1	32-2400-26-428 NUTPLATE (WEP)	EA
22	1	32-2400-27-428 NUTPLATE (WEP)	EA
23	1	32-2400-28-428 NUTPLATE (WEP)	EA
24	1	32-2400-29-428 NUTPLATE (WEP)	EA
25	1	32-2400-30-428 NUTPLATE (WEP)	EA
26	1	32-2400-31-428 NUTPLATE (WEP)	EA
27	1	32-2400-32-428 NUTPLATE (WEP)	EA
28	1	32-2400-33-428 NUTPLATE (WEP)	EA
29	1	32-2400-34-428 NUTPLATE (WEP)	EA
30	1	32-2400-35-428 NUTPLATE (WEP)	EA
31	1	32-2400-36-428 NUTPLATE (WEP)	EA
32	1	32-2400-37-428 NUTPLATE (WEP)	EA
33	1	32-2400-38-428 NUTPLATE (WEP)	EA
34	1	32-2400-39-428 NUTPLATE (WEP)	EA
35	1	32-2400-40-428 NUTPLATE (WEP)	EA
36	1	32-2400-41-428 NUTPLATE (WEP)	EA
37	1	32-2400-42-428 NUTPLATE (WEP)	EA
38	1	32-2400-43-428 NUTPLATE (WEP)	EA
39	1	32-2400-44-428 NUTPLATE (WEP)	EA
40	1	32-2400-45-428 NUTPLATE (WEP)	EA
41	1	32-2400-46-428 NUTPLATE (WEP)	EA
42	1	32-2400-47-428 NUTPLATE (WEP)	EA
43	1	32-2400-48-428 NUTPLATE (WEP)	EA
44	1	32-2400-49-428 NUTPLATE (WEP)	EA
45	1	32-2400-50-428 NUTPLATE (WEP)	EA
46	1	32-2400-51-428 NUTPLATE (WEP)	EA
47	1	32-2400-52-428 NUTPLATE (WEP)	EA
48	1	32-2400-53-428 NUTPLATE (WEP)	EA
49	1	32-2400-54-428 NUTPLATE (WEP)	EA
50	1	32-2400-55-428 NUTPLATE (WEP)	EA
51	1	32-2400-56-428 NUTPLATE (WEP)	EA
52	1	32-2400-57-428 NUTPLATE (WEP)	EA
53	1	32-2400-58-428 NUTPLATE (WEP)	EA
54	1	32-2400-59-428 NUTPLATE (WEP)	EA
55	1	32-2400-60-428 NUTPLATE (WEP)	EA
56	1	32-2400-61-428 NUTPLATE (WEP)	EA
57	1	32-2400-62-428 NUTPLATE (WEP)	EA
58	1	32-2400-63-428 NUTPLATE (WEP)	EA
59	1	32-2400-64-428 NUTPLATE (WEP)	EA
60	1	32-2400-65-428 NUTPLATE (WEP)	EA
61	1	32-2400-66-428 NUTPLATE (WEP)	EA
62	1	32-2400-67-428 NUTPLATE (WEP)	EA
63	1	32-2400-68-428 NUTPLATE (WEP)	EA
64	1	32-2400-69-428 NUTPLATE (WEP)	EA
65	1	32-2400-70-428 NUTPLATE (WEP)	EA
66	1	32-2400-71-428 NUTPLATE (WEP)	EA
67	1	32-2400-72-428 NUTPLATE (WEP)	EA
68	1	32-2400-73-428 NUTPLATE (WEP)	EA
69	1	32-2400-74-428 NUTPLATE (WEP)	EA
70	1	32-2400-75-428 NUTPLATE (WEP)	EA
71	1	32-2400-76-428 NUTPLATE (WEP)	EA
72	1	32-2400-77-428 NUTPLATE (WEP)	EA
73	1	32-2400-78-428 NUTPLATE (WEP)	EA
74	1	32-2400-79-428 NUTPLATE (WEP)	EA
75	1	32-2400-80-428 NUTPLATE (WEP)	EA
76	1	32-2400-81-428 NUTPLATE (WEP)	EA
77	1	32-2400-82-428 NUTPLATE (WEP)	EA
78	1	32-2400-83-428 NUTPLATE (WEP)	EA
79	1	32-2400-84-428 NUTPLATE (WEP)	EA
80	1	32-2400-85-428 NUTPLATE (WEP)	EA
81	1	32-2400-86-428 NUTPLATE (WEP)	EA
82	1	32-2400-87-428 NUTPLATE (WEP)	EA
83	1	32-2400-88-428 NUTPLATE (WEP)	EA
84	1	32-2400-89-428 NUTPLATE (WEP)	EA
85	1	32-2400-90-428 NUTPLATE (WEP)	EA
86	1	32-2400-91-428 NUTPLATE (WEP)	EA
87	1	32-2400-92-428 NUTPLATE (WEP)	EA
88	1	32-2400-93-428 NUTPLATE (WEP)	EA
89	1	32-2400-94-428 NUTPLATE (WEP)	EA
90	1	32-2400-95-428 NUTPLATE (WEP)	EA
91	1	32-2400-96-428 NUTPLATE (WEP)	EA
92	1	32-2400-97-428 NUTPLATE (WEP)	EA
93	1	32-2400-98-428 NUTPLATE (WEP)	EA
94	1	32-2400-99-428 NUTPLATE (WEP)	EA
95	1	32-2400-100-428 NUTPLATE (WEP)	EA

SUPPORT ASSY -
 BALANCE WEIGHT & HORN
 32-24004